UNIVERSITY OF OKLAHOMA

GRADUATE COLLEGE

TESTING AND MODELING OF UNSATURATED INTERFACES

A Dissertation

SUBMITTED TO THE GRADUATE FACULTY

in partial fulfillment of the requirements for the

degree of

Doctor of Philosophy

By

TARIQ BIN HAMID
Norman, Oklahoma
2005

UMI Number: 3162838

ProQuest Information and Learning Company
300 North Zeeb Road
P.O. Box 1346
Ann Arbor, MI 48106-1346

TESTING AND MODELING OF UNSATURATED INTERFACES

A Dissertation APPROVED FOR THE
SCHOOL OF CIVIL ENGINEERING AND ENVIRONMENTAL SCIENCE

BY

_____
Dr. Gerald A. Miller

_____
Dr. James D. Baldwin

_____
Dr. Kanthasamy K. Muraleetharan

_____
Dr. Musharraf Zaman

_____
Dr. Tohren C. Kibbey

This Dissertation is dedicated to my beloved

(Late) Mother (Fatima Begum)
and
Father (Hamid Ali Qureshi)
Whose involvement contributed to my well-being in ways immeasurable

ACKNOWLEDGEMENTS

I express my sincere thanks to my supervisor Dr. G. A. Miller for his generous advice, encouragement, and continuous support during this study. I am particularly thankful for his efforts in providing the opportunity to develop the new unsaturated interface apparatus. Presentation of the discussion and results of this research is significantly improved because of his thorough reading of the dissertation. I also wish to thank Dr. Kanthasamy K. Muraleetharan for his contribution in the development of the constitutive model presented in this dissertation. Acknowledgements are also due to Dr. James D. Baldwin, Dr. Tohren C. Kibbey, and Dr. Musharraf Zaman for serving as member of my doctoral committee.

Particular thanks are due to the workshop supervisor, Mike Schmitz, who fabricated and assemble the components of the unsaturated interface apparatus.

I would like to thank my parents, sisters, and brothers for their continuous encouragement and moral support in many ways. This work would have not been possible without the encouragement, patience, and overwhelming support of my wife, Sadia. Finally, the patience of my daughter, Fatima, and my son, Talha, during the lengthy period of this research are especially acknowledged.

This research was partly supported by the National Science Foundation (NSF) under Grant Nos. 0079785 and 0301457. The author is grateful to the NSF for the support.

TABLE OF CONTENTS

CHAPTER III

CHAPTER IV

CHAPTER V

CHAPTER VI

CHAPTER VII

CHAPTER VIII

LIST OF FIGURES

ABSTRACT

Research was conducted at the University of Oklahoma to examine the behavior of interfaces in unsaturated soil. The objectives of this research were to: (1) design and construct an apparatus for testing unsaturated interfaces and soil; (2) test unsaturated soil and interfaces in the new device to study the strength and volumetric behavior of unsaturated soil and interfaces; (3) examine application of the Mohr-Coulomb failure criterion to unsaturated interfaces; and (4) develop an elastoplastic model to account for the effect of suction and net normal stress on the behavior of an unsaturated interface.

A conventional fully automated direct shear test device was modified to achieve the objectives of this study. The newly developed device, called the Unsaturated Interface Direct Shear Apparatus (UIDSA), was equipped for applying and maintaining suction as well as net normal stress. The UIDSA can be used to conduct constant water content and constant suction tests on unsaturated soil and unsaturated interfaces.

Major device modifications included the construction of an air pressure chamber and testing cells for holding soil and counterfaces, addition of high air entry porous stones, addition of a pore water and pore air control system, and other modifications to accommodate the new apparatus. For saturated soil testing, a High Air Entry Porous Disk (HAEPD) was fixed in the bottom half of the shear box, whereas for interface testing the HAEPD was fixed in the top platen and was placed on top of the soil during testing.

The performance of the newly developed device was checked and effects of net normal stress, suction, and roughness were investigated. Net normal stresses of 105, 140, and 210 kPa were used and were conducted under constant suction values of 20, 50, and 100 kPa.

Results presented in this study suggest that the maximum shear stress of interfaces between unsaturated soil and steel is a function of net normal stress and suction. As net normal stress and suction increased, so did the shear strength. The results of this study indicate that matric suction contributed to the peak shear strength of unsaturated interfaces; however, residual shear strength did not vary with the matric suction. As opposed to the matric suction, variation in net normal stress affected both peak and residual shear stress. The influence of matric suction was more pronounced in soil than interfaces. Similar to soil samples, the rough interface showed increase in dilatancy with increase in suction, whereas the smooth interface did not show dilatancy behavior.

The extended Mohr-Coulomb failure criterion provided a good model for describing variation in interface shear strength as a function of net normal stress and matric suction. Shear strength parameters for soil and interfaces were determined to define the extended Mohr-Coulomb failure envelope.

An existing elastoplastic constitutive model was modified to predict the behavior of interfaces between unsaturated soil and steel. The model is applicable for the constant net normal and constant suction conditions. Model parameters are function of net normal stress, suction, and surface roughness. Predictions made with the modified elastoplastic model agreed well with the experimental results.

CHAPTER I

INTRODUCTION

1.1 MOTIVATION FOR STUDY

In geotechnical engineering, soil-structure interaction problems and the problems related to the mechanics of jointed rocks involve contact surface behavior. The response of soil structure systems such as shallow and deep foundations, lined tunnels, retaining walls and reinforced earth to monotonic and cyclic loads is influenced by the existence of interfaces as well as dissimilarity of the mechanical properties of each continuum. The interface can have relatively weak shear strength compared to the shear strength of soils. Thus, design of such structures is sometimes controlled by the shear strength of the interface.

The "interface" referred to above is generally defined as the contact zone or common boundary between two bodies. The interface is a thin layer through which stress is transferred from one medium to the other; therefore, it typically exhibits localized and concentrated stress and strain. An interface exists when soil is placed in contact with a man made material such as steel, concrete, or geosynthetic.

Figure 1.1 shows a steel pile embedded in soil. The total frictional resistance (skin friction), Q_s, is derived from the soil-pile interface. The load carrying capacity of the pile point is denoted by Q_p. Briaud et al. (1982) reported that for a rigid concrete shaft at one half of ultimate load, 43% of the resistance was provided by skin friction. Based on the experimental results from an instrumented concrete pile that was embedded in stiff

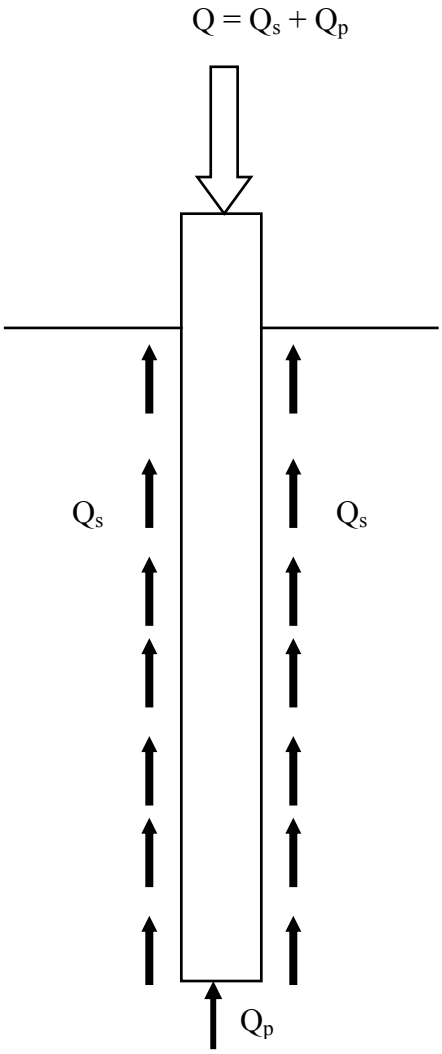

Figure 1.1: Load transfer mechanism for axially loaded pile

clay and subjected to horizontal static loading, Smith and Ray (1986) calculated that at 1/8 of the ultimate lateral load, frictional resistance Q_s contributed 84% of the soil reaction against lateral loading. The above mentioned findings show that the soil-pile interface (skin friction) plays a major part in supporting the applied load. Deep foundations are frequently used to support heavy structures, e.g., highrise buildings and bridges, and in some cases these foundations pass through unsaturated soil.

In unsaturated soils, pore spaces are filled with a mixture of two or more substances, most commonly air and water. Unlike unsaturated soil, in saturated and dry soils the pore spaces are filled with a single substance, either water or air. Most compacted soils are unsaturated with degrees of saturation much lower than one hundred percent, e.g., embankments of bridge abutments, earth dams, etc. Unsaturated soils are also found naturally in arid areas and semi-arid areas. In general, soils above the ground water table fall in the category of unsaturated soils. Matric suction plays an important role in unsaturated soil and a reasonable amount of suction controlled laboratory tests on different soil types has stressed the role of suction changes in explaining volumetric behavior and strength.

Unsaturated compacted soils are commonly used as construction materials in building embankments and dams, and for back-filling beneath foundations or behind retaining structures. Although considerable research has been done to understand unsaturated soil behavior, no data and constitutive model for the behavior of interfaces between unsaturated soil and construction material has come to the author's attention.

Unsaturated interfaces are common in geotechnical projects, e.g., friction piles embedded in unsaturated soil, retaining walls with unsaturated back fill and pipes buried

in unsaturated soil. Friction piles, for example, are commonly analyzed and designed by considering either undrained conditions (total stress approach) or drained conditions (effective stress approach). However, in cases where piles pass through an unsaturated surficial soil, as in the case of piles in fill (e.g. bridge abutments) these approaches may be inappropriate. The depth of the unsaturated soil zone may vary depending on environmental conditions in the area. The interfacial shear resistance between soil and pile in this zone presumably depends on the matric suction and net normal stress besides other factors such as void ratio, surface roughness, and overconsolidation ratio. However, there has been very little study on piles in unsaturated soil.

Unsaturated compacted soils normally have high strength and low compressibility. However, the designer must be aware of the possibility of the soil reaching a saturated state at some time during the life of the structure, due to inundation, climatic change or post construction loading. Unsaturated soil may lose some of its strength when it becomes saturated, and may also undergo large deformations during the saturation process. The loss of strength could cause slip in dams or embankments.

If the soil is at its weakest when it is saturated, it might be questioned why an understanding of unsaturated soil behavior is important. Two answers of this question may be given as: 1) there are soils that never become saturated and for these types of soils unsaturated soil mechanics theory is appropriate; and 2) if the strength parameters (e.g., undrained strength or drained strength) were evaluated when the soil was in an unsaturated state and these strength parameters were used in a saturated analysis, this could lead to an overestimation of the factor of safety, because of failing to take account of the loss of strength during saturation or even partial saturation. Only within a proper

unsaturated framework can this loss of strength be properly evaluated. The failure of a railway embankment at Notch Hill, British Columbia, Canada (Krahn et al. 1989) is a good example to show how unsaturated soil may lose some of its strength during saturation and cause failure of the structure.

Many researchers have studied interface friction between soil and other construction materials (e.g. Potyondy 1961, Tsubakihara and Kishida 1993, Tsubakihara et al. 1993, Fakharian and Evign 1996) using a variety of equipment, e.g., simple shear (Kishida and Uesagi 1987), direct shear (Potyondy1961), torsion (Yoshimi and Kishida 1981) or annular shear devices (Brumund and Leonards 1973). Fakharian and Evgin (1996) have described three dimensional monotonic and cyclic testing of interfaces for examining the influence of relative density. Some have studied the influence of overconsolidation ratio (Subba Rao et al. 2000) and surface roughness (Tsubakihara et al. 1993) on the interface behavior. However, conspicuously lacking in available literature is treatment of interfaces in unsaturated soil. Two major reasons can be identified for the lack of research on unsaturated interfaces. First, the stress system and structural arrangements within unsaturated soils are more complex than in saturated soil and this makes it difficult to identify a single effective stress variable for unsaturated soil. Second, non-availability of proper devices makes the study of behavior of unsaturated interfaces a difficult task.

In this study a new apparatus for testing of interfaces between unsaturated soil and steel was designed and constructed. The device is capable to control and/or maintain the matric suction in the soil while shearing against a steel plate. The new apparatus was used to perform unsaturated interface direct shear tests under constant suction conditions. The axis translation technique was used to control the suction.

Constitutive models for simulating the behavior of interfaces are normally required for load-deformation analysis of soil-structure systems. There are several groups of constitutive theories. The purpose of each theory is to describe the behavior of a certain class of materials under some ideal conditions. Theory of linear elasticity, for example, describes response of those materials for which stress is a unique linear function of strain. Theory of plasticity, on the other hand, describes rate independent inelastic behavior of materials. Constitutive laws based on the theory of linear and nonlinear elasticity can not describe the behavior of soil or the interface between soil and structure with reasonable accuracy. This is due to the fact that the behavior of an interface between a structure and soil is highly nonlinear and depends upon the history of deformations. The theory of plasticity describes rate independent nonlinear and inelastic response of materials. Thus, constitutive laws based on the theory of plasticity can be effectively used to characterize the behavior of soil and interfaces between soil and structures.

In the absence of relative slip in the interface, the soil-structure system can be treated as a single body and the effect of the interface may be ignored. In this case the analysis of soil-structure interaction problems can be performed using continuum mechanics principles and ignoring the presence of the interface. However, in the presence of relative slip, soil and structure have to be considered as two continuum bodies coupled through the interface. The nature and behavior of the interface is an important phenomenon in soil- structure interaction problems and the true interface action occurs only when there are relative motions at the interface.

An elastoplastic constitutive model, originally developed by Navayogarajah et al. (1992) for simulating the stress-displacement relations of interfaces between sand and

structural materials, is expanded to encompass unsaturated interfaces. The model parameters are obtained from experimental results. Subsequently the model is used for the prediction of the behavior of an unsaturated interface and the predicted results are compared with the corresponding experimental results.

1.2 SCOPE OF RESEARCH

The objectives of this research were to: (1) design and construct an apparatus for testing unsaturated interfaces and soil; (2) test unsaturated soil and interfaces in the new device to study the shearing behavior of unsaturated soil and interfaces, (3) examine the extended Mohr-Coulomb failure criterion for unsaturated interfaces, and (4) develop an elastoplastic model to account for the effect of suction and net normal stress on the behavior of an unsaturated interface.

In order to achieve the above mentioned objectives, the scope of this research may be stated as follows:

(1) Development of a new unsaturated interface direct shear apparatus capable of applying and controlling matric suction and net normal stress.

(2) Verification of the performance of the apparatus by conducting performance tests.

(3) Accomplish a series of unsaturated soil and interface tests at different suctions and net normal stresses.

(4) Expand the elastoplastic hierarchical single surface model, originally developed by Desai and co-workers and employed by Navayogarajah et al. (1992) for interface behavior, for unsaturated interfaces.

1.3 OUTLINE OF DISSERTATION

Chapter 2 presents a review of literature on the strength and volumetric behavior and testing of unsaturated soil, devices employed for interface testing, observed interface behavior, and constitutive models available for interface behavior and unsaturated soil.

Chapter 3 describes the unsaturated interface direct shear apparatus developed for this research. The major components of the apparatus, data acquisition system, and technique used to apply and control the matric suction are described.

Chapter 4 explains the testing procedures including the description of interface materials such as unsaturated soil and steel, and the specimen preparation and placement method. This chapter also describes tests conducted to evaluate the performance of the unsaturated interface direct shear device.

Chapter 5 focuses on the results of unsaturated soil and interface tests. These results are presented to explain the influence of several parameters such as net normal stress, suction, and roughness on shear strength and volumetric behavior of unsaturated soil and interfaces. Finally, a comparison is made between the results of unsaturated soil and unsaturated interfaces.

Chapter 6 presents the extended Mohr-Coulomb failure criterion for the unsaturated interface and determination of strength parameters required to define the shear strength of the unsaturated interface.

Chapter 7 describes the analogy between unsaturated soil and interfaces in unsaturated soils. An existing elastoplastic constitutive model is expanded and modified for modeling the stress-displacement relations of an unsaturated soil-steel interface under constant net normal stress and suction conditions.

Chapter 8 presents conclusions of this research and provides recommendations for future research.

CHAPTER II

LITERATURE REVIEW

The review of literature is presented in three sections. The first section covers the structure, testing, shear strength and volume change behavior of unsaturated soils. Second section deals with the experimental devices used for interface testing and the available test results for interface behavior. Section 3 discusses constitutive models proposed for interface behavior in unsaturated soil.

2.1 UNSATUARTED SOIL

Theory of soil mechanics essentially developed in the temperate climate areas (e.g., England) of the world where saturated soils are commonly found. This is one of the reasons that soil mechanics has been focused on the study of saturated soil. However, significant areas of the earth's surface are classified as arid and semi arid zones. In these areas saturated conditions are actually never reached and the limiting case of saturation is often irrelevant. Even in areas of heavy rainfall, soil structures are kept in unsaturated conditions, and saturation of these structures is considered failure of the structure. For example, efforts are made to save the fill against a retaining wall from water and different procedures of proper drainage are employed for this purpose. Geotextiles and other techniques are adopted to avoid accumulation of water underneath pavements.

Arid and semiarid areas usually have a deep ground water table and soils located above the water table have negative pore water pressure. Upon wetting, for example due to climate changes, pore water pressure increases and as a result changes occur in the

volume and shear strength of the soil. Reduction in shear strength of unsaturated soil due to change in water content is the cause of numerous slope failures. Reduction in bearing capacity and resilient modulus of soils are also associated with increase in pore water pressure. These phenomena indicate the importance of understanding the behavior of unsaturated soil and the important role that negative pore water pressure plays in controlling the mechanical behavior of unsaturated soils.

2.1.1 Soil Suction

In Figure 2.1 a clean capillary tube is shown immersed in pure water. As a result of the molecular and physico-chemical forces, water rises in the tube and for

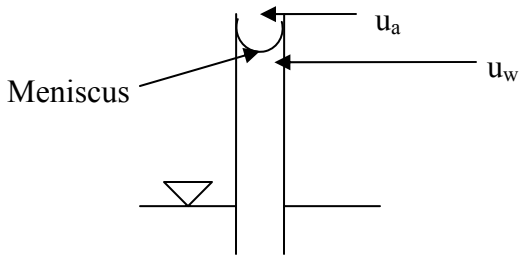

Figure 2.1: Formation of meniscus in a capillary tube

equilibrium to exist the pressure difference across the meniscus is given by,

$$(u_a - u_w) = 2T_s / R_s \qquad (2.1)$$

where:

u_a = air pressure,

u_w = water pressure,

T_s = surface tension of water, and

R_s = radius of curvature of meniscus.

Note, the contact angle between water and clean glass tube is assumed to be zero. Equation (2.1) shows that water will be in a state of tension when u_a is equal to atmospheric pressure. In Equation (2.1) the term (u_a-u_w) is known as the matric suction.

In Fig. 2.2 a model of two spherical particles with a lens of water around them is

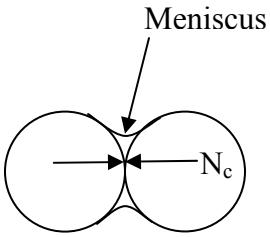

Figure 2.2: Interparticle force due to capillarity

shown. The meniscus (or lens) around grain contact points tends to draw the particles together. This attractive force, called capillary force, acts perpendicular to the grain contact surface. It has been shown that under certain conditions, capillary force, N_c, increases with an increase of suction (Kohgo et al. 1993). When suction is a relatively small value, the rate of increase in N_c is comparatively high. Increase in N_c induces an increase of shear resistance between the soil particles. This inhibits the relative sliding between the particles and the magnitude of shear resistance of soil increases. Kohgo et al. (1993) suggested that the contribution of shear resistance caused by the capillary force may be regarded as nominal cohesion. Burland and Ridley (1996) used a grain column analogy to show that the meniscus around the soil particles results in increase in stability of soil structure (Fig. 2.3). They suggested that the contact menisci can be thought of as 'bonds' holding the grains together. This bonded system can sustain some externally

applied load without collapsing. However, if these bonds are then removed by adding water to the system the column of grains will become unstable and collapse.

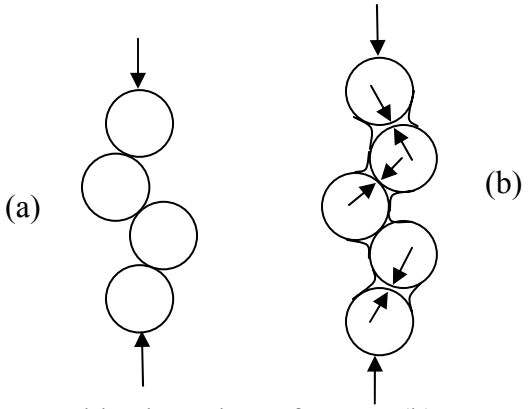

Figure 2.3: (a) Unstable boundary forces, (b) Contact menisci, stable structure (after Burland and Ridley 1996)

Unsaturated soil is a three phase system that contains solid, water and air. The mechanical behavior of unsaturated soil is strongly influenced by changes in pore air pressure, u_a, and pore water pressure, u_w. In unsaturated soil the contractile skin (meniscus) is subjected to u_a, which is greater than the water pressure u_w. As matric suction, u_a-u_w, of soil increases, the radius of curvature of the meniscus decreases. As degree of saturation decreases the meniscus withdraws into smaller pore spaces, the radius of curvature of the meniscus reduces, and therefore the matric suction increases. Because of the smaller voids, far higher suction can develop in clayey soils than in granular soils.

Soil suction (or total suction) is commonly referred to as the free energy state of soil water and is quantified in terms of the relative humidity. Total suction in soil has two components, which are called matric suction (which, is related to the curvature of meniscus) and osmotic suction (which, is related to the concentration of salts in the pore

water). Experimental evidence suggests that the shear strength and volume change behavior of unsaturated soil are primarily dependent on the matric suction rather than the total suction (Alonso et al. 1987). Therefore, the stress-strain behavior of unsaturated soil is primarily dependent on matric suction.

2.1.2 Structure of Unsaturated Soil

Fine grained soils in general have two levels of soil structure: a macro structure and a micro-structure. These structures, which are present in both natural and compacted soils are a function of type of soil, initial water content, compaction procedures and the applied stresses. The micro-structure is the arrangement of the elementary particle associations within the soil aggregate, whereas the macro-structure is arrangement of soil aggregates (Mitchell 1976). In a specimen that is compacted dry of optimum, macro-structure is more predominant. This pore structure facilitates easier drainage of water (desaturation) under an applied soil suction. In contrast to dry of optimum specimens, the pore channels in the wetter specimens are generally disconnected and offer greater resistance to the water flow. The soil in this latter condition is less pervious since the micro-structure dominates and provides resistance to the desaturation process. The specimen compacted at optimum water content lies between these two conditions. However, the behavior is more likely that of a soil compacted wet of optimum.

Seed and Chan (1959) examined the stress-strain behavior of unsaturated soils compacted at moisture contents wet and dry of optimum. High stiffness was observed for soil compacted at moisture contents dry of optimum and lower stiffness for soil compacted wet of optimum moisture content. However, the failure envelope was found to be approximately equal in both cases. Seed and Chan (1959) suggested that the reason for

equal strength was that structural changes during shearing resulted in similar structures at failure (in the failure zone) for samples compacted wet or dry of optimum. Seed and Chan (1959) also examined the influence of method of compaction. At moisture contents dry of optimum, statically and dynamically compacted samples exhibited similar stress-strain behavior. However, at moisture contents wet of optimum, statically compacted samples exhibited a significantly higher value of stiffness than dynamically compacted samples. This was attributed to the different fabrics produced by the two methods of compaction: static compaction producing a flocculated structure and dynamic compaction a dispersed or flocculated structure depending on the water content. Seed and Chan (1959) suggested that the flocculated structure caused by static compaction at moisture contents wet of optimum was the result of the smaller shear displacements caused in static compaction than in dynamic compaction.

Barden and Sides (1970) also examined the effect of structure on the behavior of compacted unsaturated soils. Barden and Sides concluded that for soils compacted dry of optimum, the settlement during loading was small and the major construction problem was collapse or swelling of soil during wetting. In soils compacted to moisture contents wet of optimum, settlement during loading was much more a problem, whereas collapse or swelling upon wetting was relatively unimportant.

Toll (1990) defined the structure of unsaturated compacted soils using the degree of saturation, and the degree of saturation was included as a variable in his analysis. A clear distinction was found between the behaviors of samples of Kinuyu gravel compacted to different values of moisture content. Toll also claimed that the structure of unsaturated soil was not destroyed even at high shear strain. This contradicted the conclusion of Seed

and Chan (1959), who stated that soil samples with different structures ended up with identical structures at failure. Toll (1990) explained the behavior of compacted unsaturated soils in terms of a two level structure involving compression of the packing arrangement of different packets and swelling of each packet. He concluded that these two different aspects of behavior would cause different volume change or pore water pressure response and the overall behavior is dependent on the relative contribution of each effect.

2.1.3 Effective Stress Concept for Unsaturated Soil

Behavior of saturated or dry soil is controlled by changes in the effective stress. According to Terzaghi's theory of saturated soil mechanics, effective stress controls strength and volume change behavior of saturated or dry soil. Effective stress is given by the following equation,

$$\sigma' = \sigma - u \qquad (2.2)$$

where:

σ' = effective stress,

σ = total stress, and

u = pore pressure.

Shear strength of soil is related to effective stress by the following equation,

$$\tau = c' + \sigma' \tan \phi' \qquad (2.3)$$

where:

c' = cohesion, and

ϕ' = effective angle of internal friction.

Effective stress concept has been verified experimentally and successfully explains the behavior of saturated and dry soils. Early researchers examined the possibility that the concept of a single effective stress could also be applied to unsaturated soils. Analysis of unsaturated soil would be greatly simplified if the concept of a single effective stress were applicable to unsaturated soil. Bishop (1959) proposed the following equation to incorporate the concept of effective stress for the analysis of unsaturated soils,

$$\sigma' = \sigma - u_a + \chi(u_a - u_w) \qquad (2.4)$$

where:

u_a = the pore air pressure,

u_w = the pore water pressure, and

χ = a parameter, which was unity for saturated soils and decreased as the degree of saturation fell, reaching zero for dry soils.

In 1960 many researchers considered the possibility of a single effective stress equation for unsaturated soils, for example Aitchison (1961), Richard (1966), and Brackley (1971). Jennings and Burland (1962) analyzed the factors affecting the use of Bishop's effective stress Equation 2.4 for unsaturated soils. Oedometer and triaxial tests were conducted on three different soils (silt, silty clay, and sand). In each test an unsaturated sample was loaded to a given value of (σ-u_a) and then soaked at constant total stress. Each sample showed an additional compression during soaking and surprisingly the final void ratio of the wetted soil fell on the virgin consolidation line for saturated soil. Jennings and Burland pointed out that, if the single effective stress concept were valid, swelling of soil samples would be expected during wetting due to the

reduction in the effective stress as defined by Equation 2.4. The reduction in soil volume observed during wetting showed that the effective stress concept as applied to volume change is not correct.

Jennings and Burland (1962) suggested a two-way mechanism to explain collapse behavior on wetting of unsaturated soils. First, bonding between the saturated soil packet structures will be removed, resulting in collapse of the packet structure into the air filled inter-pocket voids. Second, each saturated packet takes in water and swells (i.e., collapse of the "macro-structure" but swelling of the "micro-structure" of each packet). The overall volume changes are dependent on the void ratio within the packet and the strength of each packet available to prevent breakdown.

Bishop and Blight (1963) made a further attempt to validate the effective stress concept given by Equation 2.4. They conducted consolidation and shearing tests on various types of soils, adopting a variety of different stress paths. Based on their experimental results, Bishop and Blight concluded that a single effective stress, as defined by Equation 2.4, could not be used for the volume change behavior of unsaturated soils but it could be used to predict the shear strength of unsaturated soils. Bishop and Blight (1963) suggested a modified effective stress equation, in which the effective stress was a function of σ-u_a and u_a-u_w,

$$\sigma' = \sigma - u_a + f(u_a - u_w) \qquad (2.5)$$

Bishop and Blight also qualitatively represented the volume change and shear strength behavior of unsaturated soil in three dimensional plots of void ratio and strength plotted against σ-u_a and u_a-u_w. Burland (1964) rearranged the experimental results of Bishop and

Blight (1963) to demonstrate that the single effective stress concept was invalid for volume change behavior of unsaturated soils.

2.1.4 Volume Change Behavior of Unsaturated Soils

Matyas and Radhakrishna (1968) conducted a series of isotropic consolidation and K_0 tests on kaolin-flint to examine the viability of two stress state variables suggested by Bishop and Blight (1963). All the soil structures were prepared by static compaction to achieve the same initial condition for every sample. For each set of tests they plotted the void ratio (e), against suction (u_a-u_w) and mean net stress (p-u_a). The point from each test series produced a warped surface in e, u_a-u_w, p-u_a space. The results also showed the possibility of either swelling or collapse during wetting (reduction of suction to zero) depending on the value of p-u_a. These results provided strong support for the concept of two stress state variables as proposed by Bishop and Blight (1963).

Barden et al. (1969) examined the Bishop and Blight concept of two stress state variables by conducting a series of isotropic consolidation tests on Westwater Clay. Compacted unsaturated samples were consolidated at a given suction and mean net stress and then samples were taken through different stress paths involving wetting and consolidation. Several series of tests were conducted to explore the influence of water content, stress increment ratio, and clay content. Barden et al. (1969) suggested the use of (σ-u_a) and (u_a-u_w) to analyze the volume change behavior of unsaturated soil. Barden et al. (1969) found that high clay content caused swelling behavior at low mean net stress. Also, the effect of large stress increment ratios was more apparent at high clay contents.

Fredlund and Morgenstern (1976) examined the uniqueness of the surfaces of void ratio, e, plotted against net stress, σ-u_a, and suction, u_a-u_w, with a series of isotropic and

K_0 consolidation tests on three different soils. Values of the deformation moduli with respect to σ-u_a, and u_a-u_w were calculated using the deformation from small increments of stress along two different stress paths. The calculated deformation moduli were then used to compare with the anticipated deformation along a third stress path. Some samples showed a good correlation between measured and calculated deformation while others showed poor correlation. Fredlund and Morgenstern (1976) attributed this poor correlation to the non-linear nature of the constitutive surface and hysteresis of the soil behavior.

Fredlund and Morgenstern (1976) also checked the uniqueness of the constitutive surface of water phase volume plotted against σ-u_a and u_a-u_w. They found that the correlation was not as good as that of total sample volume change. This poor correlation was attributed to inaccuracy in the measurements of very small water volume changes.

In an attempt to validate the use of two stress state variables, Fredlund and Morgenstern (1977) conducted a series of null tests on unsaturated soil. Samples were isotropically consolidated to given values of σ-u_a and u_a-u_w and then equal increments of σ, u_a, and u_w were applied (i.e., without changing σ-u_a and u_a-u_w). No volume change was observed and it was concluded therefore that two stress state variables σ-u_a, and u_a-u_w could be used to analyze unsaturated soil behavior.

Lloret and Alonso (1985) examined a number of possible relationships for volume change behavior of unsaturated soils using a wide range of experimental data. They finally proposed semi-empirical equations to relate the volume change of unsaturated soils to the two stress state variables.

$$e = a + b(\sigma - u_a) + c\log(u_a - u_w) + d(\sigma - u_a)\log(u_a - u_w) \qquad (2.6)$$

or alternatively,

$$e = a + b\log(\sigma - u_a) + c\log(u_a - u_w) + d\log(\sigma - u_a)\log(u_a - u_w) \qquad (2.7)$$

e is void ratio and a, b, c, and d are constants. Equation 2.6 was best at low stress levels and Equation 2.7 was best at high stress levels. Again the constitutive Equations 2.6 and 2.7 do not satisfy saturated conditions when the suction approaches zero. However, these equations were capable of representing both swelling and collapse on wetting.

2.1.5 Shear Strength of Unsaturated Soil

An important contribution to the development of constitutive models for unsaturated soil behavior was made by Fredlund et al. (1978), who suggested a relationship between the shear strength, τ, of unsaturated soil and the two stress state variables σ-u_a and u_a-u_w.

$$\tau = c' + (\sigma - u_a)\tan\phi' + (u_a - u_w)\tan\phi^b \qquad (2.8)$$

where:

τ = shear stress on the failure plane at failure or shear strength,

c' = effective cohesion intercept,

ϕ' = effective angle of internal friction with respect to the, $(\sigma - u_a)$

ϕ^b = angle of internal friction with respect to $(u_a - u_w)$,

σ = total stress normal to the failure plane at failure,

u_a = pore air pressure on the failure plane at failure, and

u_w = pore water pressure on the failure plane at failure.

Fredlund et al. (1978) showed experimentally that the ϕ' value was similar for saturated and unsaturated conditions by conducting triaxial tests on compacted shale at constant water content. All the failure points were plotted in τ, u_a-u_w, $(\sigma_1+\sigma_2)/2 - u_a$ space. The failure points produced a planar surface. Approximate values for ϕ', ϕ^b, and c' were calculated from the results and these were used to define Equation 2.8.

Escario and Saez (1986) presented results that suggested a need to modify Equation 2.8 slightly. They conducted drained direct shear tests on compacted Guadalix Red Clay, Madrid Grey Clay and Madrid Clayey Sand at different values of controlled suction. The failure strength was plotted against suction, u_a-u_w, and net normal stress, σ-u_a, for each soil type. The results indicated that ϕ^b in Equation 2.8 was not a constant for a given soil type. The value of ϕ^b was approximately equal to ϕ' at low values of suction and then tended to decrease as suction increased. However, a stable value of ϕ^b could be found at higher suction. The suction at which the value of ϕ^b decreased differed for each type of soil. Escario and Saez (1986) also concluded that ϕ' was unaffected by changes in suction.

The non-linearity of shear strength with suction was again observed by Gan et al. (1988) in triaxial tests conducted on a glacial till. At low values of suction the value of ϕ^b was approximately equal to ϕ' and then ϕ^b started to decrease as suction increased. Gan et al. (1988) interpreted the value of suction at which ϕ^b drops from ϕ' to a lower value as the air entry value of the soil, i.e., below this critical value of suction the soil is still saturated and ϕ^b is equal to ϕ' in Equation 2.8.

The nonlinearity of shear strength with the suction was even more apparent in the direct shear tests conducted by Escario and Juca (1989). Theoretically, if the suction increases indefinitely the soil must reach a dry state and Equation 2.8 should reduce to the normal Mohr-Coulomb relationship for dry soil. To satisfy this condition ϕ^b must decrease to zero at very high values of suction.

Oloo and Fredlund (1996) proposed a simplified method for determination of ϕ^b for statically compacted soils. In this study they used a Botkin Pit Silt and Indian Head Till in saturated and as-compacted conditions. Suction values of as-compacted soil were determined by using the pressure plate apparatus. The change in matric suction resulting from the application of normal stress was estimated using the analysis proposed by Hilf (1948). All the samples were tested in an undrained condition. The value of tan ϕ^b was obtained from the slope of the shear stress versus estimated matric suction curve. The same soils were tested in modified direct shear device and unsaturated shear strength parameter ϕ^b was determined. The results from the modified direct shear tests were compared with as-compacted soils tested in conventional direct shear equipment. Results suggested that variation of shear strength with suction is similar for specimens tested in the modified direct shear and in the as-compacted state. Oloo and Fredlund (1996) proposed that the procedure is suitable for statically compacted soils that retain approximately the same soil structure when compacted to the same density at different water contents.

Vanapalli et al. (1996) proposed a method for the prediction of shear strength with respect to the soil suction. They proposed the following equation for the shear strength of soil,

$$\tau = \left[c' + (\sigma_n - u_a)\tan\phi'\right] + (u_a - u_w)\left[(\Theta^k)\tan\phi'\right] \qquad (2.9)$$

where:

k= a fitting parameter, and

Θ=normalized volumetric water content and is given by the relation $\Theta = \theta/\theta_s$, where θ is volumetric water content and θ_s is volumetric water content at a saturation of 100 %. The first part of the equation is the saturated shear strength. The second part of the equation is the shear strength contribution due to suction, which can be predicted using the soil-water characteristic curve.

Vanapalli et al. (1996) used a glacial till for the determination of soil water characteristic curves. Effective shear strength parameters were determined both under single stage and multistage testing with the soil in a saturated state. Single stage and residual shear strength testing was conducted using a conventional direct shear apparatus. Unsaturated shear strength was predicted using Equation 2.9 and results were compared with unsaturated shear strength determined using a modified direct shear apparatus. They found good comparison between the experimental results and predicted values for the range of 0-500 kPa suction for the glacial till.

2.1.6 Linking Volume Change and Shear Strength

In recent years, researchers have been attempting to analyze unsaturated soil behavior in terms of constitutive relations linking volume change, shear deformation and strength

in a single elastoplastic model. Most of this research has been concentrated on unsaturated compacted soils.

Toll (1990) conducted a series of triaxial tests on compacted Kiunyu Gravel. He prepared statically compacted samples at different moisture contents. Most of the tests were conducted by shearing at constant water content. In most of the cases, true critical states were not achieved and the sample continued to dilate even at large strain. Toll (1990) proposed the following equations for deviator stress q and specific volume v at the critical state:

$$q = M_a(p - u_a) + M_w(u_a - u_w) \tag{2.10}$$

$$v = \Gamma_{aw} - \lambda_a \ln(p - u_a) - \lambda_w(u_a - u_w) \tag{2.11}$$

where:

q = deviator stress,

v = specific volume,

p = mean stress, and

M_a, M_w, λ_a, λ_w, and Γ_{aw} = factors that changed with degree of saturation, S_r.

Toll (1990) back calculated values of M_a, M_w, λ_a, λ_w, and Γ_{aw} by conducting a regression analysis and assuming that each factor was a function of S_r only. He suggested that unique critical state relationships for q and v might be obtained if the initial structure were destroyed during shearing to produce similar structures at critical state. Toll (1990) suggested that samples with similar initial structures must be used when establishing any constitutive relationship, to avoid any influence of initial structure in the model.

Wheeler (1991) suggested an alternative form of critical state equation for deviator stress with degree of saturation, S_r, excluded from the analysis:

$$q = M(p - u_a) + f(u_a - u_w) \qquad (2.12)$$

where:

q = deviator stress,

u_a = pore air pressure,

u_w = pore water pressure

p = mean net stress, and

M = a parameter that changes with (u_a-u_w).

Wheeler (1991) also defined a critical state volumetric relationship in terms of only mean net stress and suction:

$$v_w = \Gamma - \lambda \ln(p - u_a) + f(u_a - u_w) \qquad (2.13)$$

where:

v_w = the specific water volume, which is directly related to the water content w,

Γ and λ = model parameters, and

p, u_a, and u_w were same as defined in Equation 2.12.

Equation 2.12 was validated by using Toll (1990) experimental data. Wheeler pointed out that Equation 2.12 does not provide any information on the value of the specific volume v at the critical state and hence the total volume change is not defined.

Josa et al. (1987) conducted a series of isotropic consolidation tests to examine the elastoplastic behavior of unsaturated soils. Gens et al. (1989) and Alonso et al. (1987) qualitatively expressed elastoplastic behavior of unsaturated soil. Alonso et al. (1990)

presented a mathematical formulation of an elastoplastic model and attempted to validate the theoretical concept of elastoplastic behavior of unsaturated soil with available experimental data.

Josa et al. (1987) conducted a series of isotropic consolidation tests on identical statically compacted samples of kaolin. Each sample was taken through various stress paths involving loading and unloading (changing mean net stress) at constant suction and wetting or drying (changing suction) at constant mean net stress. The results showed plastic behavior when the soil was wetted at high mean net stress and elastic behavior when the soil was wetted at low mean net stress. Alonso et al. (1990) proposed a loading collapse (LC) yield curve. They also suggested a second section of yield locus, the suction increase (SI) yield curve and expressed the possibility of coupling the LC and SI yield loci.

Wheeler and Sivakumar (1992) pointed out that the constitutive model of Alonso et al. (1990) does not include expressions for the water content, w, and therefore it can be used only for drained conditions (where the variation of suction is externally specified). They proposed a critical state frame work involving five state variables, mean net stress, p', deviator stress, q', suction, s, specific volume, v, and water content, w, for unsaturated soil. In support of their proposed constitutive model, Wheeler and Sivakumar (1992) provided experimental data from a series of triaxial shear tests on samples of compacted unsaturated kaolin. Experimental data produced straight critical state lines for any constant value of suction in q versus p' and w versus the logarithm of p' spaces, but the

critical state line was curved in plots of specific volume versus the logarithm of p′ (except for the critical state line corresponding to zero suction).

Wheeler and Sivakumar (1995), however, realized that plastic changes of water content should be calculated by the application of a flow rule (analogous to shear strain) instead of treating w as state variables (analogous to specific volume). They proposed the modified version of constitutive model of unsaturated soil in terms of four state variables: p′, q′, s, and v.

Wheeler et al. (2002) pointed out that in Alonso (1990) constitutive model of unsaturated soil there is a stress p^c at which the yield curve becomes a straight vertical line in the s-p′ plane and in practice this is unlikely to be true. Wheeler et al. (2002) suggested that the alternative elastoplastic constitutive model proposed by Wheeler and Sivakumar (1995) provides the additional flexibility required to match the normal compression lines at different values of suction, but at the expense of a more complicated mathematical expression for the LC yield curve.

Geiser et al. (2000) proposed an elastoplastic constitutive model in the framework of Disturb State Concept (DSC) to model the volumetric behavior of unsaturated soils and the loss of strength in the stress-strain relationship due to suction. The disturbed state concept was first proposed by Desai (1974) and is based on the idea that a deforming material element can be treated as a mixture of two constituent parts in the relatively intact (RI) and fully adjusted (FA) states, referred to as reference state. During external loading, the material experiences internal changes in its microstructure due to a self adjustment process, and as a consequence, the initial RI state transforms continuously to the FA state. The observed state is defined as,

$$\sigma^a = (1 - D)\sigma^i + D\sigma^c \qquad (2.14)$$

where:

σ^i = relatively intact stress,

σ^c = fully adjusted stress,

σ^a = observed stress, and

D = disturbance function ($0 \leq D \leq 1$).

The fully adjusted state of a material is considered as the stress state with D = 1. In the case of the Geiser et al. (2000) modeling it corresponds to the saturated state.

Geiser et al. (2000) made use of two independent stress variables: the saturated effective stress, σ-u_w, and the suction, u_a-u_w, to model the behavior of unsaturated soil. They proposed two yield surfaces. First a yield surface to describe the yield of soil in effective mean stress (p′)-deviator stress (q) plane at constant suction, and second, a yield surface to describe the hydric behavior in the p′-s plane at constant saturated effective mean pressure.

Several researchers (e.g., Bolzon et al. 1996, Karube and Kato 1989) have proposed elastoplastic constitutive models for unsaturated soil based on effective stress. For example, Bolzon et al. (1996) formulated a saturated soil model in the framework of generalized plasticity, considering the volumetric behavior as well as strain hardening. Bolzon et al. (1996) modified this model to incorporate the observed experimental behavior of unsaturated soil by introducing effective stress and suction as independent stress parameters and by modifying the hardening parameter and yield function to take account of the role of matric suction.

More recently, Loret and Khalili (2000) proposed a constitutive model based on an effective stress concept. They argued that the effective stress, if defined properly, provides a compact and rigorous description of unsaturated soil behavior. This argument has been examined experimentally by Geiser (2000) and Khalili (2000), who showed that a single effective stress is capable of predicting the shear strength and volume change of unsaturated soils accurately. However, in their formulation of the constitutive model Loret and Khalili (2000) included the suction as an independent variable in the yield function and plastic potential, in addition to the effective stress and the suction-dependent hardening parameter. This makes their model similar to those of Alonso (1990), which uses two stress variables.

2.1.7 Laboratory Testing of Unsaturated Soil

Laboratory tests on unsaturated soils have normally been conducted in a triaxial cell, an oedometer apparatus, or a direct shear apparatus. Different methods of soil preparation have been used. In many studies, remolded specimens formed by compacting soil at different water contents (thereby producing different soil structure) were used. In other studies, similar soil structure was obtained by compacting the soil at the same water content and bulk density and then drying or wetting the specimen to the desired water content or matric suction.

2.1.7.1 Triaxial Testing

Triaxial testing of unsaturated soil is more difficult than testing saturated samples. For unsaturated soil, a test conducted under undrained conditions is no longer a constant volume test and the sample volume change in a drained test can not be measured simply by the flow of water from the sample.

Two kinds of volume change need to be measured in triaxial testing of unsaturated soils. These are the total sample volume change and the water volume change. The water volume change can be measured in the usual manner with a burette or automatic volume change device connected to the drainage line from the sample. The overall sample volume change, due to changes in both air and water volume, can be measured in two ways: by measuring the flow of cell fluid into or out of the cell, or by measuring axial and lateral strains of the sample and calculating volumetric strain.

Bishop and Donald (1961) developed a modified triaxial cell to test unsaturated soil at Imperial College. The modified apparatus consisted of a double-walled cell with an acrylic jacket forming an inner cell wall. Mercury was used as the cell fluid in the lower part of the inner cell. The design of triaxial cell developed by Bishop and Donald (1961) was also used by Matyas and Radhakrishna (1968) to conduct isotropic consolidation tests on unsaturated soil.

Wheeler (1986) developed a double-walled triaxial cell to test unsaturated soils in the laboratory. The basic idea of the double-walled triaxial cell was that volume change of the sample could be measured by measuring the flow of water into or out of the inner cell.

The axis translation technique has been used in most laboratory research involving triaxial testing of unsaturated soil. Elevated values of pore air pressure are applied to one part of the sample boundary via a low air entry filter and lower (but still positive) values of pore water pressure are applied or measured on a different part of the sample boundary via a high air entry porous disk. Use of a high air entry porous disk does not solve the difficulty of air getting into the water drainage line. Dissolved air within the pore water

can still penetrate through the porous stone by diffusion and this air may then come out of solution in the drainage line beneath the porous stone. Bishop and Donald (1961) developed a bubble pump and Fredlund (1975) developed the Diffused Air Volume Indicator (DAVI) to remove and measure the amount of diffused air collected beneath a high air entry porous stone. The diffused air is flushed and collected from the system using a device such as a DAVI and the air volume is measured in a suitable calibrated chamber.

2.1.7.2 Oedometer Testing

Testing of unsaturated soil in an oedometer is easier than testing in a triaxial cell because in this test movement of sample takes place only in one direction. Barden and Sides (1970) developed a modified Rowe cell to conduct one-dimensional consolidation tests on unsaturated soils. They used the axis translation technique to control or measure the matric suction. Other researchers, including Fredlund and Morgenstern (1977) and Escario and Juca (1989), used the same type of apparatus with some modifications. Rahardjo and Fredlund (1996) designed an apparatus for performing consolidation tests under K_0 conditions for testing unsaturated soils. Aversa and Nicotera (2000) developed a modular system that can be configured either as an oedometer or triaxial cell.

2.1.7.3 Direct Shear Testing

In a direct shear test, a soil sample is sheared on a predetermined shear plane. The test can be conducted under constant normal stress, constant volume, or constant stiffness. This apparatus has been used for testing saturated and unsaturated soils for many years.

Escario (1980) developed a direct shear apparatus to test unsaturated soil. To apply the matric suction, the axis translation technique was employed. Elevated pore air pressure

was applied to a container surrounding the whole apparatus. The pore water pressure was then applied or measured by using the HAEPD at the sample base. The same type of apparatus was used by Gan and Fredlund (1988) to determine the shear strength parameters of unsaturated soil. Gachet et al. (2003) described a modified direct shear box to measure the shear strength of sand-glass and sand-plexiglas interfaces for different degrees of saturation. Degree of saturation was changed by using water aspiration on half of a Casagrande shear box that contained saturated sand. By using water aspiration, they estimated the degree of saturation in the sand and correlated it to the suction. However, in their paper, Gachet et al. (2003) reported only degree of saturation values and not the suction. Due to the simplicity of the method they were not able to strictly control the degree of saturation during the test.

2.2 INTERFACE TESTING AND MODELING

2.2.1 Devices Used for Interface Testing

2.2.1.1 Direct Shear Type Device

The direct shear testing of interfaces is similar to direct shear testing of soil. A hollow box, containing the soil specimen, rests on a construction material such as steel, concrete, or wood. A normal load is applied by a loading platen to the top of the soil specimen, and then a horizontal load is applied to shear the interface between the soil and the construction material.

Potyondy (1961) used the direct shear box to determine the skin friction between different type of soils and construction materials, both by stress control and strain control methods. For the strain-controlled tests, the shear box had an area of 3600 mm^2. A box with an area of 8000 mm^2 was used for the stress controlled tests. The specimens of

construction materials were placed in the lower portion of the box, and the soil was placed in the upper half.

Desai et al. (1985) have also used a shear box device to study the friction between sand and steel/concrete under the conditions of repeated loading. The bottom half of the box had a square cross-section and was made from steel plates with inner dimension of 410 mm x 410 mm. One of the materials such as concrete, ballast, and rock was inserted in the bottom half. The top part consisted of a square box (310mm x 310 mm) and contained the other material. Thus, an interface of 310 mm x 310 mm was created at the junction.

2.2.1.2 Annular Shear Type Devices

The annular shear device was used by Brummund and Leonards (1973) for experimental study of static and dynamic friction between sand and typical construction materials. It consists of a cylinder of sand encased in rubber membrane with a 28.6-mm diameter, 356-mm long rod located along its axis. By evacuating air from within the membrane, a normal stress was applied to the sand-rod interface that ranged from 8.6 kPa to 86 kPa. The rod was then caused to slip relative to the sand by gradually applying static forces to the rod in the axial direction. The dynamic test setup used the same rods as in the static tests. The dynamic force was applied using a shock tube. The coefficients of friction between sand and different materials such as steel, Teflon, cement mortar, and graphite were measured using this apparatus.

2.2.1.3 Ring Torsion Type Device

Yoshimi and Kishida (1981) used a ring torsion apparatus to study the behavior of interfaces between sand and steel. Dry sand was rained into an annular container lined with a 0.3-mm thick rubber membrane. A ring shaped metal specimen was placed on the

sand as the construction material and a static torque was applied to shear the interface under constant normal load applied with weights. In addition to measurements of circumferential and vertical displacements of the metal ring, the deformation of the sand and the slippage at the soil-metal contact were measured in some tests using x-ray radiography.

2.2.1.4 Simple Shear Type Device

Uesugi and Kishida (1986) developed a simple shear type device that was capable of measuring both sliding displacement between steel and soil as well as shear deformation of the soil mass. The contact surface between steel and sand was originally 40 mm in breadth and 100 mm in length. The area of friction surface remained constant during a test even if sliding occurred, since the steel plate was longer than the friction surface. Normal and tangential loads were applied by vertical and horizontal hydraulic actuators. The container holding the sand was a stack of 2mm thick aluminum plates with a 40 x 100 mm space in the middle. The surface of each plate was lubricated to allow the container to follow the shearing deformation of sand with minimum frictional resistance.

2.2.1.5 Dual Interface Testing Apparatus

A dual interface shear apparatus (simple or direct) was developed by Paikowsky et al. (1995) to evaluate the distribution and magnitude of friction between granular materials and solid inextensible surfaces. The apparatus was comprised of external reaction frame, shear box, instrumented friction bar, and pressure bags. The shear box consisted of two compartments separated by an instrumented friction bar. Two pairs of load cells were located in the front and rear sections of the bar for the measurement of load transformation along the interface. The shear box had a volume of 2540 cm^3 (L=400 mm,

W=125 mm, H=50.8 mm). The frames were aligned using four corner restraining pins. These pins remained in place when testing under direct shear conditions. For simple shear, these pins were removed prior to testing, allowing the frames to deform freely with the movement of the soil.

2.2.1.6 Three-Dimensional Interface Testing Apparatus

Fakharian and Evgin (1996) developed a computer controlled apparatus to study the behavior of three dimensional monotonic and cyclic loading conditions. The apparatus was capable to apply normal stress, σ_n, and two shear stresses, τ_x and τ_y. It had the capability for direct shear and simple shear testing in 3-D space. A reaction frame was designed to withstand a vertical or horizontal load up to 25 kN. The actuators used to apply the normal and tangential loads had capacities of 10 kN each. The soil was contained in a 25-mm thick hollow aluminum box, with inside area of 100 mm x 100 mm. The sand was deposited by using a multiple-sieving-pulviation method. The sand surface was leveled off by means of a vacuum so that the initial height of the sample was 20 mm. First the interface was sheared in one tangential direction up to a shear stress level less than the peak value. Then, the interface was sheared in a perpendicular direction, while the shear stress in the previous direction was maintained at a constant level. Fakharian and Evgin (1996) reported that shear stress and shear displacement increments experienced different paths, while the resultant shear stress-shear displacement curves remained the same irrespective of stress paths. Evgin and Fakharian (1996) also showed that both the direct shear box and simple shear box produced the same peak and residual shear strengths.

2.2.2 Constant Volume and Constant Normal Stiffness Testing of Interface

The stiffness of the surrounding soil (or rock), in the direction normal to the interface plane is usually denoted by K and is defined as the ratio of variations of normal stress to the variations of the normal displacement (compression or dilation), i.e., $K = d\sigma/dv$.

Constant normal stiffness tests in the laboratory have been performed by a number of researchers. However, the majority of the available results are from investigations of the mechanical properties of rock joints (e.g., Leichnitz 1985, Saeb and Amade 1992). Boulon and Plytas (1986) developed a direct shear type device to investigate the behavior of interfaces under constant volume and constant normal stiffness test conditions. The results were used for the numerical modeling of the behavior of a tension pile in sand.

In most of the available interface devices a simply supported reaction beam provides the constant normal stiffness condition. The desired stiffness may be achieved by varying the span or moment of inertia of the beam. Leichnitz (1985) described a computer controlled direct shear device capable of applying constant normal stiffness for investigation of rock discontinuities. A servo valve and a hydraulic jack were used for simulation of the constant normal stiffness condition.

2.2.3 Typical Test Results

Depending on the application requirements, either shear strength parameters or stress-displacement relations of the interface might be of interest. Shear strength parameters include adhesion denoted by $c_{a,}$ and angle of internal friction between soil and structural material, denoted by δ. The parameters are normally required for stability investigation of practical engineering problems such as retaining walls, foundations, and piles. However,

for rigorous and realistic analysis of soil-structure systems, the stress-displacement relations are essential.

Coulomb's law of friction has been widely used in physics and engineering and is stated as,

$$f = \mu N \qquad (2.15)$$

where:

f = tangential or frictional force required to induce relative displacement at the contact surface,

μ = the coefficient of friction, and

N = normal load between the two materials.

The adhesion between soil and plate is neglected in Equation 2.15. Assuming that the angle of friction between the steel plate and soil is δ, and adhesion between soil and steel plate is c_a, shear stress at failure, τ_f, under normal stress, σ_n, is given by,

$$\tau_f = c_a + (\sigma_n)_f \tan\delta \qquad (2.16)$$

The Mohr-Coulomb failure criterion for an interface is represented in Fig. 2.4 in which δ is the slope of the failure envelope and c_a is the intercept between the failure envelope and the τ axis.

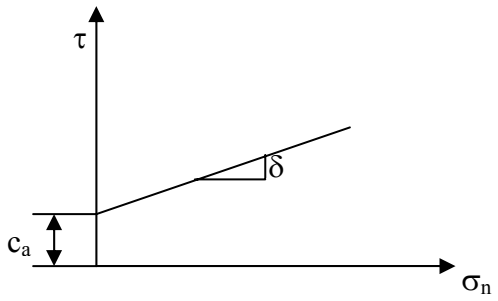

Figure 2.4: Mohr-Coulomb failure criterion

Parameters influencing the shear strength of the interface under the conditions of constant normal stress and monotonic shearing are as follows (Potyondy 1961, Fakharian 1996):

1) type of surface material (steel, concrete, wood, etc.),

2) roughness of surface (smooth, rough, medium),

3) composition of soil (sand, clay, mixture),

4) void ratio of soil,

5) grain size distribution of soil,

6) moisture content of soil,

7) magnitude of normal stress, and

8) rate of shearing.

Based on a series of tests between different type of soils (sand and clay) and construction materials, Potyondy (1961) found that four major factors determine the skin friction: the moisture content off soil, the roughness of the surface, the composition of soil, and the magnitude of the normal load.

Based on a series of tests by direct shear device, Acar et al (1982) concluded that relative density of sand and normal stress influence the angle of friction between sand

and structural materials such as steel, wood, and concrete. Angle of friction was high for low normal stress and high relative densities.

By employing an annular shear type device, Brummund and Leonards (1973) found that the coefficient of friction increases with the surface roughness and angularity of the sand grains. They also found that in the case of unlubricated surfaces, the dynamic coefficient of friction is about 20 percent greater than the static coefficient. The importance of the influence of the surface roughness on the frictional resistance was also pointed out by Yoshimi and Kishida (1981) and Kishida and Uesugi (1987).

2.2.4 Stress-Displacement Relationships

Four parameters are determined from measurement during an interface test, i.e. normal stress, σ_n, shear stress, τ, volume change or normal displacement, v, and shear displacement, u. For the common case of constant normal stress, change in shear stress and normal displacement are usually plotted versus shear displacement.

Yoshimi and Kishida (1981) reported some test results between steel and Tonegawa sand. A ring torsion apparatus was used in these experiments. Uesugi and Kishida (1986) reported similar results for the interfaces between steel and Toyoura sand, obtained from a simple shear type device. The results from both test sets indicate that the surface roughness significantly influences the peak and residual shear strengths. A more pronounced peak is observed for rough surfaces followed by strain softening until the shear stress levels off at the residual shear strength.

Volume change (or normal displacement) results indicated some initial compression for smooth surfaces followed by no volume change, whereas rough surfaces exhibited a substantial dilation after the initial compression.

Evgin and Fakharian (1996) conducted tests on an interface between quartz sand and rough steel plate. Based on the experimental results they concluded that the magnitude of the resultant peak stress ratio, $(\tau/\sigma_n)_p$ and residual stress ratio, $(\tau/\sigma_n)_r$ were independent of the stress path. They proposed that variation in the peak coefficient of friction due to normal stress may be assumed insignificant for practical purposes. However, Evgin and Fakharian (1996) found that stress paths significantly influenced the shear stress-tangential displacement and volume change behavior of interfaces.

Paikowsky et al. (1995) concluded that grain shape and the surface roughness, quantified with respect to the grain size, were the primary factors controlling the interface shear strength at a given normal stress.

2.2.5 Constitutive Models for Interface Behavior

2.2.5.1 Mohr-Coulomb Type Models

The Mohr-Coulomb failure criterion can be applied to interfaces in a manner similar to soils. The shear behavior of the interface before failure is considered as rigid (Fig.2.5a) or elastic (Fig. 2.5b) for practical applications. This is the simplest, yet frequently used model for behavior of interfaces.

The rigid-plastic model does not account for shear and normal displacements before failure or slip occurs. The elastic-perfectly plastic models consider the shear displacement, but not the non-recoverable (plastic) deformations before failure. Both models are poor in terms of modeling the normal displacement and post peak behavior of interfaces. The major advantage of such models is simplicity and applicability to some

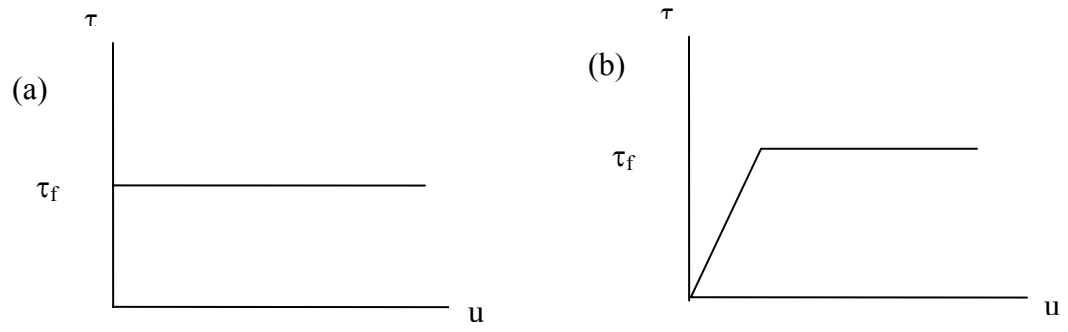

Figure 2.5: Perfectly plastic models (a) Rigid perfectly plastic (b) Elastic-perfectly plastic

conditions like those without hardening effects. But they are not suitable for granular materials in which work hardening, non-recoverable displacements before failure, non-linearity, and post-peak softening are common.

2.2.5.2 Nonlinear Elastic Models

In order to account for the nonlinearity involved in interface behavior, nonlinear elastic models have been used for interface modeling. The hyperbolic simulation is a common practice both in soil and interface modeling. Ramberg and Osgood (1943) proposed a curve fitting procedure for description of stress-strain curves by three parameters. Streeter et al. (1974) used the Ramberg-Osgood model for defining cyclic behavior of soils, and Idriss et al. (1978) used it for cohesive soils. Drumm and Desai (1986) described sand-concrete interface response, subjected to cyclic loading, using a modified form of Ramberg-Osgood model. The Ramberg-Osgood model simulates the interface behavior as piecewise nonlinear elastic. Although unloading and loading are included, inelastic deformations are not included in the sense of the theory of plasticity. The model also lacks the ability of considering the normal displacements at the contact surface.

The nonlinear elastic model developed by Clough and Duncan (1971) has been used widely in the analysis of soil structure interaction problems. The hyperbolic relationship of shear strength and relative displacement is obtained from the interface direct shear test. There are five parameters in this model. The model is not capable to capture the dilatancy behavior of an interface, which is the phenomenon consistently observed in a dense sand-structure interface.

2.2.5.3 Direction Type Models

A direction dependent constitutive relation was proposed by Boulon and Plytas (1986). This 2-D model was developed on the basis of the experimental results from the direct shear tests with constant normal stress or constant volume testing conditions. A path dependent interpolation rule was applied and the incremental shear and normal stresses of the interface were related to the incremental shear and normal displacements. This model has been employed for the analysis of soil-structure interaction problems such as axially loaded piles by Boulon and Plytas (1986).

2.2.5.4 Elastoplastic Based Models

Except for the direction type model as explained above, the other constitutive models described previously for interface behavior disregard the normal response of the interface, thus ignoring the coupling effects of shear and normal displacements. In order to account for the coupling between normal and shear behavior and also establish a meaningful framework for the behavior of the interfaces, the concept of theory of plasticity has been applied. One of the earliest attempts towards application of the theory of plasticity for interface modeling was made by Ghaboussi and Wilson (1973). An elastoplastic model was developed by Desai and Fishman (1991) for hardening behavior

of rock joints with associative and non-associative flow rules. The basic formulation of this model was the same as the one used for frictional materials by Desai (1980), Desai and Faruque (1984), and Desai et al. (1986). The same model was modified by Navayogarajah (1990) and Navayogarajah et al. (1992) for monotonic and cyclic behavior of interfaces between sand-steel and sand-concrete. Desai et al. (1984), Zaman et al. (1984), and Zaman (1982) proposed a model for joints and interfaces under dynamic loading. Boulon and Nova (1990) also applied an elastoplastic model for interfaces between dry sand and rough surfaces.

Ghionna and Mortara (2002) proposed an elastoplastic model for sand interface behavior. The model was based on the assumption that the interface can be thought of as a bidimensional (zero thickness) continuum, and had been formulated in terms of interface stresses and relative displacement. They back predicted the test results obtained from a constant normal stiffness apparatus. However, the model parameters were determined from constant normal load direct shear tests.

Zeghal and Edil (2002) presented an elastoplastic Mohr-Coulomb isochoric interface model utilizing the work hardening and nonassociative plasticity rules. They incorporated the effect of grain crushing that occurred in the interface zone. They pointed out that grain crushing played an important role in the behavior of the interface. Zeghal and Edil (2002) back predicted results of shaft-sand interface pull out tests in a satisfactory manner.

Hu and Pu (2004) performed sand-steel interface tests to obtain the stress-strain relationship. They used a charged-coupled-device camera to observe sand particles movements near the interface. They found two different failure modes during interface

shearing. An elastic perfectly plastic failure mode occurred along the smooth interface, while strain localization occurred in a rough interface accompanied by strain-softening and bulk dilatancy. Hu and Pu (2004) developed a damage constitutive model with ten model parameters based on the disturbed state concept theory. Back predicted results from this model were compared with the direct and simple shear test results. They incorporated this model into a Finite Element Model to solve soil-structure interaction problems.

2.3 SUMMARY OF LITERATURE REVIEW

Based on the literature review the following conclusions can be made:

1) Primary factors influencing the behavior of a given interface are particle angularity and size, surface roughness, void ratio, and water content.
2) Direct shear, simple shear, annular shear, and torsional shear type devices can be used to test the interfaces between soil and construction materials.
3) Behavior of unsaturated soil can not be described using the traditional single effective stress variable for saturated soils.
4) Two stress state variables, net normal stress (σ_n-u_a) and suction (u_a-u_w) can be used to describe the behavior of unsaturated soil.
5) Extended Mohr-Coulomb failure criterion can be used to describe the variation of shear strength of unsaturated soil with net normal stress and suction.
6) Elastoplastic type constitutive models are capable of capturing the main features of interfaces.
7) Cam Clay type models (e.g. Alonso et al.1990) can be used to simulate the behavior of unsaturated soils.

8) Disturbed state concept can also be used to model the behavior of unsaturated soils.

9) Conventional soil testing devices (e.g., Triaxial, Direct shear, Oedometer) have been modified to test the unsaturated soil.

10) Axis translation technique can be used to apply and maintain matric suction up to about 1500 kPa.

The foregoing review of literature also shows that, so far, regarding the behavior of interfaces between unsaturated soil and construction materials data are lacking in reported literature. The purpose of this research was to study the behavior of unsaturated interfaces. To fulfill this purpose, the existing techniques for unsaturated soil and interface testing were used with additional modifications. For example the conventional direct shear apparatus is modified following the procedure reported by Gan et al. (1988). However, as opposed to the Gan et al. (1988) device, the device developed in this study is capable of testing unsaturated soil as well as interfaces between unsaturated soil and steel plates of varying roughness.

The literature review reveals that a great deal of work has been done in the field of constitutive modeling of interfaces between soil and construction materials. However, constitutive models developed so far deal with the dry soil or saturated soil. As opposed to the existing constitutive models, the model developed in this study describes the behavior of unsaturated interfaces using two stress state variables (i.e., net normal stress and matric suction). Therefore the constitutive model reported in this study is general in the sense that it can be used to model the behavior of interfaces in dry and saturated soils as well as in unsaturated soils.

CHAPTER III

DESCRIPTION OF UNSATURATED INTERFACE DIRECT SHEAR APPARATUS

A new apparatus for testing an interface between unsaturated soil and steel was developed. The Unsaturated Interface Direct Shear Apparatus (UIDSA) has several new features compared with other available devices for interface testing such as:

- Capability to apply and maintain suction (u_a-u_w) via axis translation,
- Capability to apply and maintain net normal stress (σ_n-u_a), and
- Provisions to conduct constant suction and constant water content tests for unsaturated soil and interfaces.

A photograph of the apparatus and cross section view of the test chamber are shown in Figs. 3.1 and 3.2, respectively. The description of UIDSA is presented in the following sections.

3.1 THE BASIC DIRECT SHEAR TESTING DEVICE (WITHOUT MODIFICATIONS)

A commercially available direct shear device that can be used to perform direct shear and residual shear testing was obtained from Geocomp Corporation. It uses feedback from transducers to provide real-time control of loading. On the basis of the feedback information, the computer sends commands to the embedded controllers, which in turn generate signals to run stepper motors (vertical and horizontal). The basic device consists of a shear box to retain the sample, two loading mechanisms for horizontal and vertical

motions, four sensors (two load cells and two displacement transducers), two micro-processors (vertical and horizontal motions) for test control and data acquisition, and a PC with windows-NT compatible software to setup the test conditions and reduce the test results. The load frame contains the components that generate and measure the vertical and horizontal forces. Figure 3.3 shows the basic (unmodified) shear device.

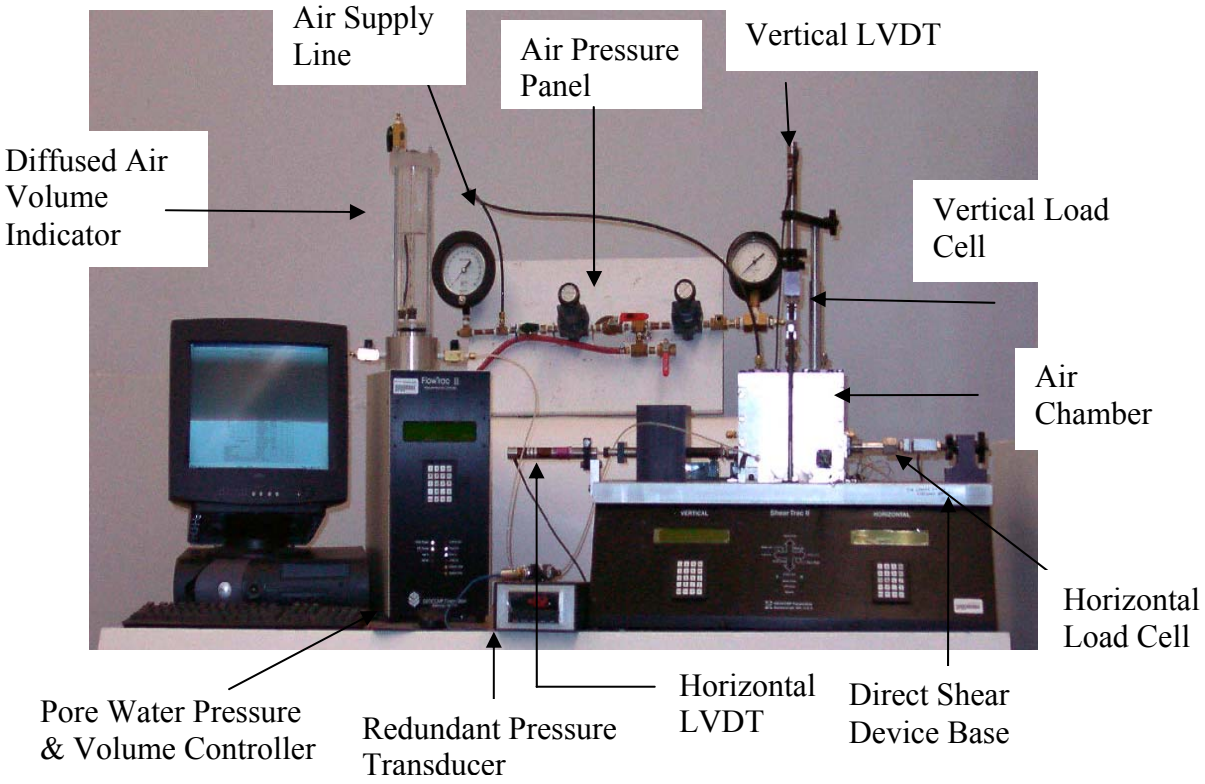

Figure 3.1: Modified Direct Shear Device

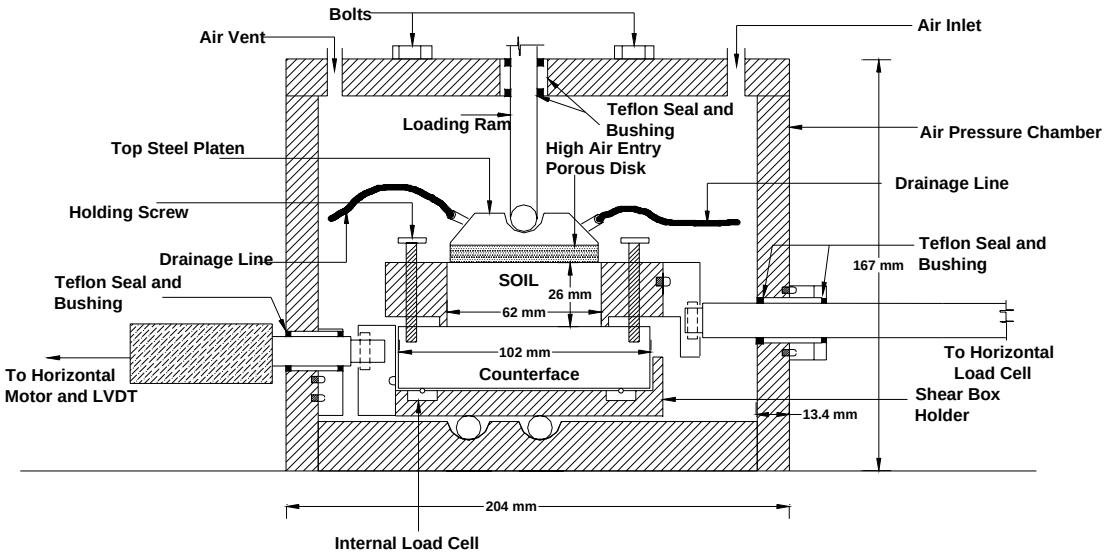

Figure 3.2: Cut Away Cross-Section View of the Air Chamber, Shear Box Holder, and Shear Box (smooth counterface shown)

Figure 3.3: Unmodified Direct Shear Device

3.2 MODIFICATIONS TO THE EXISTING EQUIPMENT

The basic device was modified to test the unsaturated soil and interface. Major modifications included: 1) relocation of the horizontal Linear Variable Differential Transformer (LVDT), 2) addition of an air pressure chamber, 3) construction of testing cells for holding soil and counterface, 4) addition of a stepper motor pump to control the pore water volume and pressure, 5) installation of plumbing for drainage lines, 6) addition of high air entry porous stones, 7) addition of a Diffused Air Volume Indicator (DAVI), and 8) internal load cells.

3.2.1 Relocation of Horizontal LVDT

In the unmodified direct shear device the horizontal displacement is measured by a Linear Variable Differential Transformer (LVDT) that is located in front of the shear box holder. However, to accommodate the air pressure chamber in the modified direct shear device the horizontal LVDT was relocated to the back of the horizontal stepper motor as shown in Fig. 3.1. In the modified device the horizontal displacement transducer is directly in contact with the drive shaft of the horizontal stepper motor.

3.2.2 Shear Box Holder

In order to slide the lower half of the shear box (containing soil or counterface) with respect to the upper half, a shear box holder was designed, as shown in Fig. 3.4 and 3.5. This holder is 108 mm in diameter and 19 mm deep and slides on rollers provided in the base of the air pressure chamber, which is described in next section. Three recesses were made in the bottom of the holder in order to fix three miniature load cells.

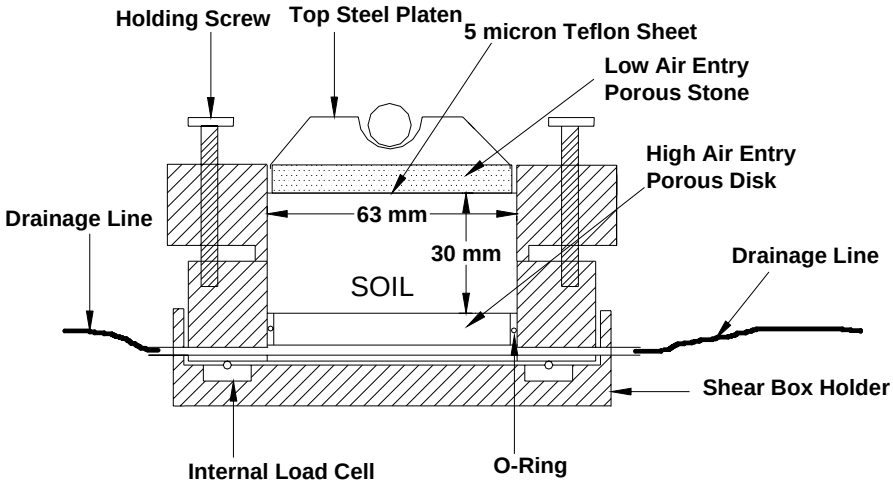

Figure 3.4: Cut Away Cross-Section View of the Soil Shear Box
(raising screws not shown)

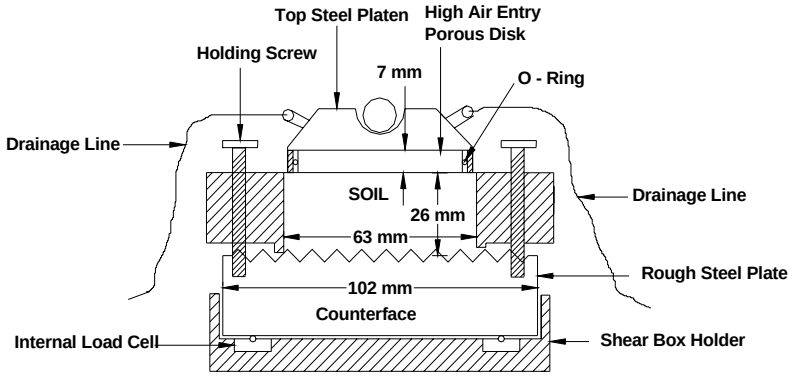

Figure 3.5: Cut Away Cross-Section View of the Interface Shear Box
(rough counterface shown)

3.2.3 Air Pressure Chamber

The interior space in the air pressure chamber is 178 mm long and 152 mm wide, as depicted in Fig. 3.2. The sides and the top are Aluminum with wall thickness of 13 mm. The top of the air pressure chamber has two air ports, one for applying the air pressure and a second for venting. The lid has six holes, each aligned with one of the screws of the shear box. The shear ring has a total of six screws, two for holding the shear ring and counterface and four screws for raising the top half of the box. The two holding screws are removed and the gap between the box and the counterface is created before applying the air pressure but after the application of a normal load increment. The two holding screws were removed using a magnetic pick-up tool. After raising the upper half of the shear box, the six holes in the lid were closed with six bolts. Each bolt has an o-ring seal to avoid leakage of air. In order to pass the vertical loading piston, a hole equipped with a low friction air tight bushing was provided in the center of the lid of the air pressure chamber. The air pressure chamber has two holes in the vertical walls in order to pass through the rods of the horizontal stepper motor and horizontal load cell. These holes were also sealed with Teflon bushings.

3.2.4 High Air Entry Porous Disk (HAEPD)

The axis translation technique was used to control/apply the suction in the soil. To control the water pressure in the soil specimen a HAEPD was used. The HAEPD has very fine pores that allow water to pass through, but not air, provided that the air pressure is less than the air entry value of the HAEPD. The air entry value is the pressure at which air will break through a wetted pore channel. For unsaturated soil testing the HAEPD was fixed in the bottom half of the shear box (Fig. 3.4). The HAEPD was fixed in a metal

(Brass) ring and an o-ring was placed around the metal ring to fix it in the lower half of the shear box.

Soil samples were prepared in the direct shear box with the HAEPD in the lower half. For interface testing the HAEPD was fixed in the top platen and was placed on the top of the soil (Fig. 3.5). Before adopting the present location of the HAEPD for unsaturated interface testing, a high air entry porous ring was tried to control the pore water pressure. However, this shape of the high air entry disk did not work because the disk was not capable of holding the air pressure in the radial directions. It seems that the high air entry disk has different properties in vertical and radial direction.

3.2.5 Plumbing for Drainage Lines

To control the pore water pressure and pore air pressure for interface direct shear testing, two ports were provided in the top platen that holds the HAEPD as shown in Fig. 3.5. One port is connected to the water pressure volume controller and the other port is connected to pore pressure transducer or diffused air volume indicator. During the flushing of air from the pore water control system this port can be connected to the diffused air volume indicator. The pore water pressure controller has the ability to precisely control the volume of water (i.e., within ±1 mm^3) or pore water pressure (i.e., within ±1 kPa). For unsaturated direct shear testing of soil the ports are provided in the lower half of the direct shear box as shown in Fig. 3.4.

All drainage lines consist of 3-mm diameter high pressure Polyvinylidene Flouride (PVDF) tubing with a wall thickness of 0.8 mm.

3.2.6 Addition of Diffused Air Volume Indicator (DAVI)

Pore air diffuses through water if the axis translation technique is used for a long time. In this study axis translation technique was used to apply/control the suction in the soil. The DAVI was used for collecting accumulated air flushed from the back of the HAEPD. The function of the DAVI is explained in detail by Fredlund and Rahardjo (1993). After every twenty four hours, air was flushed into the DAVI from the back of the HAEPD. During the flushing of air, the pore water pressure is dropped momentarily but as the drainage line is closed the volume/pressure controller quickly brings the pressure back to the target value. The volume of water moving in or out of the specimen was corrected for the volume of water drained during the flushing. It is important to mention that air pressure used during testing (70 and 120 kPa) was considerably lower than the air entry value of HAEPD (300 kPa). Therefore, little to no measurable air volume diffused into the water volume measuring system for a typical test duration, which ranged from 3 to 5 days.

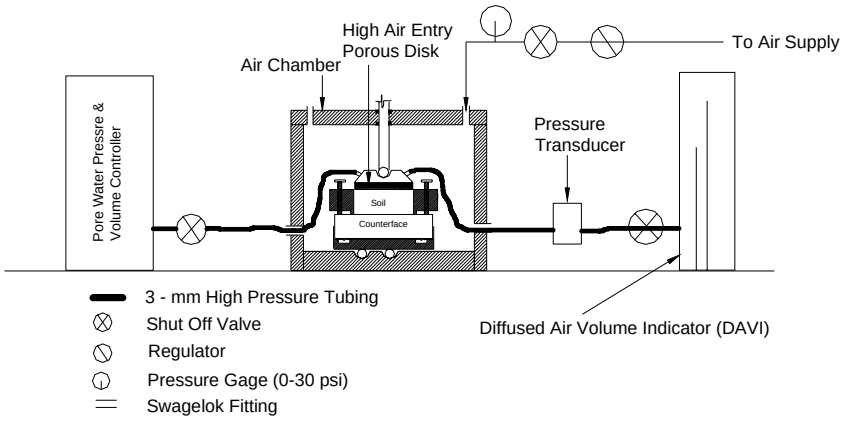

Figure 3.6: Schematic of Plumbing Arrangement for the Unsaturated Interface Direct Shear Device (Not to Scale)

3.3 CONSTRUCTION OF SHEAR BOX

3.3.1 For Unsaturated Soil Testing

The shear box consists of two halves made of stainless steel. Two screws hold these halves together. The bottom half has a high air entry porous disk with the two drainage connections, one for sending water and the other for flushing water and/or air (see Fig. 3.4). A soil sample is prepared in the shear box, which is held together by the two screws. The soil sample is 30 mm thick and 63 mm in diameter. The shear box is placed in the shear box holder over the miniature load cells and the shear box holder slides over the rollers, while the upper half of the box is fixed to the horizontal load cell shaft.

3.3.2 For Unsaturated Interface Testing

The interface shear box consists of one circular stainless steel shear ring (top half of the soil box) and counterface. Two screws hold the shear ring and counterface together. The thickness of the soil specimen in the shear ring is approximately 25 mm. After preparing the sample in the interface shear box the top loading platen with the high air entry porous disk is placed on top of the soil sample. The top loading platen was modified to hold the HAEPD (see Fig. 3.5). Two quick connecters were provided for the drainage lines, one for sending water and a second for flushing water and/or air. The interface shear box is placed in the shear box holder, over the miniature load cells. The holder, containing the counterface slides over the rollers and the upper shear ring is restrained.

The rod from the horizontal stepper motor pushes the holder, which in turn shears the soil/interface. The rod attached to the horizontal load cell restrains the top half of the

shear box. Before starting shearing, the two screws holding the shear box together are removed and the gap between the two halves of the shear box or between the shear ring and the counterface is created by raising the upper half of the box using the four screws. After creating the gap of approximately 0.6 mm, which is in the range of 10 to 20 times the D_{50} diameter of test soil (Minco Silt has D_{50}=0.05 mm), the four screws were backed off to eliminate contact with the counterface. In this way there was no contact between the metal of the upper half and the bottom half of the box or the counterface.

CHAPTER IV

TESTING PROCEDURE

This chapter describes the materials used for this study, specimen preparation and placement procedures. In addition, the calibration and performance testing is described.

4.1 INTERFACE MATERIALS

4.1.1 Soil

Soil and interface tests were performed using a locally available soil in central Oklahoma known as Minco silt. The Minco silt had a liquid limit, LL= 28 %, plasticity index, PI=8 % and 73 % fines. From a standard compaction test, the maximum dry unit weight was 17.7 kN/m^3 and optimum water content was 12.8 %. The specific gravity of soil solids was 2.68. The specimens were compacted to an initial dry density of 15.7 kN/m^3 at a moisture content of 20 $\pm$ 1%, giving a degree of saturation approximately 83%. According to Unified Soil Classification System this soil is classified as low plastic clay (CL). Minco silt was selected for this study due to availability, low plasticity and low air entry value of this soil. Low air entry value soils begin to desaturate at lower suction values than the high air entry value soils such as highly plastic clays.

4.1.2 Counterface

Two stainless steel plates (counterfaces) were prepared for this study. One steel plate was 25.5 mm thick and 102 mm in diameter with rough surface geometry as shown in Fig. 4.1. Another steel plate with polished surface was prepared with the same dimensions as the rough steel plate. Surface roughness is defined based on the roughness

profile. The maximum peak to valley height, R_{max}, for rough steel plate was 0.38 mm. Based on the literature review (ASME B46.1-1995), a value of 0.0025 mm was used as a peak to valley height for smooth steel plate. Normalized surface roughness as proposed by Uesugi and Kishida (1987) is defined as

$$R_n = R_{\max} / D_{50} \qquad (4.1)$$

where D_{50} is the grain size diameter corresponding to fifty percent finer. Based on the grain size analysis of Minco Silt, R_n= 7.6 and 0.05 was calculated for rough and smooth steel plates, respectively.

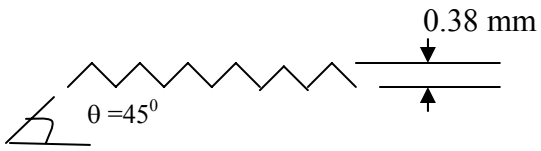

Figure 4.1: Surface geometry of rough steel plate

4.2 SAMPLE PREPARATION

The interface direct shear box is assembled by placing the upper half of the shear box on the counterface. Two screws are used to hold the counterface against the upper half of the shear box. Soil was mixed to the desired water content and stored in a humid chamber for 24 hours. After 24 hours the soil was compacted in the shear box to the required density. The compaction was done by using a tamping rod in two layers. It is important to mention that in this study all the samples were prepared at nominally the same initial moisture content and density.

4.3 SATUARTION OF HIGH AIR ENTRY POROUS DISK (HAEPD)

Prior to placing soil the HAEPD was saturated by connecting the entry port to the pore water pressure/volume controller. During saturation the water pressure was maintained at 4 kPa. Low water pressure was selected to avoid cracking of the high air entry disc and also prevent popping the disk out of the platen. Saturation was considered completed when water flooded the top surface of the disk. During the saturation process the exit port remained closed. Adequate saturation of the HAEPD took approximately 48 hours. The HAEPD used in this study had and air entry value of 300 kPa (3 bar).

To check the validity of the above mentioned saturation procedure the saturated water coefficient of permeability (k_d) of the HAEPD was determined and compared with those reported in the literature. Figure 4.2 shows the amount of water flowed through the HAEPD with respect to time during the saturation process under 4 kPa water pressure. As shown in Fig. 4.2, the hydraulic conductivity, k_d increased with time and became constant after about 2500 minutes, which corresponds to approximately 4.9 pore volumes of water passing through the stone. The hydraulic conductivity after 2500 minutes appears to be the saturated k_d value. This was verified by measuring k_d under different hydraulic gradients.

To determine k_d under different gradients, water was placed on the HAEPD and enclosed in an air tight chamber. An air pressure was then applied to the water and the amount of water flowing through the HAEPD was measured using the water volume controller.

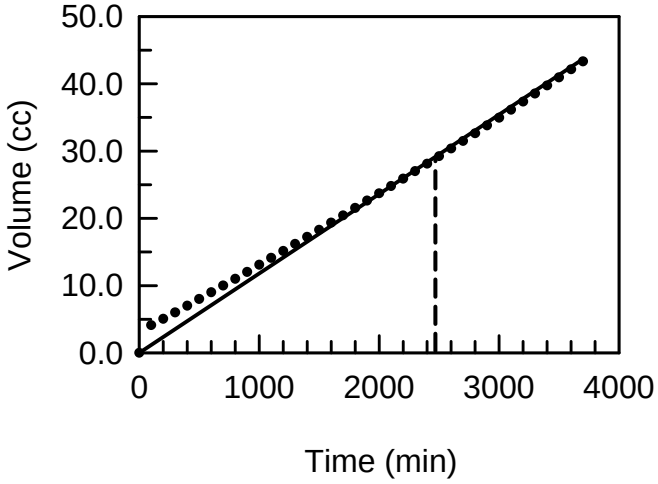

Figure 4.2: Flow of water through HAEPD; $u_a = 0$ kPa, $u_w = 4$ kPa

The water coefficients of permeability (k_d) calculated at different gradients are shown in Table 4.1 and plotted in Fig. 4.3. The values of k_d shown in Table 4.1 are approximately the same regardless of the gradient, which indicates the saturation method used in this study was satisfactory. Fredlund and Rahardjo (1993) have reported a value of 1.73×10^{-9} m/sec for k_d for a HAEPD similar to that used in this study.

4.4 ASSEMBLING OF SHEAR BOX IN THE AIR PRESSURE CHAMBER

The interface shear box, with the counterface and soil, is placed in the shear box holder in the air pressure chamber over the three miniature load cells. The drainage line from the pressure/volume controller is connected to the inlet port of HAEPD in the top platen. Outlet port is connected to the DAVI and the high air entry disk embedded in the top platen is placed on the top of the soil sample. A spherical steel ball is placed over the top platen and the air pressure chamber is closed with the lid. A gasket with vacuum grease

Table 4.1: Values of the water coefficients of permeability (k_d)

u_a kPa	u_w kPa	Hydraulic Gradient	k_d m/sec
0	4	41	1.40e-9*
0	5	51	1.40e-9
35	31	41	1.26e-9
55.2	31	247	1.22e-9
76	31	459	1.24e-9
96.6	31	669	1.27e-9
31	35	41	1.02e-9
117.3	14	1053	1.26e-9
117.3	14	1053	1.27e-9

* From the saturation procedure used during testing

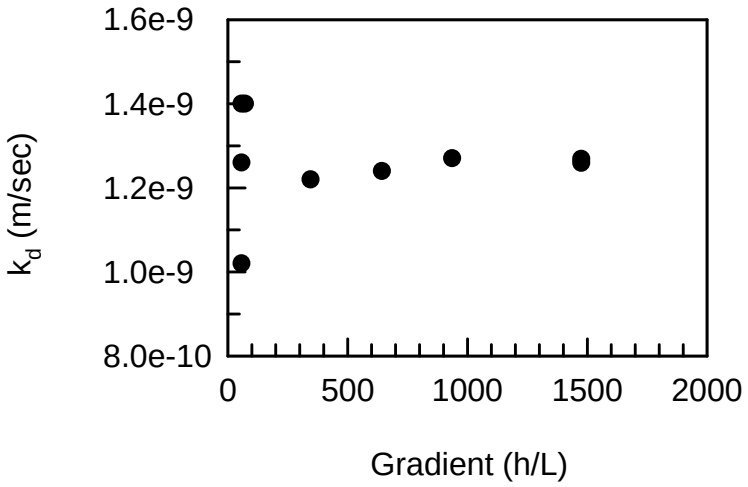

Figure 4.3: Variation of k_d with gradient

coating is placed on the air pressure chamber before placing the lid. The lid is tightened with twenty screws and the six access holes in the lid remain open until this stage. The vertical load piston is seated on the top platen ball inside the air pressure chamber and the horizontal load cell piston is tightened carefully such that no load is applied to the sample during this operation.

4.5 APPLICATION OF TARGET STATE OF STRESS

After closing the air chamber, a vertical load was applied and the specimen was allowed to consolidate under this vertical load. Vertical deformation was recorded during the consolidation procedure. Sixty minutes after applying the load, the two screws holding the upper half of the shear box and counterface (rough or smooth steel plate) were removed and brought out from the air pressure chamber using a magnetic pick-up tool. After removing the screws, the top half of the shear box was raised by turning the four raising screws, which were then backed off. The vertical load generated enough horizontal stress and shear force between the soil and box to hold the box in the raised position. In this way only soil was in contact with the counterface and there was no contact between the upper half of the shear box and the counterface. A gap of approximately 0.6 mm was created, which is in the range of 10 to 20 times the median diameter of Minco silt (D_{50} = 0.05 mm). The existence of the gap was verified at the end of each test using a small mirror with long handle. After raising the box the six access holes in the air chamber lid were sealed with bolts.

Target net normal stress (σ_n-u_a) was achieved by applying the vertical load and air pressure in stages. Vertical load was applied/increased in stages after the application of the corresponding air pressure. Once the net normal stress was achieved, target pore

water pressure (i.e., difference between the pore air pressure and the target suction) was applied to the specimen.

4.6 EQUALIZATION

Prior to shearing, each sample was allowed to equalize at the required net normal stress and suction. Equalization of the specimen was considered completed when there was no considerable change in the volume of water of the specimen. During equalization, change in volume of water and change in specimen height were recorded. A typical plot of change in water content against time during the equalization stage is shown in Fig. 4.4. Initially water flowed out at a higher rate and then gradually decreased. Initial portion of Fig 4.4a (marked as A-B) shows the movement of water at faster rate. Reaching Point B water movement slows down, which shows the equalization of the applied suction. After Point B very little water moved in or out to maintain the applied suction as is evident from the Region B-C of Fig. 4.4a

Figure 4.4b shows the change in specimen height, v, normalized with the initial specimen height (H_0), during the equalization process. During the equalization process the specimen response (Fig. 4.4b) was similar to the water movement through the specimen as shown in Fig 4.4a. As the water moved out (region A-B of Fig. 4.4a) the height of the specimen decreased (region A-B of Fig. 4.4b). The behavior of the specimen in response to the water movement during equalization indicates good saturation of HAEPD and excellent communication between the water volume controlling system and pore water. In each test water flowed out of the specimen so that the water content of the sample decreased during the equalization stage. As expected, the decrease in water content was greatest for tests where the applied suction was highest.

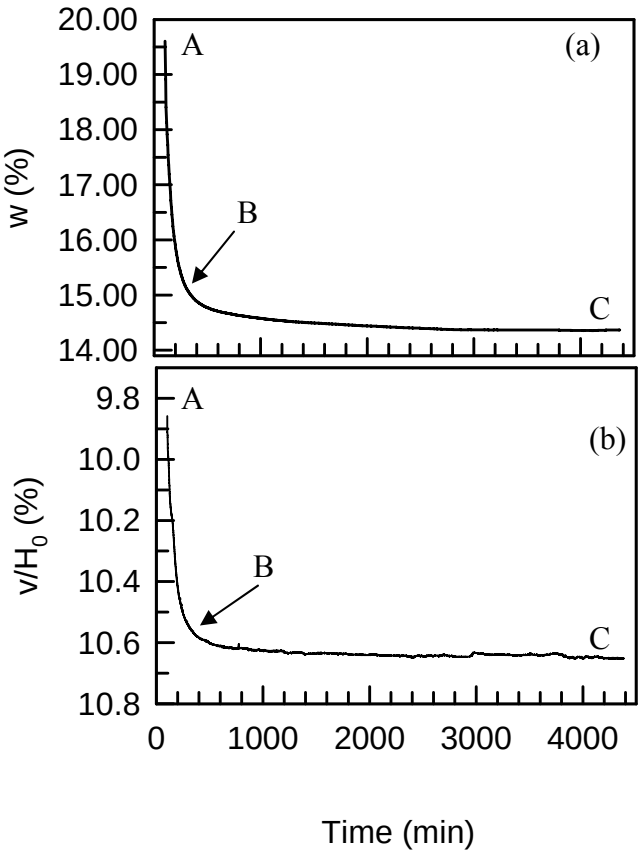

Figure 4.4: Typical (a) water content (w) and (b) vertical strain (v/H_0) during equalization (from the test of u_a-u_w = 100 kPa and σ_n-u_a = 105 kPa)

A separate specimen was prepared for each combination of suction and net normal stress used during the test program. During the application of target stresses, the approximate stress paths shown in Fig. 4.5 were adopted to achieve net normal stresses of 105, 140, and 210 kPa and suctions of 20, 50 and 100 kPa. The stress paths are shown approximately as vertical lines because the time for equalization of the matric suction was much greater than the time required to achieve a given net normal stress. The actual suction in the specimen is unknown until equalization is complete. Note that each symbol in Fig. 4.5 represents the final state of stress in a single specimen.

After equalization the specimen was subjected to the shearing load under constant suction and net normal stress. During shearing of the specimen, pore water pressure was kept constant and change in volume of water was recorded.

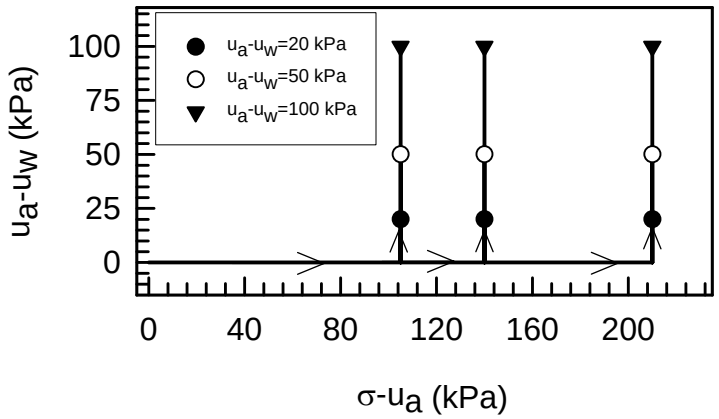

Figure 4.5: Approximate stress paths followed during application of target stresses Prior to shearing (each point represents the end of a stress path for different samples)

4.7 SHEARING

The interface was sheared up to a maximum displacement of 10 mm at a rate of 0.005 mm/min. Gan et al. (1988) reported that the value of peak shear stress of glacial till (LL = 35.5% and PI = 18.7%) was unaffected for a displacement rate less than 0.0132 mm/min. For Madrid clay (LL = 71% and PI = 35%) Escario (1980) and Escario and Saez (1986) used 0.0084 mm/min and 0.0017 mm/min displacement rate, respectively. Based on the literature review, a slow rate of shearing (i.e., 0.005 mm/min) was selected in this study to ensure drained conditions during shearing. Approximately 1% change in moisture content (w) occurred during shearing (in most of the interface tests change in w was less than 1%), which indicates that displacement rate was reasonably slow to ensure the drained conditions. However, further study is required to study the effects of displacement rate on the behavior of the soil used in this study. During shearing the horizontal load, horizontal displacement, and vertical displacement were measured and recorded, typically, at 1 minute intervals. All specimens were sheared under constant normal stress and constant suction conditions.

4.8 CALIBRATION AND PERFORMANCE TESTING

4.8.1 Calibration

All load cells and Linear Variable Differential Transformers (LVDTs) were provided with manufacturer's calibration data; however, calibrations were performed periodically in the OU Laboratory for verification. In addition, friction losses in the bushings were measured under different air pressures for corrections to vertical and horizontal loads. The 3-mm diameter, high pressure Polyvinylidene Flouride (PVDF) flexible tubing with a wall thickness of 0.8 mm was used for drainage lines to provide ease of assembly as

opposed to rigid lines. The tradeoff is that flexible tubing exhibits a small amount of compressibility that must be measured so water volume measurements can be corrected accordingly. Compressibility was determined by placing a plug on the end of the drainage system and incrementally applying pressure via the water pump. Pressure increments corresponded to the range of pressures used during testing and were maintained for a period of time corresponding to a typical test with soil. Corresponding volume changes were measured with time during application of pressure. The tubing expanded quickly with change in water pressure followed by a small amount of creep behavior as shown in Fig. 4.6. The change in water volume due to expansion of the tubing was found to be practically negligible relative to changes in water volumes during testing; nevertheless, a correction was applied to the water volume measurements to account for expansion of the tubing.

To further check the performance of the water volume measurement system, gravimetric moisture contents determined after each test by oven drying the sample were compared with moisture contents back-calculated from the volume change measurements and initial moisture contents. As shown in Fig. 4.7, the comparison is relatively good; with differences generally less than one percentage point on the water content scale. The differences are probably associated with uncertainty in the initial water content used in the back-calculation and errors associated with water loss during sample preparation and testing.

4.8.2 Performance of Stress Control System

To verify the performance of the suction and net normal stress control systems, various methods were employed. The following observations indicate that stresses were applied correctly.

1) As mentioned previously, the response of the soil specimen in terms of the vertical deformation was consistent with water volume changes during equalization under the target suction, as demonstrated in Fig. 4.4.
2) The water contents at the end of equalization decreased as the suction increased, consistent with the soil water characteristic behavior.
3) The moisture content achieved at the end of equalization was compared to similar tests performed in a suction-controlled oedometer. Gravimetric water contents obtained from each test were within one percentage point for the same suction. That the water content changes were similar suggests the suction was being controlled in similar fashion during each test. Furthermore, repeated direct shear and interface direct shear tests at the same suction resulted in similar moisture contents as shown in Fig. 4.7.
4) Null testing was performed whereby normal stress, pore water and pore air pressure were changed during equalization and shearing without changing the net normal stress or matric suction. If the presumption that net normal stress and matric suction control the soil behavior is correct, then changing the test variables (σ, u_a, u_w) should not influence the soil specimen if the stress variables (σ-u_a, u_a-u_w) are not changed.

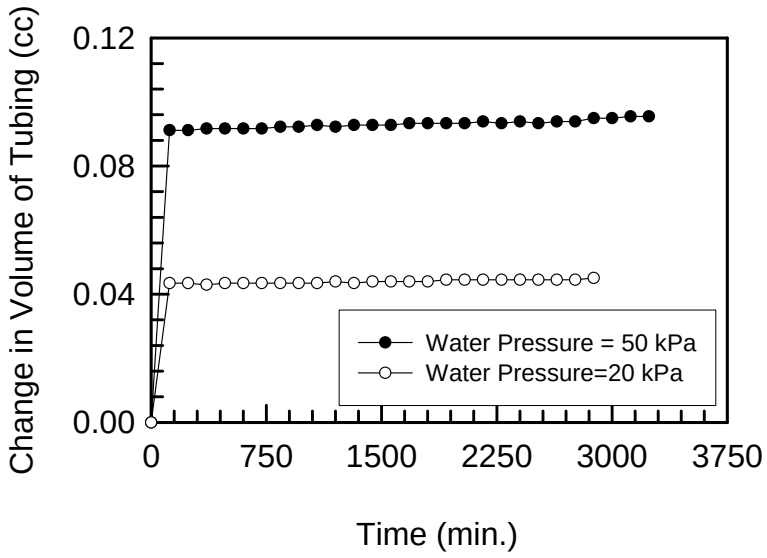

Figure 4.6: Volume Change of Tubing Versus Time After Application of Water Pressure

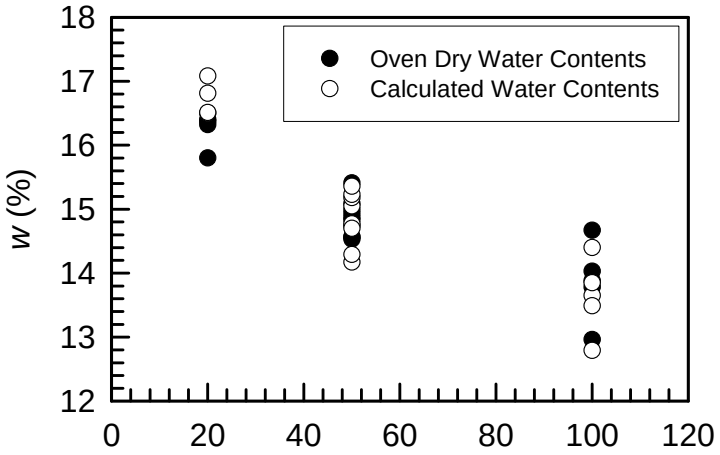

Figure 4.7: Oven dry moisture contents and those calculated using controller readings, initial moisture contents, and corrections for tubing expansion for all soil and interface Tests

In Figs. 4.8 and 4.9 the results of null testing during the equalization and shearing phases are presented. As shown, at the end of equalization the pore air and pore water pressures were increased by 21 kPa and there was virtually no response from the soil sample in terms of the vertical height or water volume change. The small amount of measured water volume change exhibited was due to the response of the pore water controller to the pressure increase signal. Toward the end of the shearing phase, pore air and pore water pressure were increased and again no appreciable change in soil response is indicated in Fig. 4.9. The small change in water content noted in Fig. 4.9c toward the end of shearing when the test variables were changed was caused by the response of the controller to the command to increase water pressure; however, the vertical deformation and shear responses were unaffected.

5) In Fig. 4.9, another test with similar values for the stress variables (σ-u_a, u_a-u_w) but different test variables (σ, u_a, u_w) is compared to the null test. The similar response of the two soil specimens demonstrates that the stress variables, and not the test variables, are controlling the soil behavior and that they are in fact similar between the two tests. Repeatability is further discussed in section 6.6 of Chapter VI.

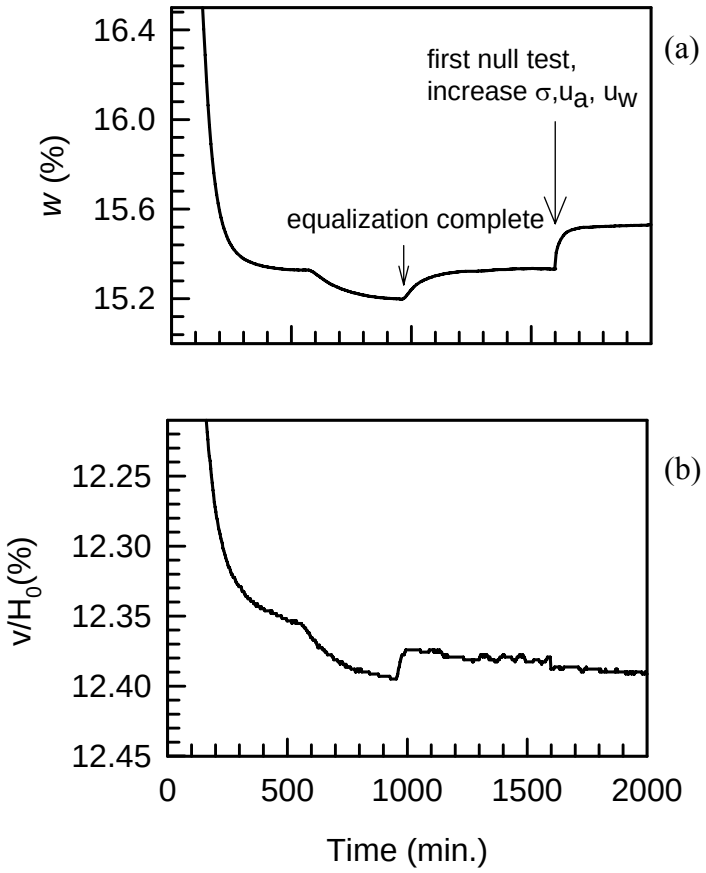

Figure 4.8: Typical (a) water content and (b) change in height during Equalization (from the null test data)

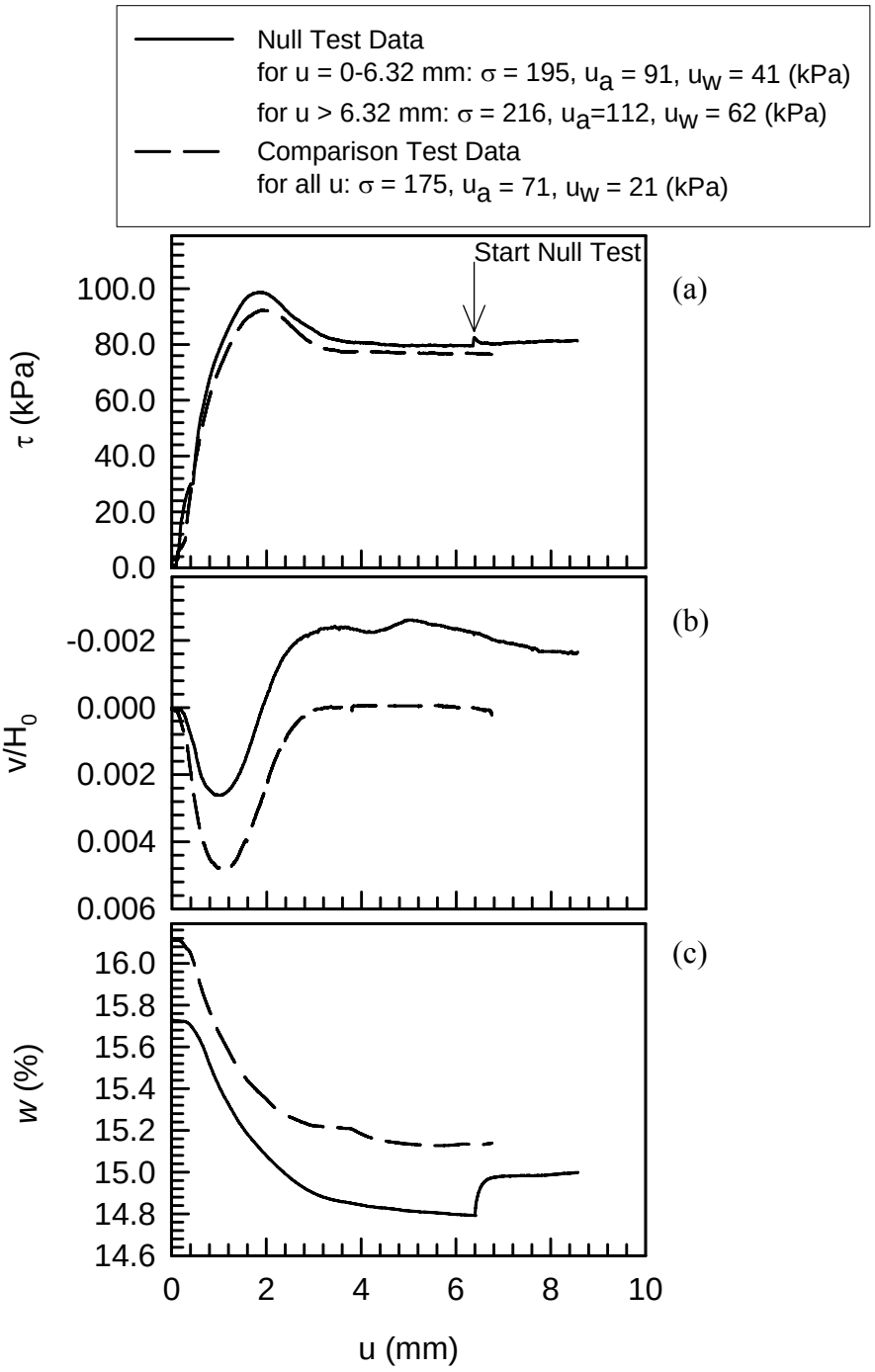

Figure 4.9: Results from shearing phase of two different tests on a rough interface with the same net normal stress and matric suction but different normal stress, pore air and pore water pressure: a) shear stress, b) vertical strain, c) water content

The null test results, and the comparison to a similar test with different test variables, but similar stress variables, suggest that the stress variables are being properly controlled. This deduction is reinforced by observations presented subsequently in the results section where it is seen that changing the stress variables has a profound influence on the soil and interface behavior.

CHAPTER V

DISCUSSION OF TEST RESULTS

5.1 INTRODUCTION

This chapter presents the results of soil and interface tests conducted under constant suction and constant net normal stress conditions in a modified direct shear box. Effects of net normal stress (σ_n-u_a), suction (u_a-u_w), and roughness on the stress-displacement and volumetric behavior of unsaturated soil and interfaces are discussed in this chapter.

5.2 EFFECT OF NET NORMAL STRESS

The effect of magnitude of net normal stress (105, 140, 155, 210 kPa) on the stress-displacement and volumetric behavior of soil and interfaces is presented in this section. Figs. 5.1-5.7 show the soil behavior, whereas Figs. 5.8-5.19 show the results of smooth and rough interface tests.

In all tests, depicted in Figs. 5.1 to 5.19, soil and interfaces were subjected to suction values of 20, 50, and 100 kPa. After equalization under the targeted state of stress, soil and interfaces were sheared to a maximum horizontal displacement of 10 mm. Horizontal displacement rate was 0.005 mm/min; normal displacement, shear stress, and horizontal displacement were recorded typically at 1.0 min intervals.

5.2.1 Effect of Net Normal Stress on Soil Behavior

5.2.1.1 Equalization Phase

Figures 5.1a, 5.3a, and 5.5a show plots of change in vertical displacement (normalized to specimen height) with time during the equalization phase. As expected, for a given suction the magnitude of compression increased with increase in net normal stress, most notably for u_a-u_w=20 kPa and 50 kPa (Fig. 5.1a, Fig. 5.3a). For u_a-u_w=100 kPa (Fig. 5.5a) similar vertical compression occurred under all three values of σ_n-u_a. Typically sixty five percent of total vertical displacement occurred under total normal stress that was applied before raising the box and before the application of target pore water pressure (u_w) and pore air pressure (u_a). Approximately 20% of total vertical displacement occurred during raising the upper half of the shear box. During the equalization process (under target σ_n-u_a and u_a-u_w) soil compressed only 20% of the total vertical displacement. These three phases of vertical displacement for a typical test are shown in Fig. 5.7.

In Fig. 5.5a, results of vertical displacement during the equalization process for u_a-u_w=100 kPa under different values of σ_n-u_a are presented. Initial moisture content for the sample tested under σ_n-u_a = 105 kPa was 21.2%, whereas for σ_n-u_a =155 kPa and σ_n-u_a = 210 kPa the initial moisture content was 20.7% and 20.2%. All three samples were subjected to the same initial vertical stress (i.e., 35 kPa). It was found that sample tested under σ_n-u_a = 105 kPa compressed approximately 22% of the total vertical compression during raising the upper half of the shear box. Samples tested under σ_n-u_a =155 kPa and σ_n-u_a = 210 kPa compressed 10% and 20 % of their total vertical displacement, respectively, during raising the upper half of the shear box. Vertical displacement at the

end of equalization was found as 3.49mm, 3.63mm, and 3.65mm for soil samples subjected to σ_n-u_a = 105 kPa, σ_n-u_a = 155 kPa, and σ_n-u_a = 210 kPa, respectively.

The similar vertical compression of the sample subjected to σ_n-u_a = 105 kPa to other two soil samples (tested under σ_n-u_a = 155 kPa and 210 kPa) can be attributed to the initial higher moisture content as compared to the other two samples.

For the soil sample tested under σ_n-u_a = 155 kPa, the target net normal stress was applied in six steps (each step size of 21 kPa) in 50 minutes, whereas for soil sample subjected to σ_n-u_a = 210 kPa, the target net normal stress was applied in five steps (each step size was 35 kPa) in 16 minutes. The similar vertical displacements for different net normal stresses (different displacements were expected) may be partly attributed to differences in the method of applying target net normal stress. Based on this observation, the method of applying net normal stress was revised and remaining tests were performed using an equal step size for a given net normal stress. However, further study is required to investigate the effect of different stress paths on the volume change behavior of unsaturated soil during equalization in a direct shear test.

Variation in volume of water (normalized by total volume of sample) for soil samples during equalization is shown in Figs. 5.1b, 5.3b, and 5.5b. As opposed to Figs. 5.1b and 5.3b, in Fig. 5.5b the lines for all net normal stresses fall in a close band, which indicates that the difference in initial moisture content of these samples was not significant and water volume controller pulled approximately the same amount of water from all three samples to maintain the required suction (i.e. 100 kPa).

Soil test for u_a-u_w = 20 kPa at σ_n-u_a = 105 kPa (solid line in Fig. 5.1b) was performed without using a Teflon membrane and a moist coarse porous stone was in direct contact with soil. During equalization the water volume controller pulled water from soil as well as from the coarse porous stone. Volume of water pulled by the water volume controller is not corrected for the water contributed by the coarse stone. Therefore, in Fig. 5.1b the plot for u_a-u_w = 20 kPa at σ_n-u_a = 105 kPa (illustrated by solid line) shows a higher amount of drained water than the other two samples, which were tested by using the hydrophobic Teflon membrane between soil and coarse porous stone.

Test results for 50 kPa suction (Fig.5.3b) at net normal stresses of 105 and 140 kPa were conducted without the Teflon membrane as well, and the volume of water pulled by the controller is different for each test. This difference is attributed to the use of the moist porous stone, which possibly contributed a different amount of water in each test. In addition, there was a difference in initial water content of two samples (solid and dash line in Fig. 5.3b). Initial moisture contents were 19.3% and 20.5 % for tests under σ_n-u_a =105 kPa and σ_n-u_a =140 kPa, respectively. Therefore, the amount of water pulled by the controller is larger for 140 kPa net normal stress than the test performed at σ_n-u_a = 105 kPa.

5.2.1.2 Shearing Phase

Shear strength of soil increased with increase in net normal stress for a given suction value as shown in Figs. 5.2a, 5.4a, 5.6a. Strain softening behavior became pronounced with increase in net normal stress for the suction (u_a-u_w) values of 50 kPa and 100 kPa (Figs. 5.4a and 5.6a), whereas samples tested at 20 kPa suction did not show the strain

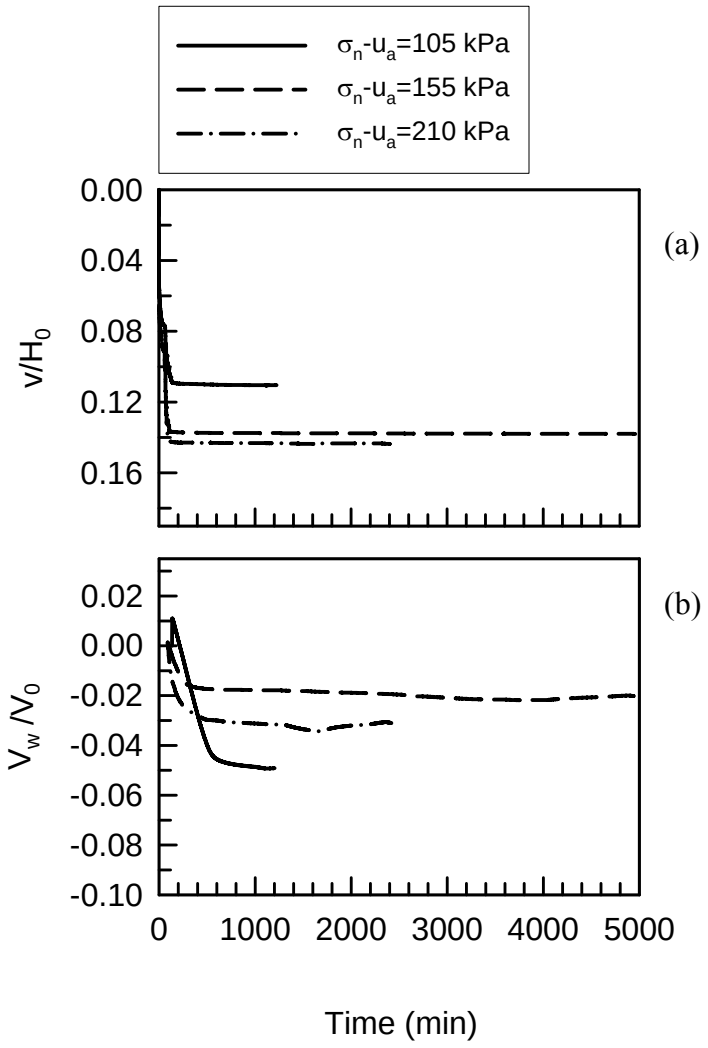

Figure 5.1: Effect of σ_n-u_a on (a) v/H_0, and (b) V_w/V_0 during equalization for soil. (u_a-u_w = 20 kPa)

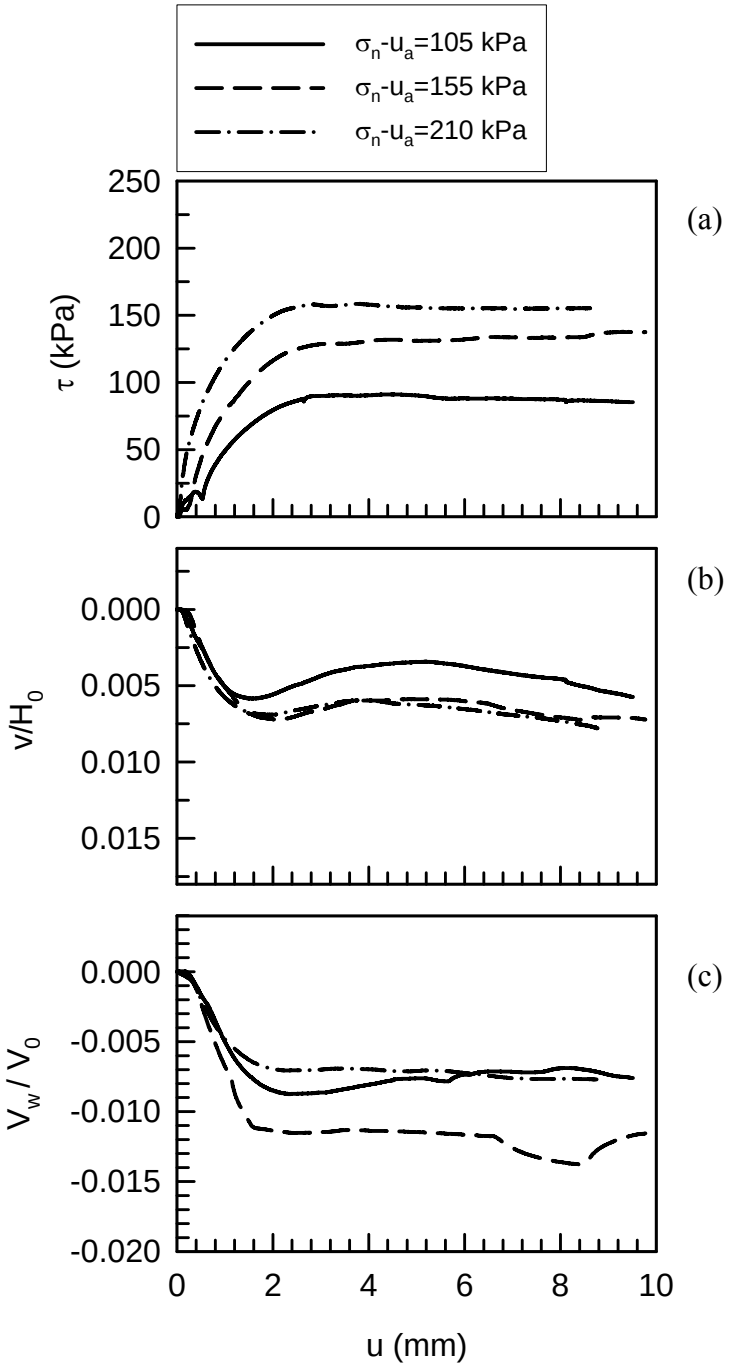

Figure 5.2: Effect of σ_n-u_a on (a) τ, (b) v/H_0, and (c) V_w/V_0 during shearing for soil. (u_a-u_w = 20 kPa)

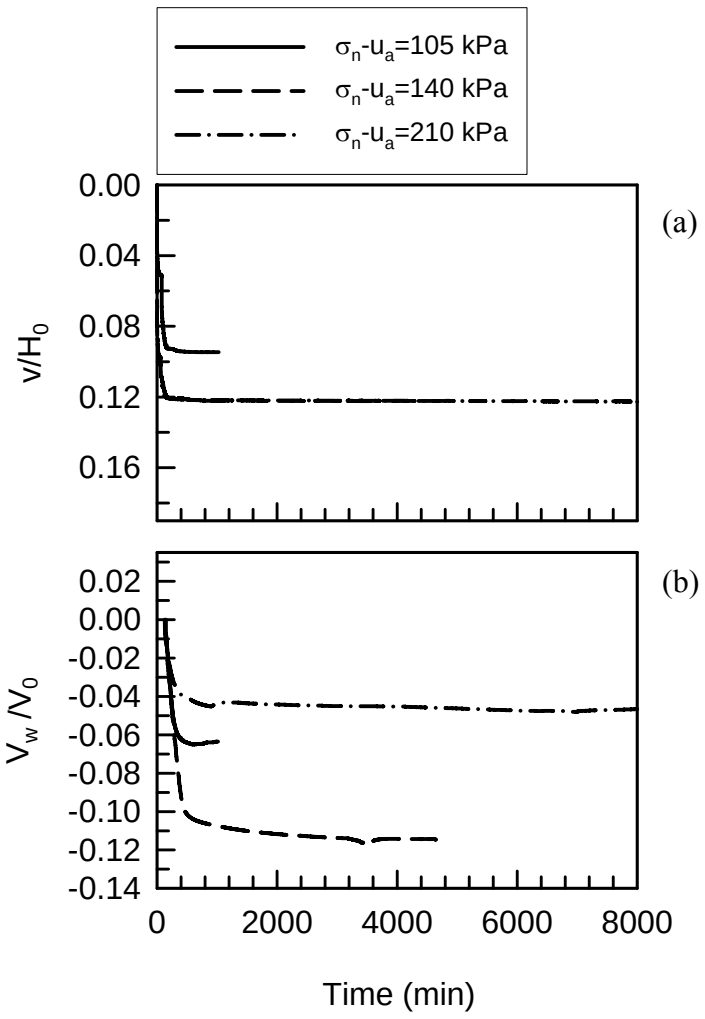

Figure 5.3: Effect of σ_n-u_a on (a) v/H_0, and (b) V_w/V_0 during equalization for soil. (u_a-u_w = 50 kPa)

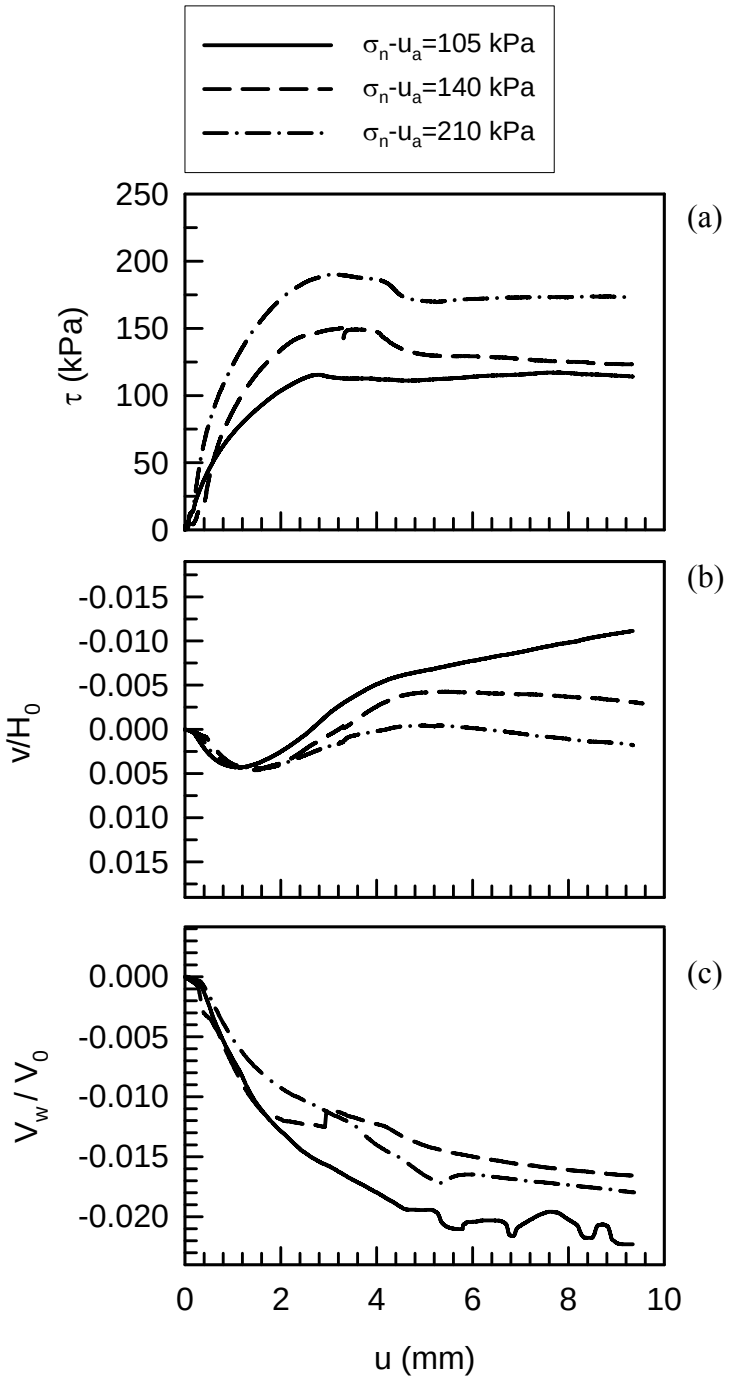

Figure 5.4: Effect of σ_n-u_a on (a) τ, (b) v/H_0, and (c) V_w/V_0 during shearing for soil. (u_a-u_w = 50 kPa)

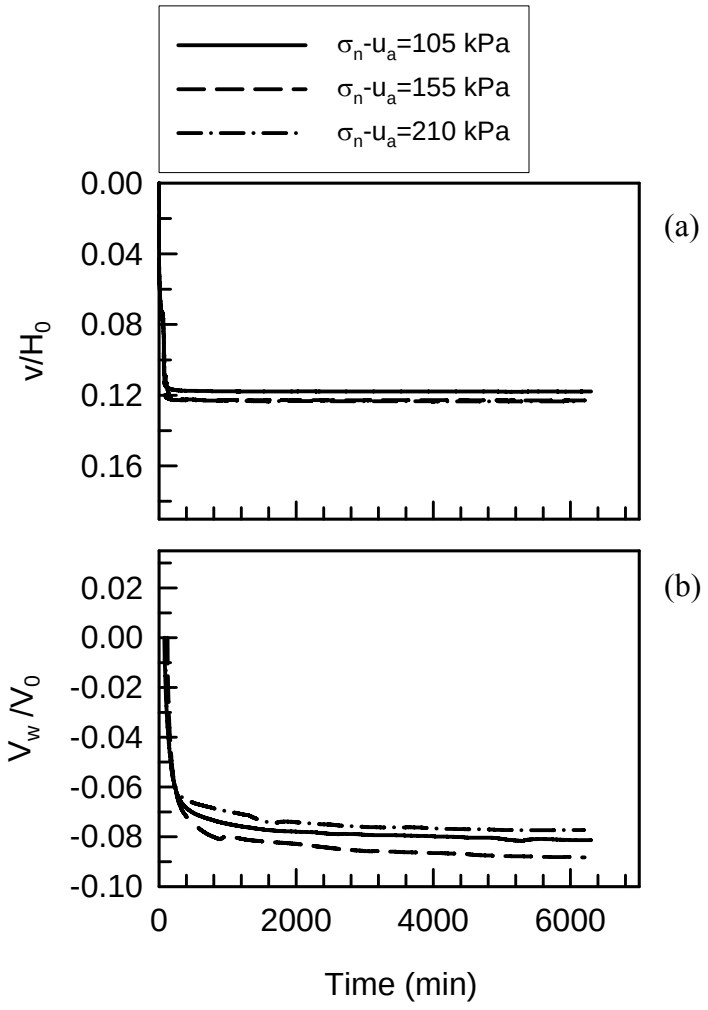

Figure 5.5: Effect of σ_n-u_a on (a) v/H_0, and (b) V_w/V_0 during equalization for soil. (u_a-u_w = 100 kPa)

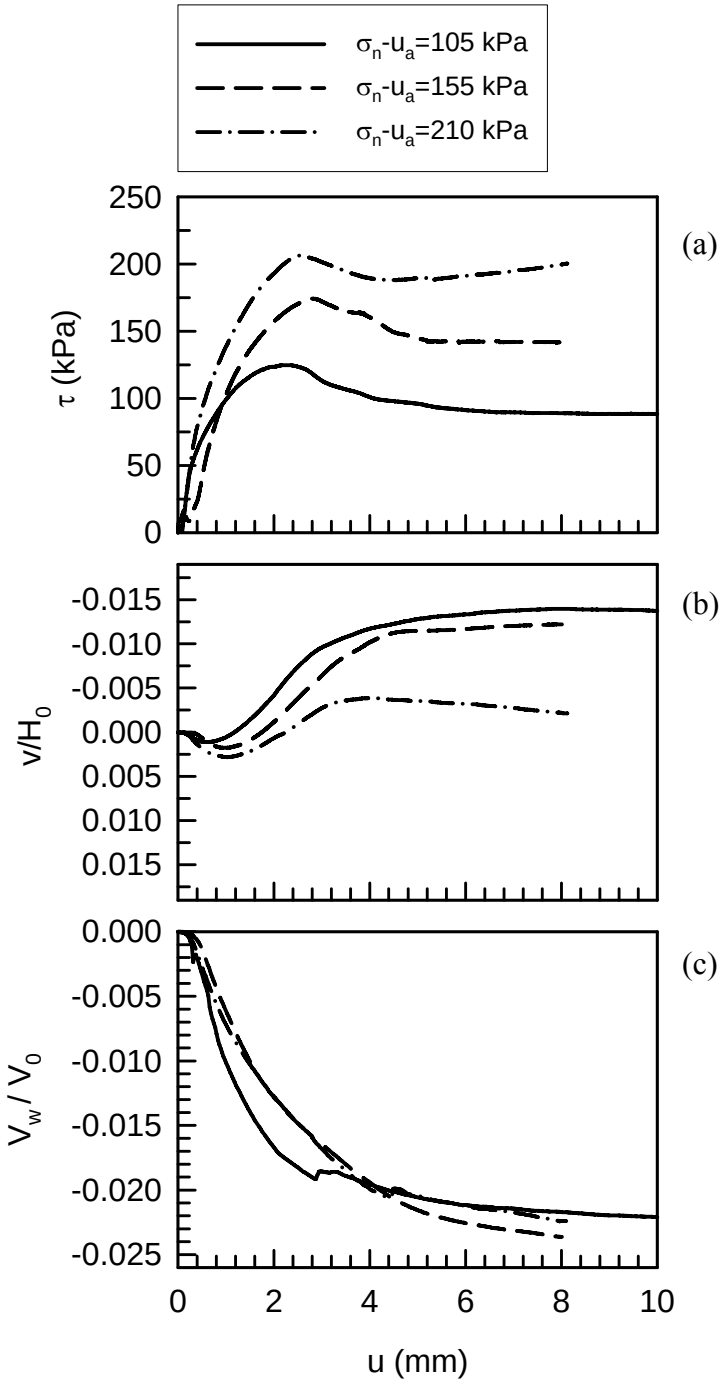

Figure 5.6: Effect of σ_n-u_a on (a) τ, (b) v/H_0, and (c) V_w/V_0 during shearing for soil. (u_a-u_w = 100 kPa)

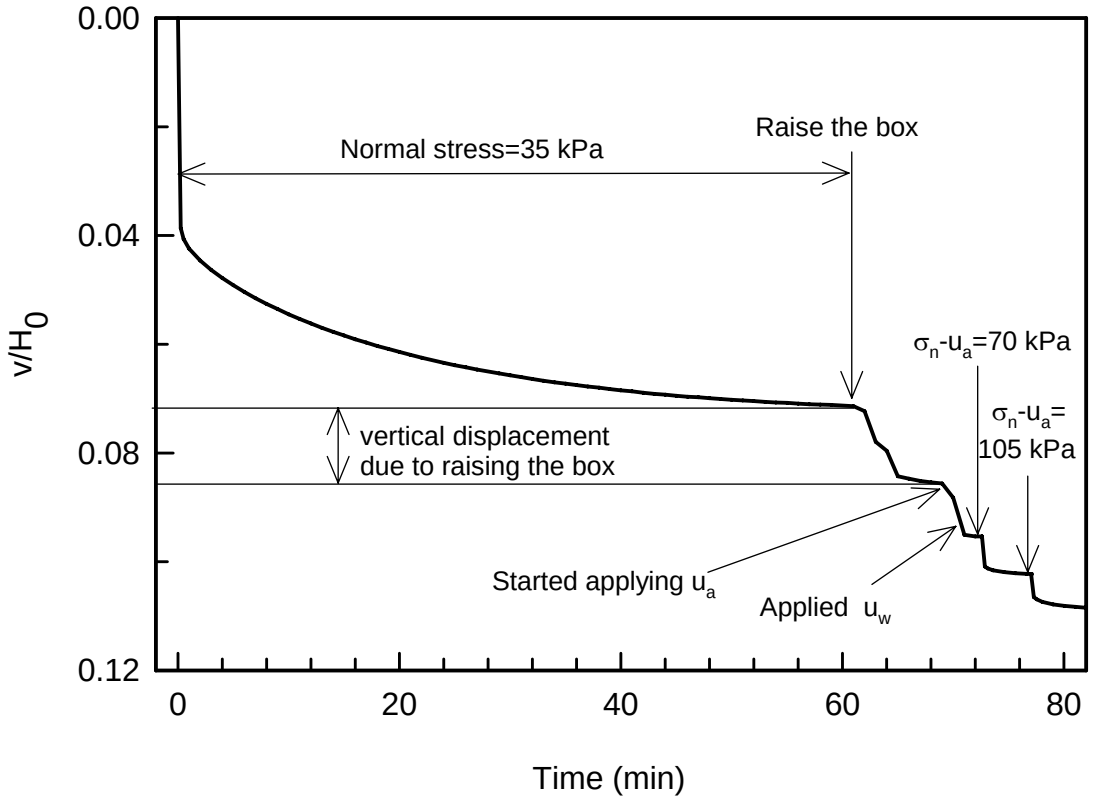

Figure 5.7: Effect of raising the box on vertical displacement and three phases of vertical displacement for a typical test

softening behavior regardless of the magnitude of net normal stress (σ_n-u_a); for 20 kPa suction, the shear stress became constant after reaching the peak. Soil samples tested at u_a-u_w =100 kPa and σ_n-u_a =210 kPa (chain line in Fg.5.6a) showed strain softening behavior followed by slight work hardening.

During shearing soil compressed initially and after reaching a horizontal displacement slightly before the displacement corresponding to maximum shear stress, soil began to dilate and this dilation behavior continued until the soil achieved the residual shear stress. In the residual shear stress region soil generally maintained steady state (i.e., little change in vertical displacement) with increasing horizontal displacement. The amount of dilation decreased as the net normal stress increased (see Figs. 5.2b, 5.4b, 5.6b). In all tests, the water volume controller pulled water from the specimen during shearing to maintain the target suction, as shown in Figs. 5.2c, 5.4c, and 5.6c. Change in volume of water tends to decrease as the horizontal displacement increases and shear strength of soil approaches the residual value.

As mentioned above the water volume controller pulled water from the soil specimen during shearing while the soil was dilating. This observation is in contrast with the behavior of saturated soil. In saturated soil mechanics, dilation indicates a tendency for generation of negative pore water pressure, which in a drained test would be manifested as an increase in volume of water. That water was being pulled out of the sample during the unsaturated test suggests that there was a tendency for increasing pore water pressure (assuming $u_a = 0$), even though the total volume change indicated dilation. This behavior is especially noticeable in Figs. 5.4 and 5.6. Based on the comparison of saturated and unsaturated soil behavior it is postulated that in unsaturated soil during dilation the

rearrangement of soil grains causes changes in the menisci between soil grains possibly even breaking of the menisci. These changes in menisci caused a tendency for increasing pore water pressure; therefore the water volume controller pulled water from the specimen to maintain constant pore water pressure while the specimen was dilating.

5.2.2 Effect of Net Normal Stress on Rough Interface Behavior

5.2.2.1 Equalization Phase

During equalization the rough interface showed the same behavior as soil and it was expected, because before shearing the interface response is dictated by soil behavior. Generally the magnitude of initial compression increased with increasing net normal stress (Figs. 5.8a, 5.10a, 5.13a). However, in Figure 5.10a, vertical displacement is higher for σ_n-u_a = 105 kPa than σ_n-u_a = 140 kPa. The reason is explained with the help of Fig. 5.11. In Fig. 5.11 results of Fig. 5.10a are re-plotted but the time scale is limited to 120 minutes from beginning of the test.

As shown in Fig. 5.11 samples were initially (from 0 to 60 minutes) subjected to a total normal stress of 35 kPa, 70 kPa and 105 kPa for σ_n-u_a =105, σ_n-u_a =140 kPa and σ_n-u_a =210 kPa tests, respectively. The amount of vertical displacement is highest for σ_n-u_a =210 kPa and lowest for σ_n-u_a = 105. After 60 minutes the upper half of the box was raised to create the gap between the steel plate and the upper ring. During this operation the sample that was subjected to lowest amount of total normal stress (i.e., 35 kPa) compressed more than the samples under total normal stress of 70 and 105 kPa, possibly due to the lower side friction between soil and upper half of the shear box. Therefore, greater vertical deformation of the test performed at σ_n-u_a =105 may be attributed to the

affect of raising the box. This observation revealed that a change in procedure was needed. Therefore, other than these three tests, all other samples were subjected to the same amount of initial total stress (i.e., 35 kPa) before raising the upper half of the shear box.

5.2.2.2 Shearing Phase

Maximum and residual shear strength of the rough interface increased with increase in net normal stress. During the shearing process the rough interface compressed and slightly before reaching the maximum shear stress it started to dilate. The rough interface kept dilating during the process of strain softening and dilation was more pronounced in samples that showed strong strain softening behavior (e.g. Figs. 5.14a and 5.14b) than those that did not show any significant strain softening behavior (e.g. Figs. 5.9a and 5.9b). Dilation ceased as the strain softening process completed and shear stress reached the residual shear strength. Figures 5.9b, 5.12b, 5.14b also illustrate that amount of dilation decreased as the net normal stress increased.

Since the rough interface compressed and dilated in the pre-peak and post-peak region, respectively, it is inferred that interlocking between the soil and the rough steel plate is the principal shearing mechanism. Moreover, as the rough interface attained the residual state, the effect of interlocking between the rough steel plate and soil completely vanished and interface kept sliding on the peaks of the rough surface at constant shear stress with out showing any noticeable change in vertical displacement and shear stress. During shearing, maximum change in volume of water occurred before the maximum shear strength value. The rate of change in volume of water decreased after maximum shear stress, as illustrated in Figs. 5.9c, 5.12c, 5.14c.

It is postulated that dilation is the result of rearrangement of soil grains and sliding of soil particles over each other and over the rough surface. As postulated for the soil test results, rearrangement and the sliding of soil grains resulted in the breaking of menisci between soil grain and between soil and steel plate. The breaking of menisci caused a tendency for increasing pore water pressure. Due to the tendency for increasing pore water pressure, the water volume controller pulled water from the sample and water volume decreased while the specimen was dilating.

5.2.3 Effect of Net Normal Stress on Smooth Interface Behavior

5.2.3.1 Equalization Phase

The smooth interface generally showed behavior similar to the rough interface and soil during the equalization process, as expected (Figs. 5.15, 5.17. 5.19).

5.2.3.2 Shearing Phase

Shear strength of the smooth interface increased with increase in net normal stress and little to no strain softening was observed follow the peak shear stress. Also, the plots of shear stress versus horizontal displacement (Fig. 5.16a, 5.18a, 5.20a) exhibit the stick-slip phenomenon. During shearing the smooth interface compressed followed by steady state behavior (i.e. did not show either compression or dilation). The change in the volume of water (normalized to the total volume of the sample) during shearing was quite erratic and varied from 0.25% to 2% (Figs. 5.16c, 5.17c, 5.19c); although the same range was observed for soil and rough interface test results. As opposed to soil and rough interface, the smooth interface did not exhibit a steady state rate of change of volume of water in the residual shear strength range. This observation may be attributed to the stick-slip

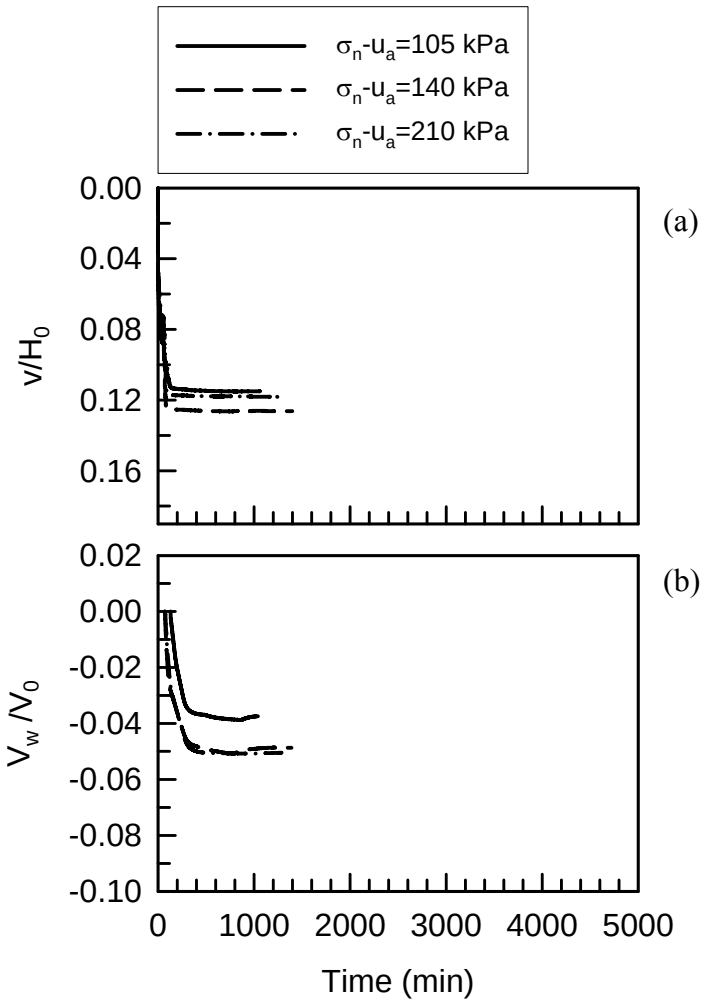

Figure 5.8: Effect of σ_n-u_a on (a) v/H_0, and (b) V_w/V_0 during equalization for rough interface. (u_a-u_w = 20 kPa)

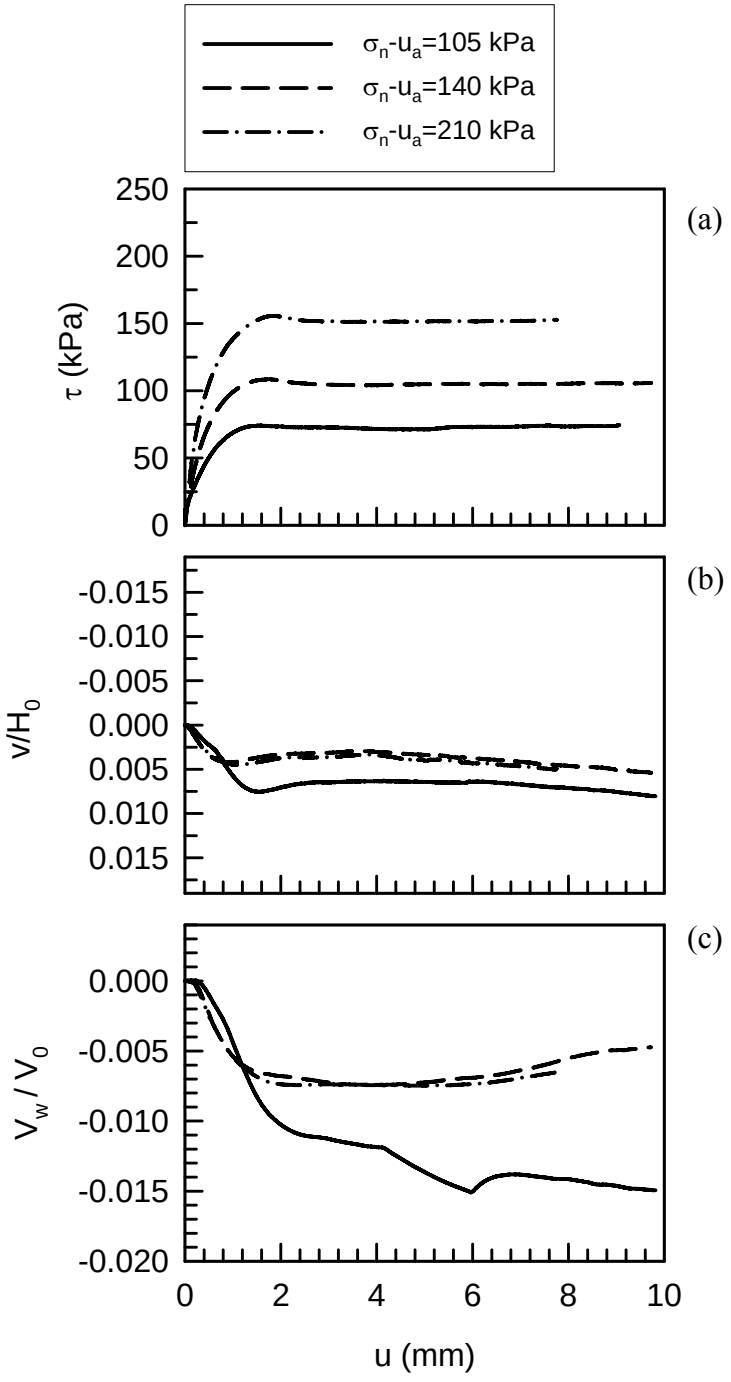

Figure 5.9: Effect of σ_n-u_a on (a) τ, (b) v/H_0, and (c) V_w/V_0 during shearing for rough interface. (u_a-u_w = 20 kPa)

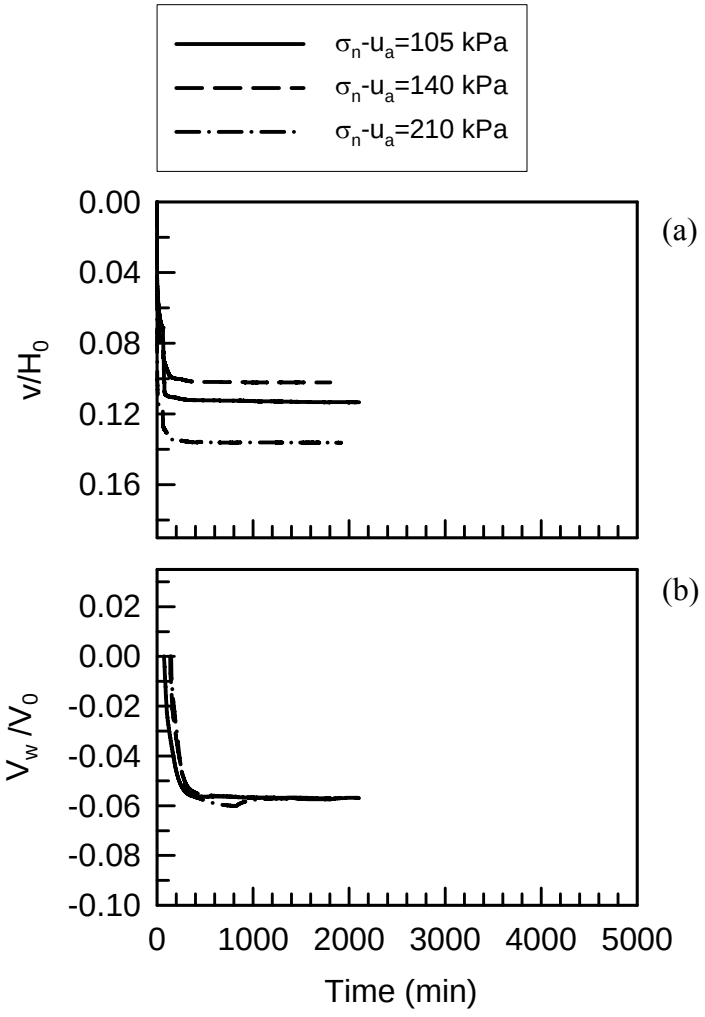

Figure 5.10: Effect of σ_n-u_a on (a) v/H_0, and (b) V_w/V_0 during equalization for rough interface. (u_a-u_w = 50 kPa)

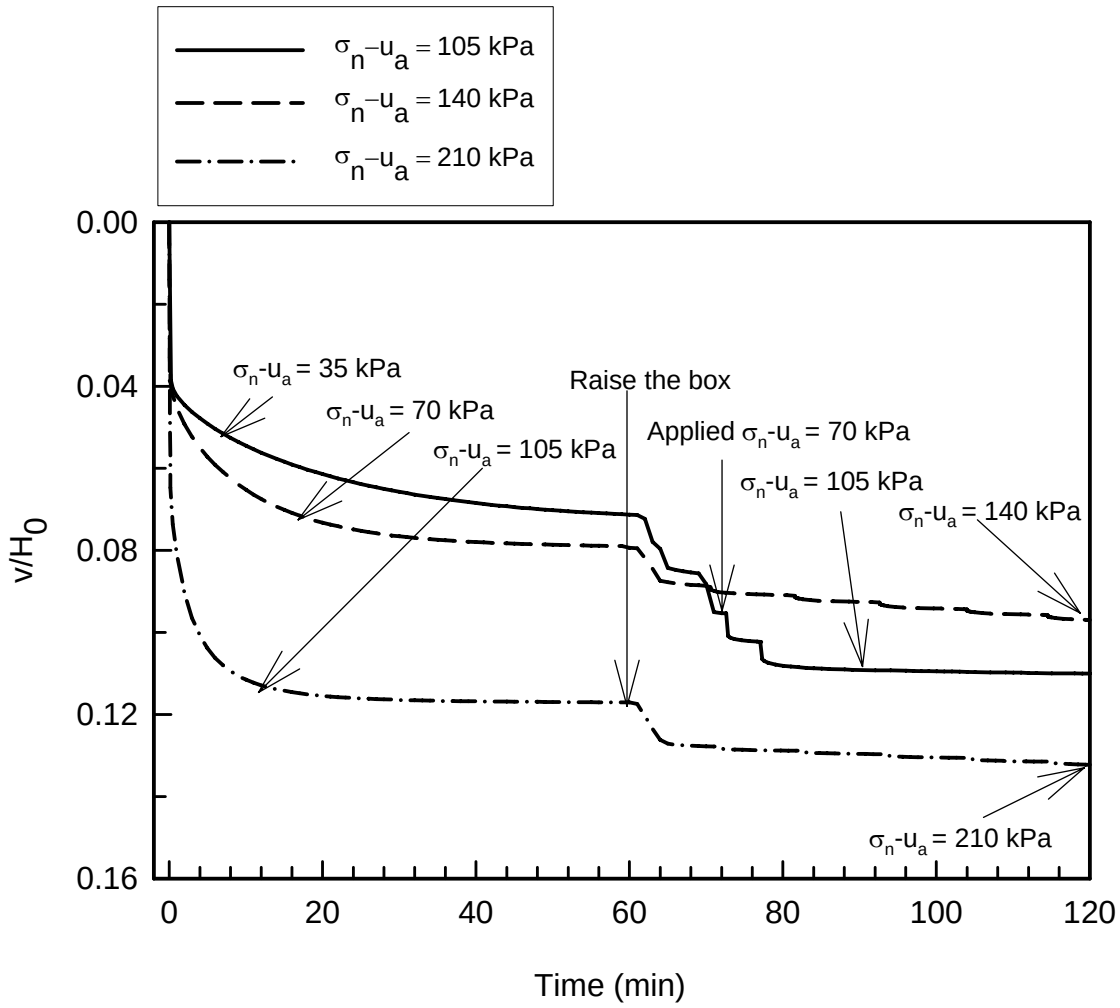

Figure 5.11: Effect of raising the box on vertical displacement

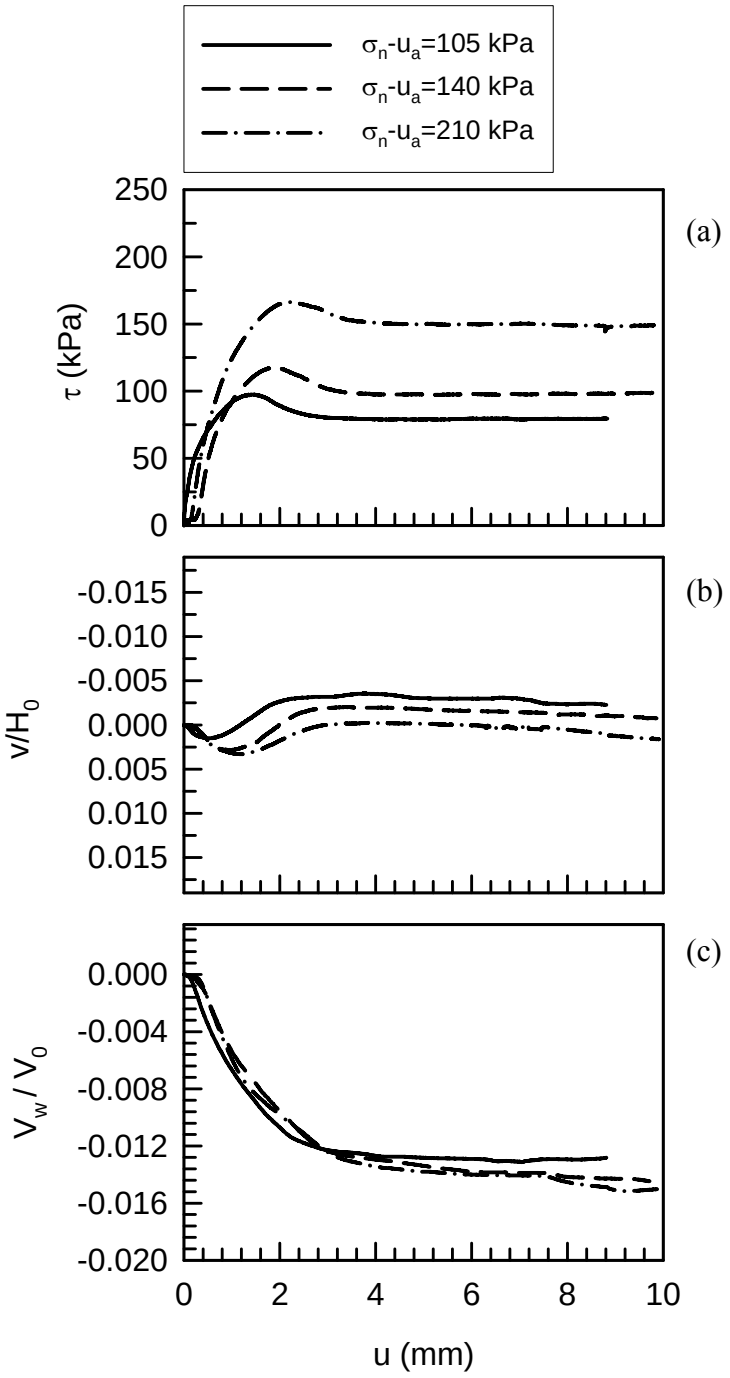

Figure 5.12: Effect of σ_n-u_a on (a) τ, (b) v/H_0, and (c) V_w/V_0 during shearing for rough interface. (u_a-u_w = 50 kPa)

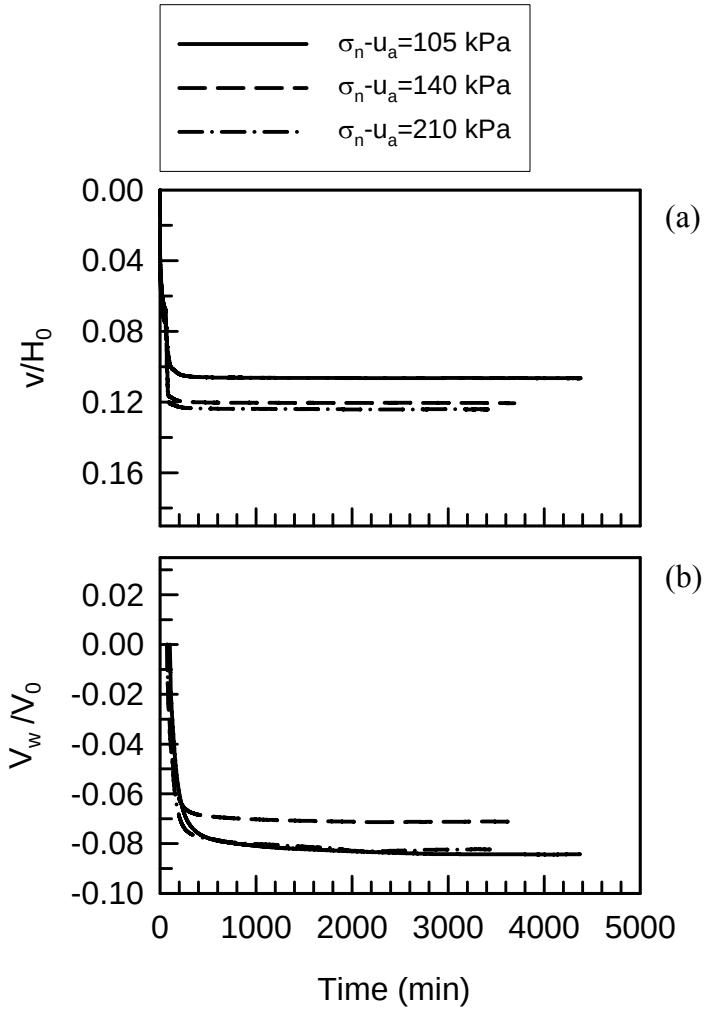

Figure 5.13: Effect of σ_n-u_a on (a) v/H_0, and (b) V_w/V_0 during equalization for rough interface. (u_a-u_w = 100 kPa)

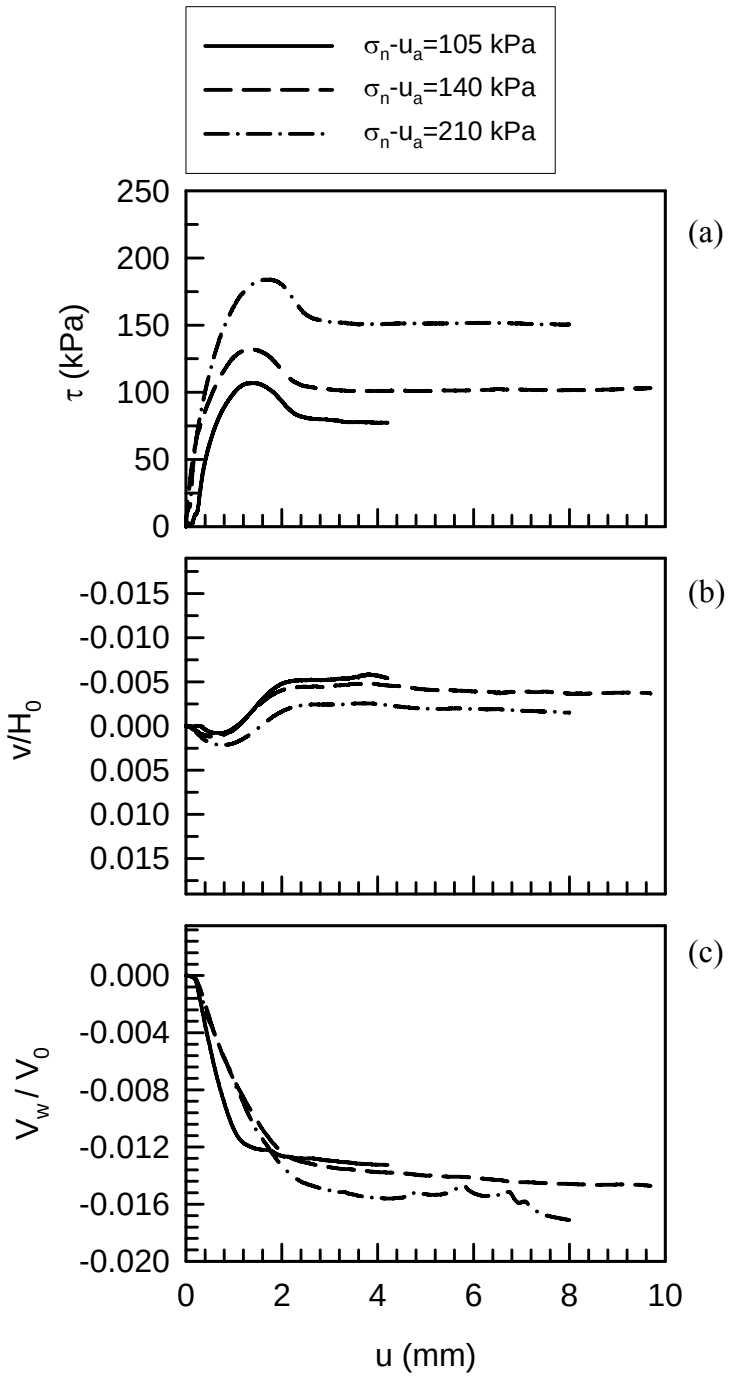

Figure 5.14: Effect of σ_n-u_a on (a) τ, (b) v/H_0, and (c) V_w/V_0 during shearing for rough interface. (u_a-u_w =100 kPa)

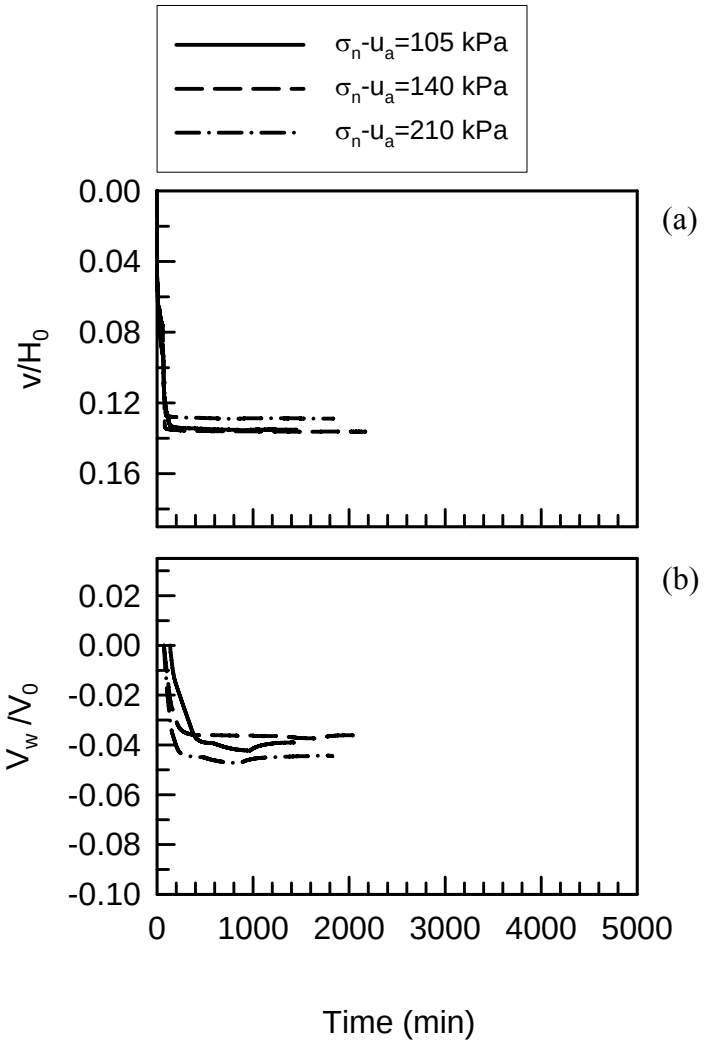

Figure 5.15: Effect of σ_n-u_a on (a) v/H_0, and (b) V_w/V_0 during equalization for smooth interface. (u_a-u_w = 20 kPa)

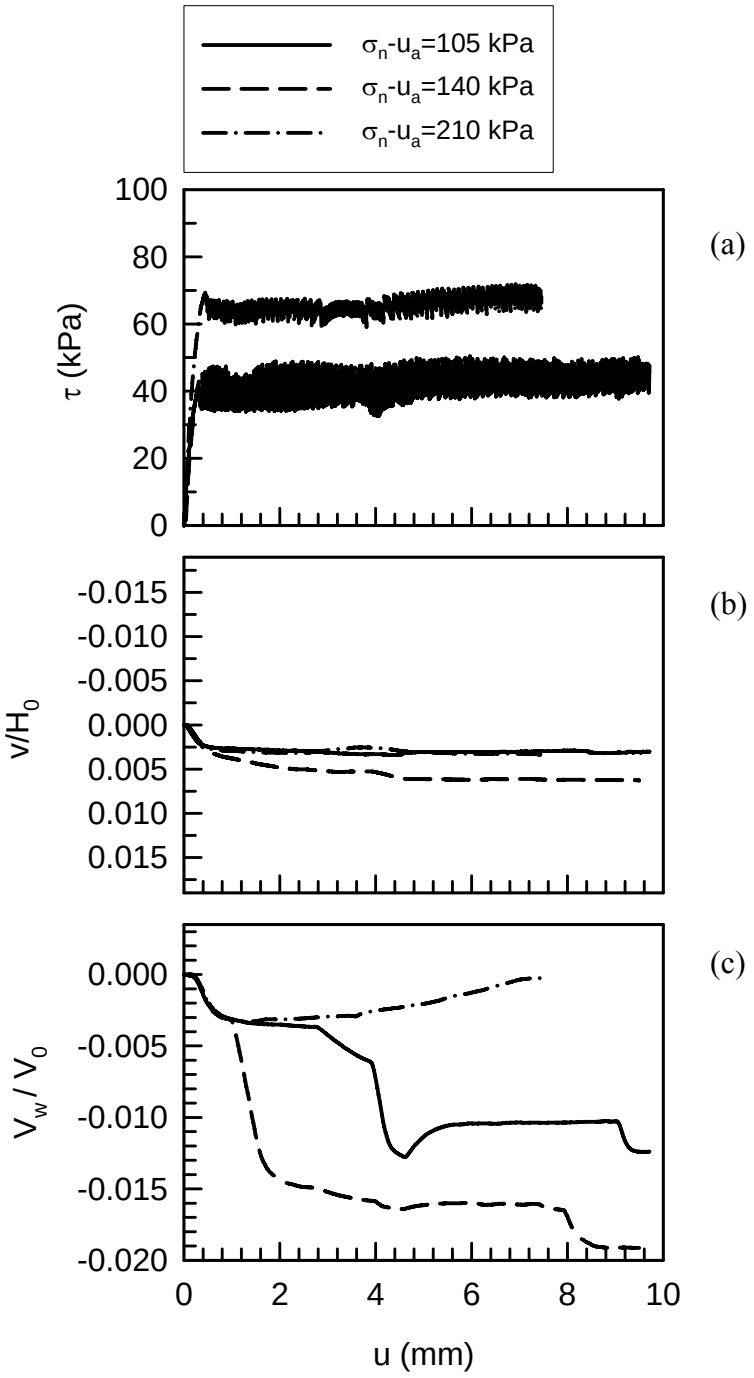

Figure 5.16: Effect of σ_n-u_a on (a) τ, (b) v/H_0, and (c) V_w/V_0 during shearing for smooth interface. (u_a-u_w = 20 kPa)

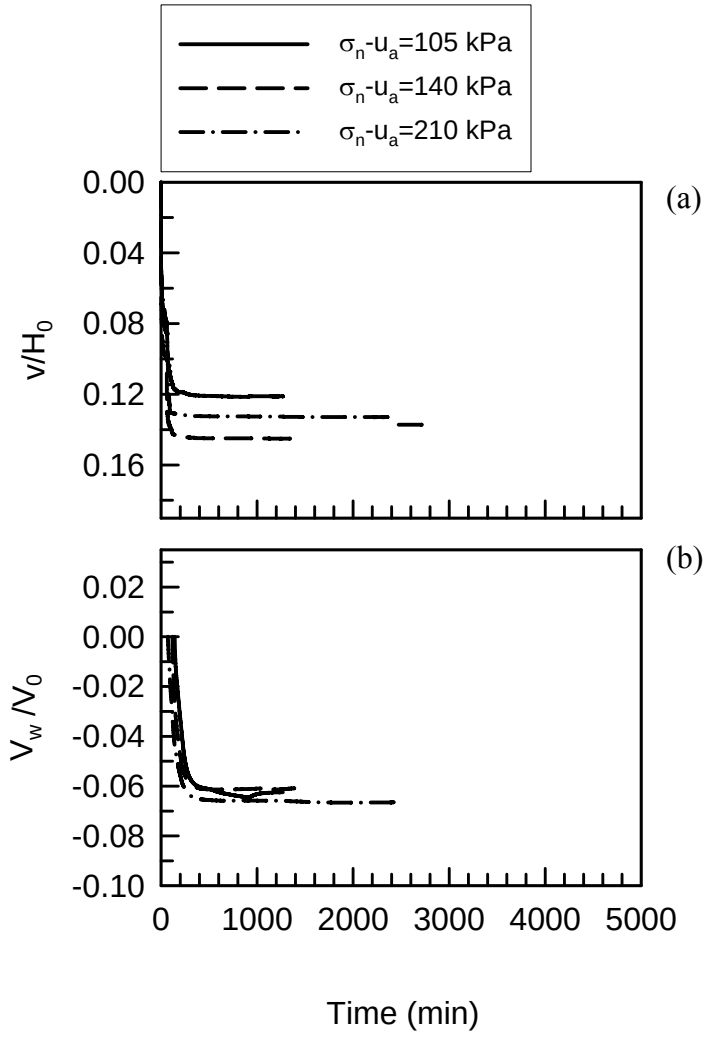

Figure 5.17: Effect of σ_n-u_a on (a) v/H_0, and (b) V_w/V_0 during equalization for smooth interface. (u_a-u_w = 50 kPa)

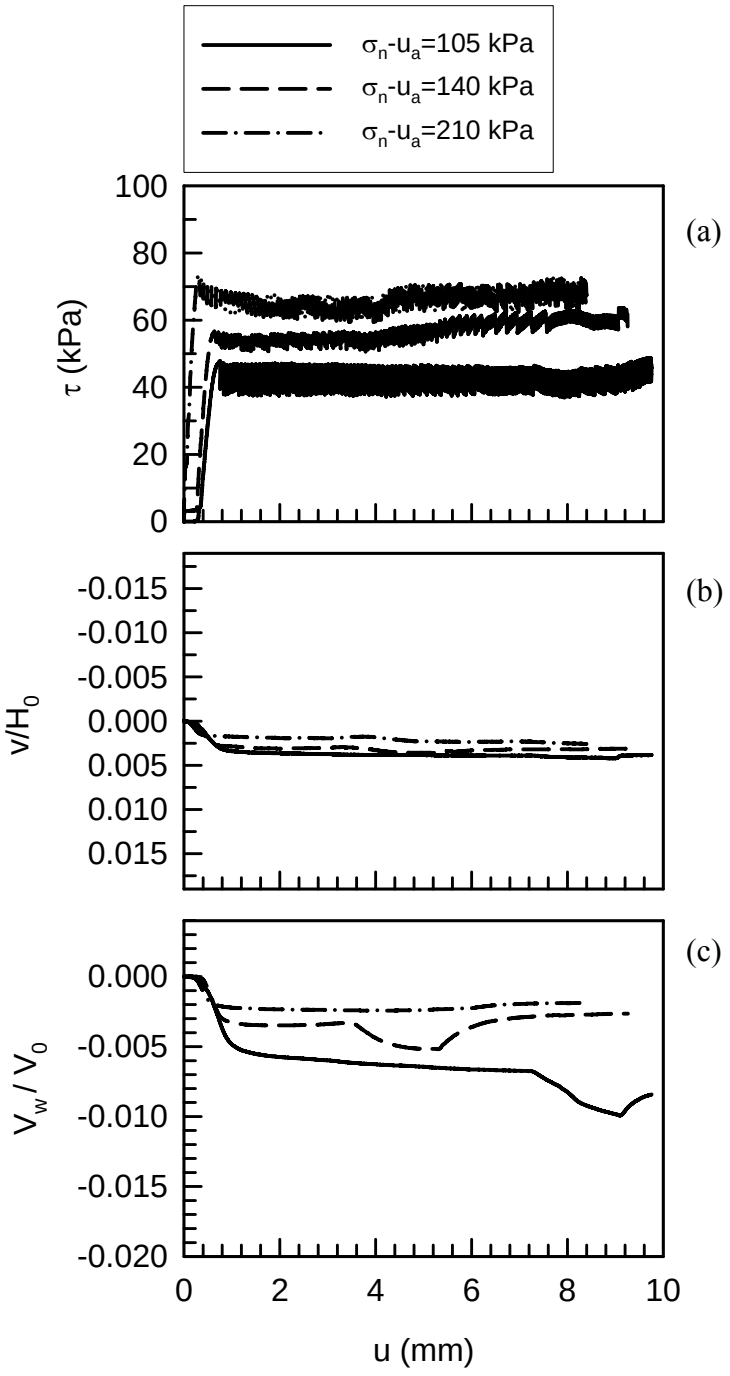

Figure 5.18: Effect of σ_n-u_a on (a) τ, (b) v/H_0, and (c) V_w/V_0 during shearing for smooth interface. (u_a-u_w = 50 kPa)

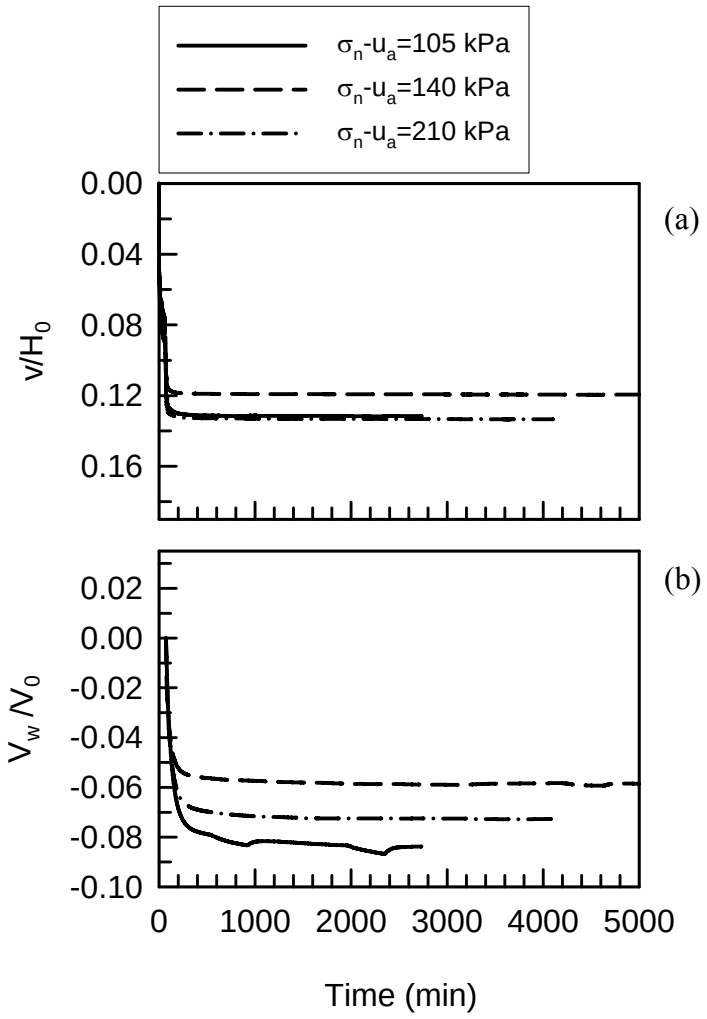

Figure 5.19: Effect of σ_n-u_a on (a) v/H_0, and (b) V_w/V_0 during equalization for smooth interface. (u_a-u_w = 100 kPa)

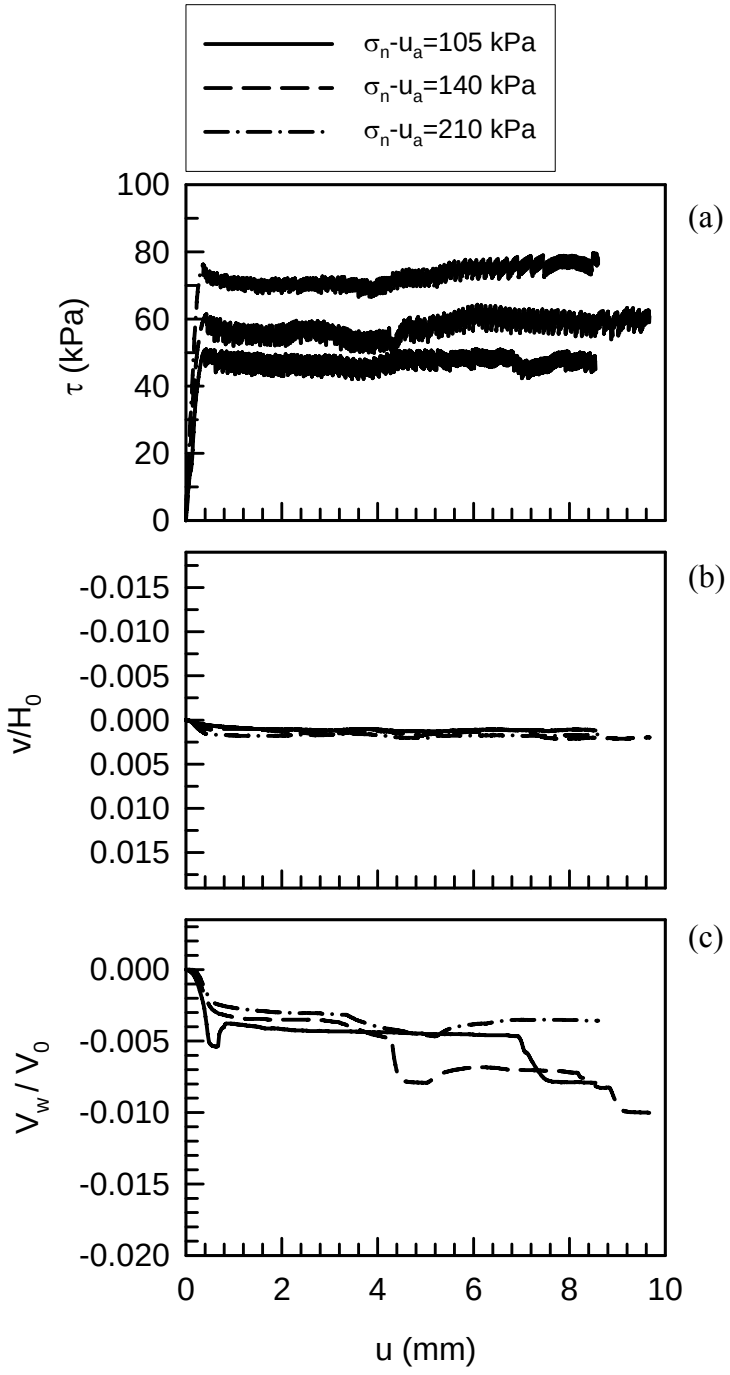

Figure 5.20: Effect of σ_n-u_a on (a) τ, (b) v/H_0, and (c) V_w/V_0 during shearing for smooth interface. (u_a-u_w = 100 kPa)

behavior of the smooth interface in the residual shear stress region because the response of pore water pressure during the stick mode would be different from the slip mode.

5.3 EFFECT OF SUCTION

Typical plots for total volume change and water volume change for different values of suction at a given net normal stress during equalization are shown in Figs. 5.21, 5.22, and 5.23 for soil, rough interface and smooth interface, respectively. Graphs for other tests are included in Appendix II.

5.3.1 Behavior of Soil and Interface During Equalization Phase

Typical plots of total volume and water volume change are shown in Figs. 5.21-5.23. As mentioned in Section 5.2.1.1, it was found that the major part of compression occurred immediately after the application of total normal stress and prior to raising the upper half of the shear box; after the application of u_a and u_w (i.e., during equalization) change in vertical displacement was less significant. Figures 5.21b to 5.23b illustrate that water (normalized by volume of specimen) drained during equalization. All curves consistently show that the amount of water drained for the lowest suction (i.e, u_a-u_w = 20 kPa, shown by solid line) was less than the amount of water drained for the highest suction (i.e, u_a-u_w = 100 kPa, shown by chain line). This observation is consistent with expectations and suggests that suction was correctly controlled.

5.3.2 Effect of Suction on Soil Behavior During Shearing

Horizontal displacement versus shear stress curves for soil at σ_n-u_a = 105 kPa under various suctions (20, 50, 100 kPa) are presented in Fig. 5.24a. Increasing suction resulted in an increase of maximum shear stress and stiffness. Strain softening behavior and a pronounced peak is obvious only for 100 kPa suction, illustrating an increasing

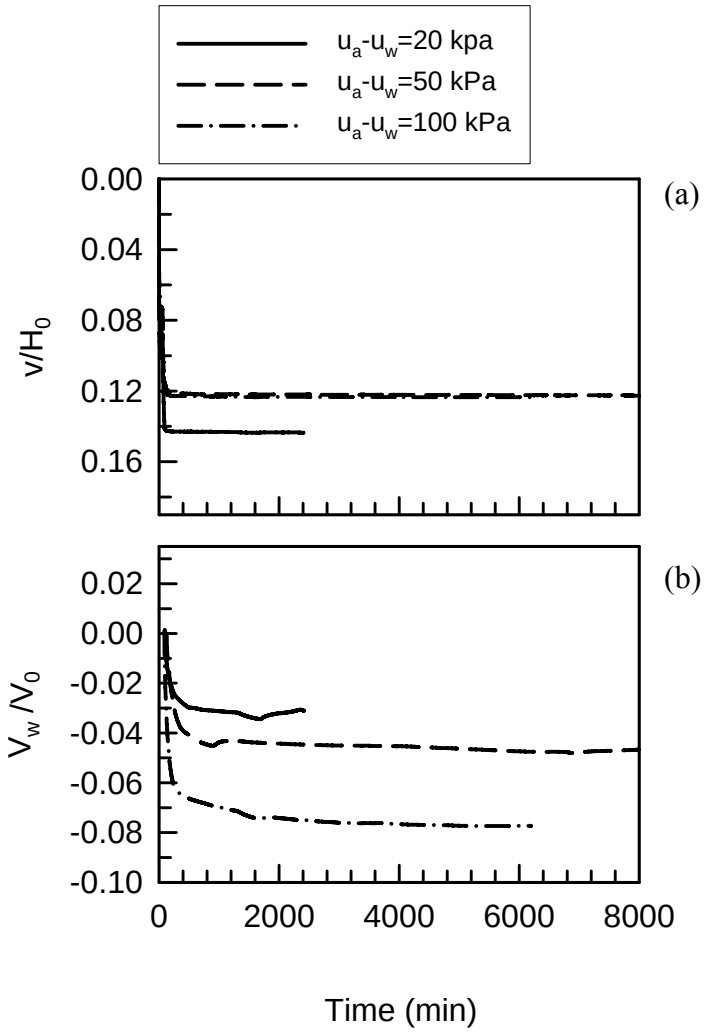

Figure 5.21: Effect of u_a-u_w on (a) v/H_0, and (b) V_w/V_0 during equalization for soil (σ_n-u_a = 210 kPa)

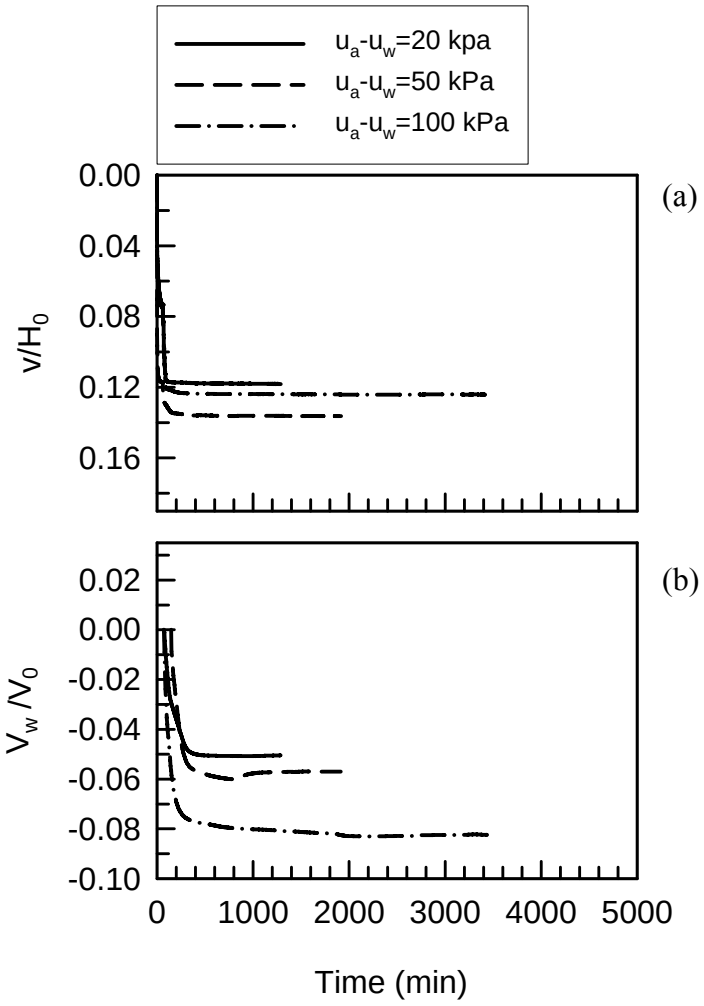

Figure 5.22: Effect of u_a-u_w on (a) v/H_0, and (b) V_w/V_0 during equalization for rough interface. (σ_n-u_a = 210 kPa)

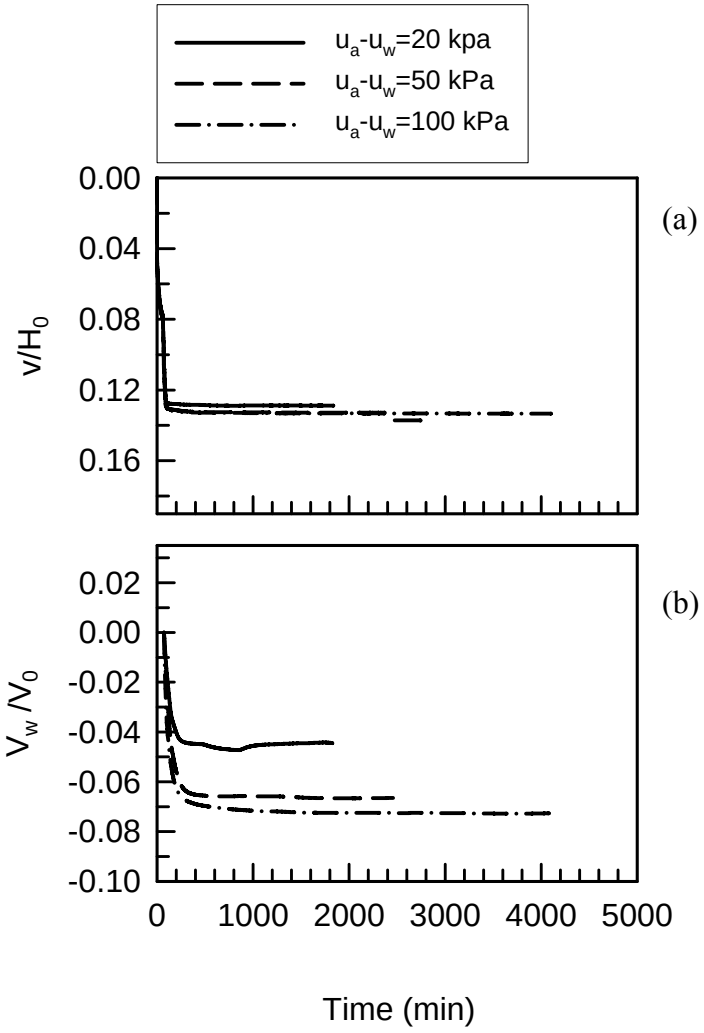

Figure 5.23: Effect of u_a-u_w on (a) v/H_0, and (b) V_w/V_0 during equalization for smooth interface. (σ_n-u_a = 210 kPa)

brittleness of the sample with increasing suction. In Fig. 5.24a, the residual shear stress of 100 kPa suction sample is similar to the residual shear strength of the sample tested at 20 kPa suction. However, the sample tested at 50 kPa suction did not show significant strain softening behavior and residual shear strength of this sample is approximately same as maximum shear stress. Soil samples tested at other net normal stresses showed some similar tendencies (Figs. 5.25a; 5.26a). That some of the curves, notably those for u_a-u_w = 20 kPa and 100 kPa in Figs. 5.24a and 5.25a, approach the same residual strength suggests that the suction is less important in the post peak region. Possibly this is due to the alteration and breaking of menisci as postulated previously.

Volume change curves (Figs. 5.24b, 5.25b, 5.26b) show that the tendency for dilation following initial compression increased with increasing suction. At a constant net normal stress, the effect of suction is opposite to that of net normal stress, since an increasing suction favors dilatancy. Generally those samples, which dilated significantly also exhibited more significant post peak softening, as expected.

Comparison of behavior of total volume and water volume change curves (Figs. 5.24, 5.25, 5.26) during shearing shows that as dilation increased so did the volume of water pulled from the sample. As discussed in section 5.2.1.2, the water volume change behavior suggests that during shearing there was tendency for increasing pore water pressure even though the total volume change behavior indicated dilation. This may be possibly attributed to changes in menisci between soil grains.

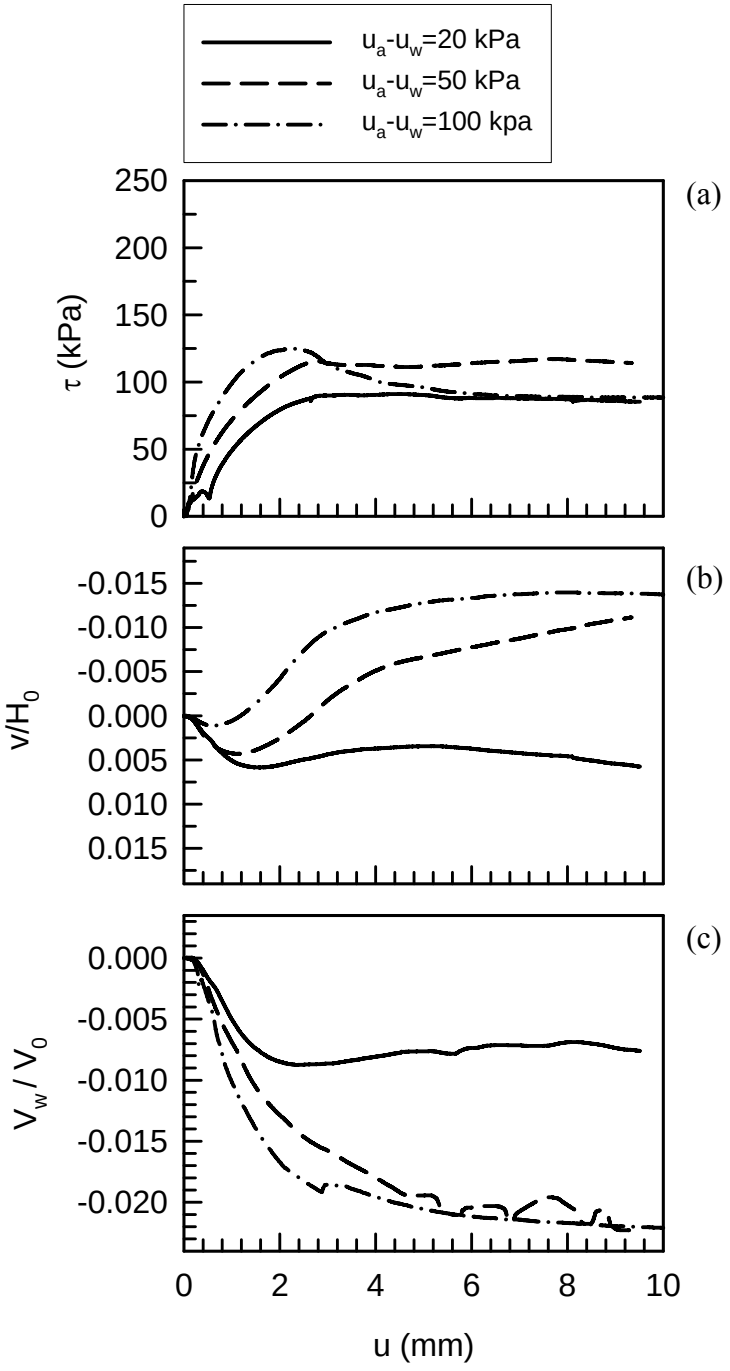

Figure 5.24: Effect of u_a-u_w on (a) τ, (b) v/H_0, and (c) V_w/V_0 during shearing for soil. (σ_n-u_a = 105 kPa)

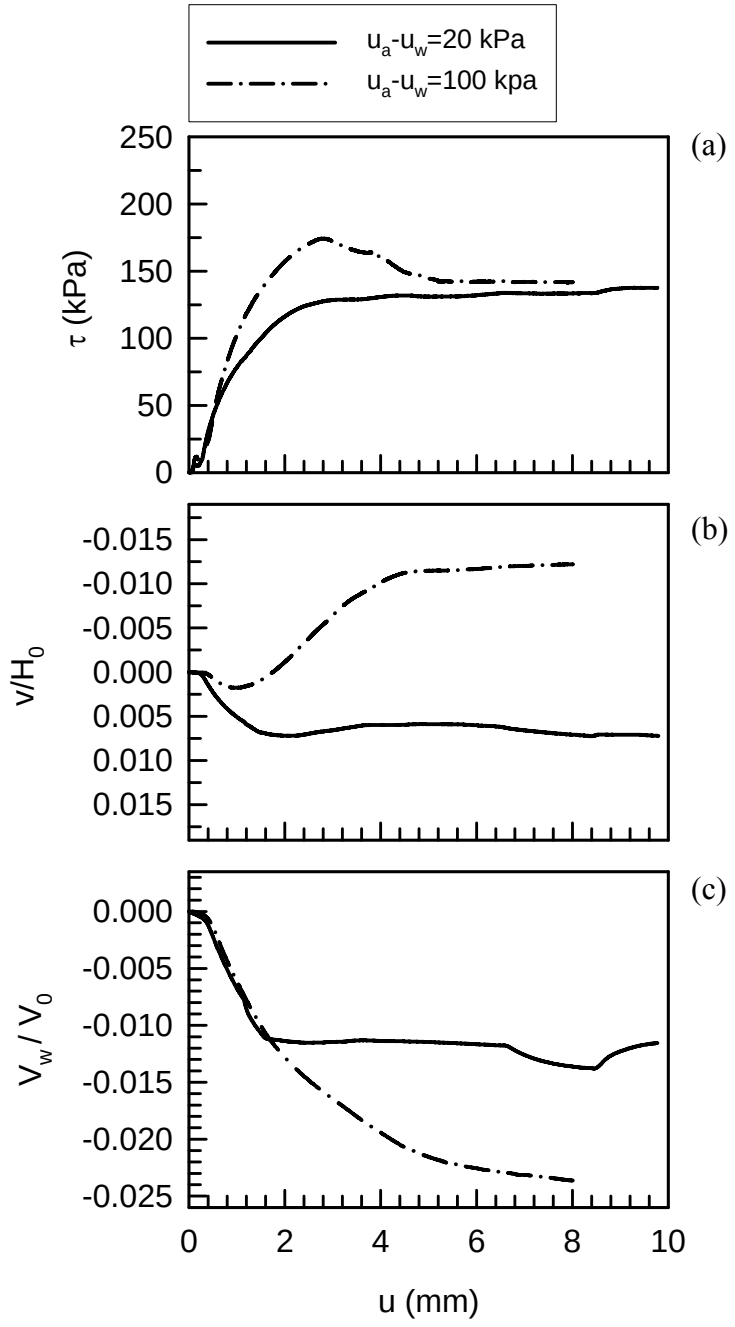

Figure 5.25: Effect of u_a-u_w on (a) τ, (b) v/H_0, and (c) V_w/V_0 during shearing for soil. (σ_n-u_a = 155 kPa)

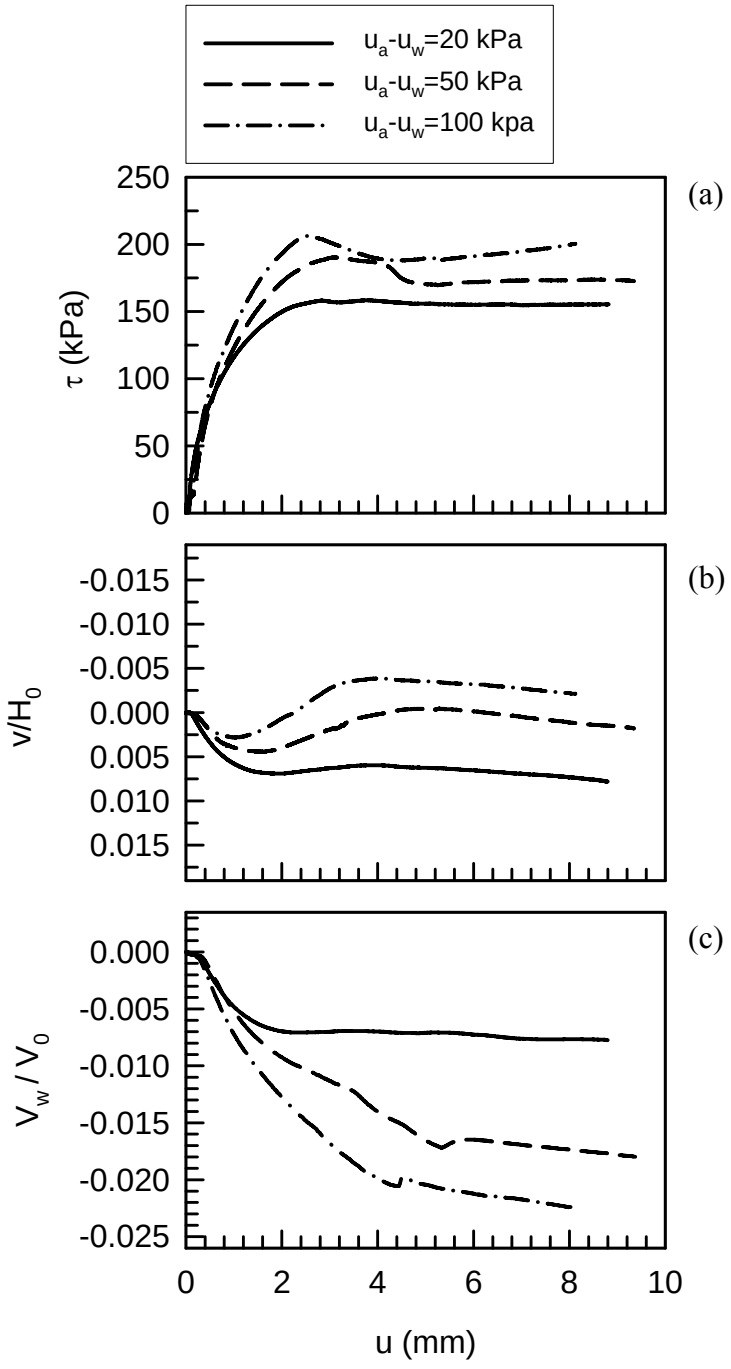

Figure 5.26: Effect of u_a-u_w on (a) τ, (b) v/H_0, and (c) V_w/V_0 during shearing for soil. (σ_n-u_a = 210 kPa)

5.3.3 Effect of Suction on Rough Interface Behavior During Shearing

Horizontal displacement versus shear stress curves for the rough interface are shown in Figs. 5.27a, 5.28a, 5.29a. These figures illustrate an increase in maximum shear stress with increase in suction for a given net normal stress, similar to the observation for soil. These figures also show that maximum shear stress occurred at lower values of horizontal displacement for increasing suction, illustrating an increasing brittleness of the sample with increasing suction. It can also be observed that strain softening behavior became pronounced with increasing suction.

Although maximum shear stress of the rough interface increased with increasing suction, values of residual shear stress did not change with increase in suction. This observation suggests, as postulated for soil, that water menisci acting in the interface are disturbed to a similar extent and that the suction has little affect on residual strength.

Corresponding volume change curves are shown in Figs. 5.27b, 5.28b, and 5.29b. These curves show initial contraction followed by dilatancy that vanished in the region of residual shear stress. Similar to soil samples, the interface showed increase in dilatancy with increase in suction. These figures also show that rough interface tested at u_a-u_w = 100 kPa contracted less than other two suction values (i.e. u_a-u_w = 20 and 50 kPa) used in this study. This trend was observed for all net normal stress values.

As discussed in the section on effect of net normal stress, the water volume controller pulled water while the rough interface was dilating during shearing and generally greater water was removed as dilation increased.

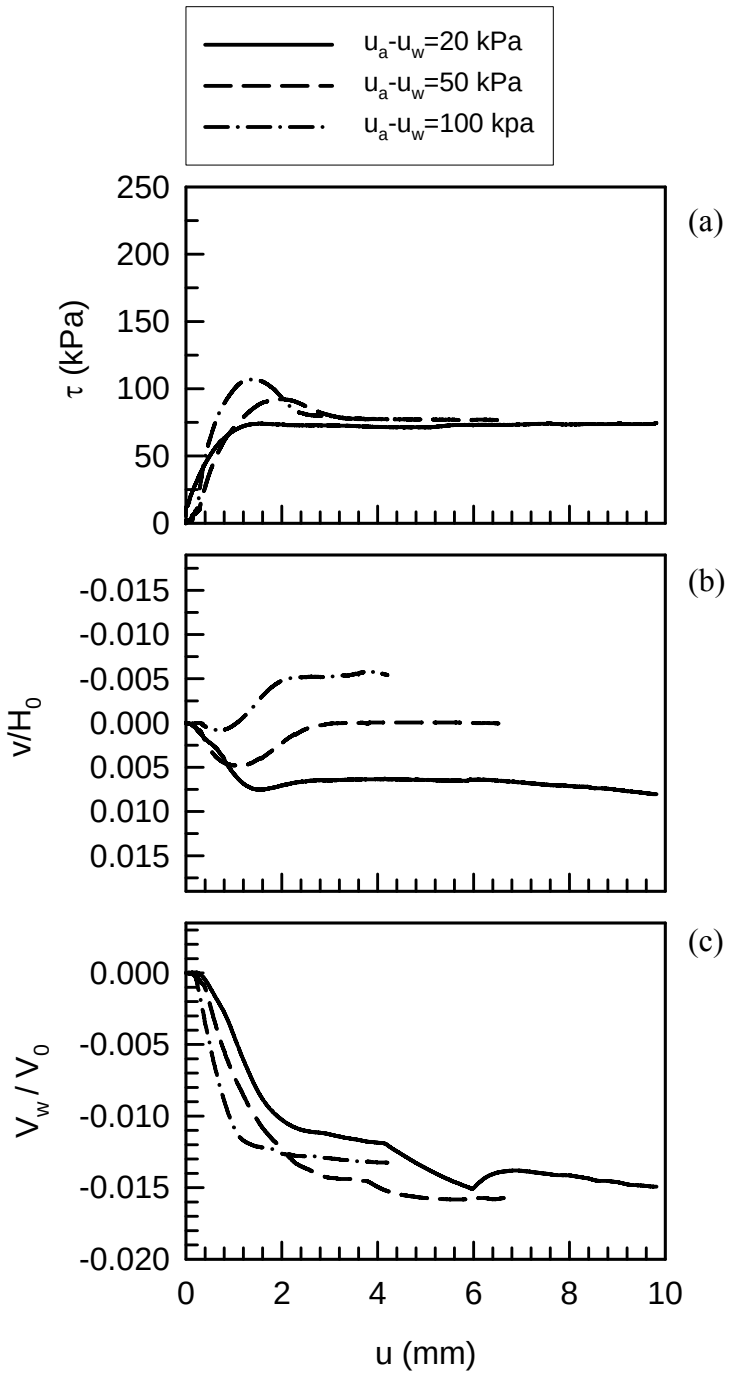

Figure 5.27: Effect of u_a-u_w on (a) τ, (b) v/H_0, and (c) V_w/V_0 during shearing for rough interface. (σ_n-u_a = 105 kPa)

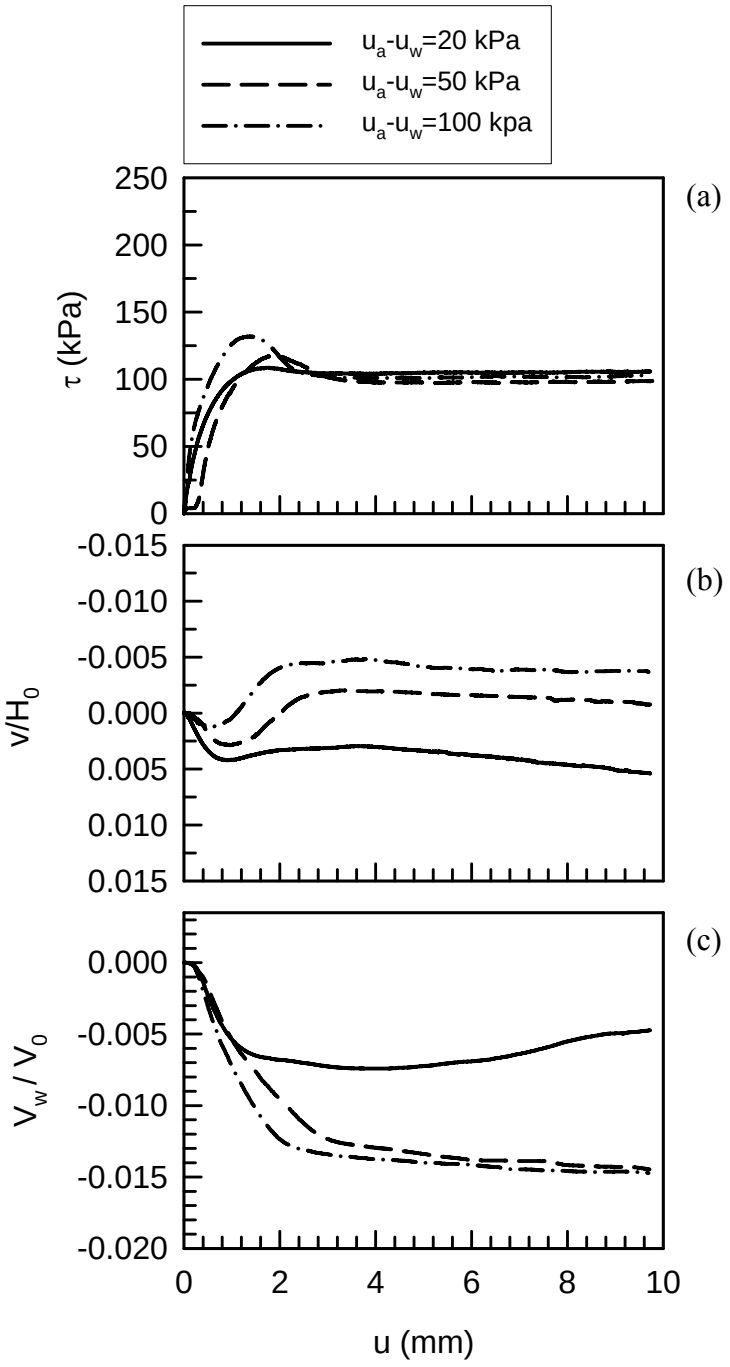

Figure 5.28: Effect of u_a-u_w on (a) τ, (b) v/H_0, and (c) V_w/V_0 during shearing for rough interface. (σ_n-u_a = 140 kPa)

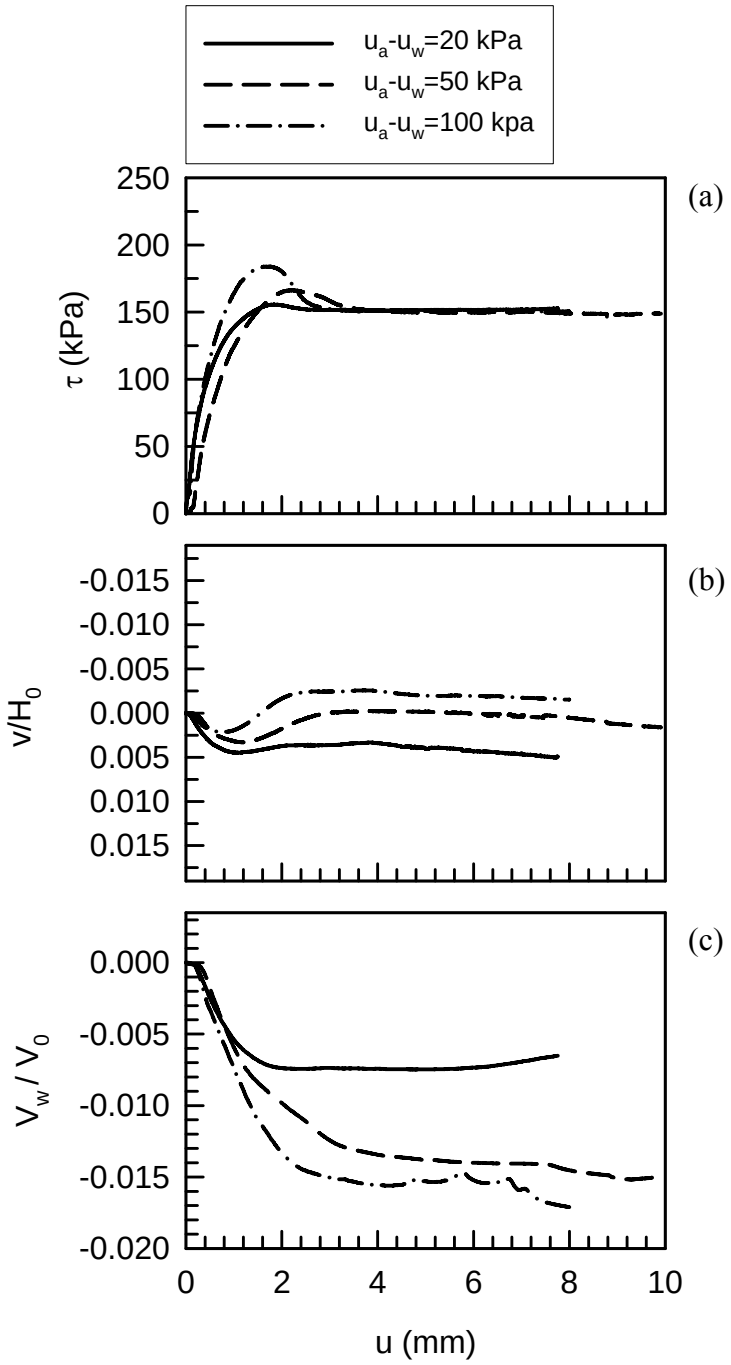

Figure 5.29: Effect of u_a-u_w on (a) τ, (b) v/H_0, and (c) V_w/V_0 during shearing for rough interface. (σ_n-u_a = 210 kPa)

5.3.4 Effect of Suction on Smooth Interface Behavior During Shearing

A typical plot of the shear stress and volume change behavior for the smooth interface during shearing is shown in Fig. 5.30. As mentioned previously, this figure shows that the smooth interface exhibited stick-slip behavior after the maximum shear stress was reached. The stick-slip process continued throughout the test. Increase in shear stress with suction, as observed in the case of soil and rough interface, can also be observed for the smooth interface. However, increase in shear strength due to suction in the case of the smooth interface is less pronounced than the soil and rough interface.

As opposed to soil and rough interface, the smooth interface did not show dilatancy behavior. For all suction (u_a-u_w) values and net normal stresses (σ_n-u_a) the smooth interface contracted initially and then the behavior remained steady after reaching the maximum shear stress. Based on this observation it is postulated that for the smooth interface the shearing mechanism is controlled by sliding rather than interlocking between soil particles or soil and smooth steel plate. Similar observations regarding the effect of suction were made for the smooth interface tested at σ_n-u_a = 105 kPa and 210 kPa. Similar to rough interface, the water volume controller pulled water from the smooth interface during shearing but as discussed previously the behavior was erratic as compared to the soil and rough interface.

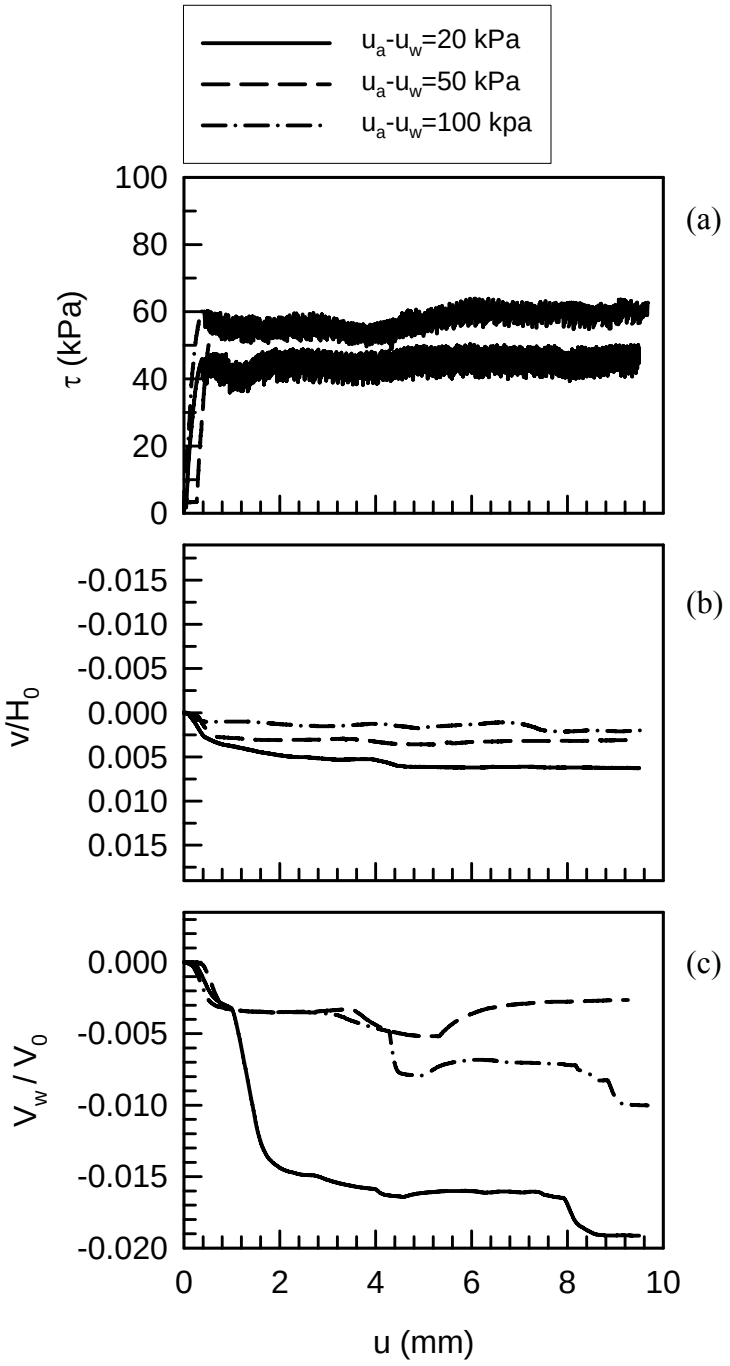

Figure 5.30: Effect of u_a-u_w on (a) τ, (b) v/H_0, and (c) V_w/V_0 during shearing for smooth interface. (σ_n-u_a = 140 kPa)

5.4 EFFECT OF SURFACE ROUGHNESS

Typical plots for the effect of surface roughness on the strength and volumetric behavior of the interface are shown in Figures 5.31 and 5.32. The presented results indicate that the surface roughness significantly affected the peak and residual shear stress as well as the volumetric behavior of interfaces. The interface response to volume change behavior became dilative as the roughness of the surface increased. Figures showing the comparison of rough and smooth surfaces for all other suction and net normal stress values are included in Appendix II. The following important observations regarding the effect of surface roughness on the behavior of the interface can be made from these typical figures.

1) A pronounced peak strength was observed for both rough and smooth surfaces.

2) The peak shear strength for the rough interface was larger and mobilized at larger horizontal deformation than that of the smooth interface.

3) The smooth interface initially compressed similar to the rough interface until the peak shear stress was reached; after the peak, the smooth interface achieved a steady state condition without showing any noticeable change in vertical displacement. As opposed to the smooth interface, the rough interface began to dilate after reaching the peak shear stress (τ_p) value and dilation continued until the residual shear stress was reached.

4) A clear stick-slip behavior was observed after the peak shear stress for the smooth surface whereas sliding of soil over the rough surface did not show stick-slip behavior.

5) Strain softening behavior was much more pronounced for the rough interface than the smooth interface, apparently due to the difference in shearing mechanisms between smooth and rough steel plates.

6) Results of the tests shown in Figs. 5.31c and 5.32c exhibit reasonably good agreement in volume of water that drained during the shearing process. Water content values for other tests at the end of equalization and shearing are given in Table I.1 in Appendix I. Table I.1 shows generally consistent water content results for a given value of suction and net normal stress. Approximately $\pm$1% difference of water content in some tests (e.g., Tests corresponding to u_a-u_w = 100 kPa and σ_n-u_a = 210 kPa) between rough and smooth interface may possibly be attributed to factors such as moisture loss between the time of preparation of sample and beginning of test, water loss during testing (through the gap between the two halves of the shear box), and different shearing mechanisms.

5.5 COMPARISON OF SOIL AND INTERFACE BEHAVIOR

Figures 5.33-5.40 show the comparison of behavior of soil and interfaces during the equalization process. These figures illustrate that before shearing, the interface acted similar to the soil because before shearing the interface response is dictated by soil behavior. As expected, during equalization process soil and interfaces compressed approximately to the same amount for a given value of net normal stress (σ_n-u_a) and suction (u_a-u_w). For example Figs. 5.39a and 5.40a show approximately the same amount of compression for soil and both interfaces. As opposed to tests shown in Figs. 5.39 and 5.40, other tests show some differences in the magnitude of vertical compression of soil and interfaces. In general, the differences in vertical compression are random, for example, in Fig. 5.33a, the smooth interface experienced maximum compression whereas in Fig. 5.34a soil compressed more than the interfaces. The difference in vertical compression may be attributed to several factors such as the difference in initial water

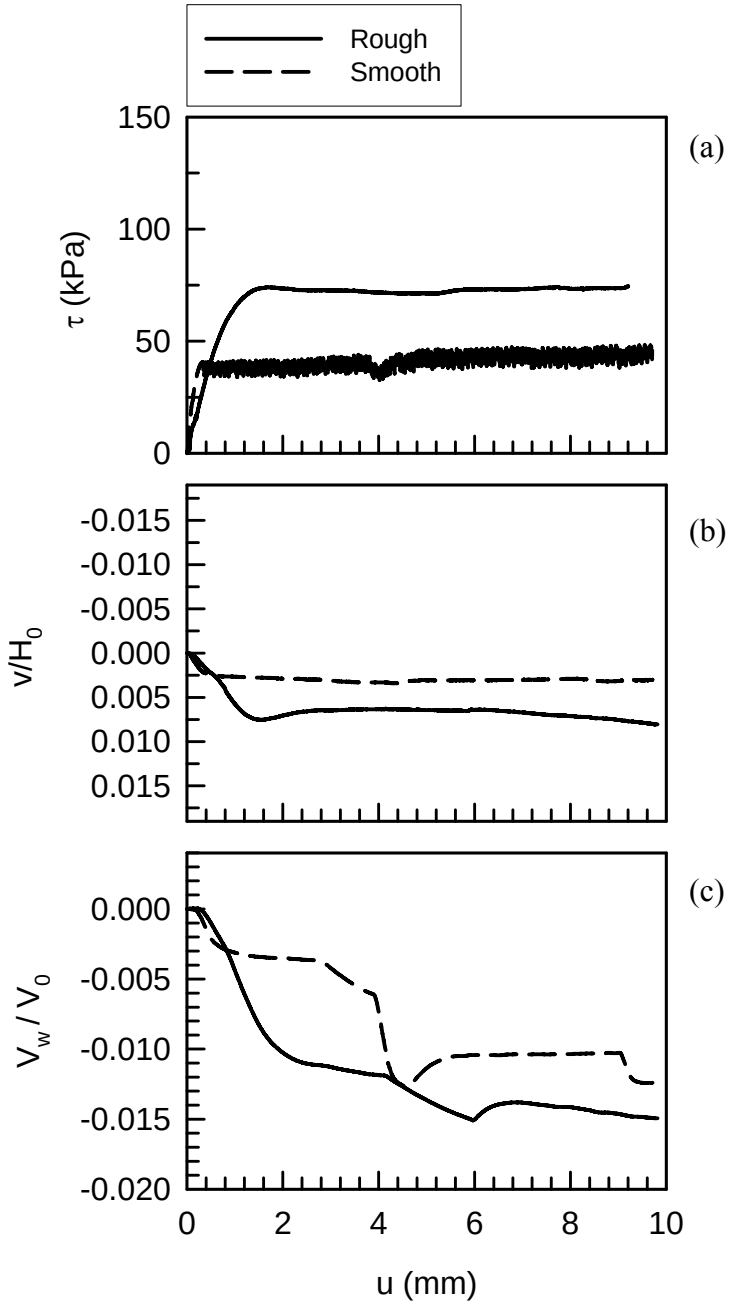

Figure 5.31: Effect of surface roughness on (a) τ, (b) v/H_0, (c) V_w/V_0 during shearing (σ_n-u_a = 105 kPa ; u_a-u_w = 20 kPa)

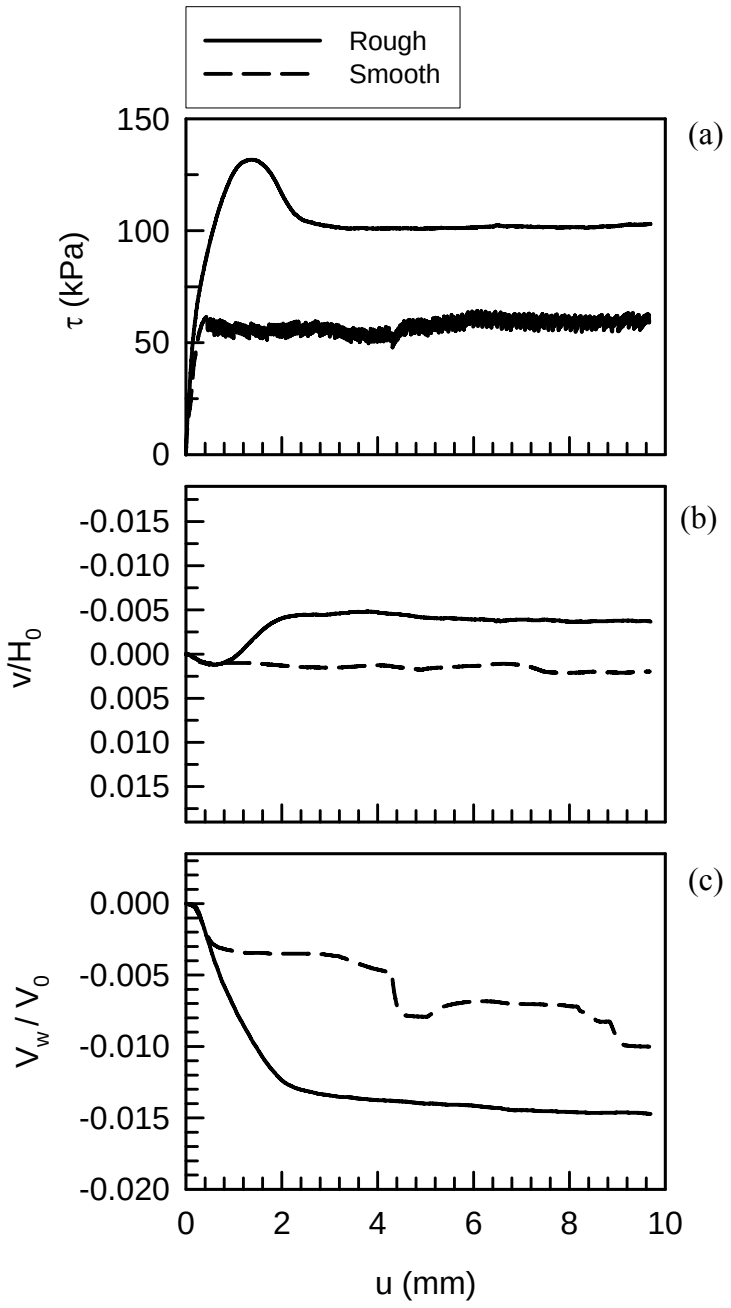

Figure 5.32: Effect of surface roughness on (a) τ, (b) v/H_0, (c) V_w/V_0 during shearing (σ_n-u_a = 140 kPa ; u_a-u_w = 100 kPa)

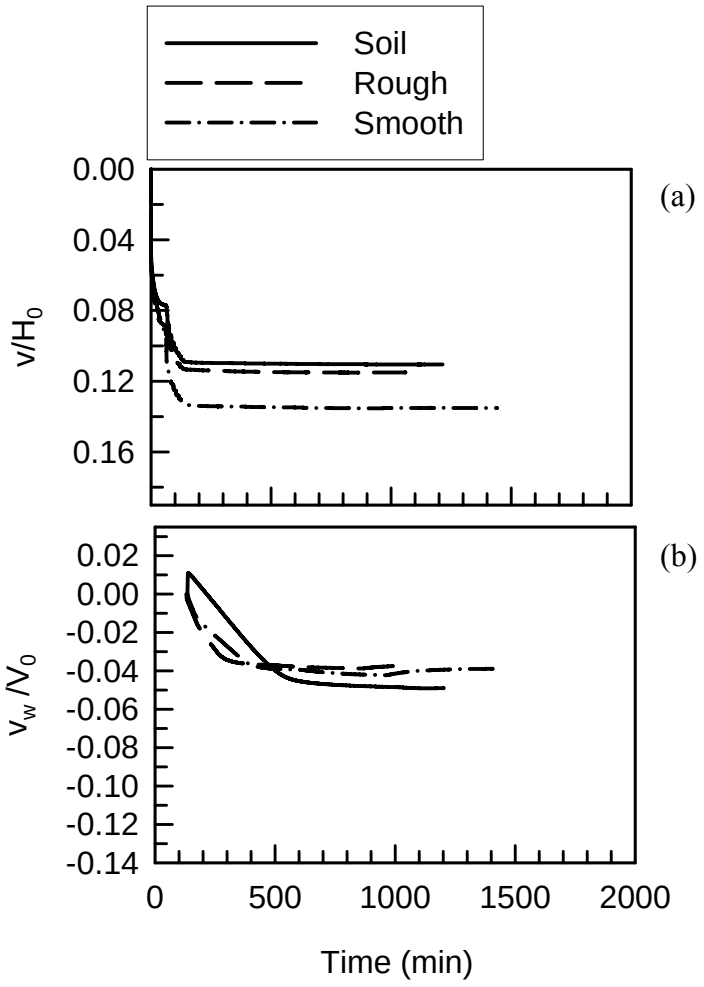

Figure 5.33: Comparison of soil, rough interface and smooth interface test results during equalization phase. σ_n-u_a = 105 kPa; u_a-u_w = 20 kPa

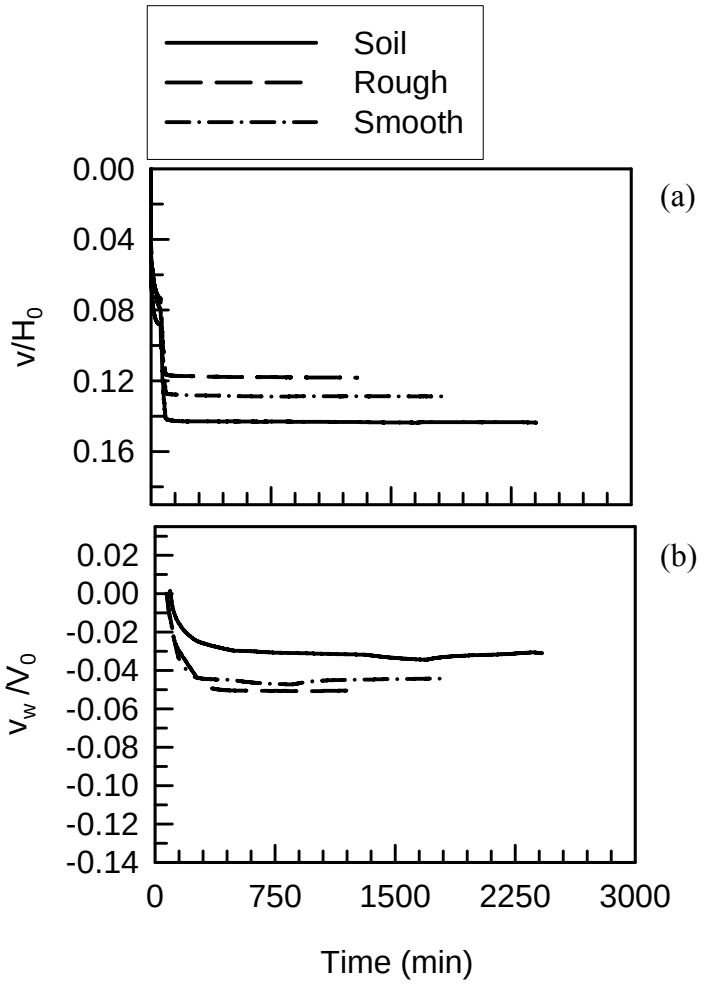

Figure 5.34: Comparison of soil, rough interface and smooth interface test results during equalization phase. σ_n-u_a = 210 kPa; u_a-u_w = 20 kPa

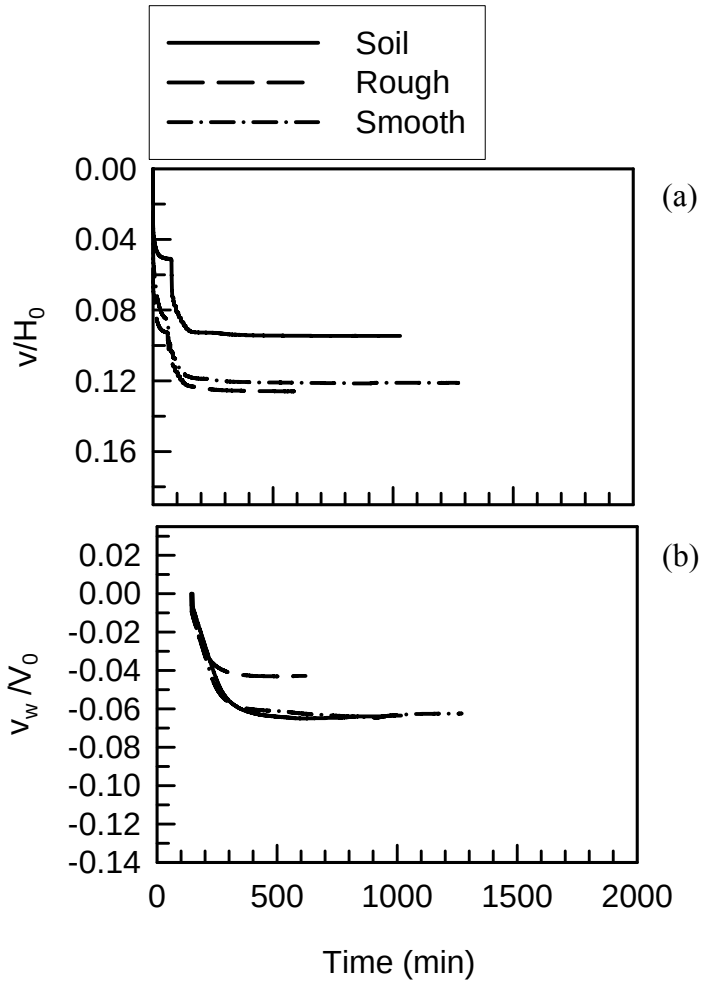

Figure 5.35: Comparison of soil, rough interface and smooth interface test results during equalization phase. σ_n-u_a = 105 kPa; u_a-u_w = 50 kPa

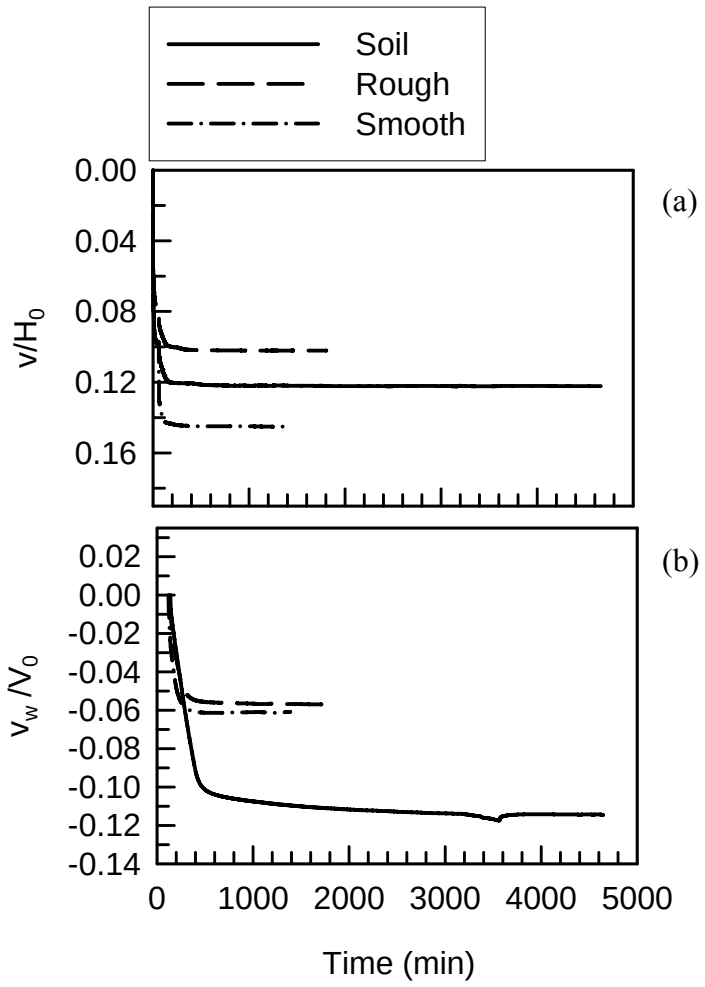

Figure 5.36: Comparison of soil, rough interface and smooth interface test results during equalization phase. σ_n-u_a = 140 kPa; u_a-u_w = 50 kPa

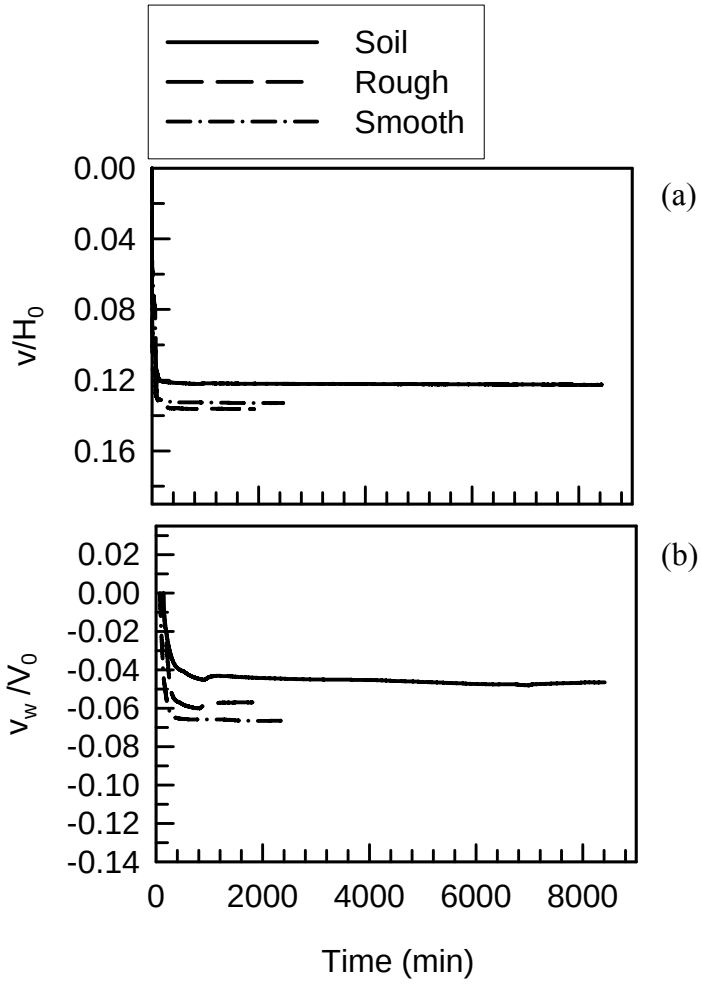

Figure 5.37: Comparison of soil, rough interface and smooth interface test results during equalization phase. σ_n-u_a = 210 kPa; u_a-u_w = 50 kPa

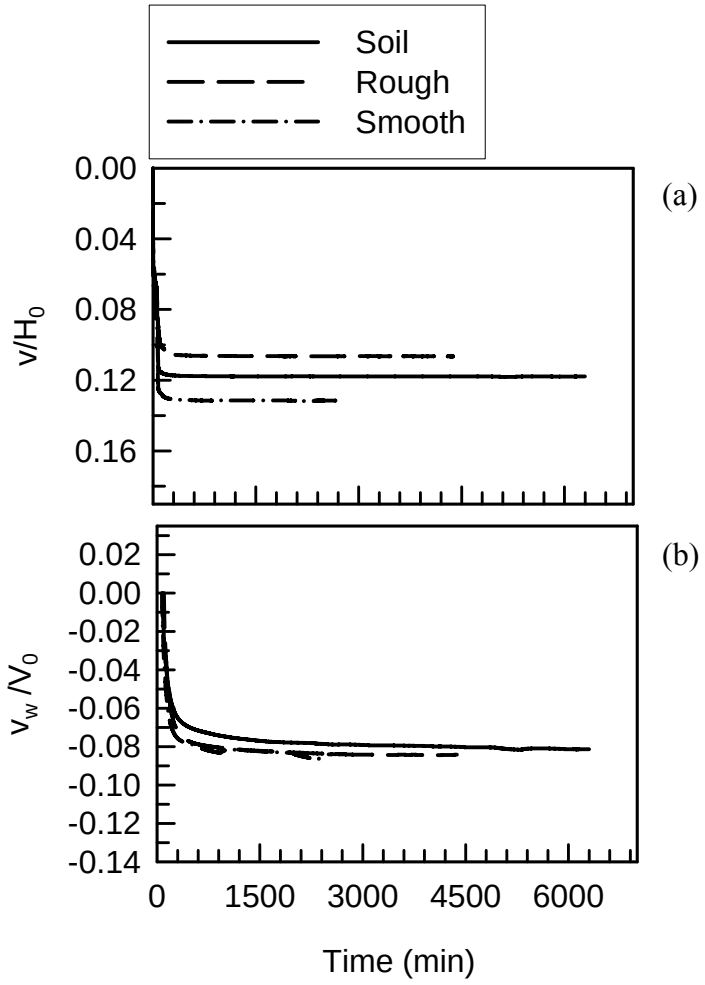

Figure 5.38: Comparison of soil, rough interface and smooth interface test results during equalization phase. σ_n-u_a = 105 kPa; u_a-u_w = 100 kPa

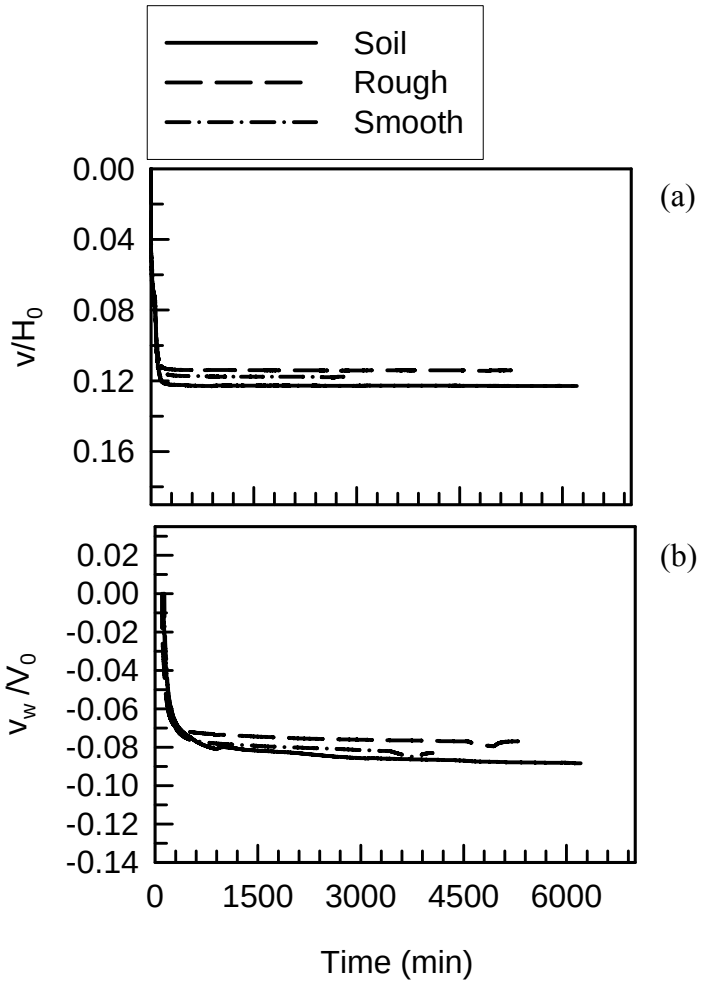

Figure 5.39: Comparison of soil, rough interface and smooth interface test results during equalization phase. σ_n-u_a = 155 kPa; u_a-u_w = 100 kPa

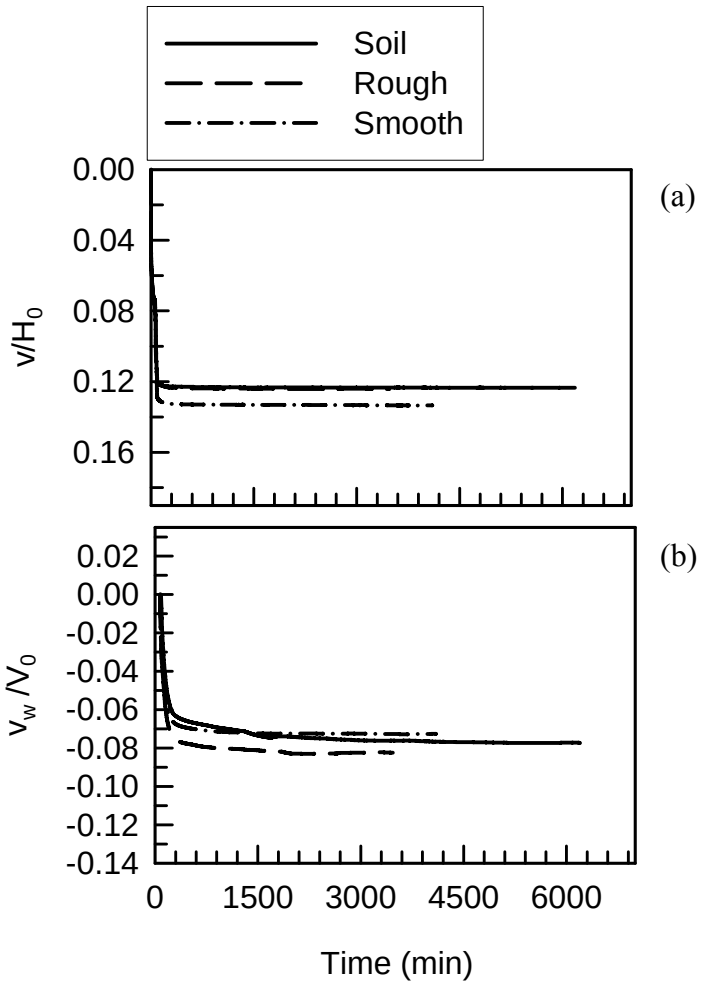

Figure 5.40: Comparison of soil, rough interface and smooth interface test results during equalization phase. σ_n-u_a = 210 kPa; u_a-u_w = 100 kPa

content of samples, variation in sample preparation, and the somewhat random effect of raising the upper half of the box.

In this study all samples were compacted by using a tamping rod to achieve the target dry density; therefore, it is expected that the surface of the samples was not perfectly level and resulting soil asperities may compress differently. Also, the seating load was not applied before the application of vertical load, which could have minimized the effects of an uneven surface. However, the total volume change behavior of soil and interfaces in the equalization phase may be considered, in general, similar in the sense that they all randomly vary approximately in a range of $v/H_0 = 0.14$ to $v/H_0 = 0.9$. Similar to vertical compression, water content at the end of equalization process was also similar in soil and interfaces for a given state of stress. For example, Figs. 5.33b and 5.38b show that approximately same amount of water drained out from the soil and interfaces during the application of target stresses. In Fig. 5.36, results of rough and smooth interfaces show that approximately same amount of water drained at the end of equalization, which is different from the amount of water drained from the soil sample. The soil test shown in Fig. 5.36 was performed without a hydrophobic Teflon membrane; therefore the water volume controller pulled more water from the soil sample than interfaces including water held in the moist porous stone. In general, for a given value of σ_n-u_a and u_a-u_w, water content varied by $\pm$ 1% (refer Table I.1 in Appendix I) this was considered satisfactory, as mentioned before, due to the factors like variation in sample preparation and initial moisture content as well as other uncertainties associated with the experiment. Approximately, similar values of vertical compression and water content for

a given value of σ_n-u_a and u_a-u_w show that prior to shearing, the behavior of soil and interfaces was similar.

Figures 5.41 to 5.48 show the comparison of shearing behavior between soil and interfaces. For u_a-u_w = 20 kPa (Figs. 5.41 and 5.42) the behavior of soil and rough interface is essentially the same in the sense that for both, the volume change and shear strength exhibited steady state after reaching the peak shear strength. However, the smooth interface showed stick-slip behavior after reaching the peak shear strength without showing noticeable change in vertical compression.

In general, the behavior of pore water volume was similar during shearing for soil and interfaces for the range of suction values used in this study. For example, for u_a-u_w = 20 kPa and σ_n-u_a = 105 (Fig. 5.41), the value of water content was approximately similar (Refer Table I.1 in Appendix I) for all three samples (soil, rough and smooth). For u_a-u_w = 20 kPa and σ_n-u_a = 210 (Fig. 5.42), smooth interface showed slightly higher water content (16.45%) than the soil (15.90%) and the rough interface (15.74%).

Results of soil, rough interface and smooth interface for u_a-u_w = 50 kPa are shown in Figs. 5.43 to 5.45. These figures illustrate the difference between the soil and interface behavior. As opposed to results of u_a-u_w = 20 kPa (Figs. 5.41 and 5.42), results presented in Figs. 5.43 to 5.45 show a peak for rough interface followed by strain softening behavior. Based on the results presented in these figures it is postulated that the pre-peak behavior of the rough interface is dictated by the neighboring soil and post peak behavior is influenced by the surface roughness. For example in Fig. 5.44a, the behavior of soil and the rough interface is essentially the same until the horizontal displacement reached

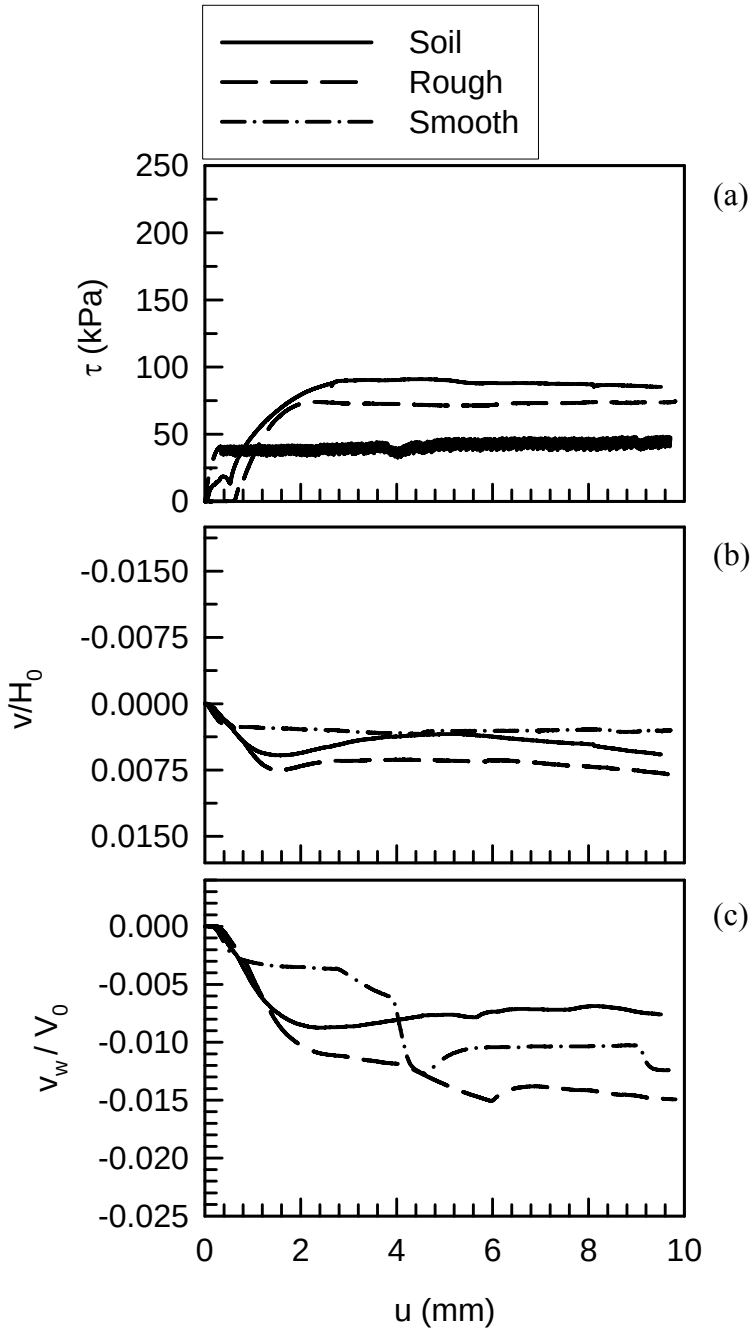

Figure 5.41: Comparison of soil, rough interface and smooth interface test results during shearing phase. σ_n-u_a = 105 kPa; u_a-u_w = 20 kPa

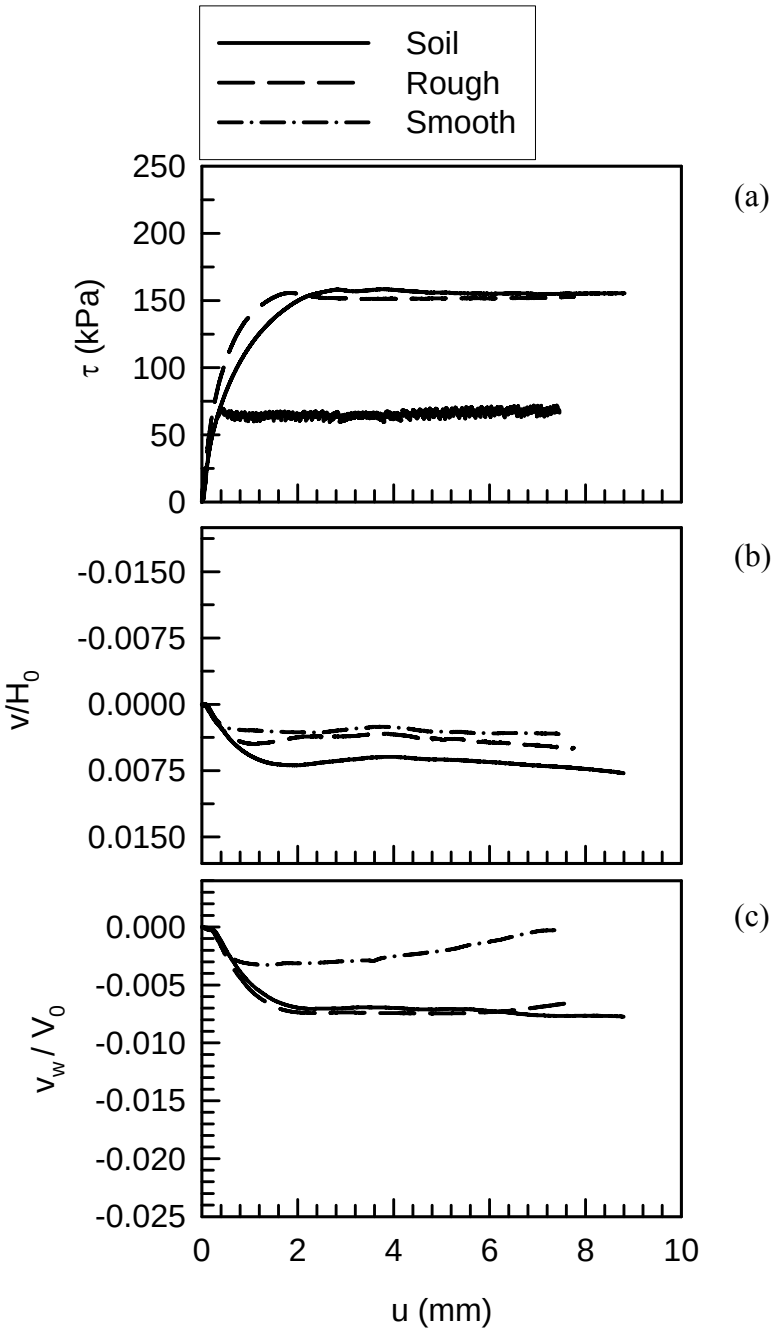

Figure 5.42: Comparison of soil, rough interface and smooth interface test results during shearing phase. σ_n-u_a = 210 kPa; u_a-u_w = 20 kPa

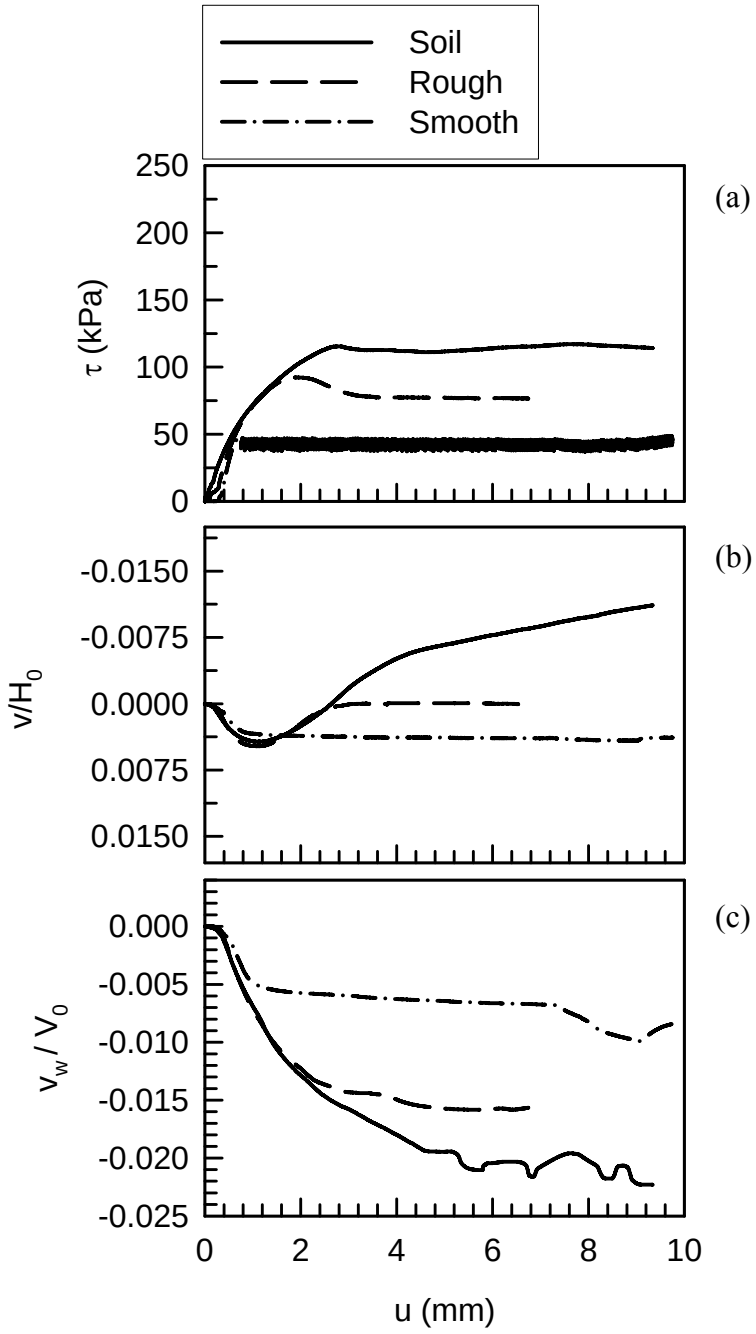

Figure 5.43: Comparison of soil, rough interface and smooth interface test results during shearing phase. σ_n-u_a = 105 kPa; u_a-u_w = 50 kPa

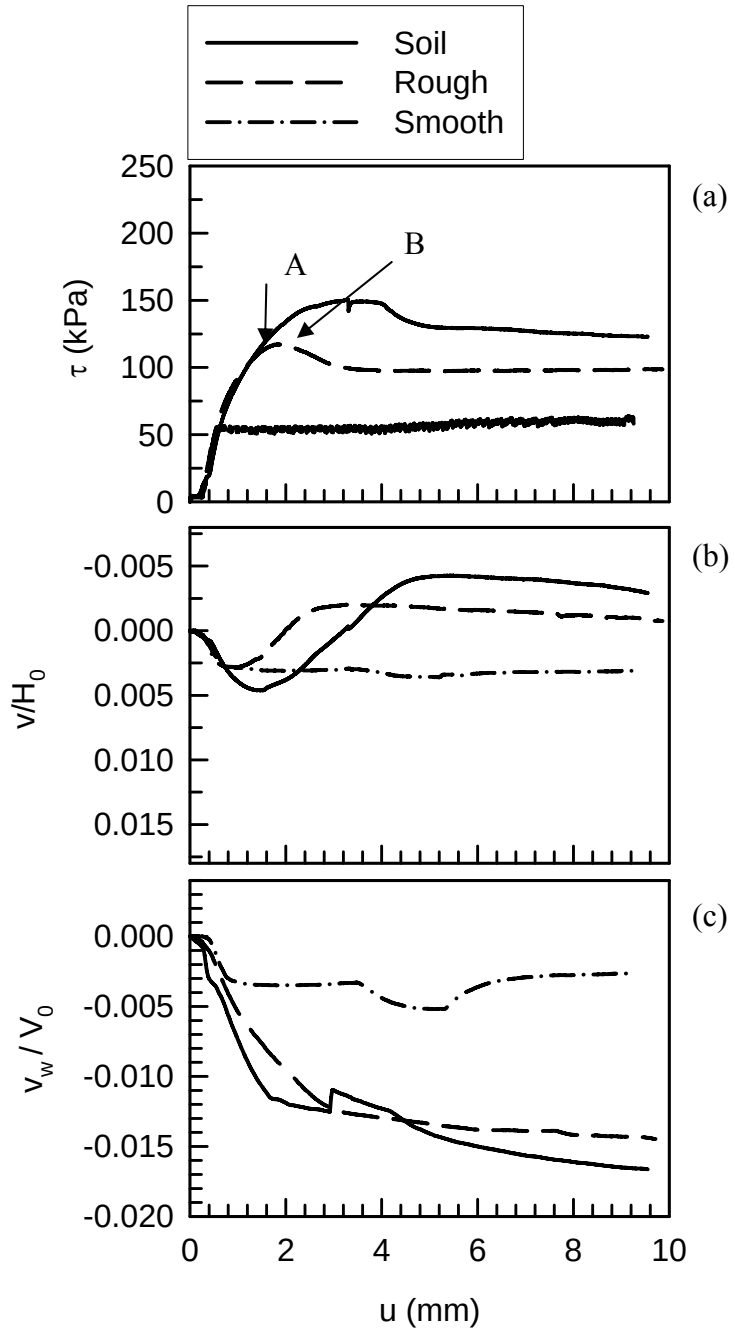

Figure 5.44: Comparison of soil, rough interface and smooth interface test results during shearing phase. σ_n-u_a = 140 kPa; u_a-u_w = 50 kPa

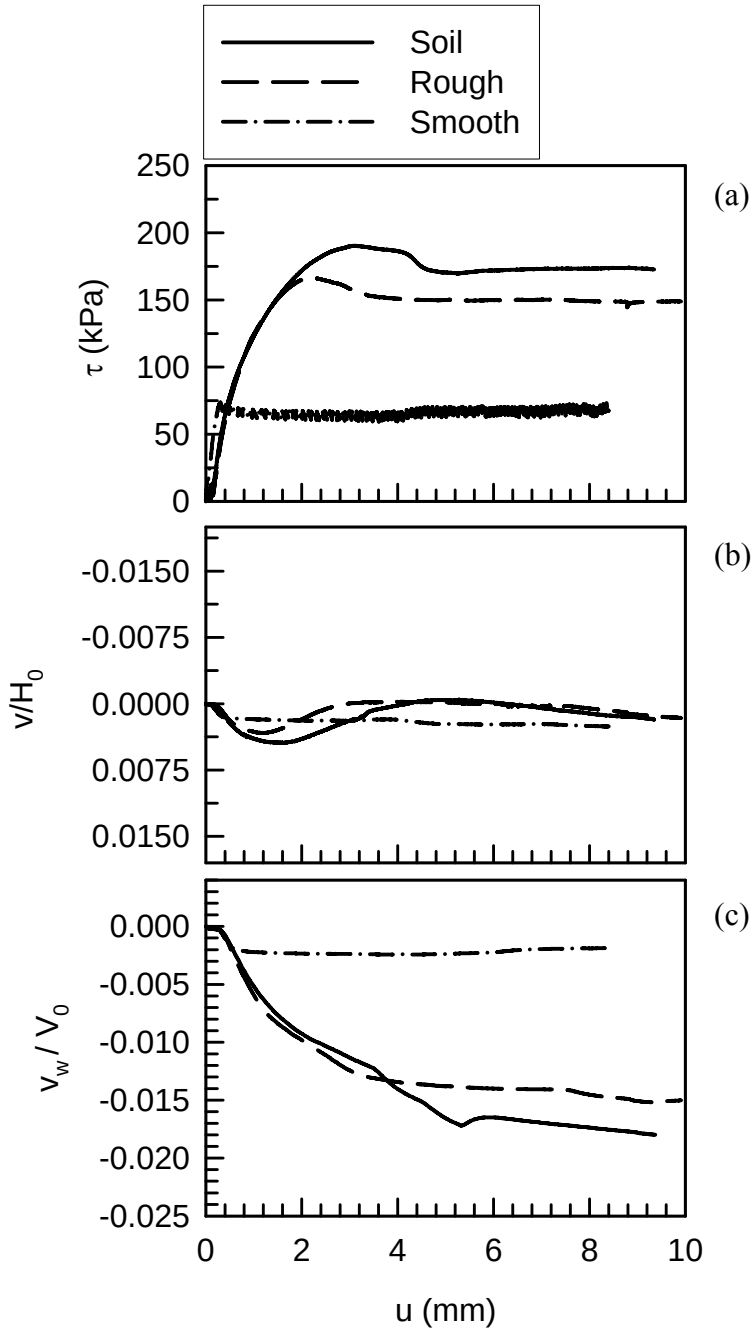

Figure 5.45: Comparison of soil, rough interface and smooth interface test results during shearing phase. σ_n-u_a = 210 kPa; u_a-u_w = 50 kPa

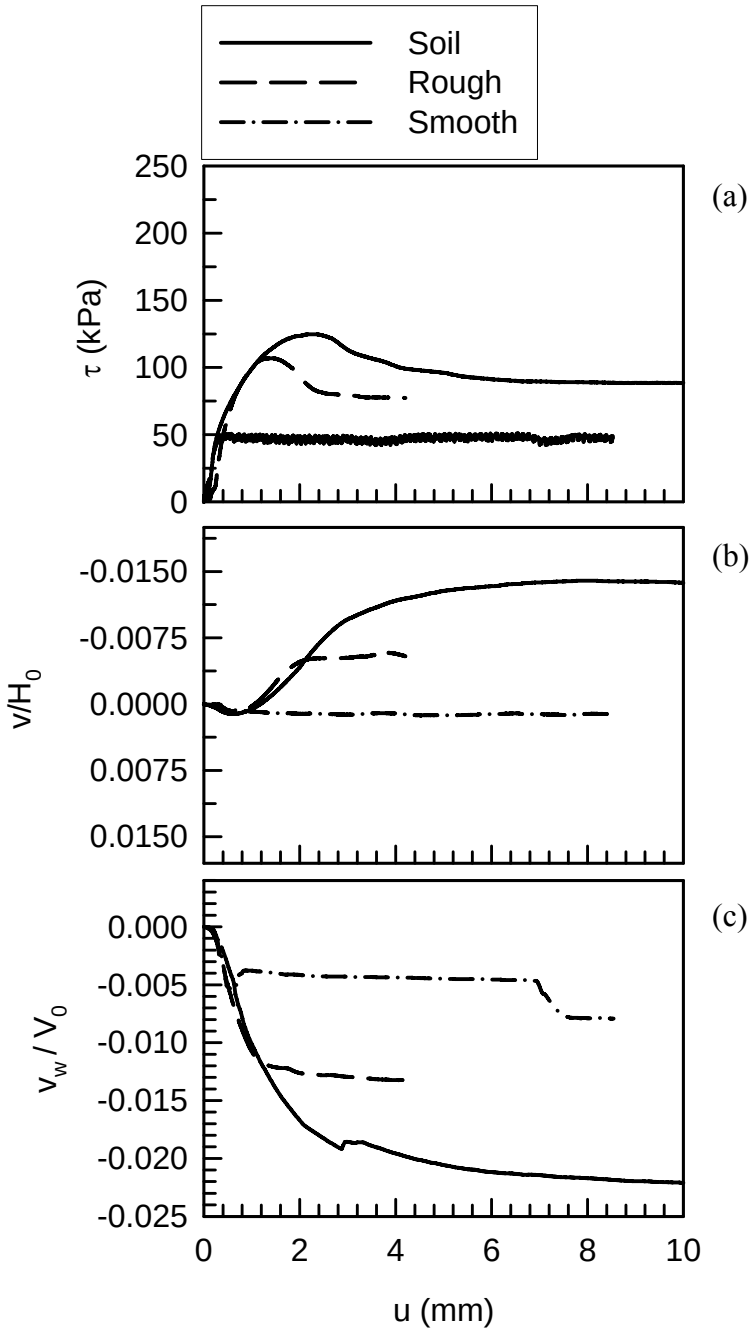

Figure 5.46: Comparison of soil, rough interface and smooth interface test results during shearing phase. σ_n-u_a = 105 kPa; u_a-u_w = 100 kPa

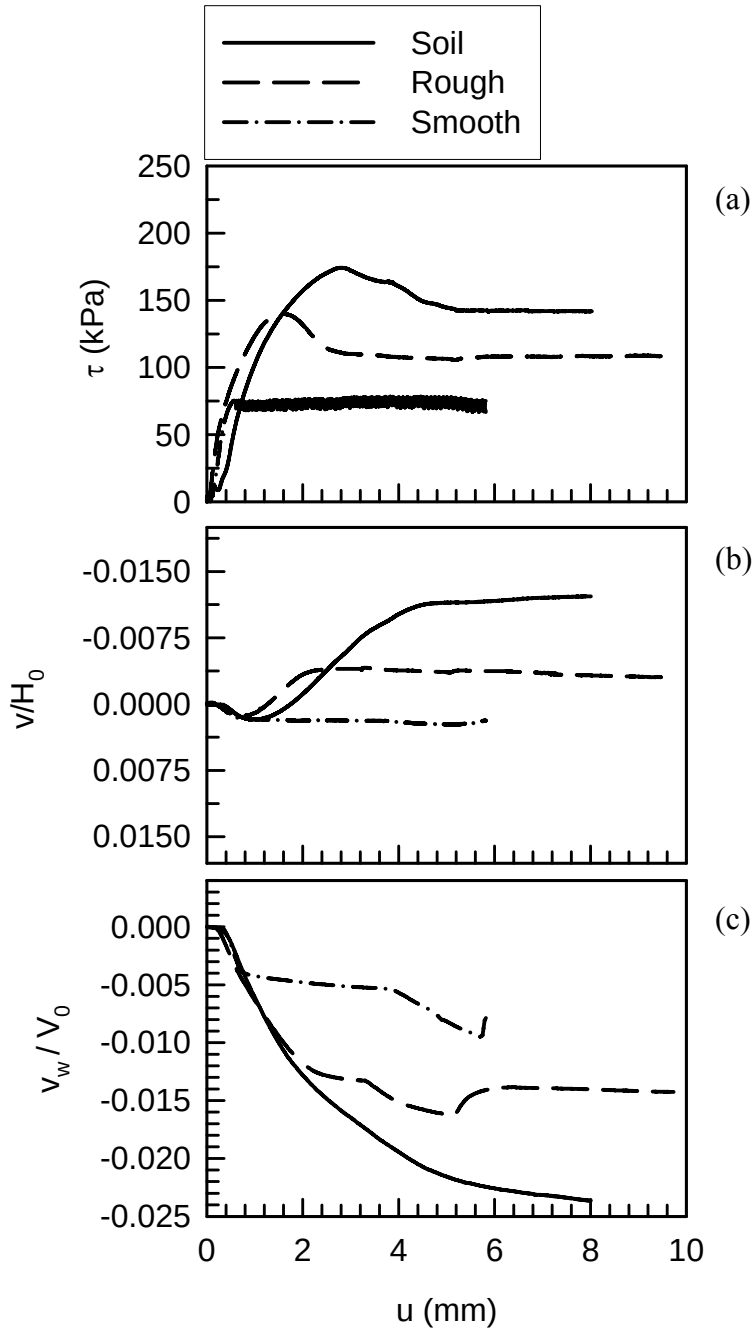

Figure 5.47: Comparison of soil, rough interface and smooth interface test results during shearing phase. σ_n-u_a = 155 kPa; u_a-u_w = 100 kPa

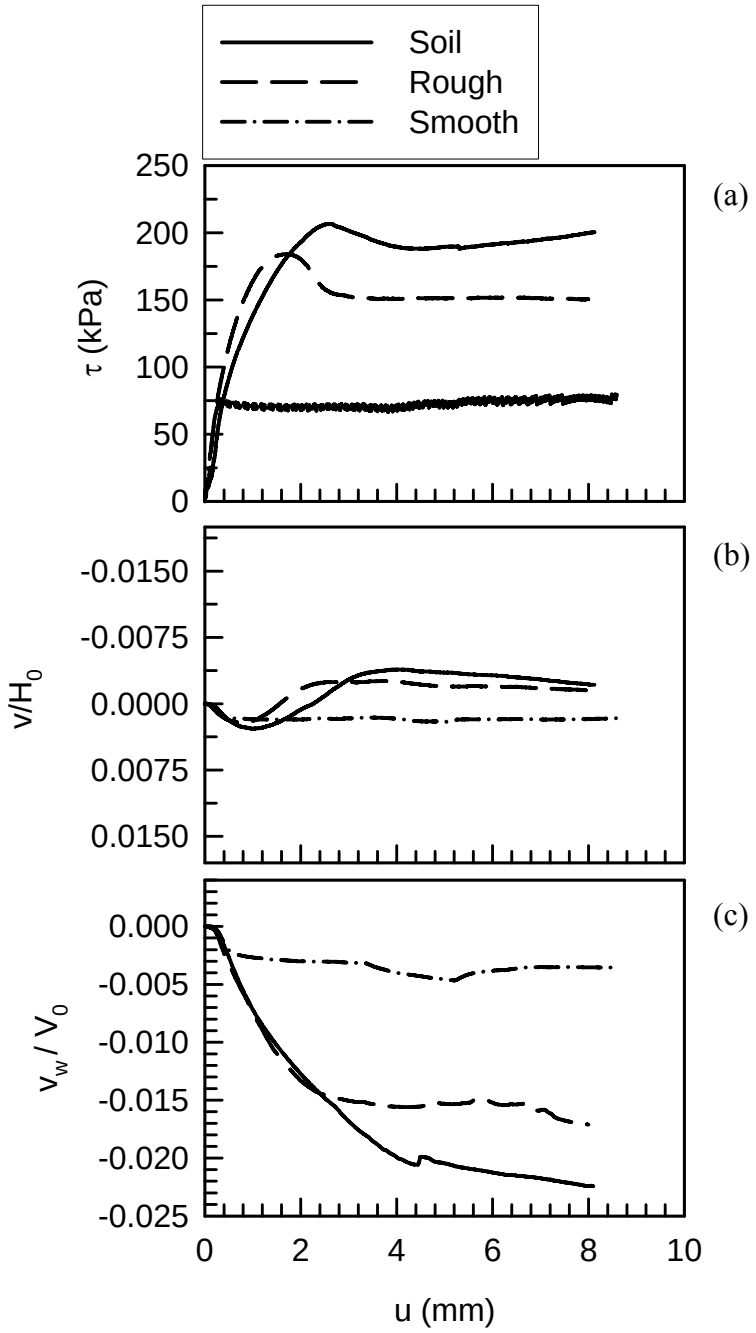

Figure 5.48: Comparison of soil, rough interface and smooth interface test results during shearing phase. σ_n-u_a = 210 kPa; u_a-u_w = 100 kPa

1.57-mm (point A in Fig. 5.44a), i.e., slightly before the peak shear strength. In this region the behavior of the rough interface is controlled by the overlain soil and both have approximately the same stiffness and vertical compression. However, after reaching the peak shear strength (point B in Fig. 5.44a), the behavior of the rough interface deviated from the soil in the sense that rough interface started dilating whereas soil followed compression behavior. In addition to volumetric behavior, rough interface showed strain softening behavior after reaching peak shear strength, i.e., point B in Fig. 5.44a, while the shear stress of soil was still increasing.

The smooth interface exhibited peak shear strength at a smaller horizontal displacement than the rough interface, which implies that the surface roughness started controlling the behavior of the smooth interface at a smaller horizontal displacement than the rough interface. Based on these observations it is postulated that before reaching peak shear strength the shearing behavior of interfaces is similar to the soil. After reaching peak shear stress, the rough interface dilates follows by the steady state behavior whereas smooth interface follows steady state behavior (i.e., no noticeable change in vertical displacement) after reaching peak shear strength.

Although the maximum shear strength of soil was higher than the rough interface for all values of net normal stress and suction, strength behavior of soil and the rough interface was similar in the sense that both showed strain softening behavior followed by steady state. However, the smooth interface showed stick-slip behavior after reaching peak shear strength and the maximum shear strength of smooth interface was less than the soil and rough interface for all states of stress used in this study.

It is postulated in this study that in the direct shear testing of interfaces, the volumetric behavior observed during shearing represents the behavior of interfaces. However, it is important to mention that vertical deformation was measured at the top of the specimen (i.e., not at the interface); therefore, the observed behavior of the interface may exhibit some influence of soil above the interface. Keeping in view the limitations of the interface direct shear device, the above mentioned technique to differentiate the behavior of soil and the interface seems appropriate.

For u_a-u_w = 50 kPa, water content values (Refer Table I.1 in Appendix 1) for soil and rough interface were approximately the same at the end of shearing. For example for u_a-u_w = 50 kPa and σ_n-u_a = 105 kPa, water content values for soil and rough interface were 14.6% and 14.9%, respectively. At the end of shearing, the smooth interface showed slightly higher water content than the soil and rough interface. For example the value of water content was 15.5% for smooth interface for u_a-u_w = 50 kPa and σ_n-u_a = 210 kPa, whereas soil and rough interface showed water content values of 14.6% and 14.8%, respectively.

Similar to tests conducted at 50 kPa suction, peak shear strength and strain softening behavior is obvious for u_a-u_w = 100 kPa (Figs. 5.46-5.48). As observed for u_a-u_w = 50 kPa, the results presented in Figs. 5.46 to 5.48 show that the surface roughness started controlling the behavior of the interface before reaching the peak shear strength. For u_a-u_w = 100 kPa and σ_n-u_a = 210 kPa, soil and rough interface dilated approximately to the same amount. Similar observations can be made for u_a-u_w = 50 kPa and σ_n-u_a = 210 kPa. The behavior of smooth interface when tested under 100 kPa suction was similar to the

tests under u_a-u_w = 20 kPa and 50 kPa suction values (i.e., stick-slip behavior after peak shear strength and steady state after initial compression). Water content values were similar for soil and rough interface for u_a-u_w = 100 kPa (Refer Table I.1 in Appendix I). For example water content values were 13.7% and 13.9%, for u_a-u_w = 100 kPa and σ_n-u_a = 210 kPa, for soil and rough interface, respectively. However, smooth interface showed higher moisture content (15.1%) than the soil and rough interface at the end of shearing for u_a-u_w = 100 kPa and σ_n-u_a = 210 kPa.

5.6 VARIATION OF WATER CONTENT AND DEGREE OF SATURATION

Figure 5.49 shows the variation of water content (w) and degree of saturation (S_r) at different stages of a typical rough interface test. Figure 5.49a shows that all specimens were prepared at approximately the same water content. During compression water squeezed out from the specimen and thickness of the specimen decreased. At this stage the specimen was subjected to the vertical normal stress only and drainage lines were open. It is observed that computed degrees of saturation increased to more than 100 percent (Fig. 5.49b) and water content decreased (Fig. 5.49a) during compression under the application of vertical load (i.e., prior to application of pore air and pore water pressure). Degrees of saturation greater than 100 percent indicate that samples were completely saturated before the application of target net normal stress and suction values and that free water was present at the top of the specimen. However, at the end of equalization the water content and degree of saturation both decreased and the reduction of w and S_r is consistent with the target suction values. This figure also illustrates that during the shearing stage the water content of specimens decreased. Figures 5.50 and 5.51 show the variation in w and S_r at various stages of the smooth interface and soil

tests, respectively. Similar observations were made for rough (Fig. 5.51) and smooth interfaces and soil. Figures 5.49, 5.50 and 5.51 also illustrate that water content and degree of saturation decreased with increase in suction.

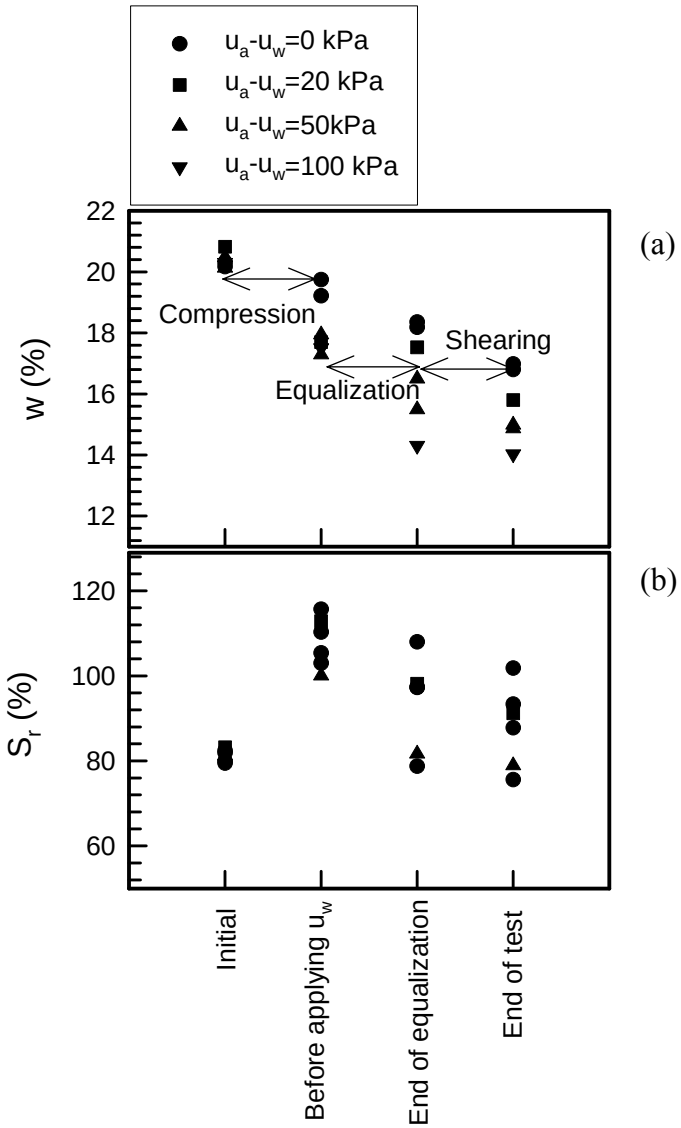

Figure 5.49: Variation of w and S_r at various stages of rough interface tests. (σ_n-u_a = 105 kPa)

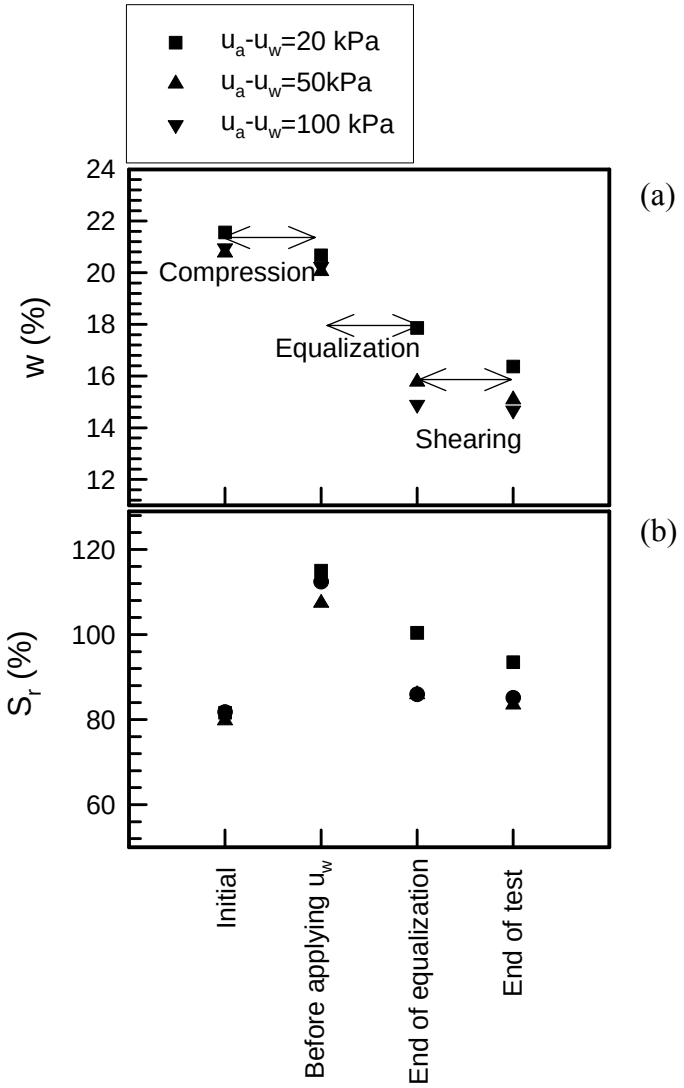

Figure 5.50: Variation of w and S_r at various stages of smooth interface tests. (σ_n-u_a = 105 kPa)

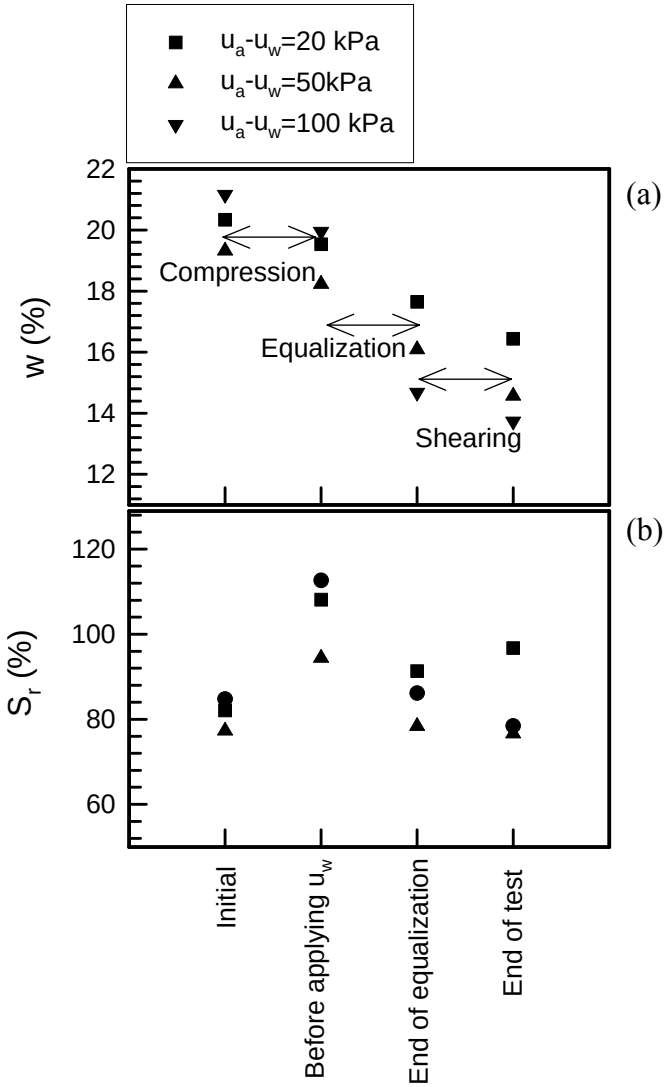

Figure 5.51: Variation of w and S_r at various stages of soil tests. (σ_n-u_a = 105 kPa)

CHAPTER VI

EXTENDED MOHR- COULOMB FAILURE CRITERION

6.1 EXTENDED MOHR-COULOMB FAILURE CRITERION FOR INTERFACES IN UNSATURATED SOIL

For saturated soils the shear strength on a plane can be represented as a function of the effective stress normal to that plane as given by the following Mohr-Coulomb failure model,

$$\tau = \sigma_n^{'} \tan\phi' + c' \qquad (6.1)$$

where:
τ = shear strength or shear stress on the failure plane at failure,
$\sigma_n^{'}$ = effective stress normal to the failure plane at failure = $\sigma_n - u_w$,
σ_n = total stress normal to the failure plane at failure,
u_w = pore water pressure at failure,
ϕ' = effective angle of internal friction, and
c' = effective cohesion.

Equation 6.1 has been successfully applied to the prediction of strength of soil-structure interfaces (e.g., pile skin friction) where drained conditions are assumed to prevail, as in the following form (e.g., Chandler 1968),

$$f_s = \sigma_{hc}^{'} \tan\delta^{'} + c_a \qquad (6.2)$$

where:

$\sigma_{hc}^{'} = K_c \sigma_{v0}^{'}$ = effective lateral stress on the pile,
K_c = lateral stress ratio,
$\sigma_{v0}^{'}$ = initial vertical effective stress before pile installation,
δ' = the interface friction angle, and
c_a = the cohesion intercept.

The state of stress for the unsaturated soil can be described by using two stress variables (σ_n-u_a, and u_a-u_w) as shown on an extended Mohr-Coulomb failure envelope in Fig. 6.1. The equation corresponding to the limit or failure conditions (i.e. shear strength equation) can be written as,

$$\tau = c' + (\sigma_n - u_a)\tan\phi' + (u_a - u_w)\tan\phi^b \qquad (6.3)$$

where:

c' = effective cohesion intercept,
ϕ' = effective angle of internal friction with respect to the $(\sigma_n - u_a)$,
ϕ^b = angle of internal friction with respect to $(u_a - u_w)$,
σ_n = total stress normal to the failure plane at failure,
u_a = pore-air pressure on the failure plane at failure,
u_w = pore-water pressure on the failure plane at failure, and
τ = shear stress on the failure plane at failure or shear strength.

Equation 6.3 can be written in a form similar to that used for saturated soils:

$$\tau = c + (\sigma_n - u_a)\tan\phi' \qquad (6.4)$$

The total cohesion, c, is written as

$$c = c' + (u_a - u_w)\tan\phi^b \qquad (6.5)$$

The plot of Equation 6.4 is shown in Fig. 6.1 (b).

It was postulated in this study that unsaturated interface shear strength (e.g., skin friction on pile in unsaturated soil) can be represented by an equation of a form similar to Equation 6.3, following the similarity between Equation 6.1 and 6.2. Thus an, expression for interface shear strength in unsaturated soils is proposed as:

$$\tau_s = c_a^{'} + (\sigma_n - u_a)\tan\delta^{'} + (u_a - u_w)\tan\delta^b \qquad (6.6)$$

where:

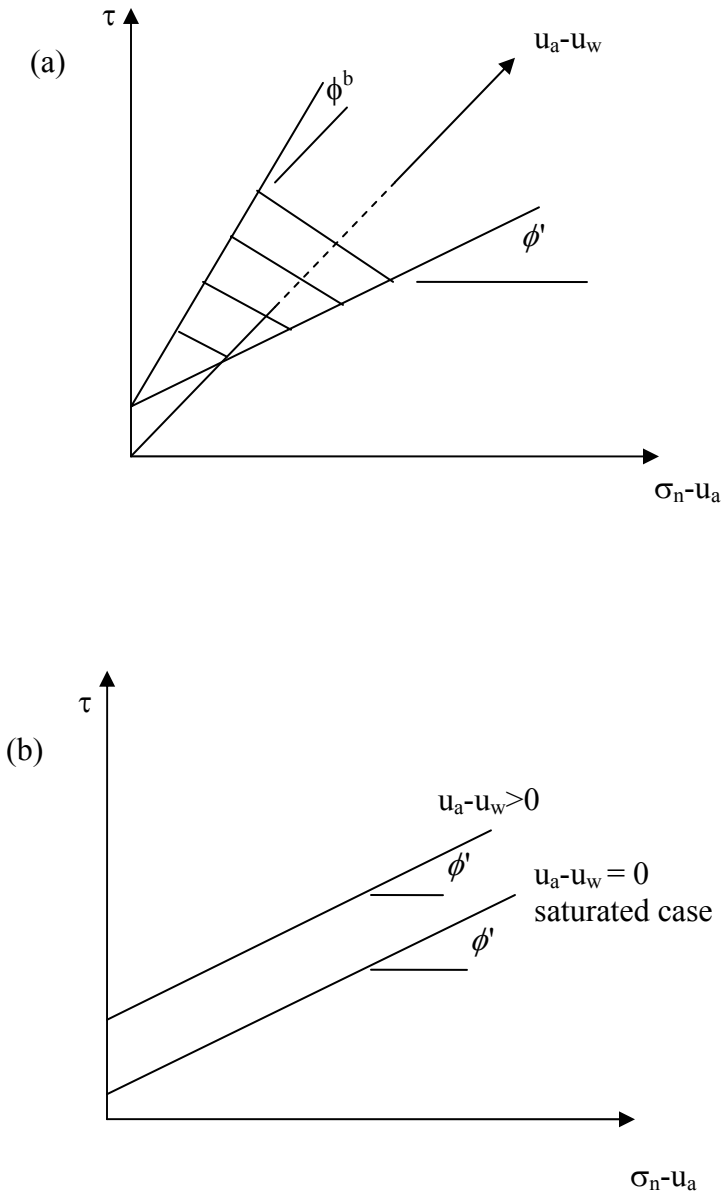

Figure 6.1: Failure envelope for unsaturated soil. (a) Extended Mohr-Coulomb failure envelope; (b) Failure envelope projection on the net normal stress plane

$c_a^{'}$ = adhesion intercept
σ_n = normal stress on the interface at the failure,
u_a = pore air pressure at failure,
δ' = the angle of friction between soil and counterface with respect to (σ_n-u_a),
u_w = pore water pressure at failure,
δ^b = the angle of friction between soil and counterface with respect to (u_a-u_w), and
u_a-u_w = s, matric suction at failure.

Equation 6.6 is a more general form for shear strength of an interface in that it also models saturated conditions, where $u_a = u_w$ and $c_a^{'}$ and δ' are effective stress strength parameters (analogus to c′ and ϕ′ for saturated soil); in this case Equation 6.6 becomes the same as Equation 6.2. Using the same equation form as unsaturated soil for unsaturated interfaces has the advantage that the extended Mohr-Coulomb failure envelope and other concepts can easily be modified to accommodate interface shear strength. It is simply necessary to remember that unsaturated shear strength parameters c_a and δ are determined from the unsaturated interface shear strength tests.

6.2 DETERMINATION OF UNSATURATED INTERFACE SHEAR STRENGTH PARAMETERS

Plots of shear stress, τ, versus net normal stress, σ_n-u_a, corresponding to failure, for soil, rough, and smooth interfaces are shown in Figs. 6.2a, b, and c, respectively. The peak shear stress was used as the shear stress at failure. The lines plotted through the data points in Fig. 6.2 form Mohr-Coulomb failure envelopes for the unsaturated soil and interface. Mohr-Coulomb failure envelopes shown in Fig. 6.2 represent the frontal plane of extended Mohr-Coulomb failure envelope graph shown in Fig. 6.1. Slopes and intercepts of these envelopes are presented in Tables 6.1 and 6.2 for soil and interfaces,

respectively. For soil, slope of the failure envelope is denoted by ϕ' and intercept is denoted by c. For interfaces, the slope of the failure envelope on τ versus (σ_n-u_a) plane is denoted by δ', whereas, the intercept of this failure envelope yields the values of adhesion of interface (c_a).

In Figures 6.3a, b, and c, the same results shown in Figure 6.2a, b, and c, are redrawn, but plotting the abscissa as (u_a-u_w). Each curve of Fig. 6.2a, b, and c corresponds to a different value of σ_n-u_a. For soil (Fig. 6.3a), the slope of the failure envelope in τ- (u_a-u_w) plane yields angle of internal friction with respect to suction and is denoted by ϕ^b and intercept of the plot indicates cohesion with respect to suction and is denoted by c''. For interfaces the slope of the failure envelope on τ versus (u_a-u_w) plane is denoted by δ^b (i.e. angle of friction between soil and counterface), whereas, the intercept of this failure envelope yields adhesion of interface (c_a''). The values of slopes and intercepts of these plots are summarized in Tables 6.3 and 6.4.

6.3 DISCUSSION OF TEST RESULTS

In Fig. 6.2 variation in shear strength with σ_n-u_a is represented in all cases (soil, rough, smooth) by straight lines. Fredlund et al. (1978) assumed that the failure envelopes for different values of (u_a-u_w) are parallel. However, for soil (Fig. 6.2a), a tendency for divergence can be observed ($\phi' = 32.5^0$, 35.2^0, 37.5^0 for u_a-u_w = 20, 50, 100 kPa, respectively). This indicates that angle of internal friction ϕ' is not constant but changes with change in suction. However, considering the experimental error such as variation in sample preparation and initial moisture content, failure envelopes can be assumed parallel

Table 6.1: Unsaturated shear strength parameters (c, ϕ') for different suction values.

	u_a-u_w	c	ϕ'	R^2
	(kPa)	(kPa)	(Degree)	
Soil	20	26.4	32.5	0.9868
	50	44.4	35.2	0.9849
	100	47.6	37.5	0.9827

Table 6.2: Unsaturated interface shear strength parameters (c_a, δ') for different suction values.

Interface Type	u_a-u_w	c_a	δ'	R^2
	(kPa)	(kPa)	(Degree)	
Rough Interface	20	-2. 8	37.3	0.9900
	50	18.2	35.2	1.0000
	100	28.1	36.4	0.9992
Smooth Interface	20	10.4	15.2	0.9747
	50	23.3	13.2	1.0000
	100	26.7	13.4	0.9900

Table 6.3: Unsaturated shear strength parameters (c'', ϕ^b) for different σ_n-u_a values.

	σ_n-u_a	c''	ϕ^b	R^2
	(kPa)	(kPa)	(Degree)	
Soil	105	87.6	21.9	0.8647
	210	103.2	29.6	0.8790

Table 6.4: Unsaturated interface shear strength parameters (c_a'', δ^b) for different σ_n-u_a values.

Interface Type	σ_n-u_a	c_a''	δ^b	R^2
	(kPa)	(kPa)	(Degree)	
Rough Interface	105	68.4	21.6	0.9603
	140	103.2	15.1	0.9993
	210	148.4	19.5	1.0000
Smooth Interface	105	39.7	6.7	0.8624
	140	43.9	10.6	0.9008
	210	66.9	5. 5	0.9764

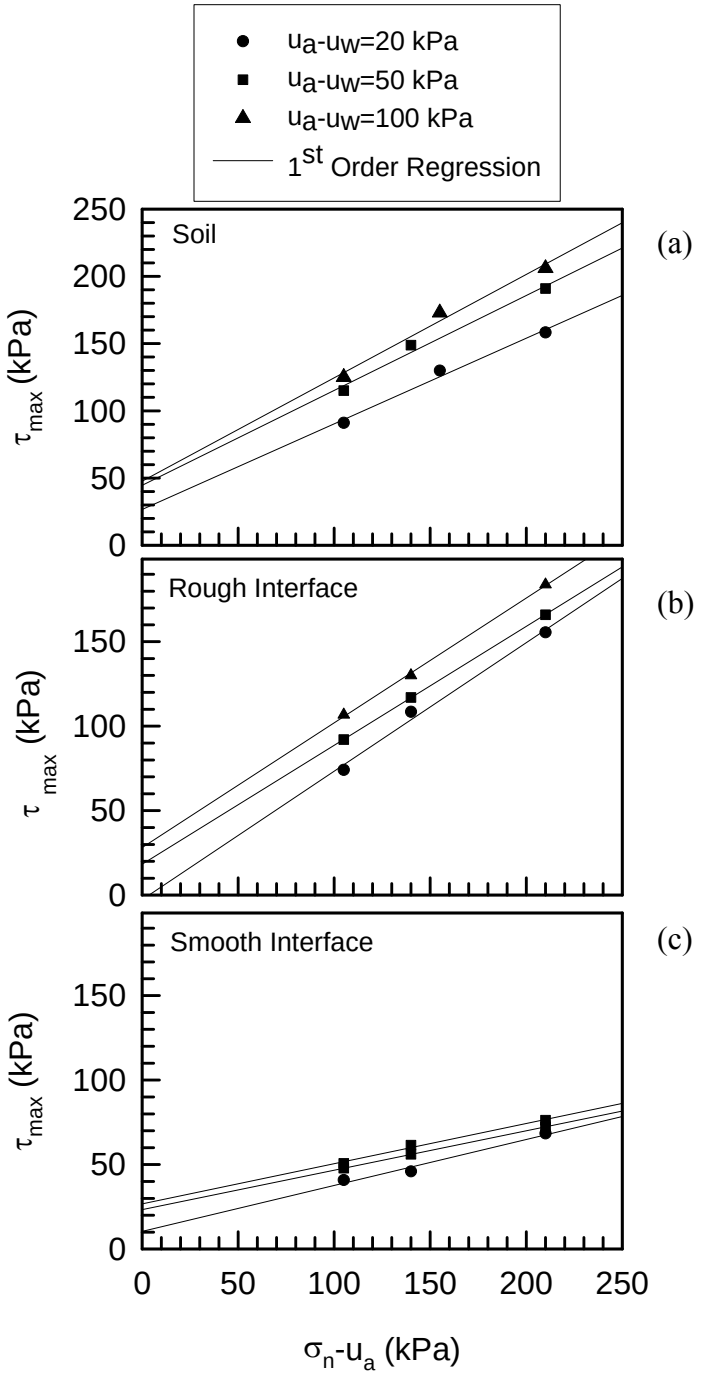

Figure 6.2: Failure envelope projections from unsaturated (a) soil, (b) rough, and (c) smooth interface direct shear tests on (σ_n-u_a)-τ_{max} plane

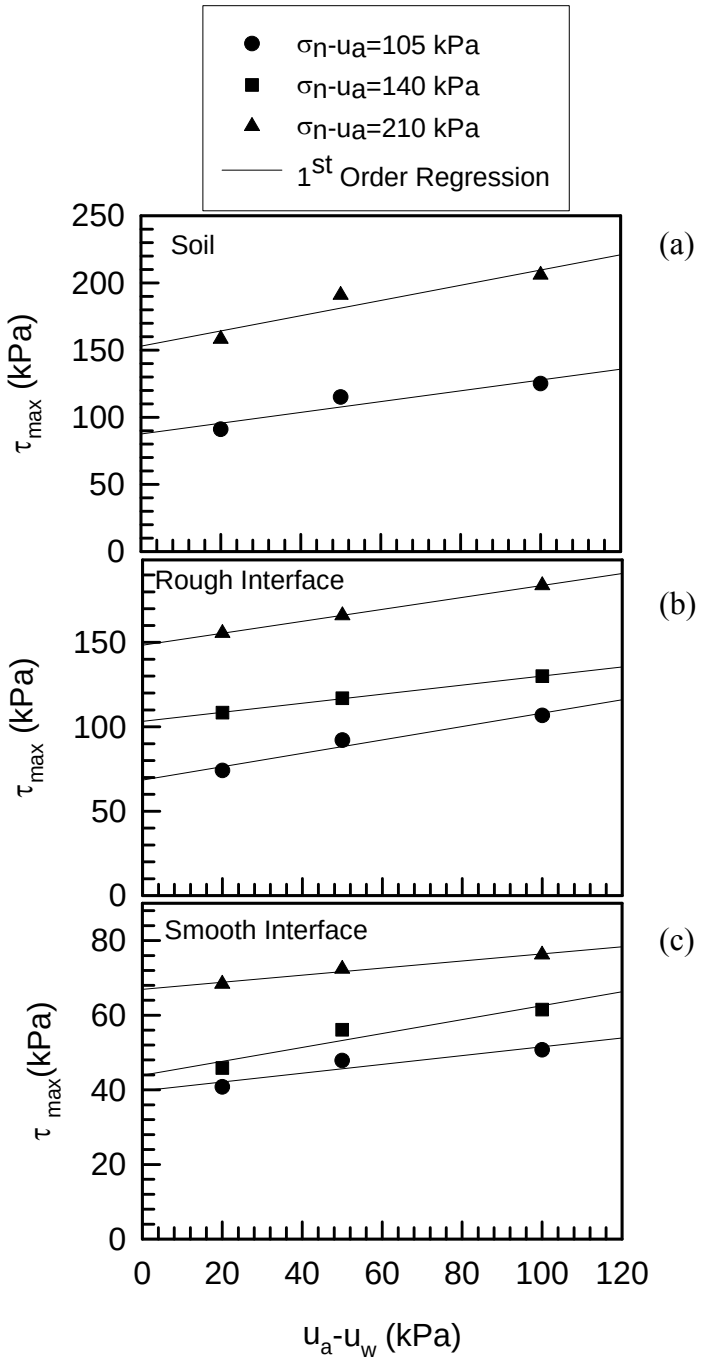

Figure 6.3: Failure envelope projections from unsaturated (a) soil, (b) rough, and (c) smooth interface direct shear tests on (u_a-u_w)-τ_{max} plane

(i.e., constant ϕ'). It can also be noticed that the intercepts of failure envelopes with the shear strength axis increase as suction increases, which indicates an increase in cohesion.

For rough and smooth interfaces, failure envelopes are approximately parallel and it is postulated that the above stated assumption of Fredlund et al. (1978) (i.e., failure envelopes for different values of (u_a-u_w) are parallel) is also valid for interfaces.

A comparison of Figures 6.2a and 6.2b shows that the values of ϕ' and δ' are approximately the same for all values of suction used in this study (also see Tables 6.1 and 6.2). However, cohesion (c) of soil is greater than adhesion (c_a) of the rough interface. This can be explained by considering the different shear failure mechanisms in soil and interface.

Shear strength of soil consists of two parts: interlocking and cohesion. Shear strength contributed by interlocking is represented by the angle of internal friction and effective cohesion represents the part of the shear strength contributed by the cohesion (physico-chemical bonding between soil grains).

In the case of a rough interface, interlocking exists at two levels; the first level of interlocking exists between the soil grains of thin layer adjacent to the counterface and the second level of interlocking exists between rough counterface and soil grains. Identical values of ϕ' and δ' indicates that interlocking between rough surface and soil grains was approximately similar to interlocking between soil grains in the thin layer of soil adjacent to the rough surface.

As can be seen from the data presented in Tables 6.1 and 6.2, cohesion, c, of soil is greater than adhesion, c_a, of rough interface, which implies that the bonding due to

physico-chemical and capillary forces between the soil grains is stronger than the bonding between the soil and rough steel plate.

For the case of the smooth interface, the values of δ' and c_a are much smaller than values of ϕ' and c, which indicates that interlocking between smooth surface and soil grains is weaker than interlocking between soil grains themselves. Similarly, adhesion forces between soil and smooth steel surface are weaker than the cohesion forces between the soil particles. Therefore, the failure occurred between soil layer and smooth steel plate.

However, the values of adhesion (c_a) of the smooth interface are greater than the values of c_a for the rough interface, which indicates stronger physico-chemical bonding of soil grains with the smooth surface. Failure mechanisms of rough and smooth interfaces that may explain these differences are discussed in Section 6.5 of this chapter.

Figure 6.3a presents the plot of τ versus u_a-u_w for soil. The failure envelope is assumed linear and 1st order regression is performed to calculate the value of ϕ^b and c′′. The slope of failure envelopes changes with changing (σ_n-u_a); the greater the net normal stress (σ_n-u_a), the steeper the failure envelope. This means that the effect of suction is more pronounced at high net normal stress. However, the same graph is redrawn in Fig. 6.4a and nonlinearity can be easily observed. An increase in matric suction results in reduction of pore water; therefore, the increase in shear strength with increasing matric suction gradually decreases due to the reduced interfacial area between soil particles and water. Theoretically at very high matric suction, when soil becomes dry, matric suction will not affect the shear strength of soil at all. The nonlinearity (curvature) of τ versus (u_a-u_w) has

also been observed by other researchers (e.g. Escario and Saez 1986; Fredlund et al. 1987).

Shear strength (τ) versus matric suction (u_a-u_w) relationship for rough and smooth interfaces is shown in Figs. 6.3b and 6.3c, respectively. Failure envelopes are obtained by performing linear regressions and values of slope (δ^b) and intercept (c_a'') are given in Table 6.4. Similar to soil, nonlinearity of these failure envelopes is obvious in Figs. 6.4b and 6.4c and nonlinearity decreases with increasing σ_n-u_a.

A comparison of Figs.6.3a, b, and c shows that the suction effect is more pronounced for soil than interfaces. As is shown in Table 6.3 and 6.4, ϕ^b and c'' are greater than δ^b and c_a'' for all values of (σ_n-u_a) used in this study (see Tables 6.3 and 6.4). Smaller values of δ^b and c_a'' as compared to ϕ^b and c'' suggest that bonding due to menisci between soil and counterface is not as strong as between soil grains themselves. This phenomenon may be attributed to the differences between surface chemistry of counterface and soil grains.

The angle of friction, δ^b, and adhesion, c_a'', between soil and rough surface are greater than the values of δ^b and c_a'' of the smooth interface for all values of (σ_n-u_a) used in this study. This trend shows the effect of surface roughness on δ^b and c_a''; for a given value of suction, the rough interface has larger value of δ^b than the smooth counterface.

Effect of suction on residual shear strength of rough and smooth interfaces is shown in Figures 6.5a and 6.5b, respectively. These figures illustrate that unlike maximum shear

strength, residual shear strength does not change with change in suction. This phenomenon can be explained as follows:

As the suction is applied, air enters the spaces between the rough plate and soil grains and water is squeezed out. At this stage water forms a meniscus at the contact point of grain and counterface. This meniscus creates a bond between soil grain and counterface. This bonding force, called the capillary force, acts perpendicular to the contact point of counterface and soil grain. The relationship between suction and capillary forces has been discussed in detail by Kohgo et al. (1993). Sliding will occur between soil grains and counterface when the applied horizontal force overcomes the interlocking and capillary forces.

Once the soil grains starts sliding over the counterface the meniscus between the counterface and soil grain is broken and capillary forces become negligible. Therefore, the residual stress is not affected by the suction values. In other words, after the peak shear stress the bond between the counterface and soil grains is broken and at this stage the meniscus does not exist. Constant residual shear strength regardless of the suction value is the direct consequence of meniscus breaking.

Residual adhesion ($c''_{a\,,\,\text{residual}}$) between steel plate (rough and smooth, both) and soil increased with increase in net normal stress. However, angle of friction ($\delta^{b}_{\text{residual}}$) between steel plate and soil with respect to suction remained nearly constant and almost zero with increase in net normal stress (Fig. 6.6).

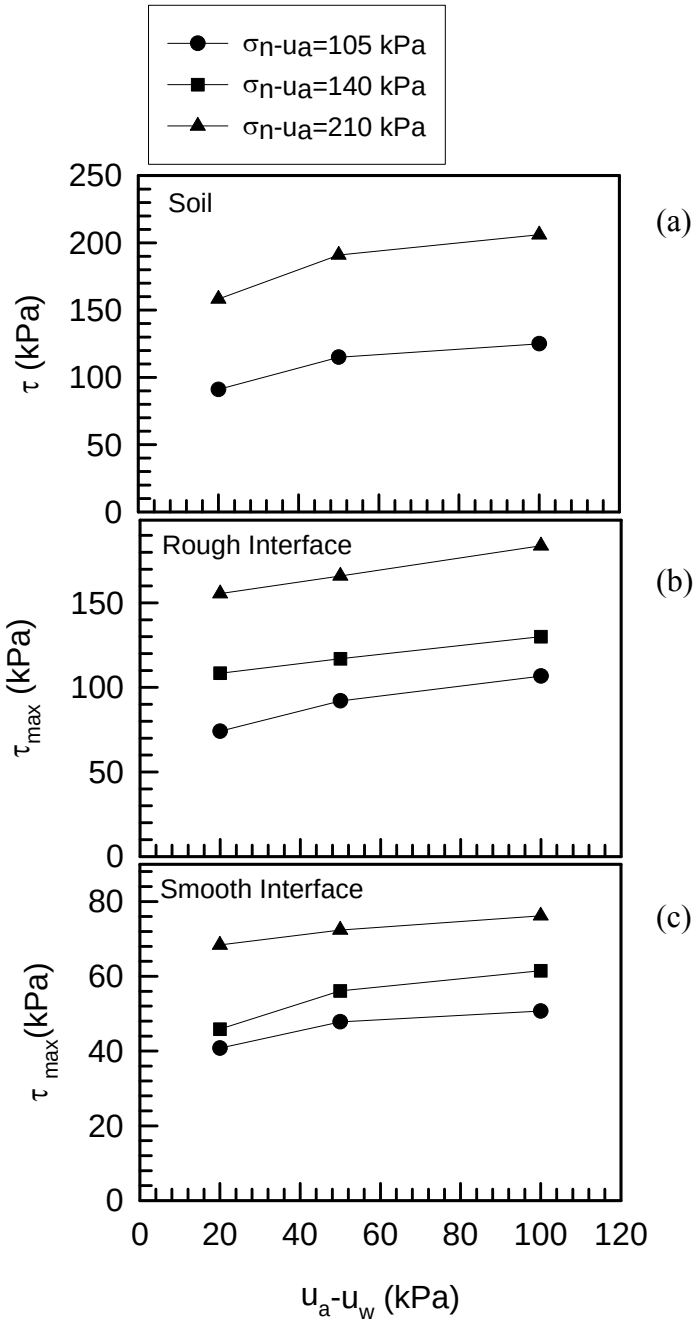

Figure 6.4: Nonlinear failure envelope projections from unsaturated (a) soil, (b) rough, and (c) smooth interface direct shear tests on (u_a-u_w)-τ_{max} plane

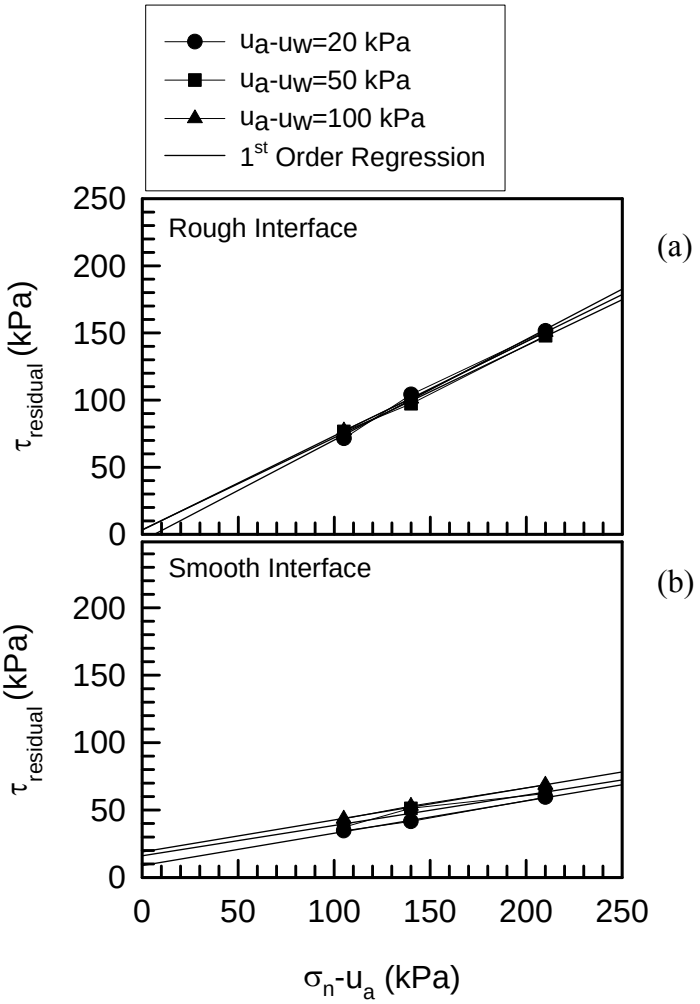

Figure 6.5: Failure envelope projections for unsaturated (a) rough and (b) smooth interfaces on (σ_n-u_a)-$\tau_{residual}$ plane

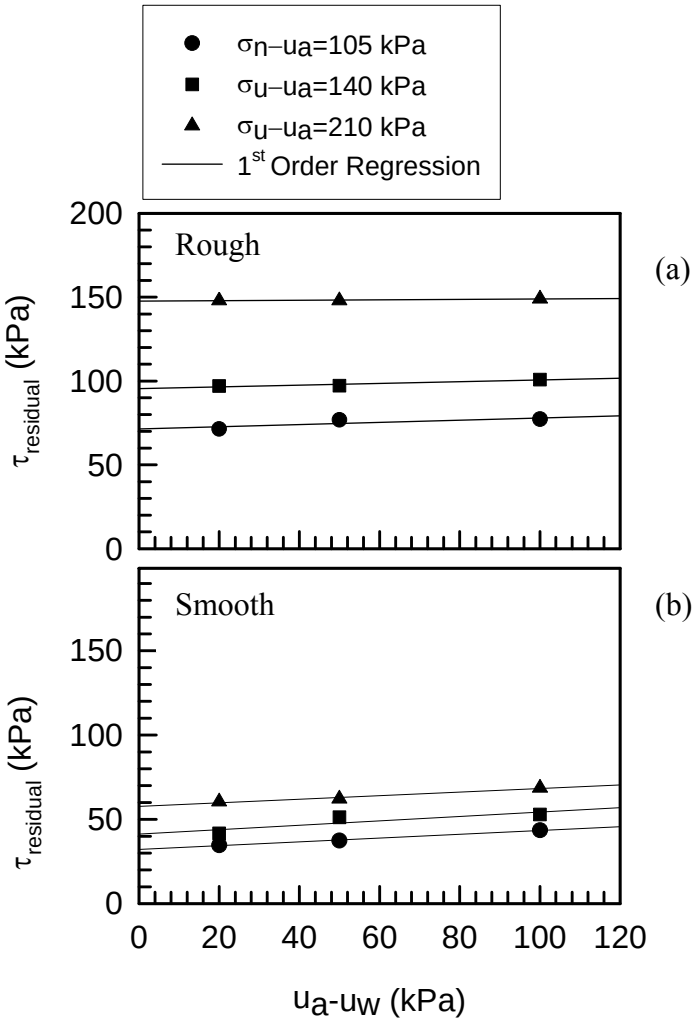

Figure 6.6: Failure envelope projections for unsaturated (a) rough and (b) smooth interface on (u_a-u_w)-$\tau_{residual}$ plane

6.4 DETREMINATION OF EXTENDED MOHR-COULOMB ENVELOPE STRENGTH PARAMETERS

In this study a simplified approach was adopted to determine the effective cohesion/adhesion corresponding to zero suction. As mentioned in the previous section, failure envelope projections on (u_a-u_w)-τ_{max} planes were not linear; however, considering the experimental errors such as variation in sample preparation and initial water content, failure envelopes are assumed to be linear. To verify the observed nonlinearity in experimental data further testing and study is required. Based on the assumption that failure envelopes are linear, an average value of the angle of internal friction was used as the slope of failure envelopes of soil and interfaces. Best fit lines (failure envelopes) were drawn through experimental data points using average values of ϕ', ϕ^b, δ', and δ^b. In Figs. 6.7-6.12, original data points obtained from the soil, the rough interface, and the smooth interface are shown and best fit lines are shown using thick solid lines in Figs. 6.7-6.12. Slopes and intercepts of these best fit lines are summarized in Table 6.5.

The intercepts of best fit lines (i.e., the value of c'', c_a'') of Figs. 6.7-6.9 are plotted as ordinate and u_a-u_w as abscissa in Fig. 6.13. Intercepts and slopes of lines shown in Fig. 6.13 represent the effective cohesion/adhesion corresponding to $\sigma_n-u_a = 0$ kPa and angle of internal friction ϕ^b, δ^b, respectively, and their values are given in Table 6.6.

In Fig. 6.14, the intercepts of best fit lines (i.e., the values of c, c_a) of Figs. 6.10-6.12 are plotted as ordinate and σ_n-u_a as abscissa. Intercepts and slopes of lines shown in Fig. 6.14 represent the effective cohesion/adhesion corresponding to $\sigma_n-u_a = 0$ kPa and angles of internal friction (ϕ',δ'), respectively, and their values are given in Table 6.7.

Theoretically, the intercept values ($c', c_a^{'}$) given in Tables 6.6 and 6.7 should be identical; however, a small difference is obvious in the values of c′, $c_a^{'}$ when the experimental data is plotted in (u_a-u_w)-τ_{max} plane. This difference may be attributed to the nonlinear behavior of the soil and the interface with increasing suction. Due to this uncertainty, failure envelopes plotted in (σ_n-u_a)-τ_{max} plane are more appropriate than failure envelopes plotted in (u_a-u_w) - τ_{max} plane for the determination of the effective cohesion/adhesion. Based on this assumption the values of effective cohesion given in Table 6.7 are considered as representative values of the Minco Silt used in this study. Equations 6.3 (for soil) and 6.6 (for interface) are given below with shear strength parameter values determined in this study for Minco Silt and interfaces between Minco Silt and steel.

$$\tau = 14 + (\sigma_n - u_a)\tan(34.5^0) + (u_a - u_w)\tan(26.6^0) \qquad (6.7) \quad \text{(For Soil)}$$

$$\tau = 0 + (\sigma_n - u_a)\tan(35.5^0) + (u_a - u_w)\tan(17.7^0) \qquad (6.8) \quad \text{(For rough interface)}$$

$$\tau = 10 + (\sigma_n - u_a)\tan(15^0) + (u_a - u_w)\tan(8.9^0) \qquad (6.9) \quad \text{(For smooth interface)}$$

Table 6.5: Values of unsaturated shear strength parameters from best fit lines shown in Figs. 6.7-6.12.

	ϕ', δ'	c, c_a (kPa)			ϕ^b, δ^b	c'', c_a'' (kPa)			
		u_a-u_w				σ_n-u_a			
		20	50	100		105	140	155	210
	(DEGREES)	(kPa)	(kPa)	(kPa)	(Degrees)	(kPa)	(kPa)	(kPa)	(kPa)
Soil	35.1	17	45	59	24.9	88	-	118	160
Rough	36.3	2	15	28	18.7	75	100	-	150
Smooth	13.9	13	21	26	7.6	40	47	-	66

Table 6.6: Values of effective cohesion/adhesion corresponding to σ_n-u_a = 0 kPa and angle of internal friction (u_a-u_w)-τ_{max} plane.

	ϕ^b, δ^b	c', c_a' (kPa)
	(Degrees)	(kPa)
Soil	26.6	12
Rough	17.7	-3
Smooth	8.9	11

Table 6.7: Values of effective cohesion/adhesion corresponding to u_a-u_w = 0 kPa and angle of internal friction (σ_n-u_a)-τ_{max} plane.

	ϕ' , δ'	c' , c_a' (kPa)
	(Degrees)	(kPa)
Soil	34.5	14
Rough	35.5	0
Smooth	15.0	10

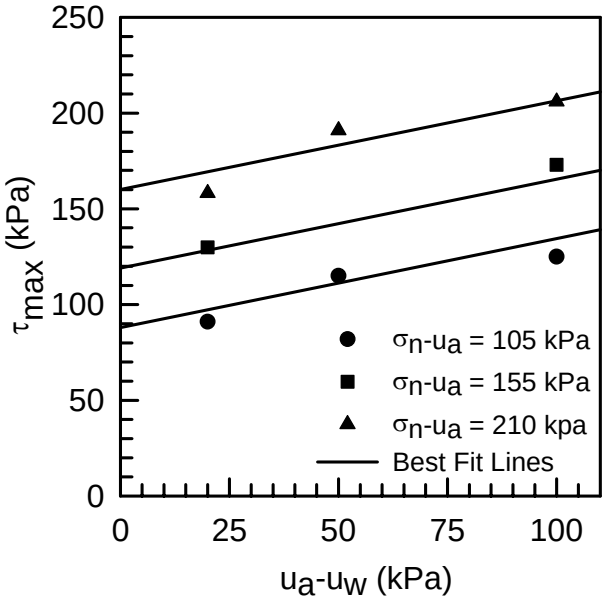

Figure 6.7: Experimental data points from soil tests and best fit lines to determine the values of c″ and ϕ^b

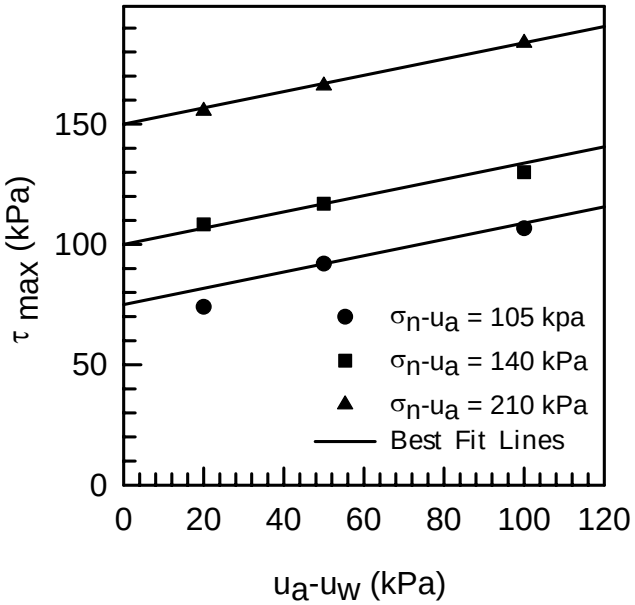

Figure 6.8: Experimental data points from rough interface tests and best fit lines to determine the values of c_a'' and δ^b

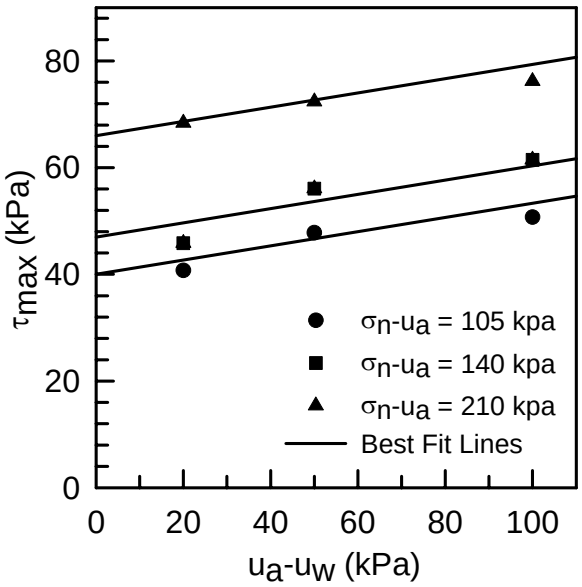

Figure 6.9: Experimental data points from smooth interface tests and best fit lines to determine the values of $c_{a''}$ and δ^b

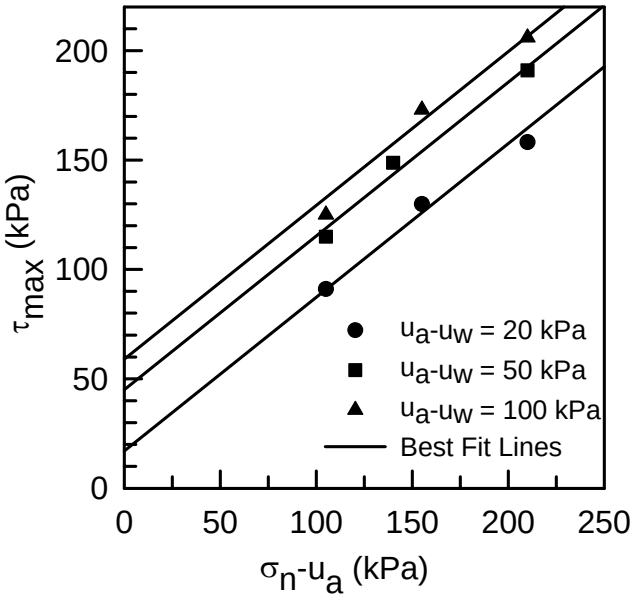

Figure 6.10: Experimental data points from soil tests and best fit lines to determine the values of c and ϕ'

.

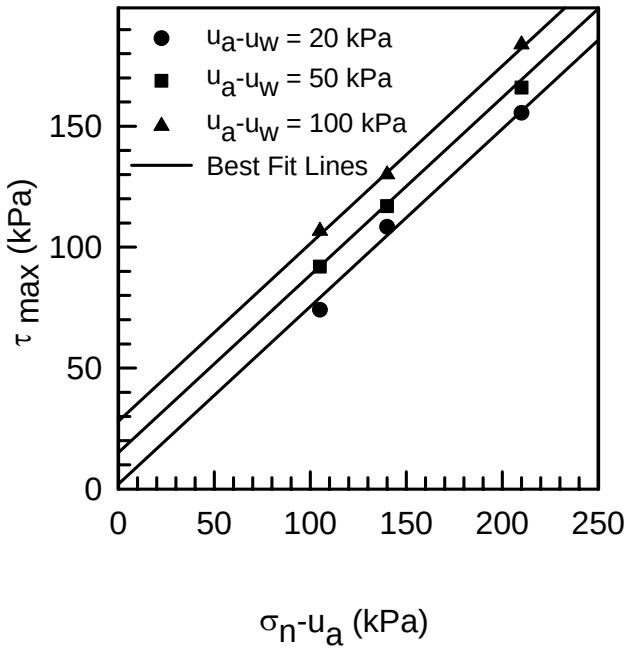

Figure 6.11: Experimental data points from rough interface tests and best fit lines to determine the values of c_a and δ

.

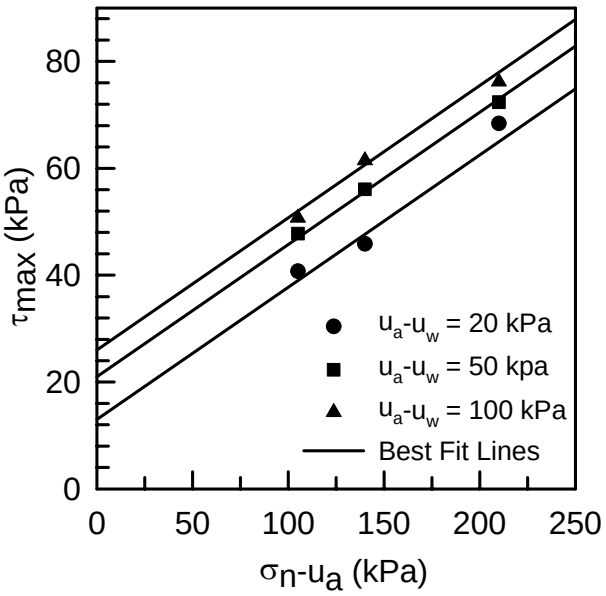

Figure 6.12: Experimental data points from smooth interface tests and best fit lines to determine the values of c_a and δ

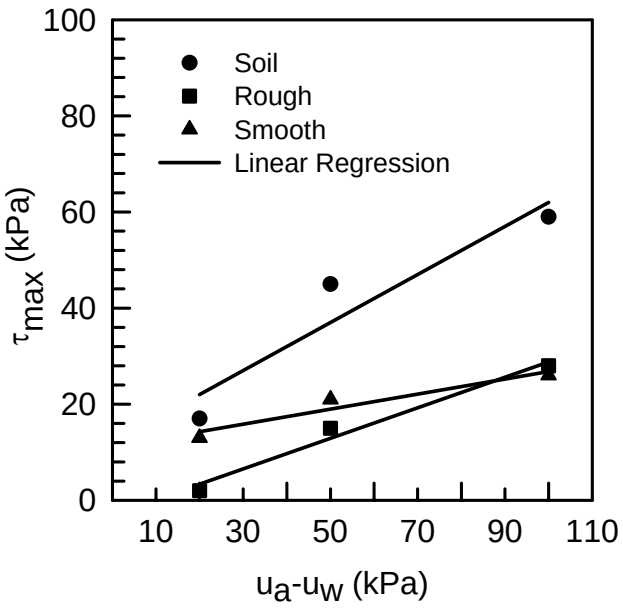

Figure 6.13: Failure envelope for the determination of effective cohesion in (u_a-u_w)-τ_{max} plane ($\sigma_n-u_a = 0$ kPa)

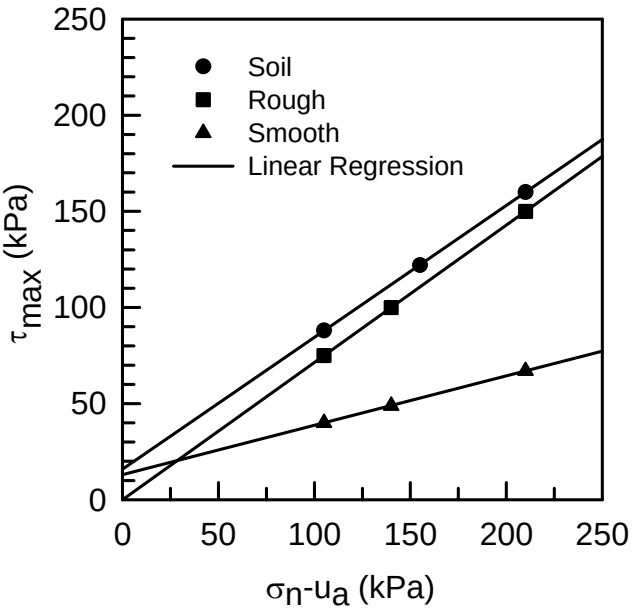

Figure 6.14: Failure envelope for the determination of effective cohesion in (σ_n-u_a)-τ_{max} plane ($u_a-u_w = 0$ kPa)

6.5 POSTULATED FAILURE MECHANISM OF INTERFACES

This section describes failure mechanisms of rough and smooth interfaces. Figure 6.15 shows the idealized curves of shear stress versus horizontal displacement and vertical displacement versus horizontal displacement for the rough interface. Figures 6.16 and 6.17 show the postulated failure mechanism between soil and rough interface. Based on the tests results of this study it is assumed during shearing until point B (Fig. 6.15) is reached (i.e., before yielding) that the soil mass in the gap between upper half of the ring and the counterface is distorted as a continuum. In other words the movement between soil particles and adjacent rough surface has not yet started. In region A-B (Fig. 6.15) some of the initial micro cracks and particles contacts are closed (Desai 2001). In region B-C of stress-displacement curve, which shows strain hardening behavior, soil mass above the rough surface continues distorting, but in this region soil particles adjacent to the rough surface start moving (see soil block 1c-2c-3c-4c in Fig. 6.16(b)). In other words the soil-surface interaction is mobilized. In this region soil mass has been compressed to its maximum value and before reaching peak shear strength (τ_p) the dilation behavior is started. Due to disturbance that soil particles experienced during the movement (horizontal and vertical) from region A-B to B-C the adhesion between soil and surface becomes weaker than the cohesion between soil particles. Therefore, it is assumed at point B, the bond due to physico-chemical forces between soil and rough surface is reduced (i.e., contact adhesion is lost or decreased) and yielding starts. However, in the case of a direct shear test on soil, where soil particles slide over each other (i.e., the interference due to rough surface is not present) the physico-chemical forces (cohesion) are maintained to a larger horizontal displacement than the rough interface. The

difference in mechanisms affecting physico-chemical forces around the interface zone is the primary reason why adhesion of a rough interface is less than the cohesion of soil as seen in the failure envelopes in Fig. 6.14 and Table 6.7. In region C-D (i.e., strain softening zone) shear strength reduces due to further reduction of adhesion force and decreasing influence of dilation. In region D-E the adhesion and dilation no longer contribute to increasing shear strength. Beyond point D, it is assumed that friction is primarily responsible for the continued shear strength of the rough interface.

Figure 6.18 shows the idealized curves of shear stress versus horizontal displacement and vertical displacement versus horizontal displacement of the smooth interface. In region A-B, the behavior of the smooth interface is assumed similar to the rough interface. However, in region B-C the soil particles adjacent to the counterface start sliding relative to the smooth surface without showing dilation behavior (Fig. 6.19). As opposed to the rough interface, in the case of smooth interface the bonding between counterface and soil particles due to physico-chemical forces is at a maximum when the peak shear strength is reached. It should be pointed out that failure envelopes are obtained by plotting the peak shear strength (i.e., shear strength corresponding to point C in Fig. 6.15 and shear strength corresponding to point B in Fig. 6.18). In Fig. 6.15 (for rough interface) when shear strength reached the maximum value at point C, the contact adhesion was reduced due to the movement (or disturbance) of the soil particle from point B to C (see Fig. 6.16(b)). As opposed to the rough interface, for the smooth interface point B of Fig. 6.18 is used to obtain failure envelopes. At point B (i.e., peak

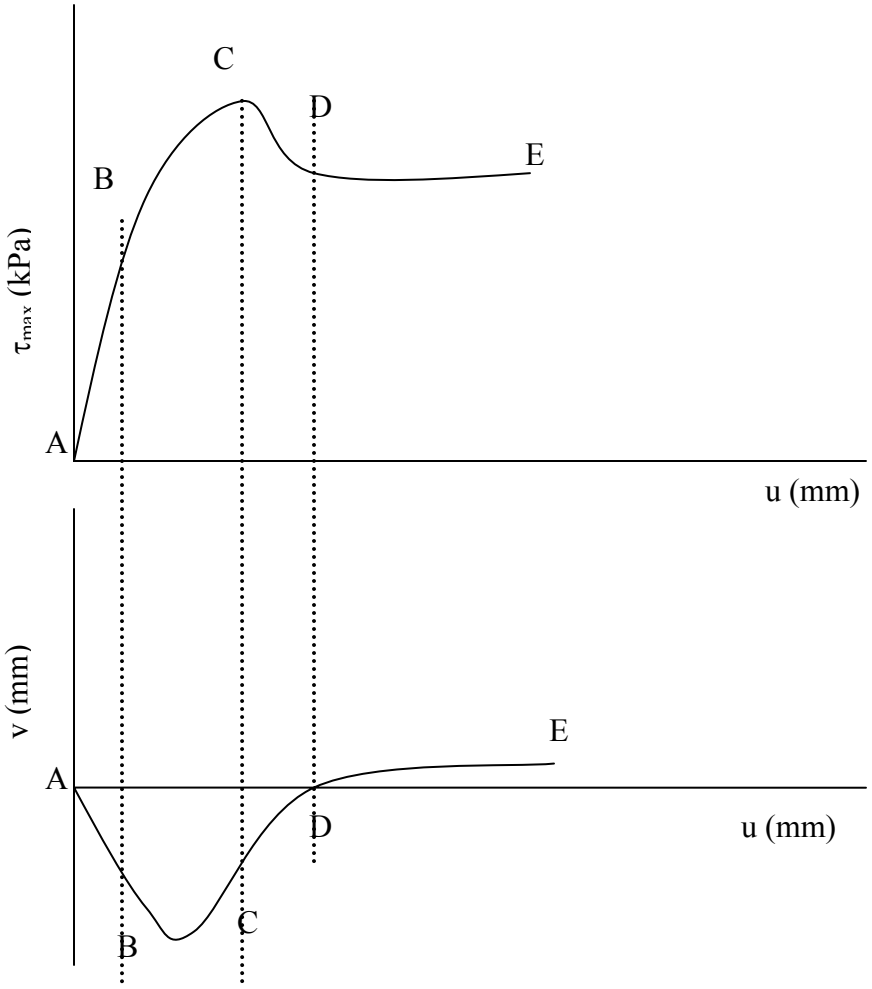

Figure 6.15: Idealized shear stress-horizontal displacement, vertical displacement vs. horizontal displacement curve for the rough interface

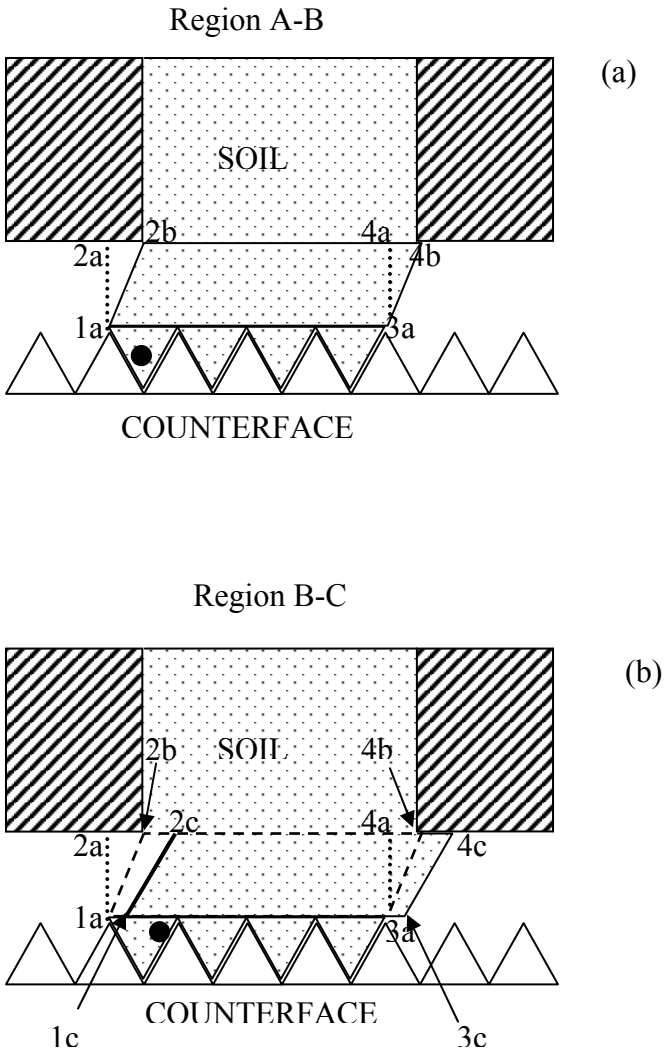

Figure 6.16: Postulated failure mechanism for the rough interface in regions A-B and B-C of Fig. 6.15

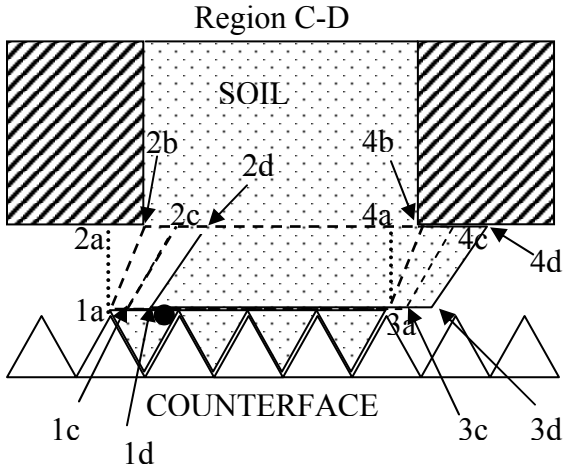

(a)

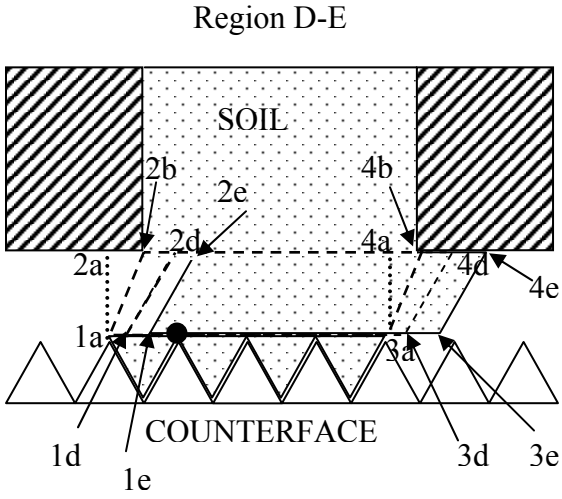

(b)

Figure 6.17: Postulated failure mechanism for the rough interface in regions C-D and D-E of Fig. 6.15

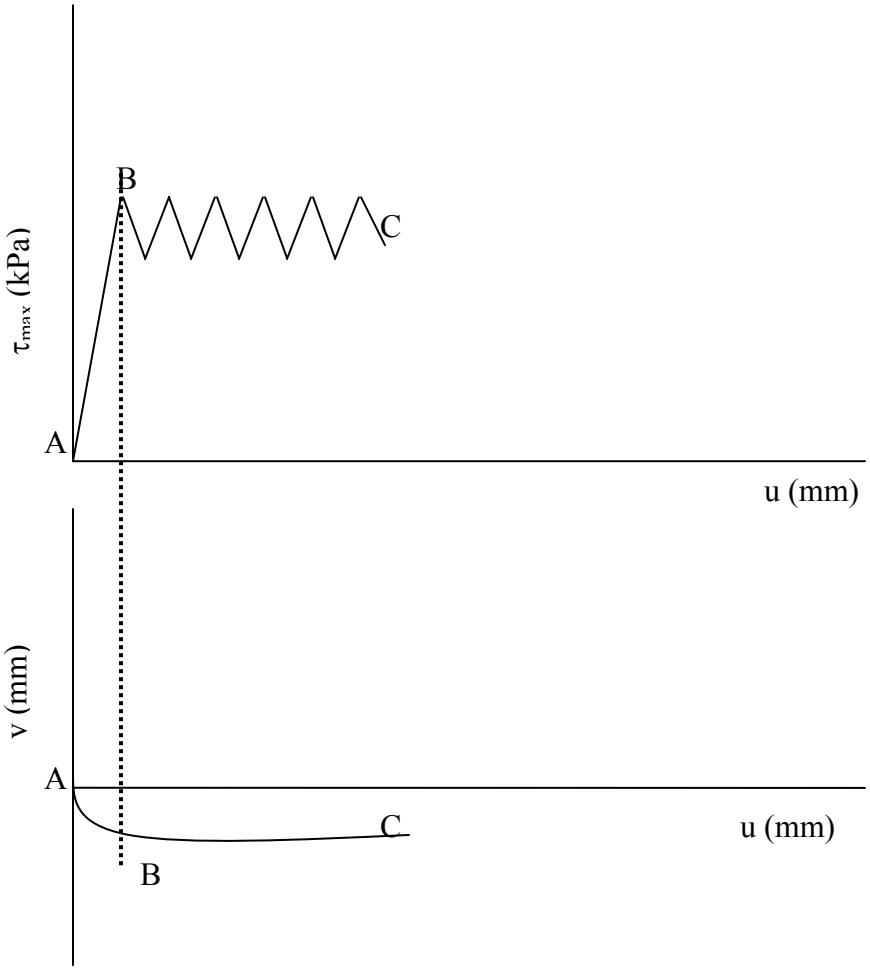

Figure 6.18: Idealized shear stress vs. horizontal displacement and vertical displacement vs. horizontal displacement curve for the smooth interface

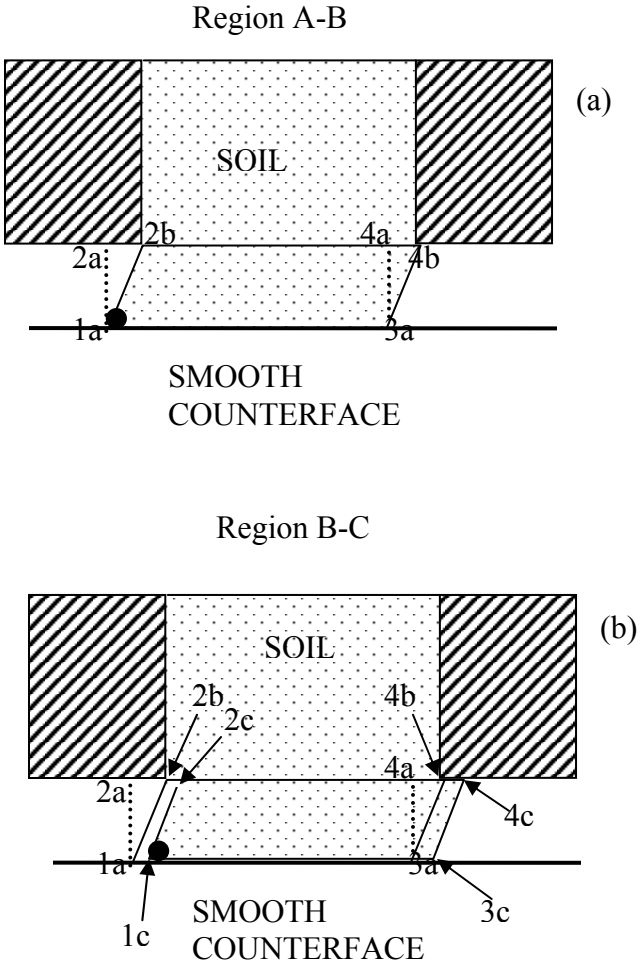

Figure 6.19: Postulated failure mechanism for the smooth interface in regions C-D and D- E of Fig. 6.18

shear strength) the soil particle (shown by black circle in Fig. 6.19(a)) has not started moving and the adhesion force is the maximum at the peak shear strength. Thus, this explains why c′ for the smooth interface is greater than the rough interface.

6.6 REPEATABILITY

Repeatability of test results was mentioned in Chapter IV and is further discussed in this section. As mentioned in Chapter IV all samples were compacted manually by using a tamping rod. Table I.1 (in Appendix I) shows that for soil samples, initial moisture content varied from 20.9% to 19.3%; variation in initial water content was 20.1% to 20.8% for the case of rough interface and 20.2% to 21.6% for the smooth interface testing. Therefore, a variation in initial dry density occurred, which may affect the results of two samples tested at the same stress conditions.

Figures 6.20 to 6.25 show the comparison of test results repeated at the same stress conditions. Comparison of Figs. 6.20 to 6.25 shows that in general the repeatability of test results is satisfactory. For example, Fig. 6.21 shows that values of maximum shear stress, magnitude of vertical displacement, and water content are approximately the same for two tests conducted at u_a-u_w = 0 kPa and σ_n-u_a = 105 kPa. However, some differences in tests results were expected, even though stress conditions were same, due to the variation in sample preparation, variation in initial moisture content, and dry density. For example, Fig. 6.23 shows results of two samples tested at σ_n-u_a = 105 kPa and u_a-u_w = 20 kPa, a difference in maximum shear stress, vertical displacement and water content is obvious. The difference may be attributed to the factors mentioned above. In addition to the above mentioned factors, the sequence of application of target net normal stress and target suction was different in both tests. Both samples were subjected to the same

normal stress (i.e., 35 kPa) for approximately 60 minutes; however, in Test ID# 051504, target net normal stress was applied in seven steps (approximately 10 kPa per step) whereas in Test ID# 021905 target net normal stress was applied in two steps (35 kPa per step). To eliminate the influence of the size of stress increments, all other tests were performed using 35 kPa increments of normal stress. Table 6.8 shows the values of maximum shear stress and water content values for the tests conducted at the same stress conditions.

Keeping in view the variation in initial conditions and experimental errors, it can be expected that the parameters of the Mohr-Coulomb equation (c', c_a', ϕ',δ', ϕ^b, δ^b) can also vary from those reported in Section 6.4. Figures 6.26 to 6.29 show the best fit parallel lines with original data points and error bars that indicate a 5% difference from the trend line at each normal stress. It is obvious from these figures that in most cases the error between the expected data point (i.e., a point that will fall on the solid line) and actual data point is less than 5%. Tests repeated at 0 kPa, 20 kPa, and 50 kPa suction values are also plotted on Fig. 6.29. Tests results repeated at 0 and 50 kPa suction fall within 5% error bar. The difference between the maximum shear stress for the tests conducted at 20 kPa suction is greater than 5%; however, the average of the peak shear strength from two tests lies within the 5% error bars.

Table 6.8: Comparison of tests conducted at the same stress conditions

Test ID#	u_a-u_w (kPa)	σ_n-u_a (kPa)	τ_{max} (kPa)	w (%) (at the end of shearing)
011405	0	105	79	17.0
121004	0	105	78	16.8
051504*	20	105	74	15.8
021905*	20	105	92	15.9
042604	50	105	92	15.0
042004	50	105	91	14.90

* for these two tests, significant differences in the net normal stress increments existed.

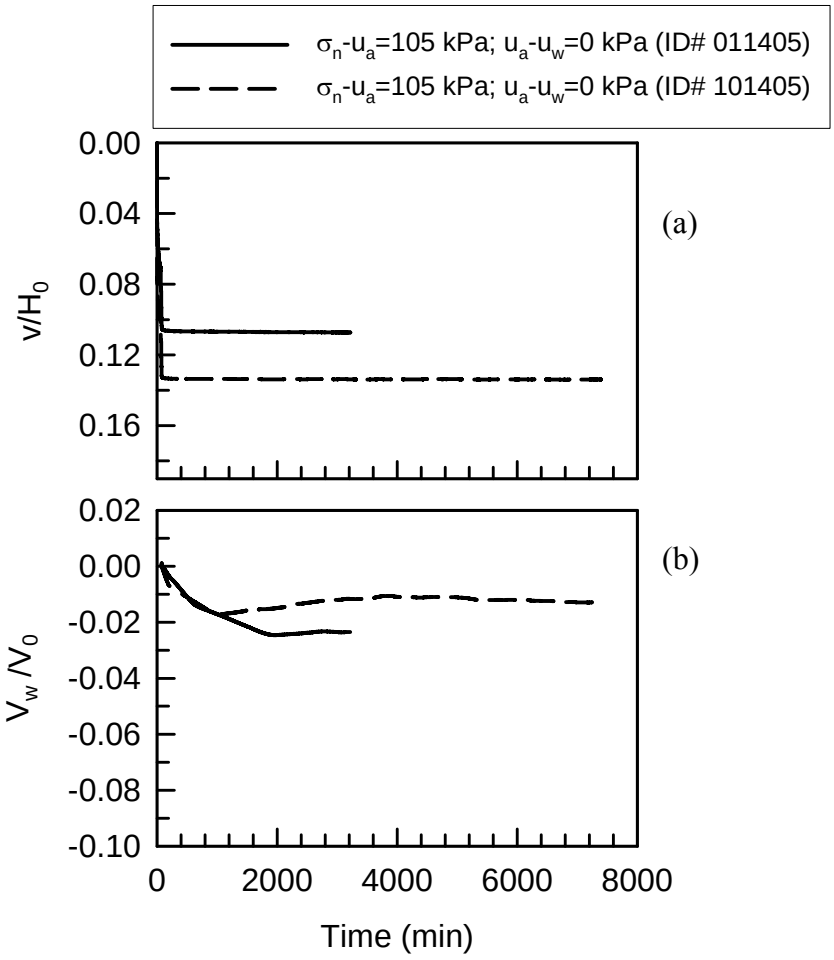

Figure 6.20: Comparison of variation in (a) v/H_0 and (b) V_w/V_0 during equalization phase for tests conducted at the same stress conditions (u_a-u_w = 0 kPa; σ_n-u_a = 105 kPa)

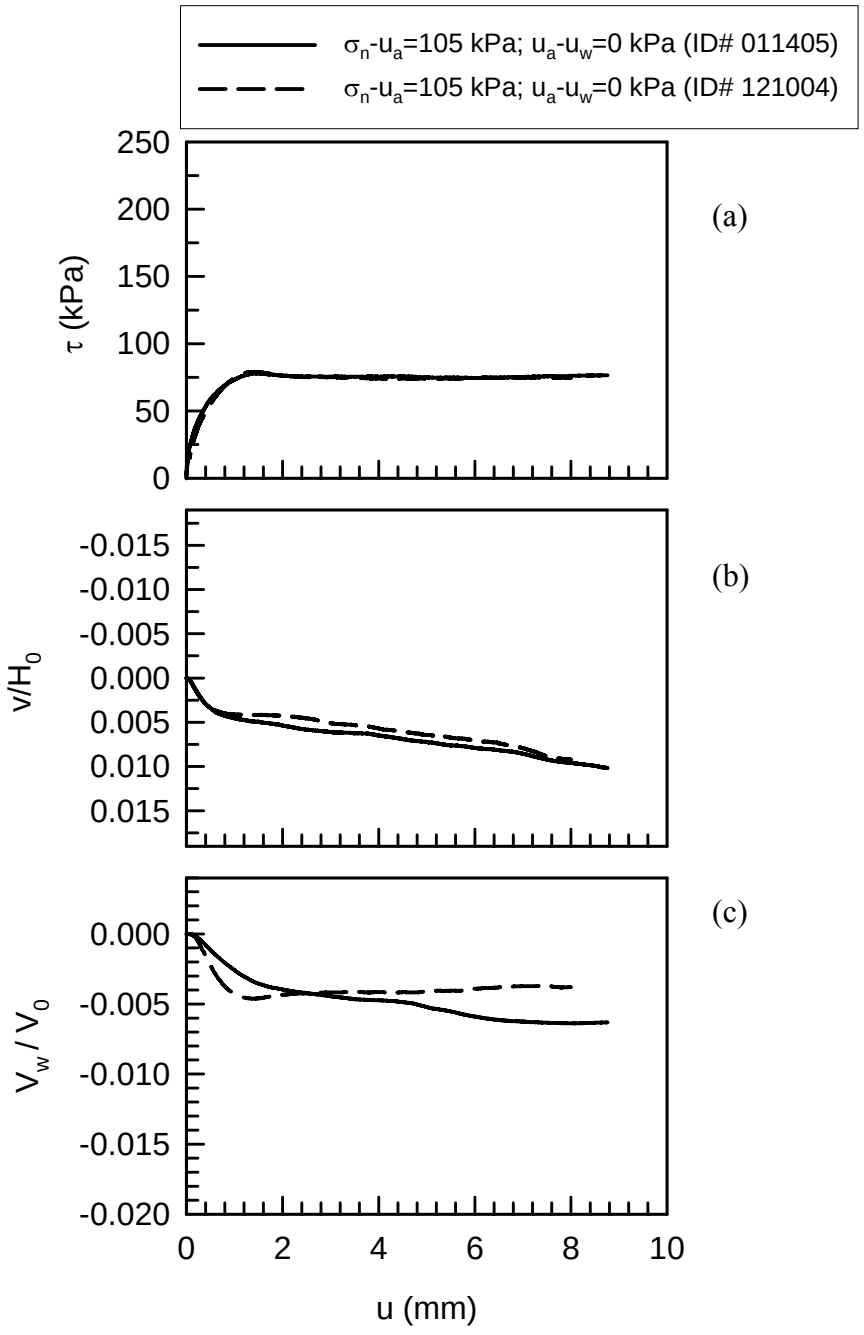

Figure 6.21: Comparison of variation in (a) τ, (b) v/H_0, and (c) V_w/V_0 during shearing phase for tests conducted at the same stress conditions. (u_a-u_w = 0 kPa; σ_n-u_a = 105 kPa)

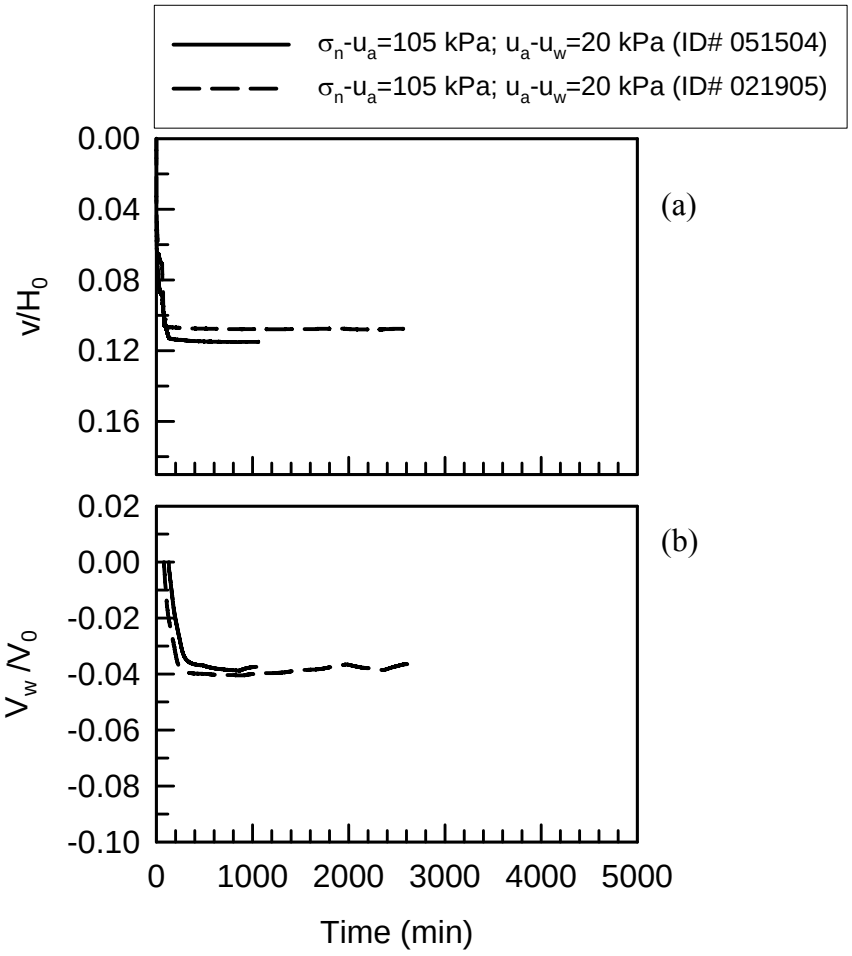

Figure 6.22: Comparison of variation in (a) v/H_0 and (b) V_w/V_0 during equalization phase for tests conducted at the same stress conditions (u_a-u_w = 20 kPa; σ_n-u_a = 105 kPa)

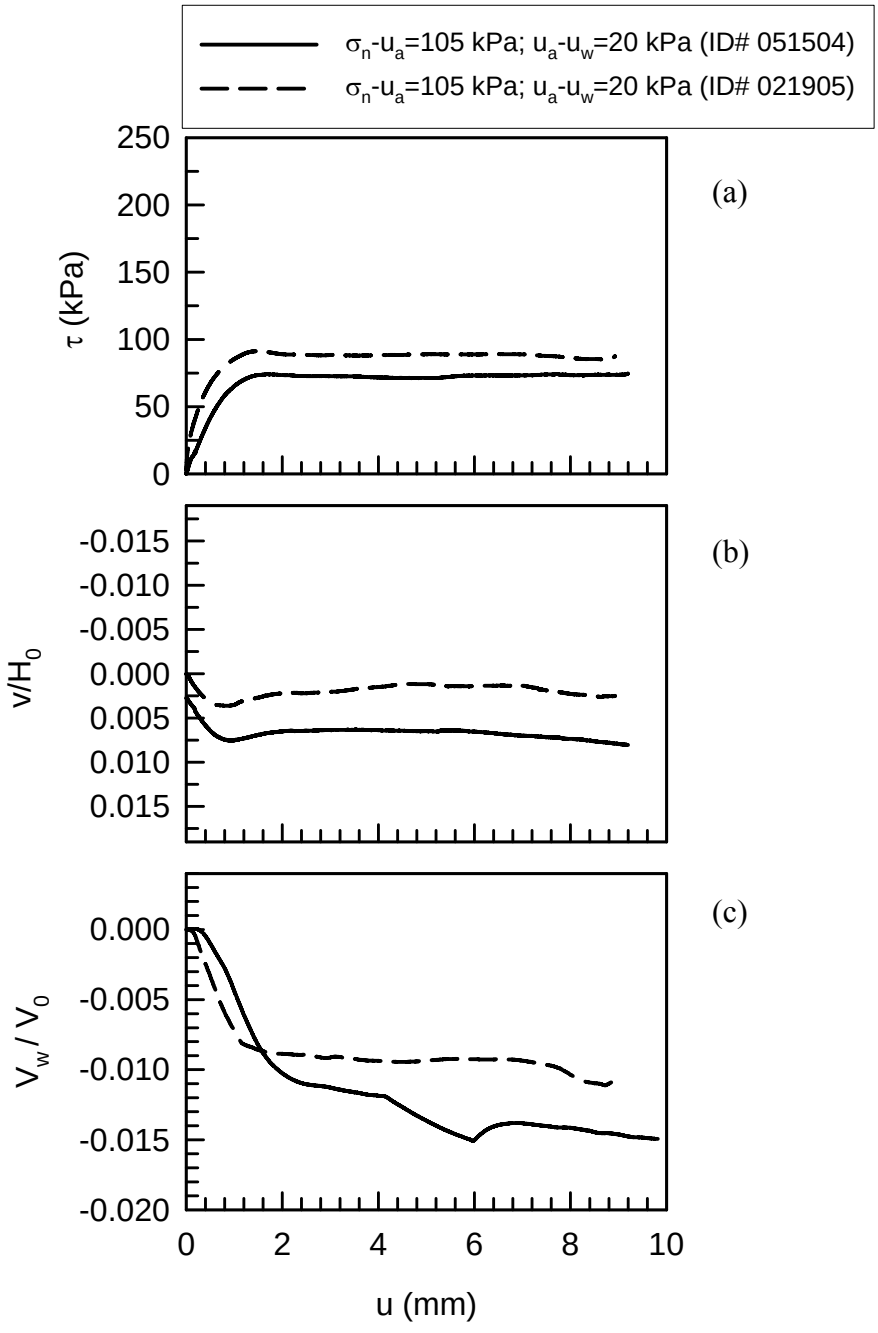

Figure 6.23: Comparison of variation in (a) τ, (b) v/H_0, and (c) V_w/V_0 during shearing phase for tests conducted at the same stress conditions (u_a-u_w = 20 kPa; σ_n-u_a = 105 kPa)

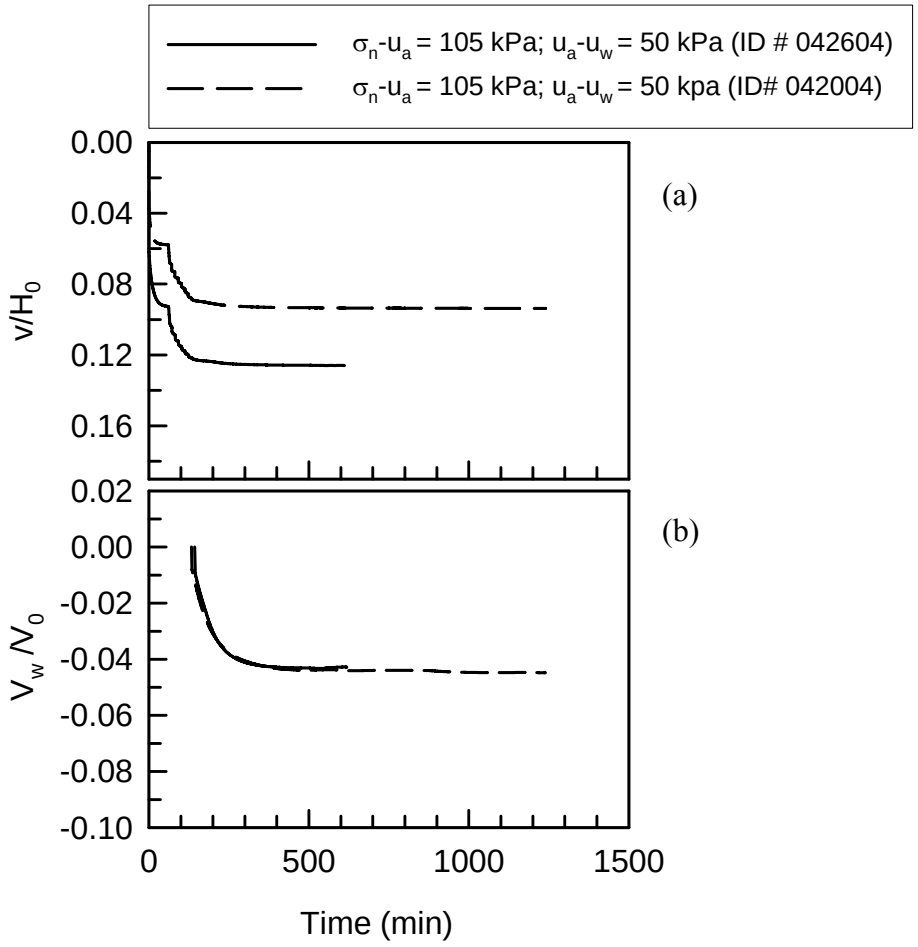

Figure 6.24: Comparison of variation in (a) v/H_0 and (b) V_w/V_0 during equalization phase for tests conducted at the same stress conditions (u_a-u_w = 50 kPa; σ_n-u_a =105 kPa)

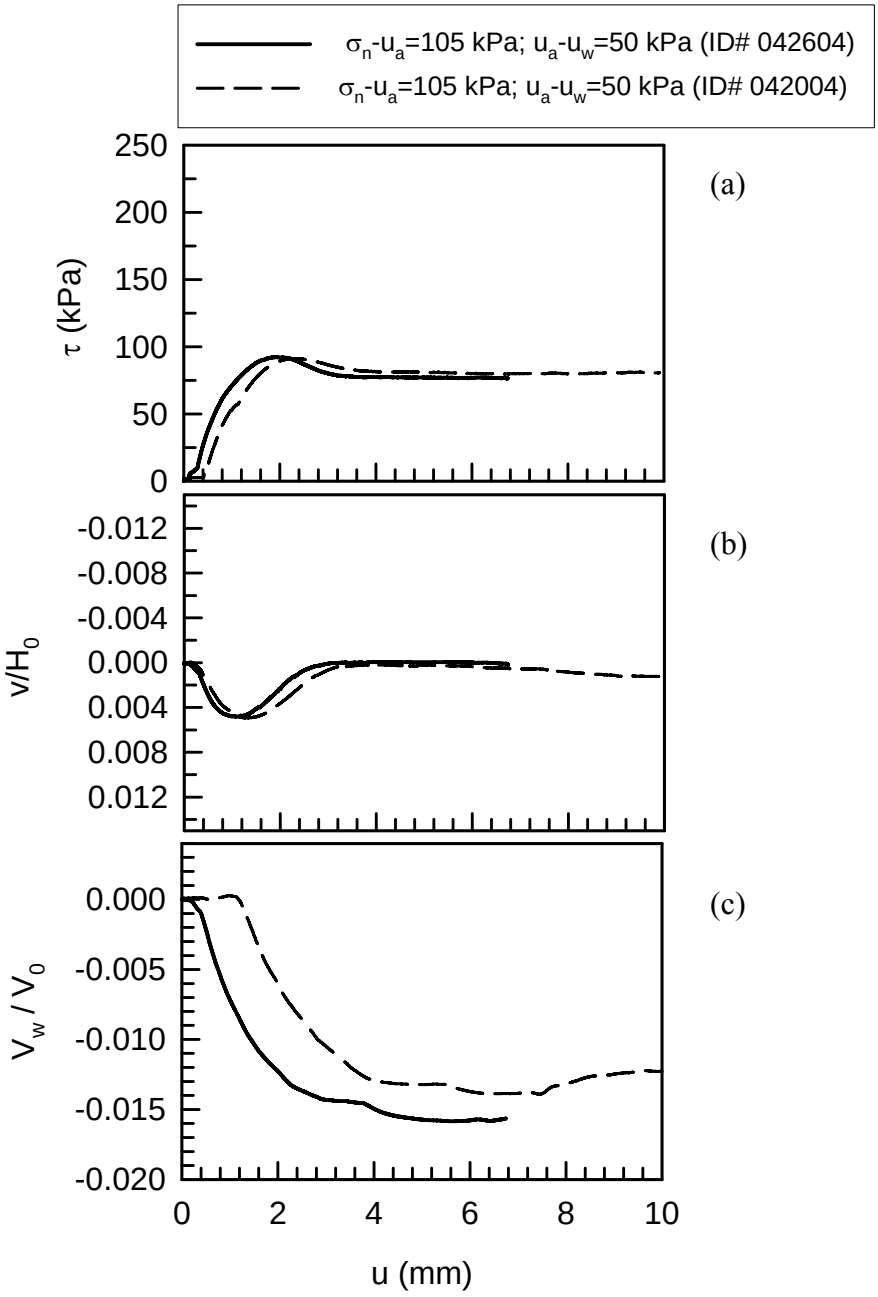

Figure 6.25: Comparison of variation in (a) τ, (b) v/H_0, and (c) V_w/V_0 during shearing phase for tests conducted at the same stress conditions. (u_a-u_w = 50 kPa; σ_n-u_a =105 kPa)

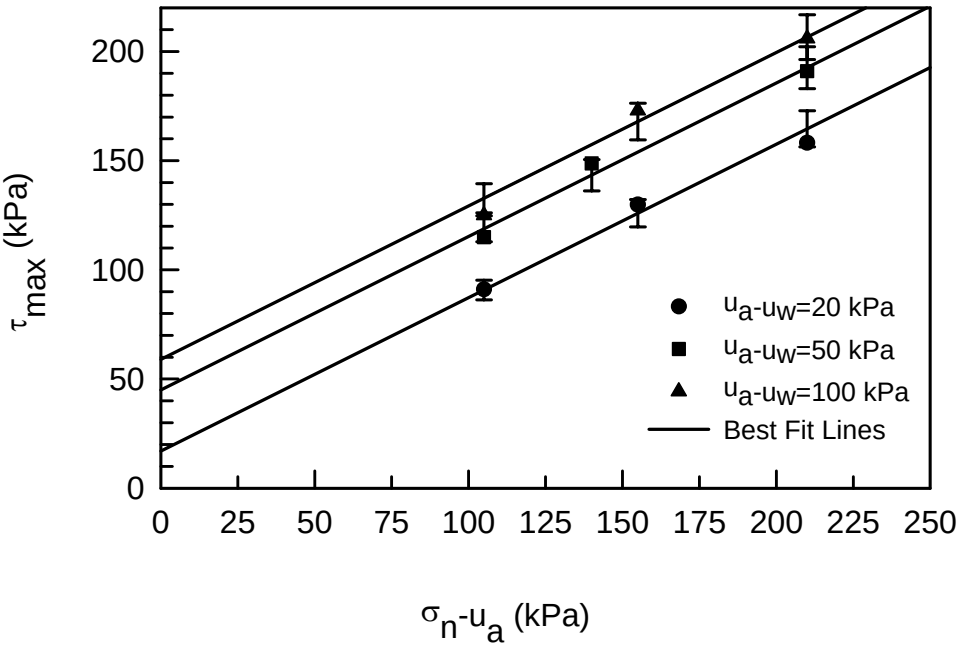

Figure 6.26: Failure envelopes of soil in (u_a-uw)-τ_{max} plane with 5% error bars

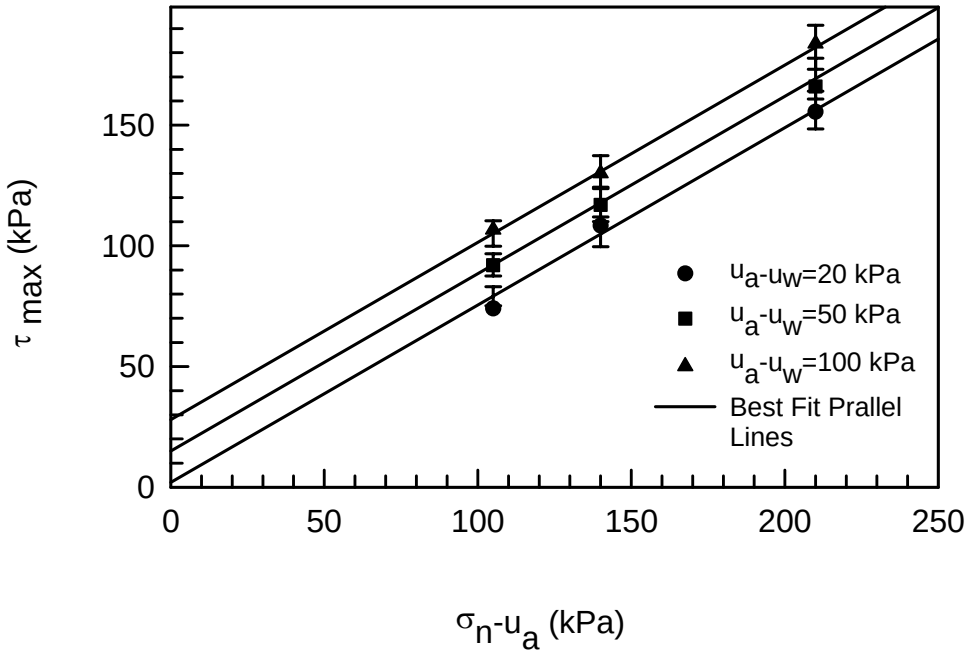

Figure 6.27: Failure envelopes of the rough interface in (u_a-uw)-τ_{max} plane with 5% error bars

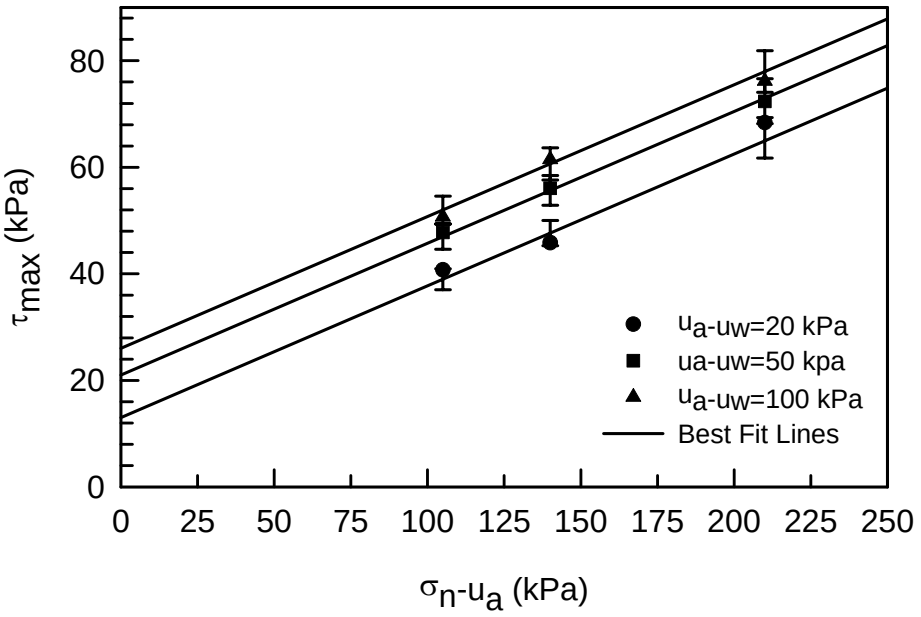

Figure 6.28: Failure envelopes of the smooth interface in $(u_a\text{-}uw)\text{-}\tau_{max}$ plane with 5% error bars

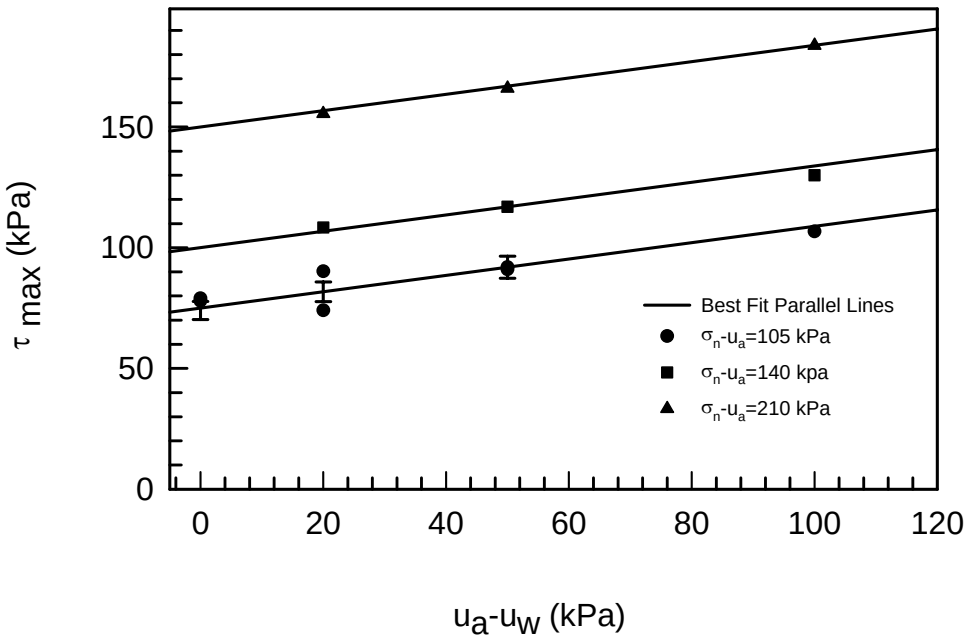

Figure 6.29: Tests of the rough interface repeated at $u_a\text{-}u_w$ = 20 kPa, 50 kPa, and 100 kPa for constant $\sigma_n\text{-}u_a$ = 105 kPa

CHAPTER VII

ELASTOPLASTIC CONSTITUTIVE MODELING

7.1 INTRODUCTION

A brief review of elastoplasticity based models for interface behavior was presented in Subsection 2.2.5.4. The modified model by Navayogarajah et al. (1992) was selected to be expanded and applied for simulating the suction-controlled interface direct shear test results presented in this study. The model was originally developed for simulating the behavior of frictional materials by Desai and co-workers (Desai 1980, Desai and Faruque 1984, Desai et al. 1986). This model is generally a hierarchical approach in the sense that a progressively refined version of the model (associative model with isotropic hardening) can be modified to obtain a model having nonassociativeness, strain softening, and cyclic loading capability.

The hierarchical approach was specialized by Desai and Fishman (1991) for modeling the behavior of rock joints. Navayogarajah et al. (1992) employed the same model for idealization of sand-steel and sand-concrete interfaces, based on comprehensive experimental results using a simple shear type interface device by Uesugi and Kishida (1986) and Uesugi et al. (1989, 1990). The model was modified to simulate the strain softening and cyclic loading behavior of interfaces between sand and steel or concrete.

The original model is modified within the framework of the disturbed state concept, which has been used successfully to model saturated and unsaturated soil behavior. Disturbed state concept has also been employed to predict the behavior of joints in rocks

and interfaces between different materials. However, the interface models reported in the literature have not incorporated the effect of suction on the behavior of interfaces.

Navayogarajah et al. (1992) model was selected in this study to be modified and extended for modeling the behavior of unsaturated interfaces under constant net normal stress conditions in the direct shear device. The choice was made on the following considerations:

- The model has been formulated based upon the general framework of the theory of plasticity and thus, has a strong and meaningful theoretical basis.
- The model is capable of simulating nonassociativeness and strain softening behavior of interfaces.
- The 3-D generalized form of this model has been successfully used to model the behavior of unsaturated soil.

Analogies between the behavior of unsaturated soil mass and unsaturated interface behavior are presented in Section 7.2. The procedure for expanding the model to unsaturated interfaces is described in Section 7.3. The model validation is presented in Section 7.4 by reproducing some of the predictions presented by Navayogarajah (1990), for the monotonic behavior of an interface between Toyoura sand and steel. Section 7.5 explains the procedure for the determination of model parameters for the test results, and predictions of unsaturated interface test results are presented in Section 7.6. Section 7.7 presents the effect of variation of model parameters.

7.2 ANALOGIES BETWEEN SOIL BEHAVIOR AND INTERFACE BEHAVIOR

Boulon and Nova (1990) provided an analogy based on the similarities of drained and undrained triaxial test results for sand, and constant normal load and constant volume

interface test results, respectively. Figure 7.1 represents typical experimental results for an interface between sand and steel, which were obtained from a direct shear type device. Shear stress-tangential displacement and normal displacement-tangential displacement curves under constant normal stress are shown in Fig. 7.1a. Figure 7.1b presents the results from tests performed under constant volume conditions.

Drained and undrained triaxial test results on sand are presented in Figs. 7.2a and 7.2b, respectively. p' is the effective mean pressure, q is the deviator stress, and ε_v and ε_s are volumetric and deviatoric strains.

Similarity exists between constant normal load results of Fig. 7.1a and drained triaxial test results of Fig. 7.2a as well as constant volume test results of Fig. 7.1b and undrained triaxial test results of Fig. 7.2b, respectively.

In drained triaxial tests, the deviatoric stress, q, increases to a peak and then the soil strain softens until a residual stress state is reached, after which soil deforms without noticeable change in stresses and volume. Volumetric strain, ε_v, is initially compressive, then well before peak shear stress the sample starts dilating. Eventually, the dilation rate becomes very small and the stress-strain curve becomes horizontal. One can describe the constant normal stress test results for an interface, Fig. 7.1a, in a similar sense, except that the deviatoric stress, q, is substituted by the shear stress, τ, the deviatoric strain, ε_s, is substituted by the tangential relative displacement, w, and finally, the role of confining pressure is played by the normal stress, σ_n.

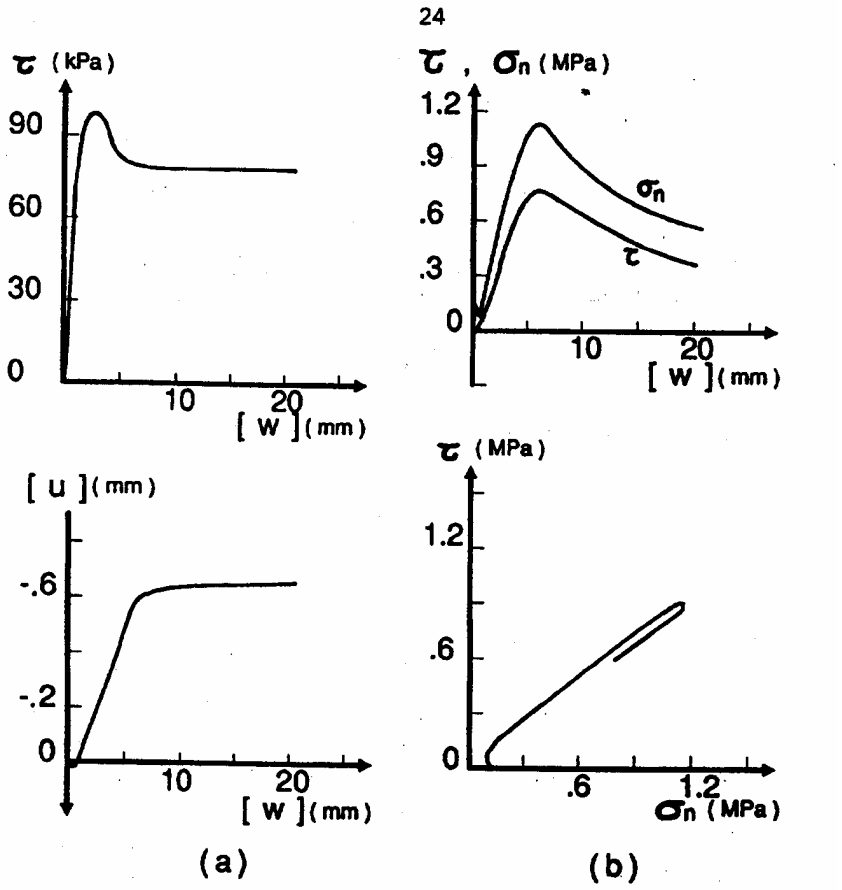

Figure 7.1: Direct shear tests on dense coarse Hostun Sand, σ_{n0} =122 kPa: (a) Constant normal stress (b) Constant volume. (After Boulon and Nova, 1990)

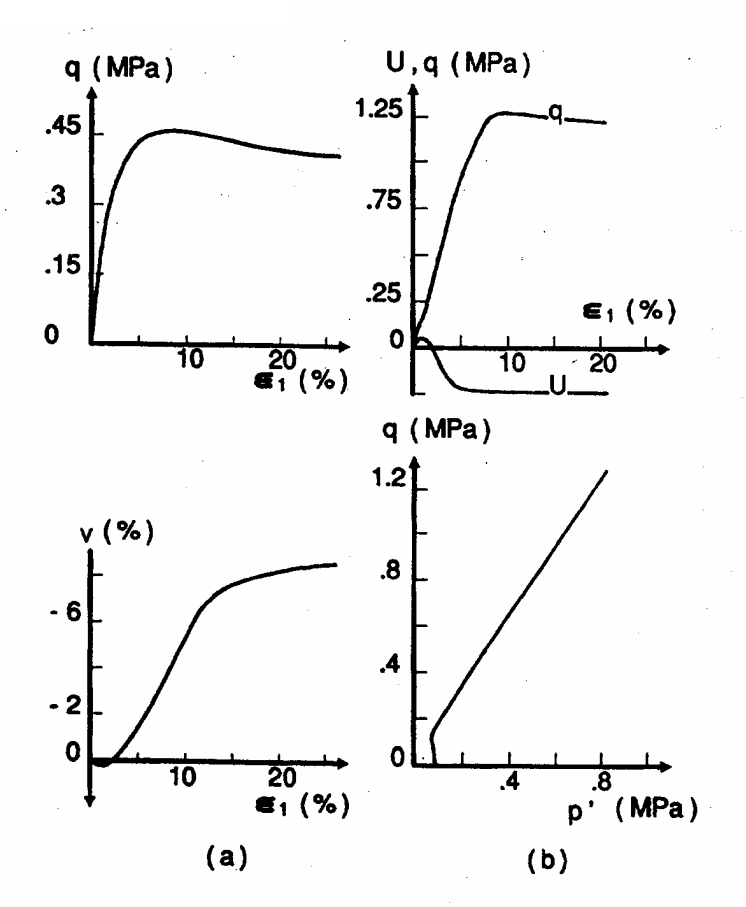

Figure 7.2: Triaxial tests on dense coarse Hostun Sand, σ_3 = 100 kPa: (a) Drained (b) Undrained (After Boulon and Nova, 1990)

Cui and Delage (1996) presented suction controlled triaxial test results, which are shown in Fig. 7.3. The following observations can be made about these results:

- As the suction, u_a-u_w, increases, the peak in the stress-strain plot becomes more pronounced.
- Maximum deviator stress, q, increases with increase in suction.
- Soil shows initial compression and slightly before the maximum deviator stress dilation begins.
- Dilation behavior becomes pronounced as the suction value increases.
- At higher suction values strain softening behavior is more pronounced. After reaching the maximum shear strength value, deviatoric stress decreases and becomes constant.
- At low suction values soil did not show a peak in deviatoric stress-axial strain plot; after reaching the maximum shear stress, shear strength remains constant with increasing axial strain.
- The soil exhibited much less dilative behavior for the lowest suction value (i.e., u_a-u_w = 200 kPa) used in the experimental program by Cui and Delage (1996).

Similar observations can be made for the results from this study and presented in Fig. 7.4, which represent typical tests on an unsaturated interface between unsaturated soil and a rough steel counterface. Following the approach of Boulon and Nova (1990), an analogy is established between the unsaturated triaxial test results and the unsaturated interface direct shear test results presented in Fig.7.3 and Fig.7.4, respectively.

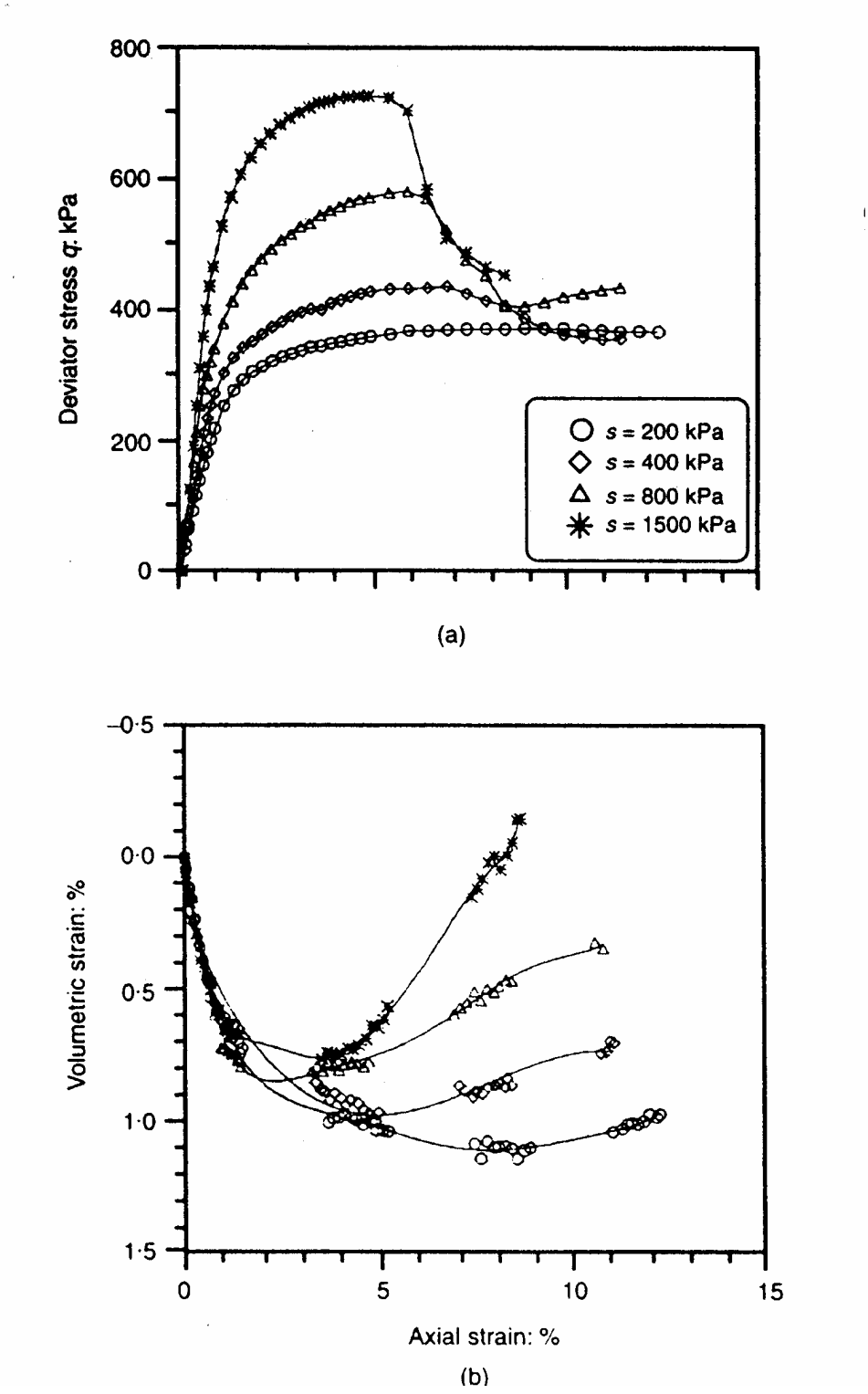

Figure 7.3: Stress-strain and volume change curves at σ_3 = 50 kPa and various controlled suctions from triaxial tests on Jossigny silt (After Cui and Delage, 1996)

The analogous quantities for unsaturated triaxial tests and unsaturated interfaces are presented in Table 7.1.

Table 7.1 Analogous quantities for unsaturated soil and interfaces

Unsaturated Soil	Unsaturated Interface
q	τ
$p = (\sigma_1 + \sigma_2 + \sigma_3/3) - u_a$	$\sigma_{net} = \sigma_n - u_a$
ε_v	v
ε_s	u
u_a-u_w	u_a-u_w

7.3 ELASTOPLASTIC UNSATURATED INTERFACE CONSTITUTIVE MODEL

The elastoplastic model for an unsaturated soil-steel interface is presented in this section. Emphasis is given on the effect of suction and net normal stress on the strength and volumetric behavior. The Navayogarajah et al. (1992) model for sand-steel interface was modified to integrate the effect of suction and net normal stress on the interface behavior.

The modified model presented in this section is capable of capturing the important features of unsaturated soil-interface observed in the laboratory and describes the behavior in terms of two stress state variables, suction, u_a-u_w and net normal stress, σ_n-u_a.

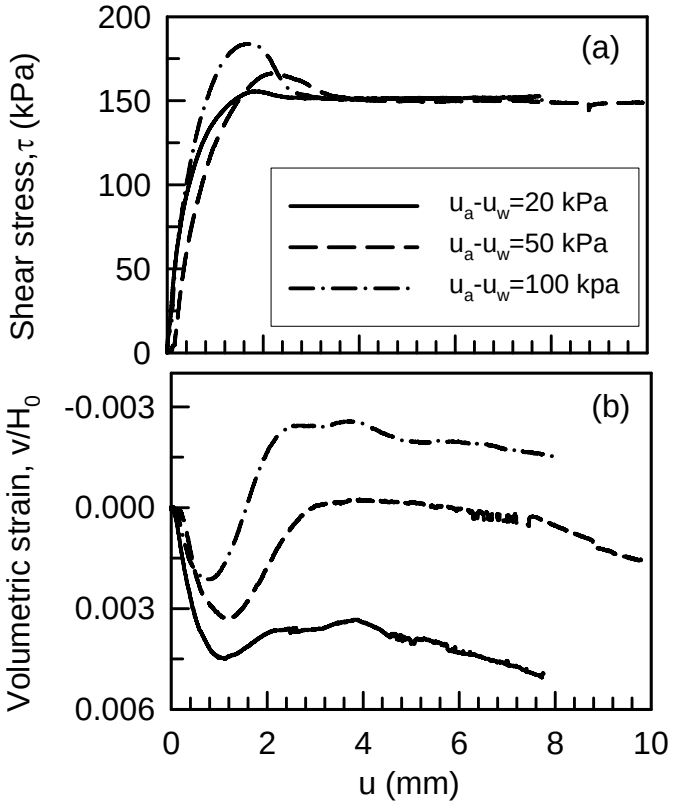

Figure 7.4: Effect of suction on shear stress and volumetric strain for rough interface during shearing (σ_n-u_a = 210 kPa)

7.3.1 Incremental Stress Displacement Relations

The total incremental relative displacement, in normal and tangential directions, is decomposed into elastic (recoverable) part and plastic (non-recoverable) parts;

$$dv = dv^e + dv^p \tag{7.1}$$

$$du = du^e + du^p \tag{7.2}$$

where *dv* and *du* are the total relative displacements normal and tangential to the contact surface, respectively. Superscripts *e* and *p* denote the elastic and plastic parts of the displacements, respectively.

Failure is considered when slip occurs between the two bodies in contact and when,

$$F = 0 \tag{7.3}$$

where F is the yield function. It is also assumed that any hardening or softening is due to the plastic normal and plastic tangential displacements. The consistency condition

$$dF = 0 \tag{7.4}$$

yields the following expression

$$dF = \frac{\partial F}{\partial \sigma_{net}} d\sigma_{net} + \frac{\partial F}{\partial \xi_D} d\xi_D + \frac{dF}{d\xi_v} d\xi_v = 0 \tag{7.5}$$

where: net normal stress = $\sigma_{net} = \sigma_n - u_a$, $\xi_v = \int \left| dv^p \right|$ (accumulation of plastic vertical displacement), and $\xi_D = \int \left| du^p \right|$ (accumulation of plastic tangential displacement).

Elastic displacements are related to the net normal and shear stresses by the following relationship:

$$\begin{Bmatrix} d\sigma_{net} \\ d\tau \end{Bmatrix} = \begin{bmatrix} K_n & 0 \\ 0 & K_s \end{bmatrix} \begin{Bmatrix} dv^e \\ du^e \end{Bmatrix} \tag{7.6a}$$

or

$$d\sigma = C^e dU^e \tag{7.6b}$$

where: C^e = elastic constitutive matrix of the interface, K_n and K_s = elastic normal and shear stiffness of the interface, respectively. It is assumed that elastic normal and shear behavior of interface are uncoupled.

The permanent relative displacement due to sliding and normal displacement are related to the plastic potential function by the flow rule,

$$\begin{Bmatrix} dv^p \\ du^p \end{Bmatrix} = \lambda \begin{bmatrix} \partial Q/\partial \sigma_{net} \\ \partial Q/\partial \tau \end{bmatrix} \tag{7.7}$$

where:

$\lambda = 0$ if $F<0$ or $dF<0$,

$\lambda>0$ if $F = 0$ or $dF = 0$, and

Q = Potential function.

Combining Equations 7.5-7.7 and eliminating the λ we can write the incremental stress-relative displacement relationship as

$$\{d\sigma\} = \left[C^e\right] \left(\{dU\} - \frac{\left(\frac{\partial F}{\partial \{d\sigma\}}\right)^T \left[C^e\right] \{dU\} \left(\frac{\partial Q}{\partial \{d\sigma\}}\right)}{\left(\frac{\partial F}{\partial \{d\sigma\}}\right)^T \left[C^e\right] \left(\frac{\partial Q}{\partial \{d\sigma\}}\right) - H} \right) \tag{7.8}$$

where: $\left[C^e\right]$ is elastic stiffness, $\{dU\}$ is the increment of relative plastic displacement, F and Q are the yield and potential functions, respectively, and H is the plastic modulus given by

$$H = \left(\frac{\partial F}{\partial \xi_v}\right)\left(\left|\frac{\partial Q}{\partial \sigma_{net}}\right|\right) + \left(\frac{\partial F}{\partial \xi_D}\right)\left(\left|\frac{\partial Q}{\partial \tau}\right|\right) \qquad (7.9)$$

7.3.2 Yield and Potential Functions

In this study a single yield surface is proposed to capture the response of unsaturated soil-steel interface under constant net normal stress for a given value of suction.

The following yield function, F, written in terms of stress variants was proposed by Geiser et al. (2000) for an unsaturated soil continuum,

$$F = \frac{j_{2D}}{{p_a}^2} - \left[-\alpha(s)\left\{\frac{j'_1 + R(s)}{p_a}\right\}^n + \gamma\left\{\frac{j'_1 + R(s)}{p_a}\right\}^2\right]F_s \qquad (7.10)$$

where:

j_{2D} = second invariant of the deviatoric stress tensor,

j_1' = first invariant of the saturated effective stress tensor,

$R(s)$ = bonding stress,

p_a = a constant equal to atmospheric pressure,

γ and β = ultimate state parameters, and

$F_s = 1 - \beta \bar{S}_r$

$\bar{S}_r$ = stress ratio = $\bar{S}_r = \sqrt{27/2}\, j_{3D} . j_{2D}^{-3/2}$,

where:

j_{3D} = third invariant of the deviatoric stress tensor,

α (s) = growth or hardening function of strain trajectories $\xi = \int \left(d\varepsilon_{ij}^p d\varepsilon_{ij}^p\right)^{1/2}$, and

suction = s = u_a-u_w.

Following the analogies between solid and interface, as shown in Table 7.1, a yield function for unsaturated soil-steel interface is obtained as a special case of Equation (7.10);

$$F = \tau^2 + \alpha(s)\left[\sigma_{net} + R(s)\right]^n - \gamma(s)\left[\sigma_{net} + R(s)\right]^2 \qquad (7.11)$$

R(s) represents the increase in the strength of the unsaturated interface with the increase in suction; it can be thought as the value of effective cohesion in the net normal stress-shear stress plane.

$\gamma(s)$ is a material parameter and its value is given as

$$\gamma(s) = \left[\frac{\tau}{\left(\sigma_{net} + R(s)\right)}\right]^2 \qquad (7.12)$$

$\alpha(s)$ is a hardening parameter which defines the evolution of the yield surface during deformation. $\alpha(s)$ is defined as,

$$\left.\begin{array}{ll} \alpha(s) = \gamma(s)\exp(-a\xi_v)\left(\frac{\xi_D^* - \xi_D}{\xi_D^*}\right)^b & \text{For } \xi_D < \xi_D^* \\ \text{and } \alpha(s) = 0 & \text{For } \xi_D \geq \xi_D^* \end{array}\right\} \qquad (7.13)$$

n is a phase change parameter. Parameters a, b, n, and ξ_D^* are functions of R(s) and roughness ratio $R_n = R_{max}/D_{50}$. R_{max} is defined as the maximum height between peak and valley of rough surface and D_{50} is the median diameter of soil grains. $\xi_d = \int \left| dv^p \right|$ and ξ_D^* is the value of ξ_D when shear stress reaches the peak value.

Figure 7.5 shows the typical yield curves given by Equation 7.11. For solids the parameter Fs in Equation 7.10 controls the shape of the yield functions plotted in principal stress space (Fishman, 1988). However, in unsaturated interfaces yield always

occurs on a specified plane. Therefore, the yield function is written and plotted in terms of the net normal stress (σ_{net}) and shear (τ) stress components instead of stress invariants and therefore, Fs is taken as unity. Parameter, n, is related to the state of stress at which transition from compaction to dilation occurs or at which the change in the volume vanishes.

The following function is proposed as the nonassociative flow rule,

$$Q = \tau^2 + \alpha_Q(s)[\sigma_{net} + R(s)]^n - \gamma(s)[\sigma_{net} + R(s)]^2 \qquad (7.14)$$

where the function $\alpha_Q(s)$ is given by the following expression.

$$\alpha_Q(s) = \alpha(s) + \alpha_{ph}\left(1 - \frac{\alpha(s)}{\alpha_i}\right)\left[1 - \kappa\left(1 - \frac{D}{D_u}\right)\right] \qquad (7.15)$$

κ is a material parameter (nonassociative parameter) and is related to the normalized roughness, net normal stress and suction. The value of κ is computed using the procedure described by Navayogarajah (1990) and is given by Equation 7.16.

$$\kappa = -[\gamma(s)]^{-1/2} * (dv^p / du^p)\Big|_{\xi_D = \xi_D^*} \qquad (7.16)$$

The α_{ph} and α_i are the values of $\alpha(s)$ at the phase change point and initiation of nonassociativeness. The value of α_{ph} is determined by differentiating Equation 7.11 with respect to net normal stress. Therefore,

$$\alpha_{ph} = \frac{2\gamma(s)}{n}(\sigma_{net} + R(s))^{2-n} \qquad (7.17)$$

Nonassociativeness, for a direct shear test is considered to occur just after the normal stress has been applied prior to the initiation of shear (Fishman, 1988). Using this

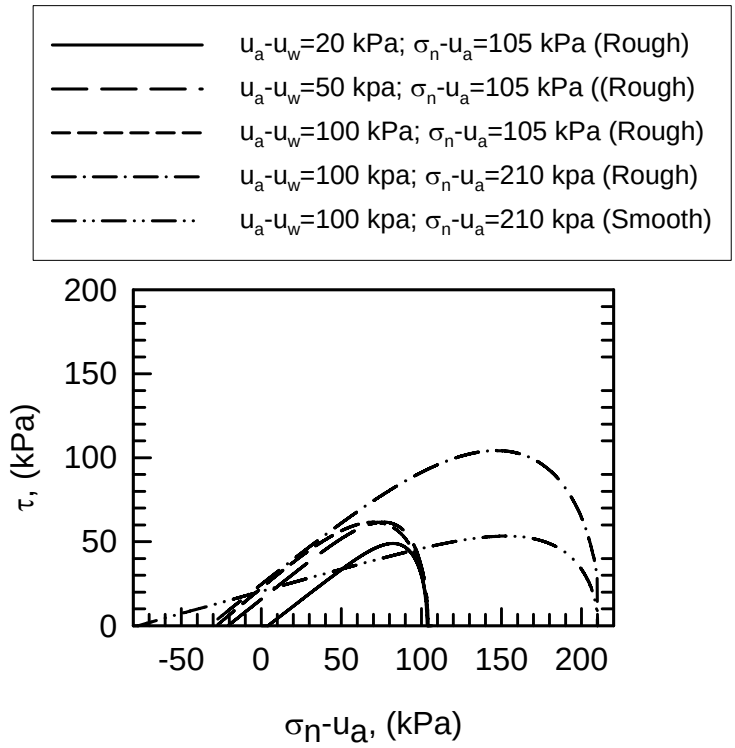

Figure 7.5: Typical yield surfaces for different u_a-u_w and σ_n-u_a for unsaturated interface

assumption

$$\alpha_i = \gamma(s)(\sigma_{net}+R(s))^{2-n} \qquad (7.18)$$

Damage function D, in Equation 7.15 is given as

$$D=0 \qquad \text{for } \xi_D < \xi_D^* \qquad (7.19)$$

$$D = D_u - D_u \exp[-(\xi_D - \xi_D^*)^2] \qquad \text{for } \xi_D \geq \xi_D^* \qquad (7.20)$$

where $D_u = \dfrac{\tau_p - \tau_r}{\tau_p}$ and τ_p and τ_r are the peak and residual shear stress, respectively.

Note that the form of $\alpha_Q(s)$ is same as proposed by Navayogarajah et al. (1992); however, as opposed to the original model, the parameters in Equation 7.15 are dependent on suction and net normal stress as well as on roughness.

Strain softening was observed in all unsaturated interface testing and was more pronounced for higher suction values. To model the strain softening behavior the disturbed state concept is employed. Desai & Ma (1992) and Navayogarajah et al. (1992) have already used disturbed state concept to model the interface behavior without the influence of suction. In disturbed state concept the observed or average stress is defined as the sum of the stress in the relative intact parts part and stress in the fully adjusted parts. The following relationship for the observed stresses is proposed:

$$\begin{Bmatrix} \sigma_{net} \\ \tau \end{Bmatrix} = (1-D)\begin{Bmatrix} \sigma_{net}^{t} \\ \tau^{t} \end{Bmatrix} + D\begin{Bmatrix} \sigma_{net}^{t} \\ 0 \end{Bmatrix} \qquad (7.21)$$

Superscript 't' in Equation 7.21 shows the intact part of the material, and this also shows that the normal stress is not affected by damage, only shear stress is affected.

7.4 DETERMINATION OF MODEL PARAMETERS

7.4.1 Elastic Constants, K_n, K_s

Elastic moduli are calculated from unloading/reloading slopes of unsaturated interface shear tests. Net normal stress vs. normal displacement and shear stress vs. shear stress displacement plots for a rough interface are shown in Figs. 7.6 and 7.7, respectively. Slopes of the unloading curves shown in Figs. 7.6 and 7.7 give values for elastic normal stiffness, K_n, and elastic shear stiffness, K_s, respectively.

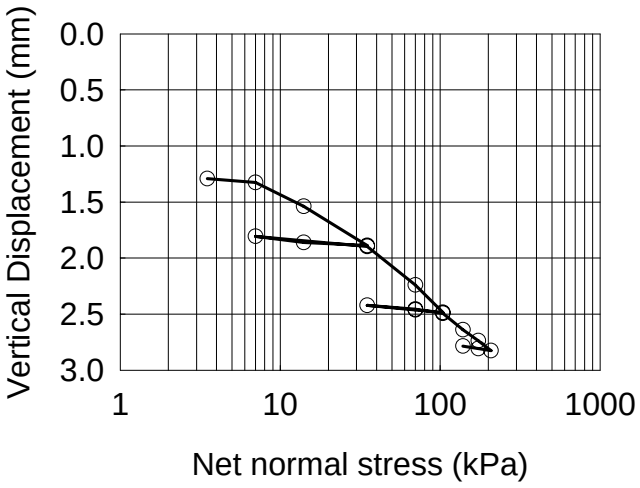

Figure 7.6: Loading-unloading results for σ_n-u_a versus v, to determine K_n

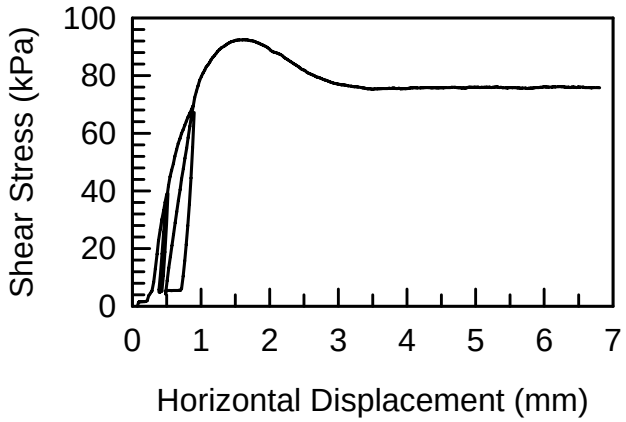

Figure 7.7: Loading-unloading results for τ versus u, to determine K_s

7.4.2 Ultimate Parameter, γ(s)

Peak shear stress condition of the interface is given by α(s) = 0 in the yield function, F. At ultimate condition (i.e. F = 0 and α(s) = 0) Equation 7.11 reduces to

$$\tau_p^2 - \gamma(s)\left(\sigma_{net} + R(s)\right)^2 = 0 \qquad (7.22)$$

$$\gamma(s)^{1/2} = \tau_p \big/ (\sigma_{net} + R(s)) \qquad (7.23)$$

Dependence of $\gamma(s)$ on roughness ratio R_n is given by

$$\gamma(s)^{1/2} = \mu_p = \tau_p / (\sigma_{net} + R(s)) = [\mu_{p1} + \mu_{p2} R_n] \qquad (7.24)$$

The slope and intercept of $\gamma(s)^{1/2}$ vs. R_n will give material constants μ_{p2} and μ_{p1}, respectively. The plot of $\gamma(s)^{1/2}$ vs. R_n from test results of 105 kPa and 210 kPa net normal stress and suction values of 20 and 100 kPa is shown in Fig. 7.8.

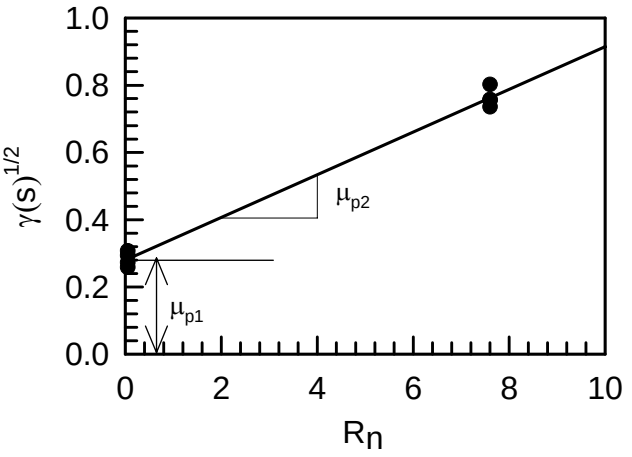

Figure 7.8: Determination of μ_{p1} and μ_{p2}

7.4.3 Determination of Hardening Parameters, ξ_D^*, a, b

Experimental results show that ξ_D^* is not only dependent on roughness, its value also changes with change in suction. Therefore, the following expression is proposed for ξ_D^* :

$$\xi_D^* = \left[\xi_{D1}^* + \xi_{D2}^* \left(R_n + R(s)/P_a \right) \right] \qquad (7.25)$$

P_a is the atmospheric pressure with units of stress. The slope and intercept of ξ_D^* vs. $\left[R_n + (R(s)/P_a)\right]$ will give material constants ξ_{D1}^* and ξ_{D2}^*, respectively (Fig. 7.9). Constants 'a' and 'b' in Equation 7.13 are found by the slope of the best fit line between $[\{\ln\gamma(s) - \ln\alpha(s)\}/\ln\{(\xi_D^* - \xi_D)/\xi_D^*\}]$ and $[\xi_v/\ln\{(\xi_D^* - \xi_D)/\xi_D^*\}]$; the slope of this

plot yields the value of 'a' and the intercept gives the value of 'b' (Figure 7.10). To plot $[\{\ln\gamma(s)-\ln\alpha(s)\}/\ln\{(\xi_D^*-\xi_D)/\xi_D^*\}]$ vs. $[\xi_v/\ln\{(\xi_D^*-\xi_D)/\xi_D^*\}]$, data points are selected between 0 to ξ_D^*. For each interface roughness and suction value 'a' and 'b' are computed and the average values of 'a' and 'b' are used. Predictions made by using the average values of 'a' and 'b' yield satisfactory results. Hardening parameters 'a' and 'b' both control the compression and dilation of the interface and also control the transition of shear stress from peak to residual. High values of both parameters result in increased dilation and decreased compression of a rough interface. For the smooth interface, high values of both parameters produce increase in initial compression. A higher value of parameter 'a' results in abrupt change from peak shear stress to residual shear stress instead of a smooth transition.

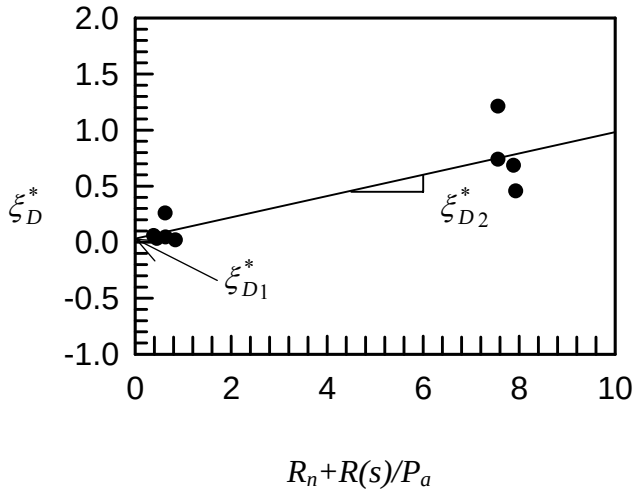

Figure 7.9: Determination of ξ_{D1}^* and ξ_{D2}^*

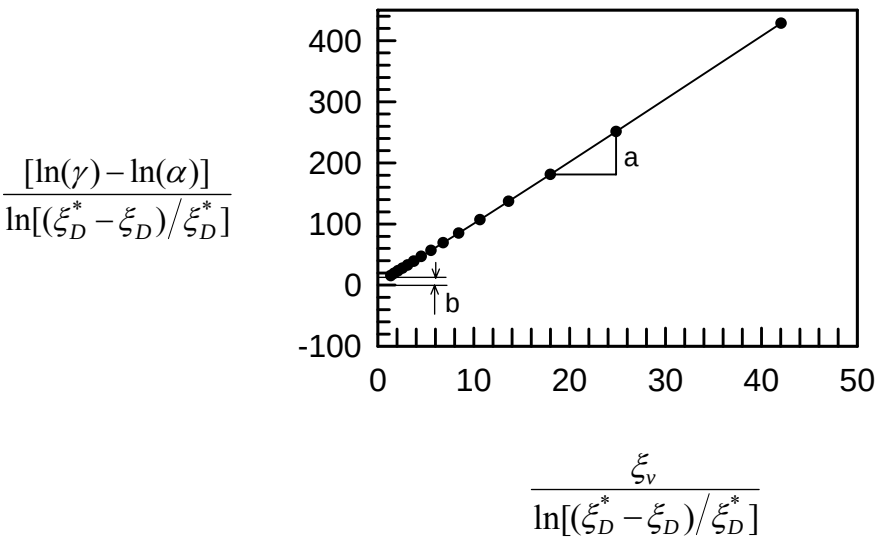

Figure 7.10: Typical plot for determination of parameters 'a' and 'b' from typical test results of rough interface

7.4.4 Phase Change Parameter, n

The phase change parameter, n, is related to a state of stress at which the material passes through a state of zero volume change. The zero plastic volume change occurs when the normal plastic displacement vanishes. The phase change parameter expression used in this study is the modified form of the expression proposed by Wathugala (1990).

$$[\gamma_t^{1/2}/\gamma(s)^{1/2}] = [(n-2)/n]^{1/2} \qquad (7.26)$$

$\gamma(s)^{1/2}$ is the slope of the ultimate line and $\gamma_t^{1/2}$ is the slope of the line connecting the crest of all the yield surfaces (i.e. phase change line).

For u_a-u_w = 20 kPa, the value of 'n' was determined to be approximately 7 for all values of net normal stress. However, the value of 'n' was calibrated by matching the experimental and analytical results. In this way the value of 'n' was determined to be 8

and was used in the back prediction of results of 20 kPa suction. Similarly, for 100 kPa suction, the value of n was in the range of 3.9 to 5.7. After calibration of parameter 'n', a value of n = 4 was used for the back prediction.

7.4.5 Non-Associative Flow Parameter, κ

κ is related to R_n, R(s), and σ_{net} as

$$\left.\begin{aligned} \kappa &= [\kappa_1 + \kappa_2 \{R_n + (R(s)/P_a)\}] \\ \kappa &= [\kappa_1 + \kappa_2 \{R_n + (R(s) + \sigma_{net})/P_a\}] \end{aligned}\right\} \quad \begin{aligned} &\text{for } u_a\text{-}u_w \leq 50 \text{ kPa} \quad (7.27) \\ &\text{for } u_a\text{-}u_w > 50 \text{ kPa} \quad (7.28) \end{aligned}$$

By plotting κ vs. $[R_n + R(s)/P_a]$ or κ vs. $[R_n + \{R(s) + \sigma_{net}\}/P_a]$ the constants κ_1 and κ_2 can be computed. As opposed to Equation 7.27, κ is dependent on σ_{net} in Equation 7.28. Two equations were proposed for κ based on the experimental results. For 20 and 50 kPa suction, the difference in initial compression was negligible for all net normal stress values (i.e. 105, 140, 210 kPa). For 100 kPa suction initial compression of the interface increased and dilation decreased as the net normal stress increased.

To simulate this observation, κ is made dependent on σ_{net} for 100 kPa suction. However, further test data is required to verify this observation. Figure 7.11 shows a plot for determination of κ for u_a-u_w = 100 kPa for the rough interface.

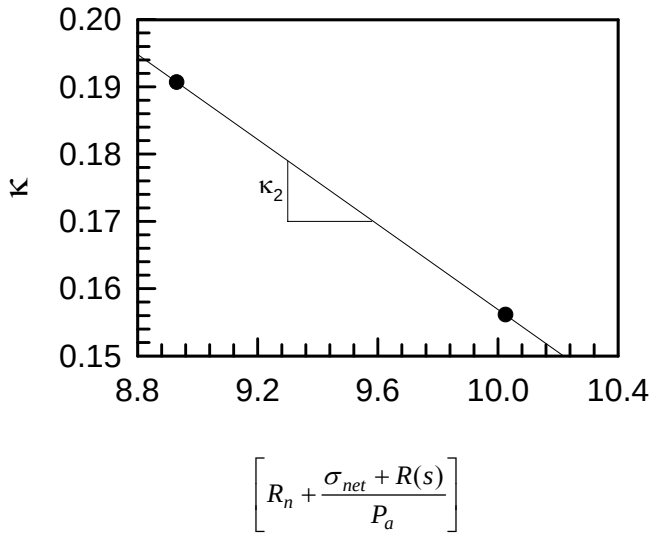

Figure 7.11: Typical plot for determination of κ for u_a-u_w = 100 kPa for rough interface

For the smooth interface, initial compression was observed followed by steady state. Differences in vertical displacement for 20 and 50 kPa suction values were negligible and the predictions were made by using the average value of κ for 20 kPa suction only. For 100 kPa suction, vertical displacement increased as the net normal stress increased. Therefore, for the smooth interface also, Equation 7.28 was used to predict the results of 100 kPa suction.

Figure 7.12 shows the back predictions made using the Equation 7.27 (i.e., without incorporating σ_n-u_a). It is obvious from Fig. 7.12 that Equation 7.27 can not capture the change in the specimen height during shearing. Use of Equation 7.28 improves the back prediction of tests conducted at u_a-u_w = 100 kPa.

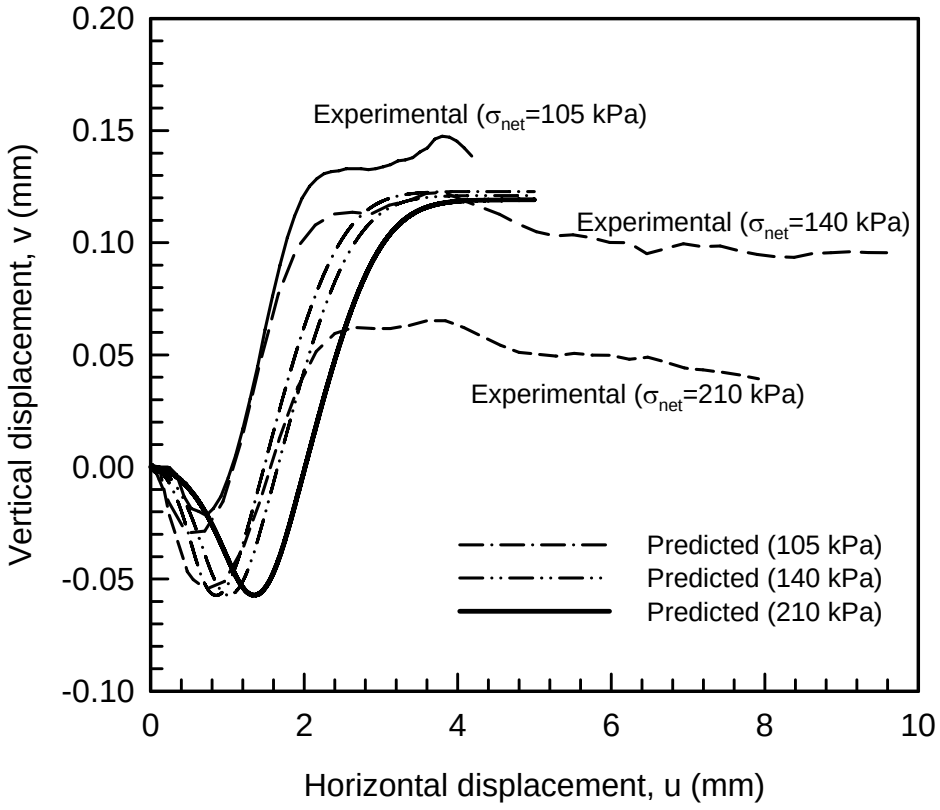

Figure 7.12: Predictions made by Equation 7.27 for u_a-u_w = 100 kPa

Parameters κ_1 and κ_2 were determined by using the results of tests conducted under 20 and 100 kPa at σ_n-u_a = 105 kPa and 210 kPa. For the smooth interface parameters κ_1 and κ_2 were calibrated by matching the experimental results and analytical results of 20 and 100 kPa suction tests. It was found and shown in Section 7.7 that a slight change in the value of κ results in a large change in volumetric behavior of the interface. However, further study is required to verify the volumetric behavior of interfaces during shearing under different suction values. Availability of more data than used in this study can help to improve the model capability of predicting the volume change behavior of unsaturated interfaces.

7.4.6 Determination of Residual Parameter, μ_0

Experimental results show that residual shear stress, τ_r , is not affected by the suction; therefore, in this study τ_r is related to R_n only in a manner similar to the original model:

$$\mu_0 = \frac{\tau_r}{\sigma_{net}} = \left[\mu_{01} + \mu_{02} R_n\right] \qquad (7.29)$$

μ_{01} and μ_{02} are the intercept and slope of the plot μ_0 versus R_n (Fig. 7.13).

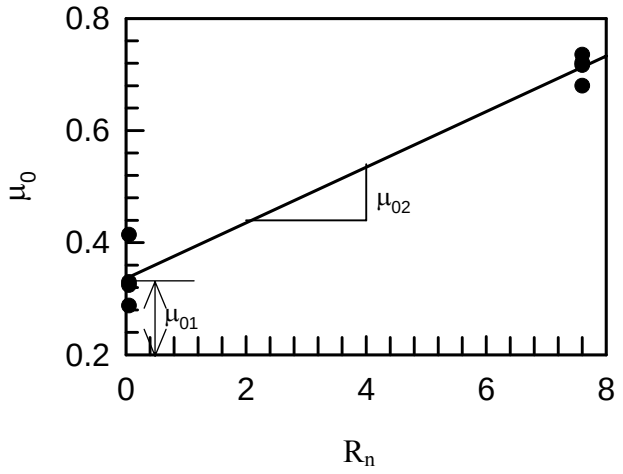

Figure 7.13: Determination of parameter $\mu_{01}$and μ_{02}

As mentioned before, the smooth interface did not exhibit steady state behavior after reaching peak shear strength (it followed stick-slip behavior). Residual shear stress of the smooth interface was approximated based on the lowest shear stress in the post peak region. To back predict the behavior of the smooth interface in post peak region, the value of μ_{01} was slightly modified (Refer Table 7.2) due to the scatter in data (see Fig. 7.13).

7.4.7 Determination of Parameter, R(s)

The following equation is proposed for R(s):

$$R(s) = \lambda(s) * (u_a - u_w) + \lambda_1 R_n + \lambda_2 \qquad (7.30)$$

Data points are plotted for all suction (u_a-u_w) values against R(s) and the slope of this plot yields the value of $\lambda(s)$ (Fig. 7.14a). Intercept of u_a-u_w vs. R(s), i.e., λ^* for each net normal stress is plotted against R_n as shown in Fig. 7.14b. Slope and intercept of plot R_n vs. λ^* yield parameters λ_1 and λ_2.

7.5 VERIFICATION OF THE MODEL

A computer code was written in MATLAB for the back prediction of test results using the elastoplastic model described in this chapter. The computer code was used to back predict the behavior of the interface between Toyoura Sand (D_r = 90%) and a steel plate with the model parameters reported by Navayogarajah (1990). Figure 7.15 shows the back predictions made by Navayogarajah (1990) and Fig. 7.16 shows the back predictions for three surface roughnesses of 40, 19, and 9.6 mm by using the computer code written in this study. Stress ratio (τ/σ_n) versus horizontal displacement (u) results compare well with those predicted by Navayogarajah (1990) and reproduced in Figure 7.15. Similarly, the volume change predictions were in agreement with those reported by Navayogarajah (1990) for surface roughnesses of 9.6 and 18 μm, whereas the volume change behavior for the surface roughness of 40 μm was over estimated as compared with prediction made by Navayogarajah (1990). Fakharian (1996) also back predicted the results of the interface between Toyoura Sand (D_r = 90%) and steel plate with the model parameters reported by Navayogarajah (1990) and the results for the roughness of 40μm

determined in this study were in agreement with those reported by Fakharian (1996). These comparisons were considered satisfactory and indicate that the model has been correctly formulated in the computer code.

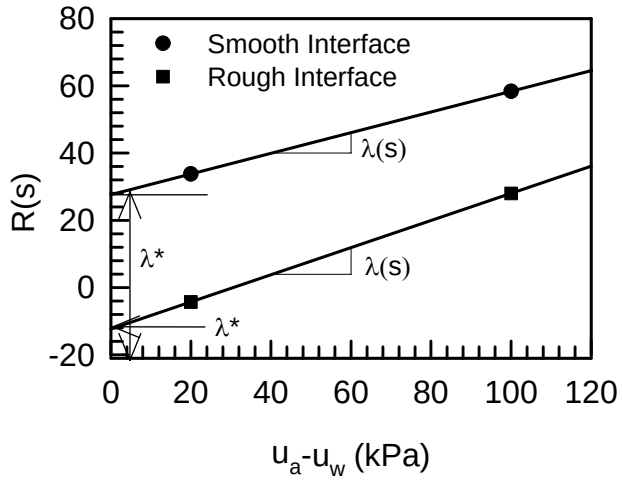

(a)

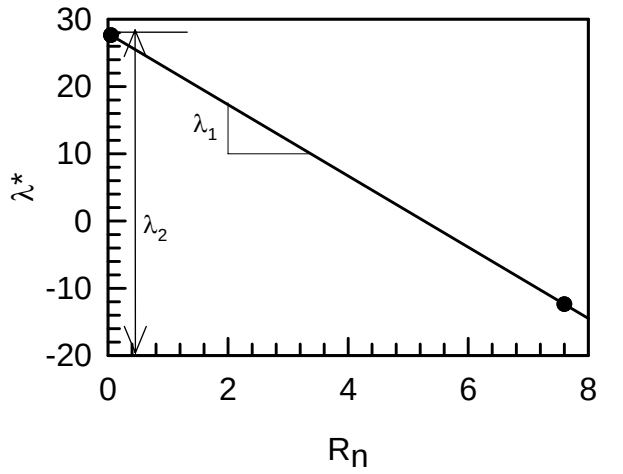

(b)

Figure 7.14: Determination of parameters for determining R(s): (a) determination of λ^* and $\lambda(s)$ (b) Determination of λ_1 and λ_2

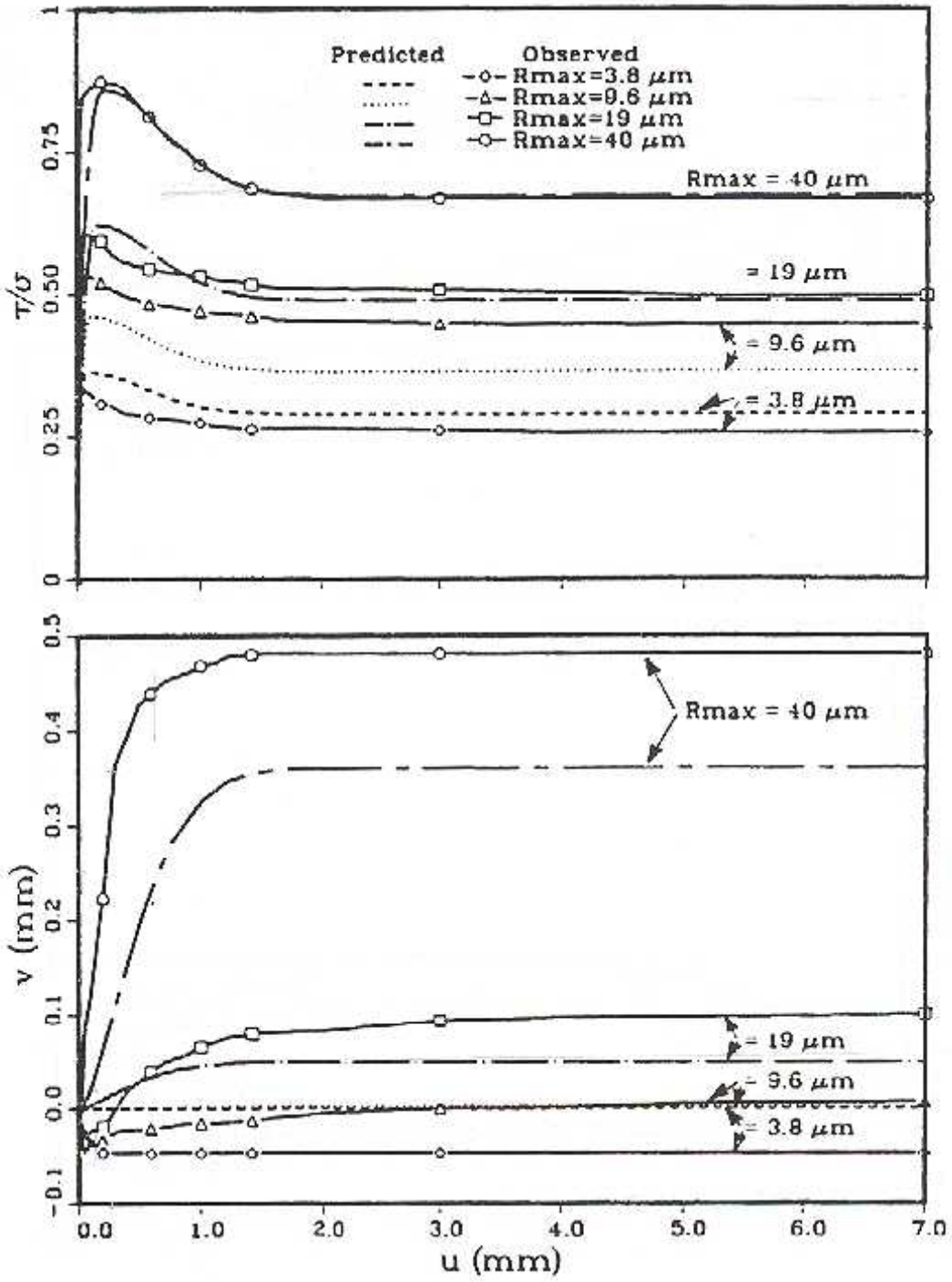

Figure 7.15: Predicted results for σ = 98 kPa, D_r = 90%, Steel-Toyoura Sand interface, monotonic loading (Fig. 5.9 of Navayogarajah 1990)

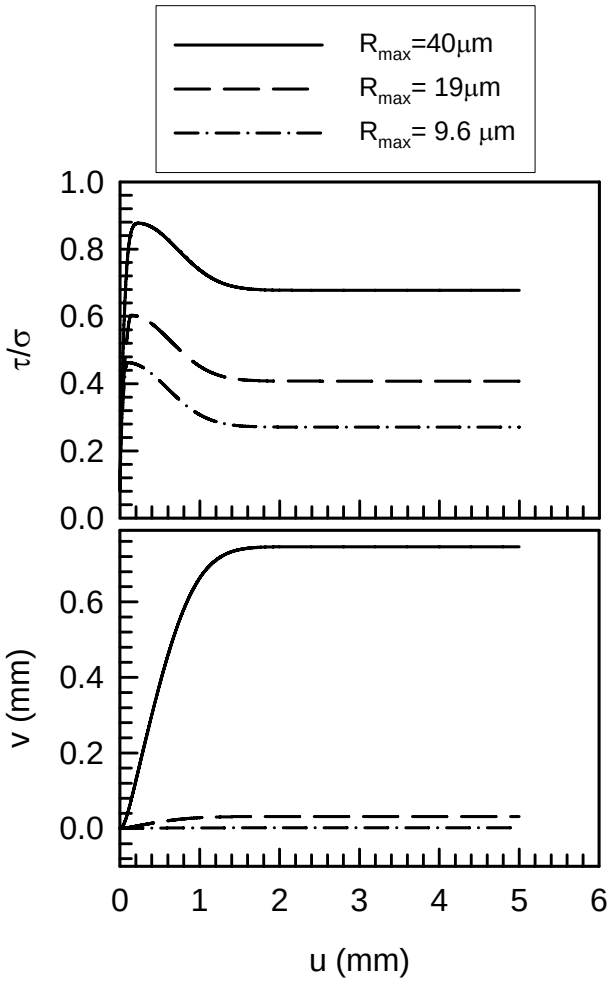

Figure 7.16: Predictions using the Navayogarajah et al. (1992) model for the test results shown in Fig. 7.15

7.6 PREDICTIONS FOR UNSATURATED INTERFACE TEST RESULTS

In this section, the experimental results are back predicted with the proposed unsaturated interface model. Figures 7.17 to 7.27 show the comparison between predictions and experimental results. Parameters used for the simulations are given in Tables 7.2 and 7.3. Test data corresponding to u_a-u_w = 50 kPa and σ_n-u_a = 140 kPa were not used to calculate the model parameters to show the predictive capability of the model. In this section, results of only two smooth interface tests are presented in Figures 7.26 and 7.27; the rest of the results for smooth interface are included as Appendix II. Model parameters γ, κ, and ξ_D^* are dependent on roughness ratio, R_n, as well as on suction (u_a-u_w). Hardening parameters 'a' and 'b' are also a function of roughness and suction. However, it was found that these parameters were not very sensitive to the suction; therefore, the back predictions are made by using the average values of 'a' and 'b' for all suction values. Experimental data for interfaces suggested an increase in peak shear strength with suction but a constant residual shear stress for a given net normal stress regardless of suction. Therefore, parameter μ_0 depends only on roughness. The smooth interface showed stick-slip behavior; however, no attempt was made to incorporate this behavior in the model.

Comparisons between back predictions and experimental results show that the proposed model is capable to capture the important behavior of an unsaturated soil-steel interface such as:

1) increasing peak shear strength of unsaturated soil-steel interface with increasing suction,
2) constant residual shear strength of unsaturated interface regardless of suction value, and
3) pronounced strain softening effect for higher suction and higher net normal stress values.

Figures 7.17b to 7.25b show the comparison of back predicted results with the experimental data in shear displacement-vertical displacement plane for the rough interface. Figures 7.26b and 7.27b show the volumetric behavior of the smooth interface. Back prediction results show that the model is capable of capturing the following important volume change behavior of unsaturated interfaces, as observed in the laboratory:

1) the rough interface initially compresses and then dilates or remains steady, and
2) the smooth interface initially shows compression and then exhibits little or no volume change.

Experimental data presented in Figures 7.17b to 7.25b illustrate that dilation reduces with increase in net normal stress for rough interface and comparison of experimental data with predicted results showed that the model is capable of simulating this effect.

The comparison presented in this section showed that the model is capable of capturing all important aspects of the strength and volumetric behavior of the interface between unsaturated soil and steel. It is important to mention that the proposed model is applicable for constant suction and constant net normal stress conditions; however, parameters are a function of suction and net normal stress.

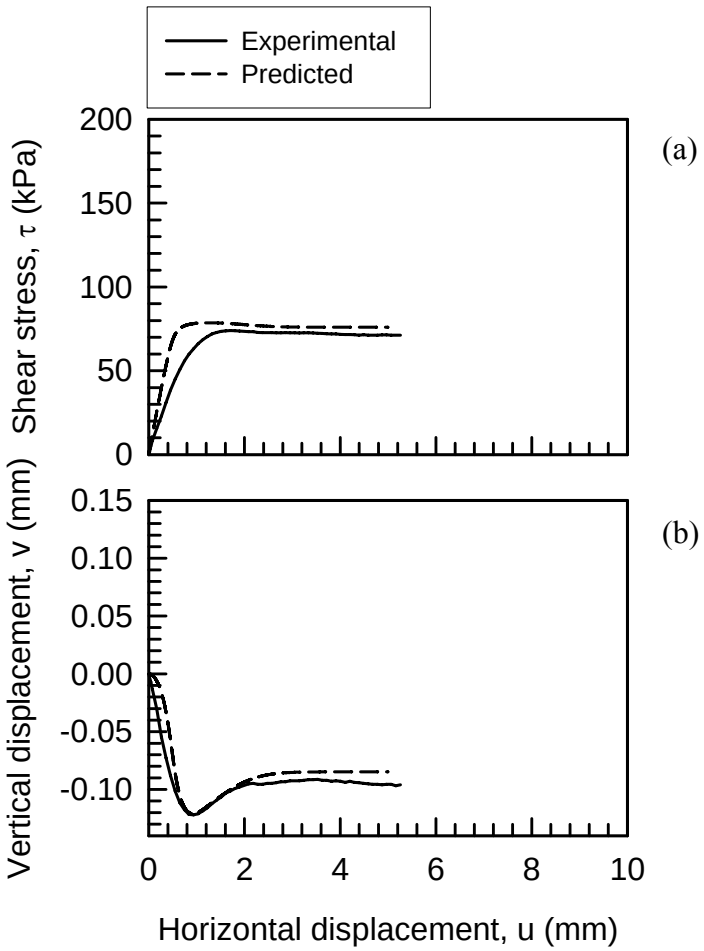

Figure 7.17: Comparison between predicted and experimental results for u_a-u_w = 20 kPa and σ_n-u_a = 105 kPa; rough interface

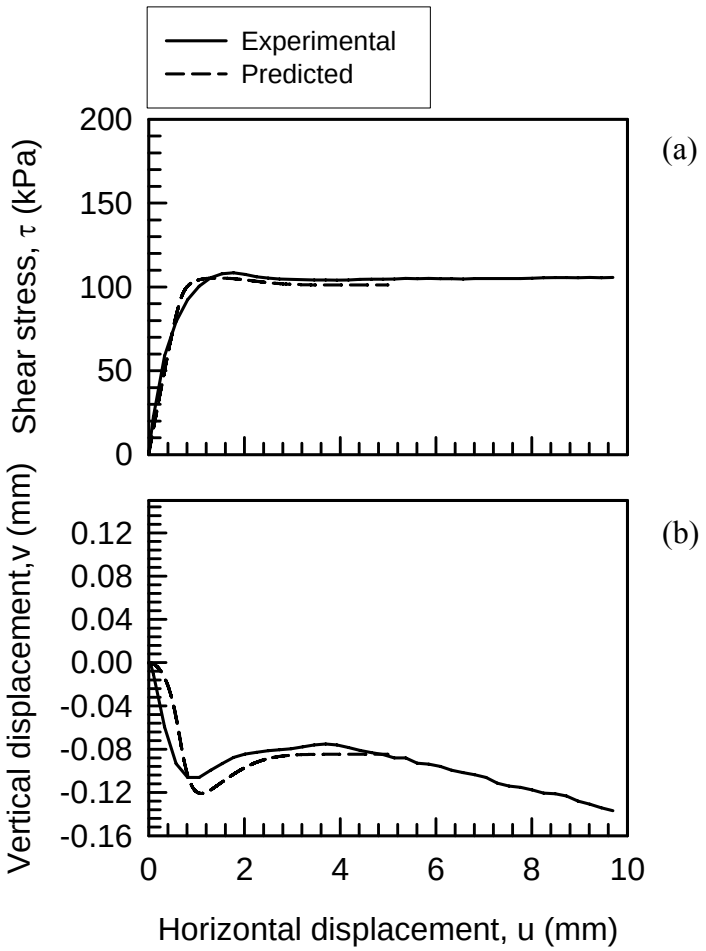

Figure 7.18: Comparison between predicted and experimental results for u_a-u_w = 20 kPa and σ_n-u_a = 140 kPa; rough interface

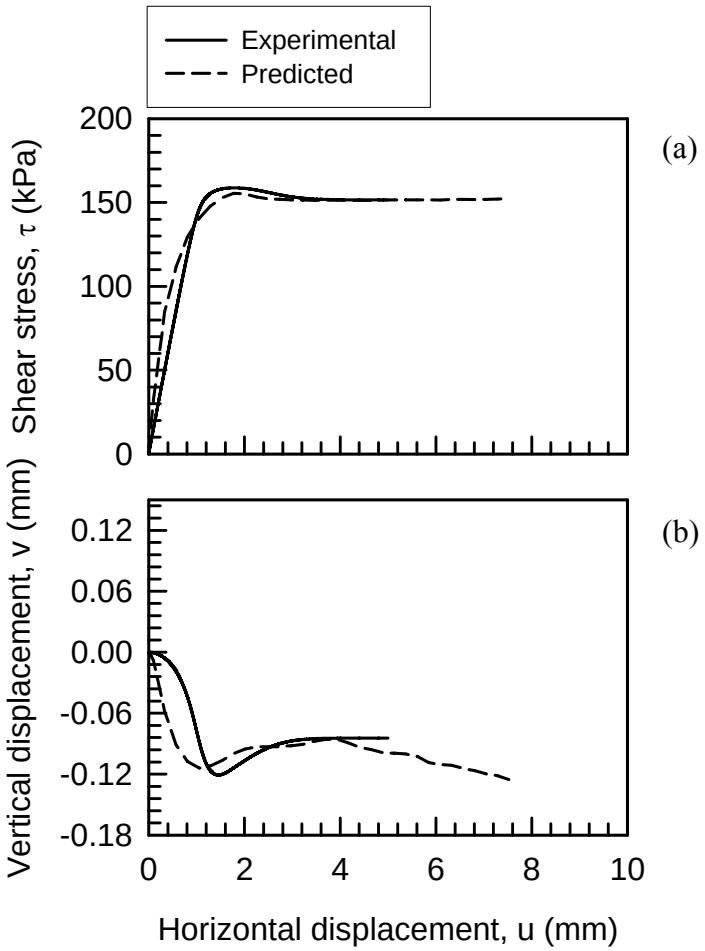

Figure 7.19: Comparison between predicted and experimental results for u_a-u_w = 20 kPa and σ_n-u_a = 210 kPa; rough interface

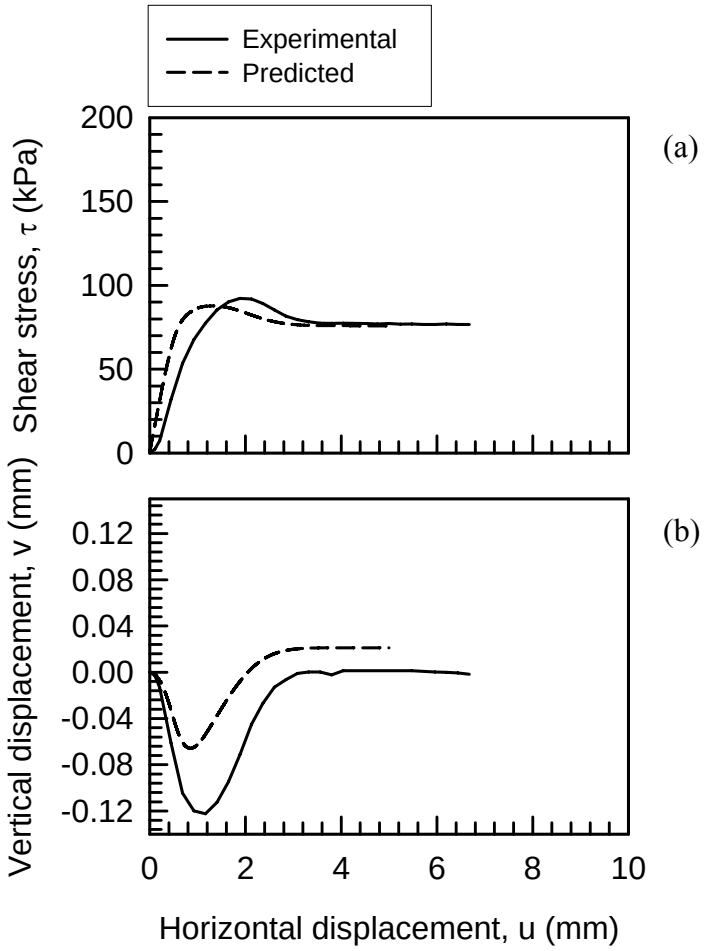

Figure 7.20: Comparison between predicted and experimental results for u_a-u_w = 50 kPa and σ_n-u_a = 105 kPa; rough interface

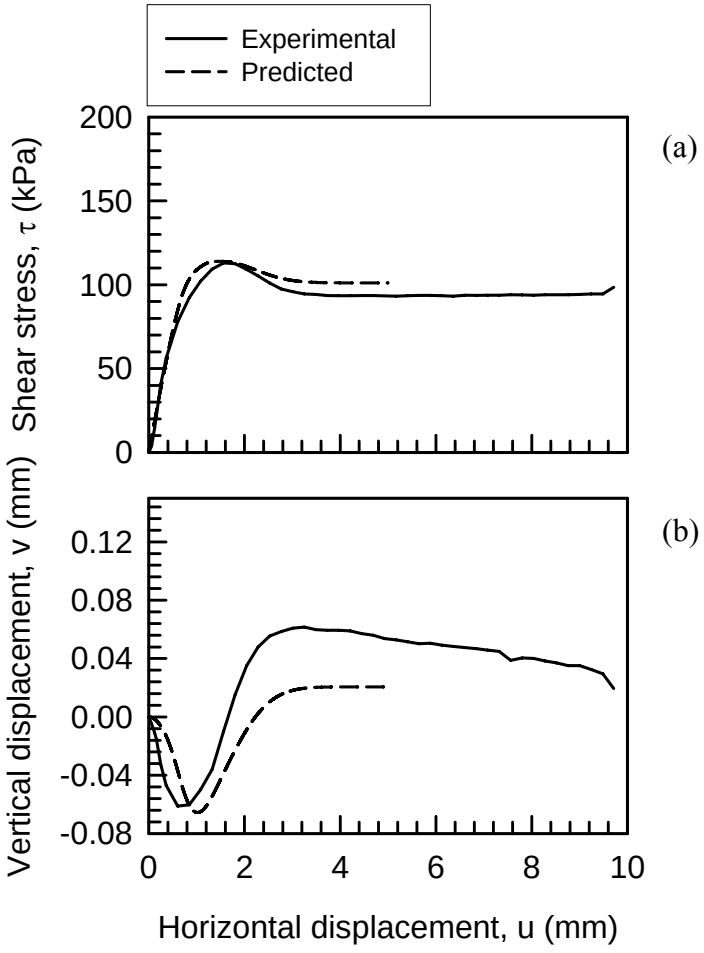

Figure 7.21: Comparison between predicted and experimental results for u_a-u_w = 50 kPa and σ_n-u_a = 140 kPa; rough interface

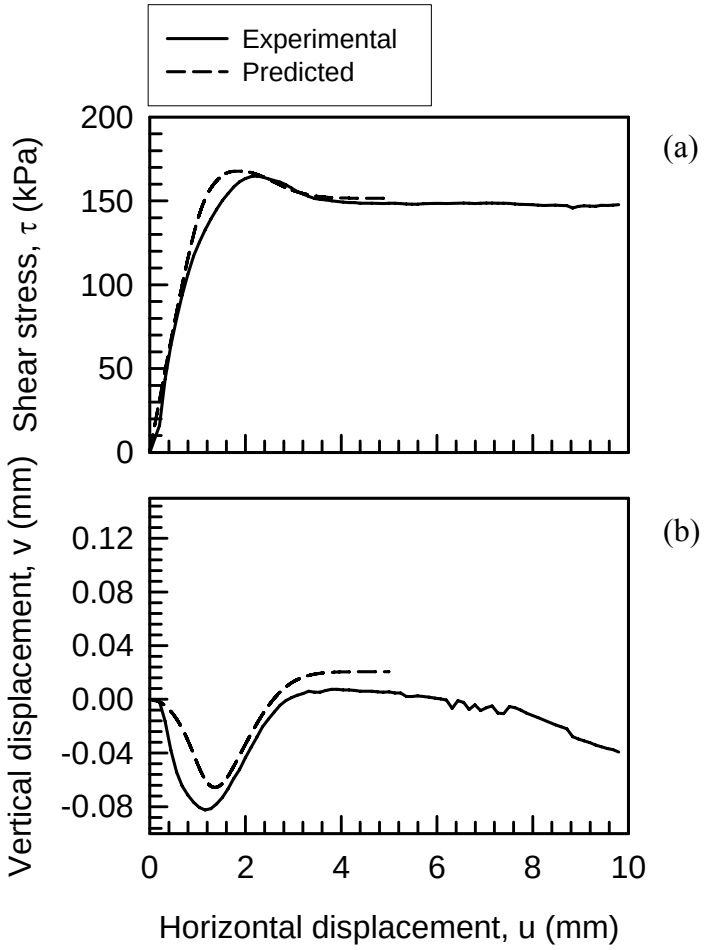

Figure 7.22: Comparison between predicted and experimental results for u_a-u_w = 50 kPa and σ_n-u_a = 210 kPa; rough interface

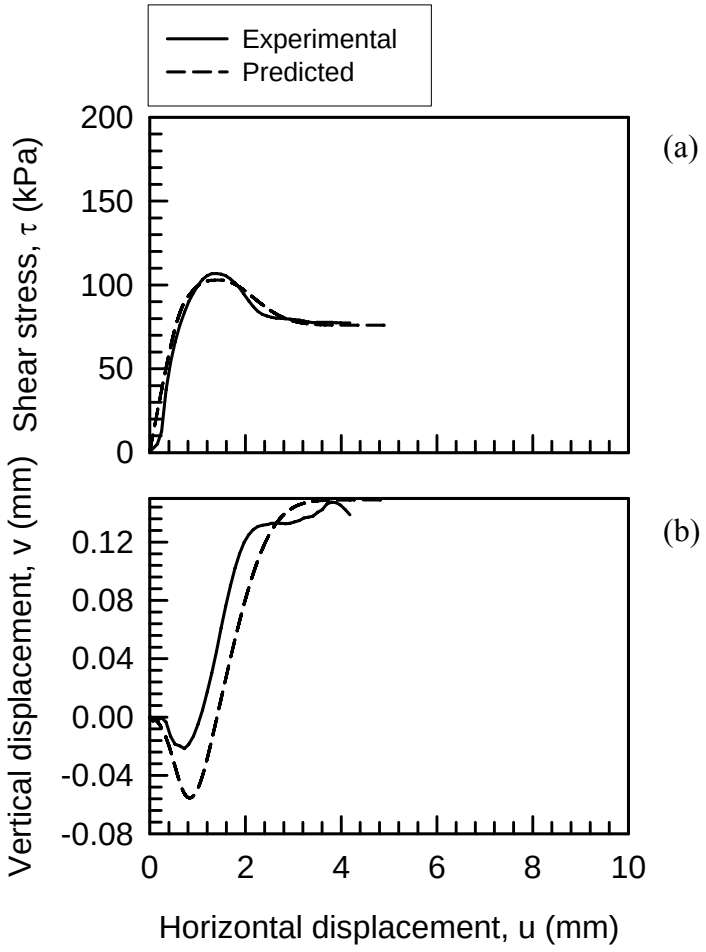

Figure 7.23: Comparison between predicted and experimental results for u_a-u_w = 100 kPa and σ_n-u_a = 105 kPa; rough interface

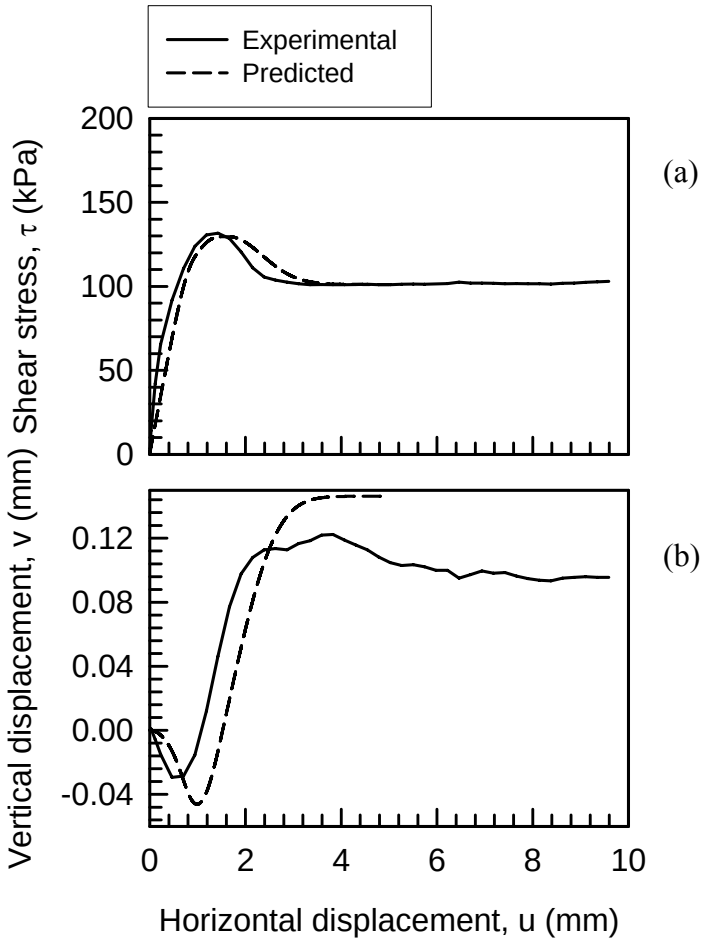

Figure 7.24: Comparison between predicted and experimental results for u_a-u_w = 100 kPa and σ_n-u_a = 140 kPa; rough interface

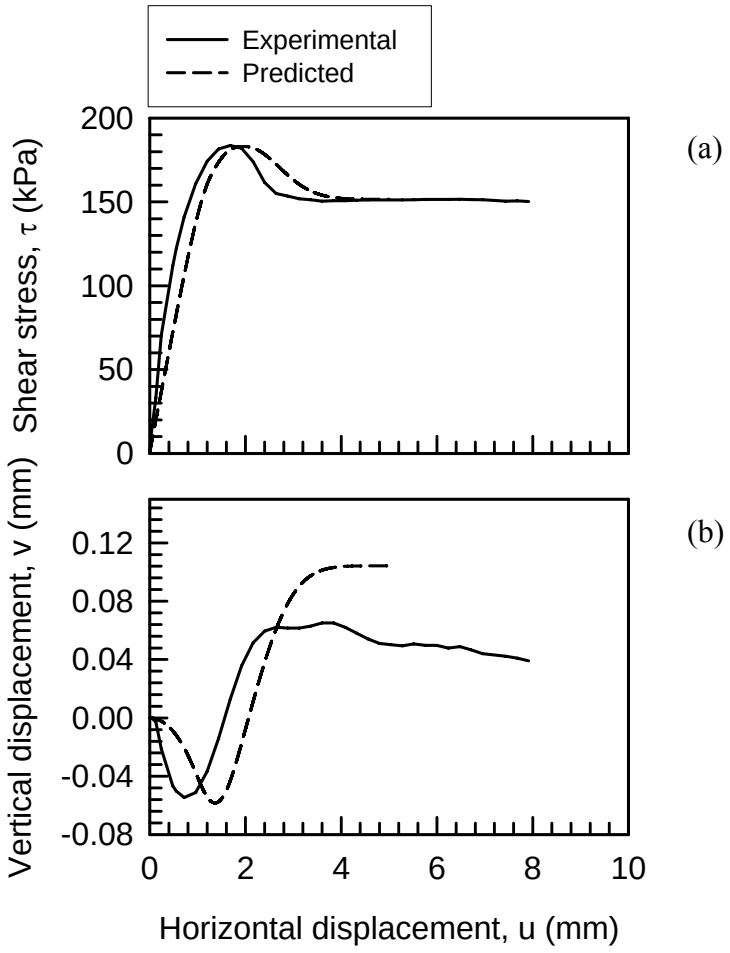

Figure 7.25: Comparison between predicted and experimental results for u_a-u_w = 100 kPa and σ_n-u_a = 210 kPa; rough interface

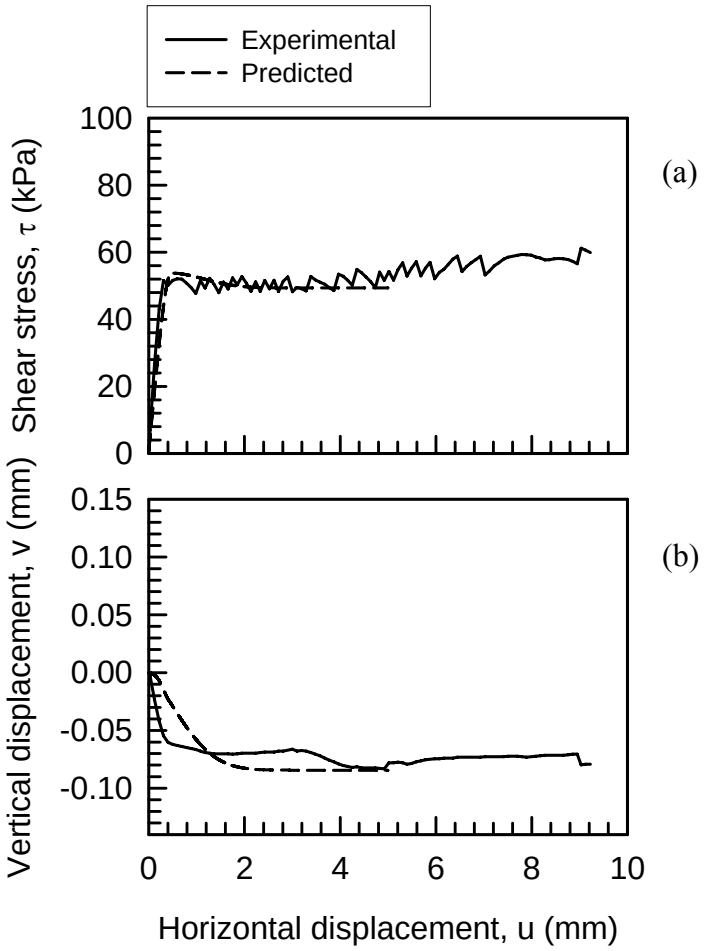

Figure 7.26: Comparison between predicted and experimental results for u_a-u_w = 50 kPa and σ_n-u_a = 140 kPa; smooth interface

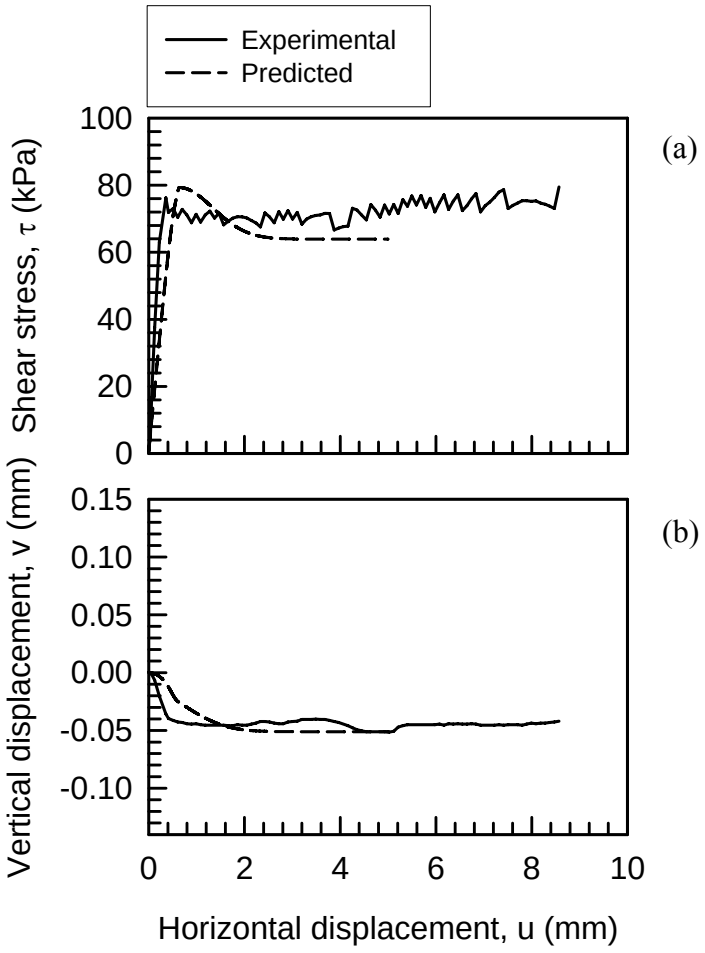

Figure 7.27: Comparison between predicted and experimental results for u_a-u_w = 100 kPa and σ_n-u_a = 210 kPa; smooth interface

Table 7.2: Model Parameters for Rough Interface

ROUGH INTERFACE										
u_a-u_w (kPa)		20			50			100		
σ_n-u_a (kPa)		105	140	210	105	140	210	105	140	210
ξ_D^* (mm)	ξ_{D1}^*	0.0318	0.0318	0.0318	0.0318	0.0318	0.0318	0.0318	0.0318	0.0318
	ξ_{D2}^*	0.0951	0.0951	0.0951	0.0951	0.0951	0.0951	0.0951	0.0951	0.0951
n		8	8	8	4	4	4	4	4	4
γ(s)	μ_{p1}	0.2796	0.2796	0.2796	0.2796	0.2796	0.2796	0.2796	0.2796	0.2796
	μ_{p2}	0.0635	0.0635	0.0635	0.0635	0.0635	0.0635	0.0635	0.0635	0.0635
μ_0	μ_{01}	0.3479	0.3479	0.3479	0.3479	0.3479	0.3479	0.3479	0.3479	0.3479
	μ_{02}	0.049	0.049	0.049	0.049	0.049	0.049	0.049	0.049	0.049
κ	κ_1	-2.9927	-2.9927	-2.9927	-2.9927	-2.9927	-2.9927	0.4728	0.4728	0.4728
	κ_2	0.4004	0.4004	0.4004	0.4004	0.4004	0.4004	-0.0316	-0.0316	-0.0316
a		17.4	17.4	17.4	17.4	17.4	17.4	17.4	17.4	17.4
b		2.85	2.85	2.85	2.85	2.85	2.85	2.85	2.85	2.85
R(s)	λ(s)	0.3990	0.3990	0.3990	0.3990	0.3990	0.3990	0.3990	0.3990	0.3990
	λ_1	-5.2285	-5.2285	-5.2285	-5.2285	-5.2285	-5.2285	-5.2285	-5.2285	-5.2285
	λ_2	29.4865	29.4865	29.4865	29.4865	29.4865	29.4865	29.4865	29.4865	29.4865
K_n (kPa)		1000	1000	1000	1000	1000	1000	1000	1000	1000
K_s (kPa)		150	150	150	150	150	150	150	150	150

Table 7.3: Model Parameters for Smooth Interface

SMOOTH INTERFACE										
u_a-u_w (kPa)		20			50			100		
σ_n-u_a (kPa)		105	140	210	105	140	210	105	140	210
ξ_D^* (mm)	ξ_{D1}^*	0.0318	0.0318	0.0318	0.0318	0.0318	0.0318	0.0318	0.0318	0.0318
	ξ_{D2}^*	0.0951	0.0951	0.0951	0.0951	0.0951	0.0951	0.0951	0.0951	0.0951
n		7	7	7	7	7	7	7	7	7
γ(s)	μ_{p1}	0.2796	0.2796	0.2796	0.2796	0.2796	0.2796	0.2796	0.2796	0.2796
	μ_{p2}	0.0635	0.0635	0.0635	0.0635	0.0635	0.0635	0.0635	0.0635	0.0635
μ_0	μ_{01}	0.3479	0.3479	0.3000	0.3479	0.3479	0.3000	0.3479	0.3479	0.3000
	μ_{02}	0.049	0.049	0.049	0.049	0.049	0.049	0.049	0.049	0.049
κ	κ_1	0.2308	0.2308	0.2308	0.2308	0.2308	0.2308	0.0229	0.0229	0.0229
	κ_2	-	-	-	-	-	-	-0.0318	-0.0318	-0.0318
a		56	56	56	56	56	56	56	56	56
b		1	1	1	1	1	1	1	1	1
R(s)	λ(s)	0.3990	0.3990	0.3990	0.3990	0.3990	0.3990	0.3990	0.3990	0.3990
	λ_1	-5.2285	-5.2285	-5.2285	-5.2285	-5.2285	-5.2285	-5.2285	-5.2285	-5.2285
	λ_2	29.4865	29.4865	29.4865	29.4865	29.4865	29.4865	29.4865	29.4865	29.4865
K_n (kPa)		1000	1000	1000	1000	1000	1000	1000	1000	1000
K_s (kPa)		150	150	150	150	150	150	150	150	150

7.7 EFFECT OF VARIATION OF MODEL PARAMETERS

Figures 7.28 to 7.40 show the qualitative and quantitative influence of various parameters of the interface constitutive model. To study the effect of variation of model parameters, values of parameters were selected in such a way that the effect of variation becomes clear. The qualitative influence of varying shear stiffness of the interface (K_s) is shown in Fig. 7.28. Increase in K_s results in stiffer behavior of the interface; however, the variation in K_s does not affect the peak shear strength and maximum compression or dilation. The change in normal stiffness (K_n) does not affect the behavior of the interface during shearing.

The effect of variation in μ_{p1} and μ_{p2} ($\gamma(s)$) is depicted in Fig. 7.30. It is obvious from this figure that an increase in μ_{p1} and μ_{p2} (or $\gamma(s)$) results in an increase in the peak shear strength of the interface and reduction in the value of μ_{p1} and μ_{p2} (or $\gamma(s)$) causes reduction in the peak shear strength. The value of maximum compression was not affected by variation in $\gamma(s)$; however, as $\gamma(s)$ reduces, so does the dilation behavior.

The influence of varying model parameters ‘a’ and ‘b’ is shown in Fig. 7.31. Variation in ‘a’ and ‘b’ does not affect the strength behavior of the interface (see Fig. 7.31a). However, the values corresponding to maximum compression and dilation vary with change in these parameters. For example when the parameter ‘a’ was increased from 17.4 to 36, keeping the value of ‘b’ constant (as 2.85), the maximum compression decreased and dilation behavior increased. Similar behavior was observed when the value of ‘b’ was increased from 1.7 to 2.85 with a = 17.4.

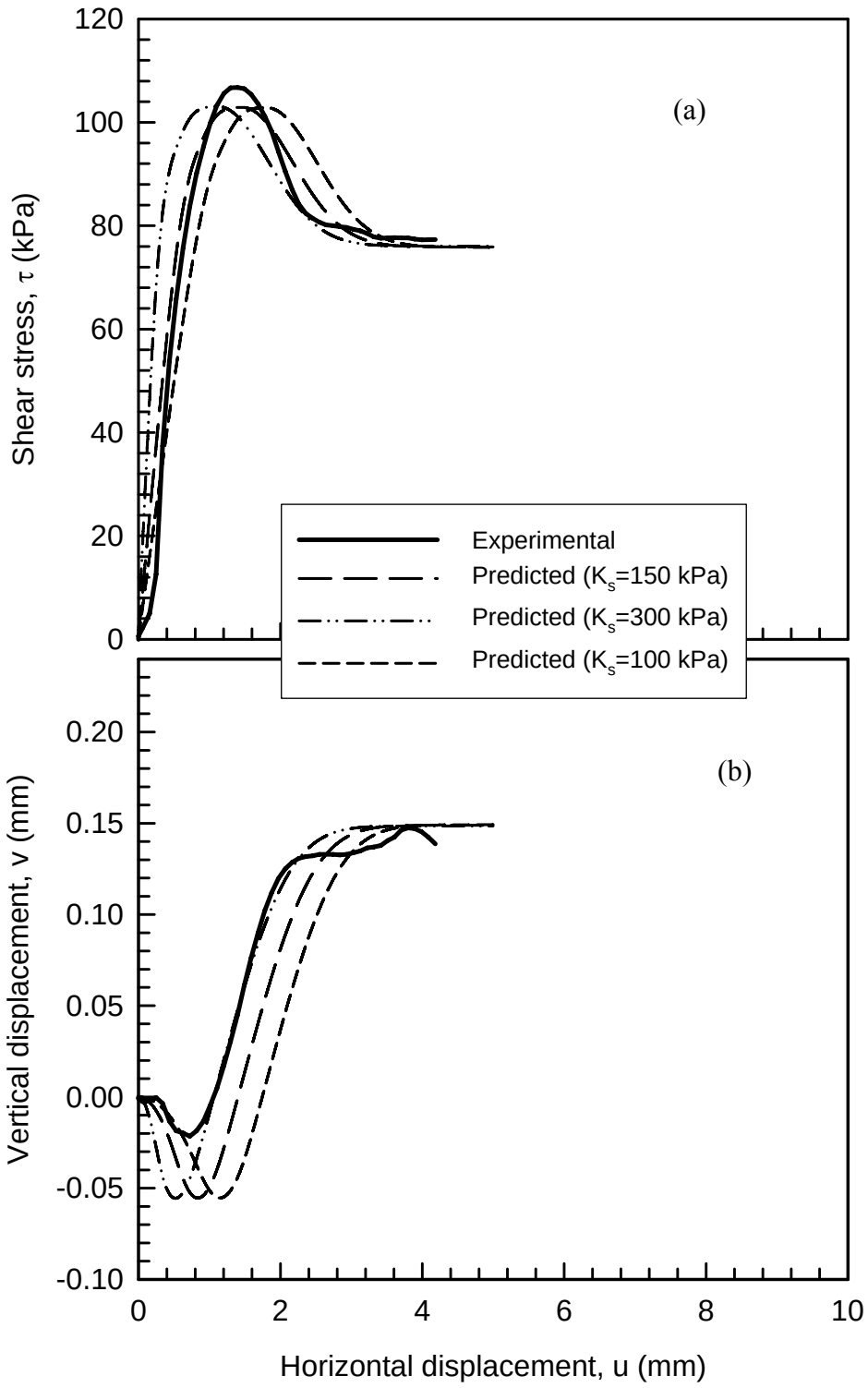

Figure 7.28: Effect of varying K_s on the predicted (a) τ vs. u and (b) u vs. v response of the rough interface at u_a-u_w = 100 kPa and σ_n-u_a = 105 kPa

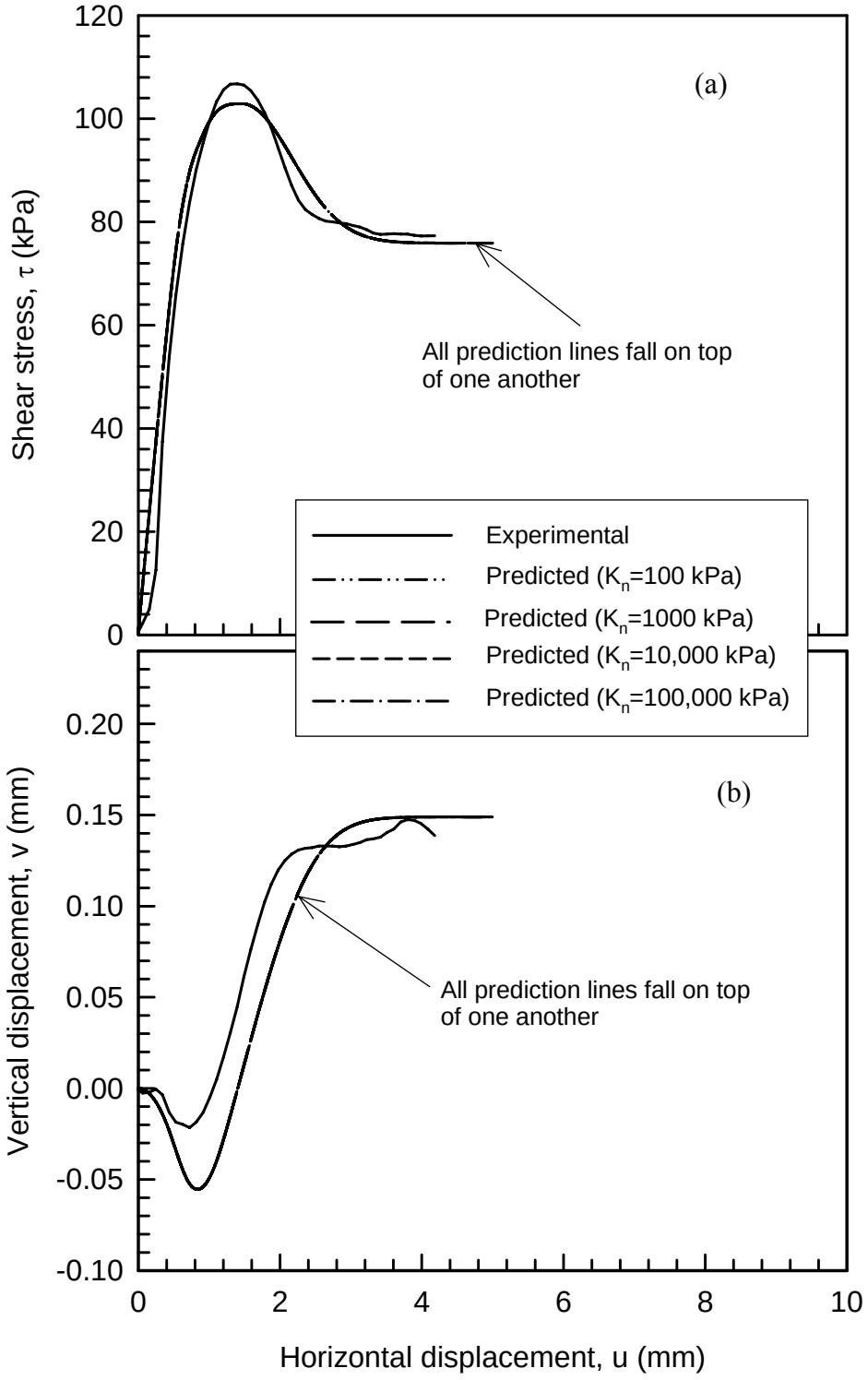

Figure 7.29: Effect of varying K_n on the predicted (a) τ vs. u and (b) u vs. v response of the rough interface at u_a-u_w = 100 kPa and σ_n-u_a = 105 kPa

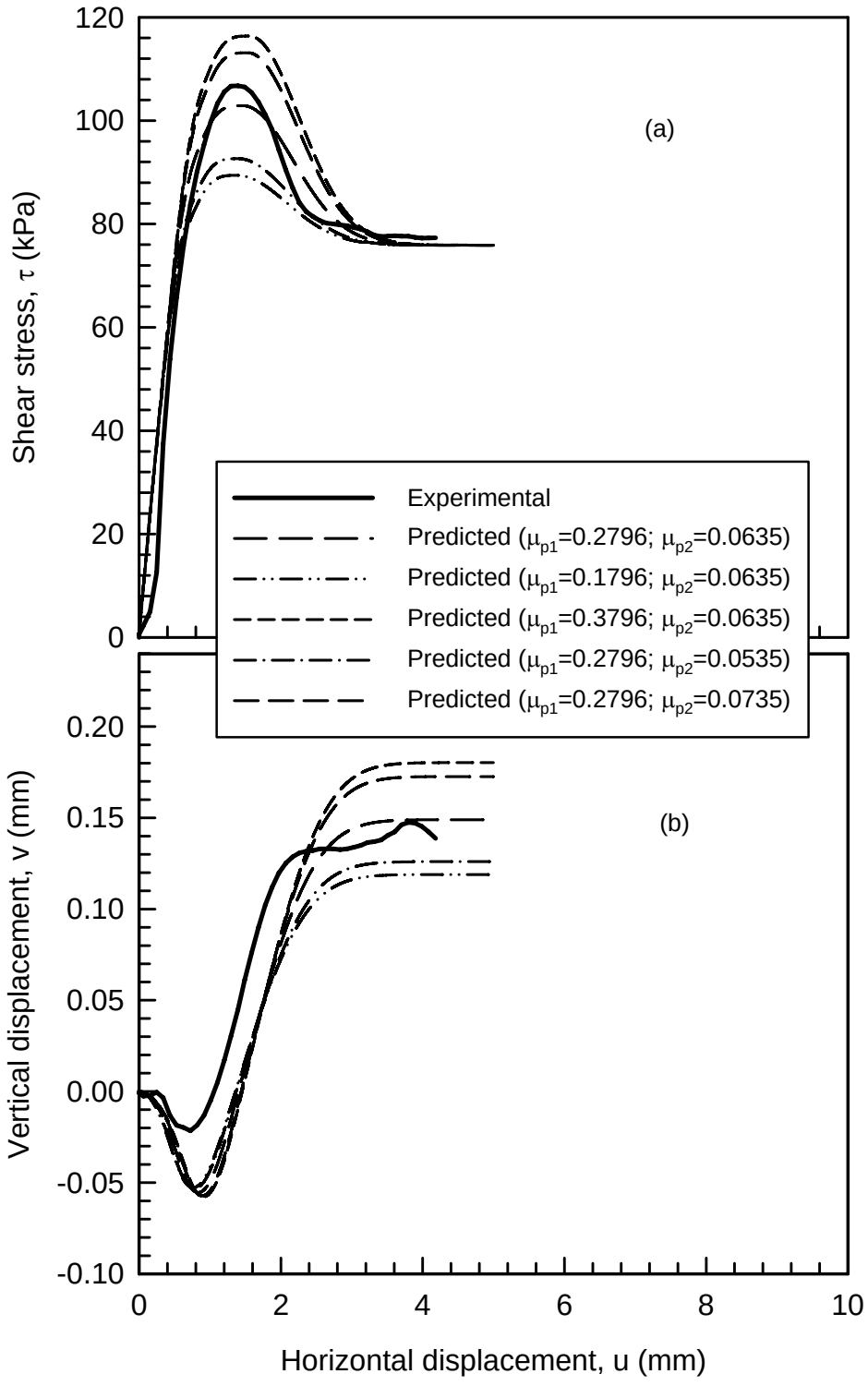

Figure 7.30: Effect of varying μ_{p1} and μ_{p2} on the predicted (a) τ vs. u and (b) u vs. v response of the rough interface at u_a-u_w = 100 kPa and σ_n-u_a = 105 kPa

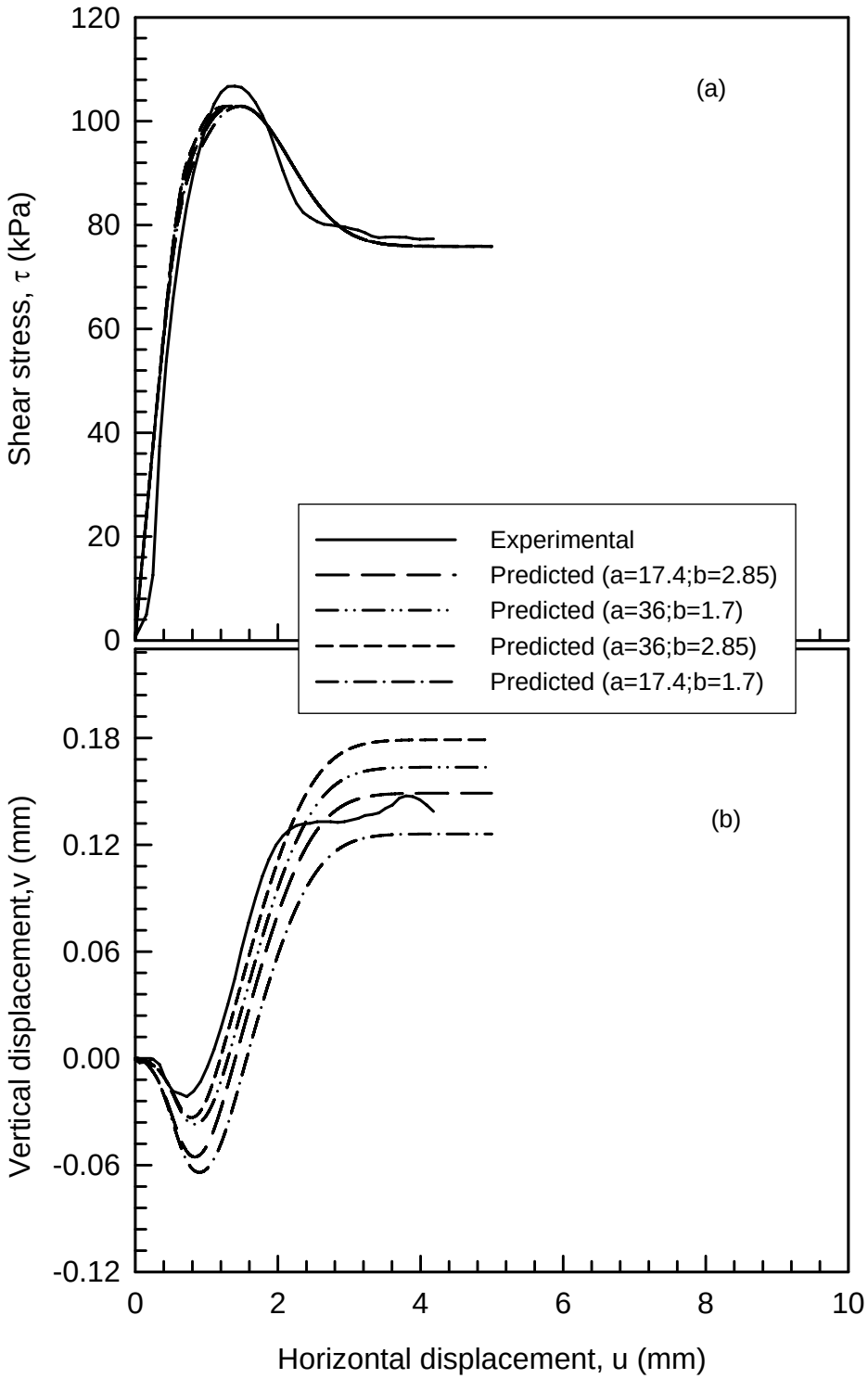

Figure 7.31: Effect of varying "a" & "b" on the predicted (a) τ vs. u and (b) u vs. v, response of the rough interface at u_a-u_w = 100 kPa and σ_n-u_a = 105 kPa

Model parameter ξ_D^* is a function of suction and surface roughness. Comparison of Figs. 7.32 and 7.33 shows that the parameter ξ_{D1}^* does not affect the interface behavior; however, increase in ξ_{D2}^* shifts the location of occurrence of peak shear strength. Increase in ξ_{D2}^* also caused increase in maximum compression and dilation.

The qualitative influence of varying phase change parameter (n) is shown in Fig. 7.34. As the value of 'n' increases, so does vertical compression. Variation in 'n' does not influence the strength behavior of the interface.

Figures 7.35 and 7.36 show the effect of nonassociative parameter κ on the volumetric and strength behavior of the interface. It is obvious that variation in κ does not affect the strength behavior of the soil. An increase in κ_1 results in increase in dilation behavior and negligible change in maximum compression. On the other hand, when the value of κ_2 decreased, the dilation behavior of the interface decreased with negligible change in vertical compression.

The parameter μ_0 is a function of roughness and depends on μ_{01} and μ_{02}. The parameter μ_0 controls the residual shear strength and the strain softening behavior of the interface. Reduction in the value of μ_{01} and μ_{02} results in a decrease in residual shear strength and increase in these parameters causes an increase in residual shear strength as shown in Fig. 7.37.

Figure 7.38 shows that a decrease in absolute value of λ_1 caused an increase in peak shear strength and an increase in absolute value of λ_1 resulted in an increase in peak shear strength of the interface. Figure 7.39 shows that λ_2 affect on the strength and volumetric behavior of the interface less than λ_1 and $\lambda(s)$; Fig. 7.40 shows the significant effect of

$\lambda(s)$ on the behavior of interface, where an increase in $\lambda(s)$ results in an increase of shear strength. The effect of $\lambda(s)$ on volume change behavior of the interface is negligible. Although the effects of model parameters on predictions are presented for selected tests, similar effects were observed (as presented in Figs. 7.28-7.40) for other tests conducted in this study.

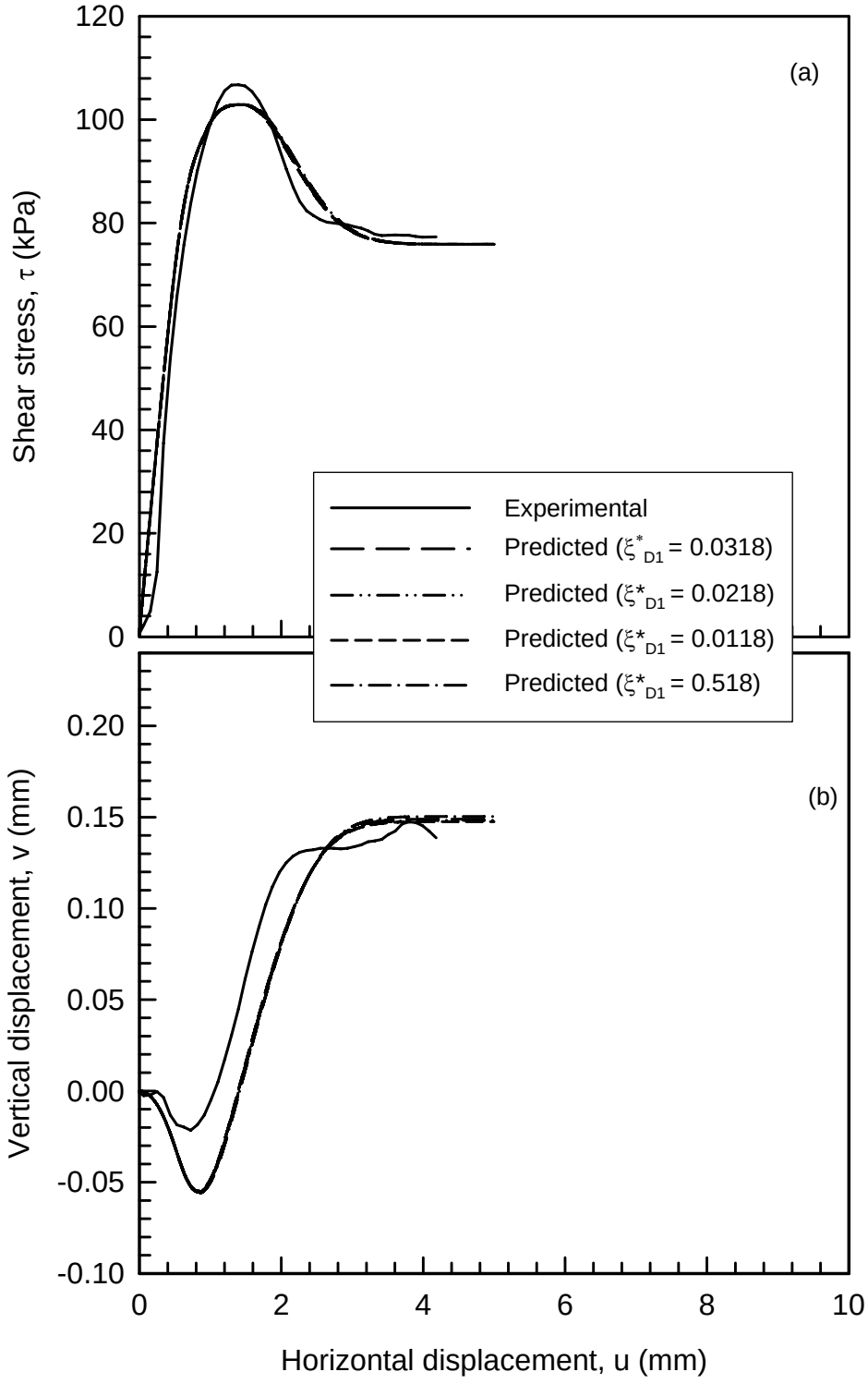

Figure 7.32: Effect of varying ξ^*_{D1} on the predicted (a) τ vs. u and (b) u vs. v, response of the rough interface at u_a-u_w = 100 kPa and σ_n-u_a = 105 kPa

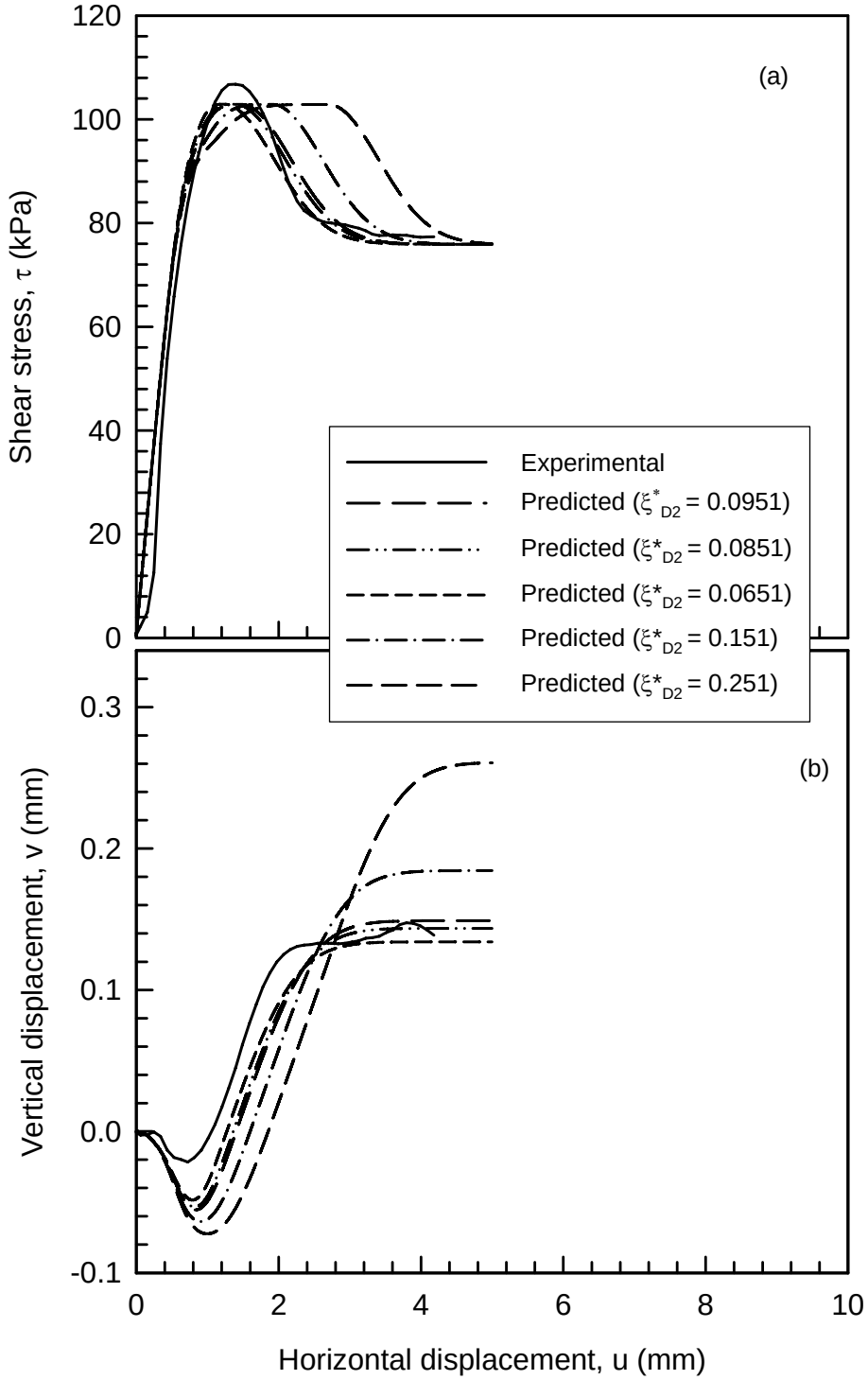

Figure 7.33: Effect of varying ξ^*_{D2} on the predicted (a) τ vs. u and (b) u vs. v response of the rough interface at u_a-u_w = 100 kPa and σ_n-u_a = 105 kPa

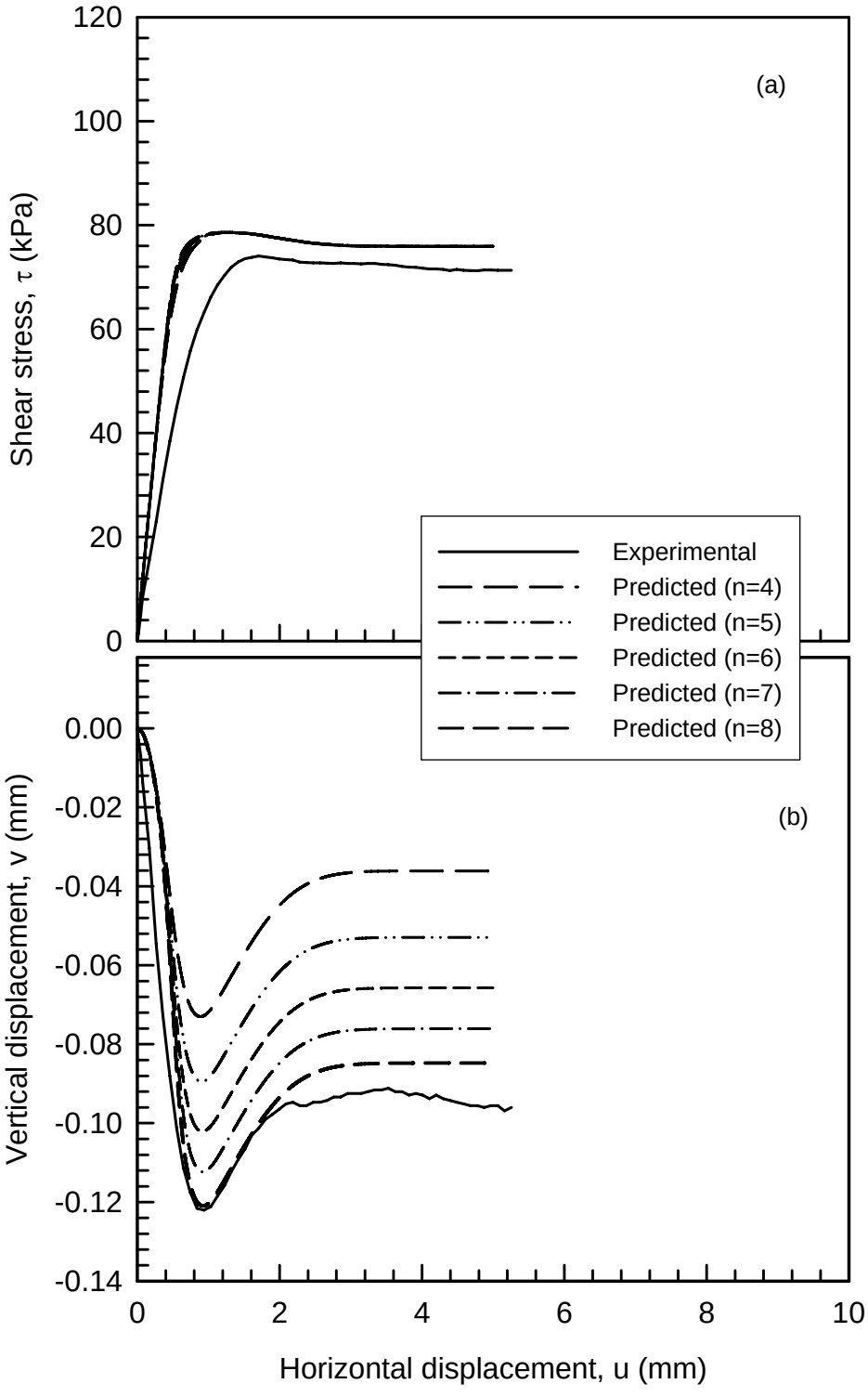

Figure 7.34: Effect of varying "n" on the predicted (a) τ vs. u and (b) u vs. v response of the rough interface at u_a-u_w = 20 kPa and σ_n-u_a = 105 kPa

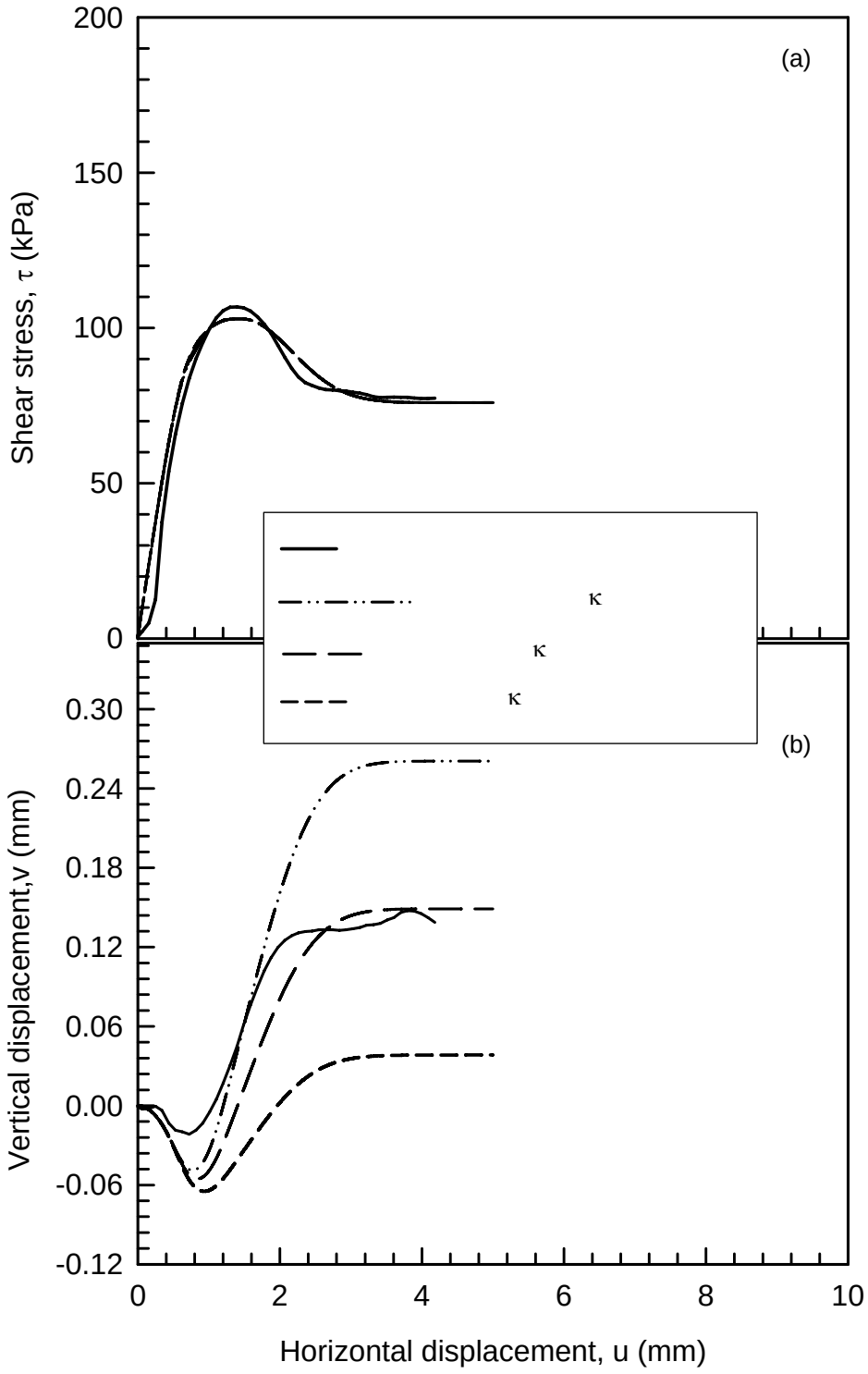

Figure 7.35: Effect of varying κ_1 on the predicted (a) τ vs. u and (b) u vs. v response of the rough interface at u_a-u_w = 100 kPa and σ_n-u_a = 105 kPa

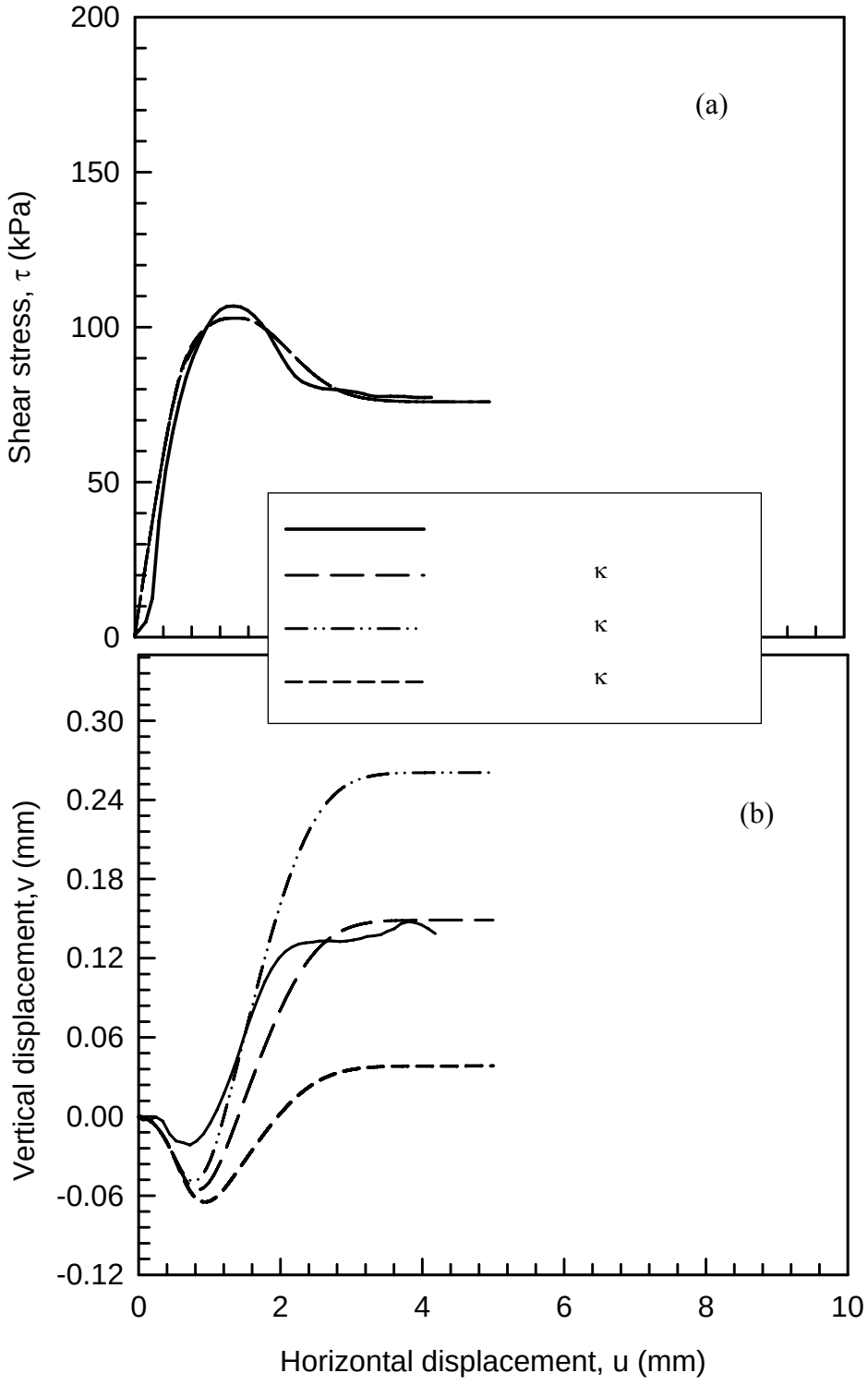

Figure 7.36: Effect of varying κ_2 on the predicted (a) τ vs. u and (b) u vs. v response of the rough interface at u_a-u_w = 100 kPa and σ_n-u_a = 105 kPa

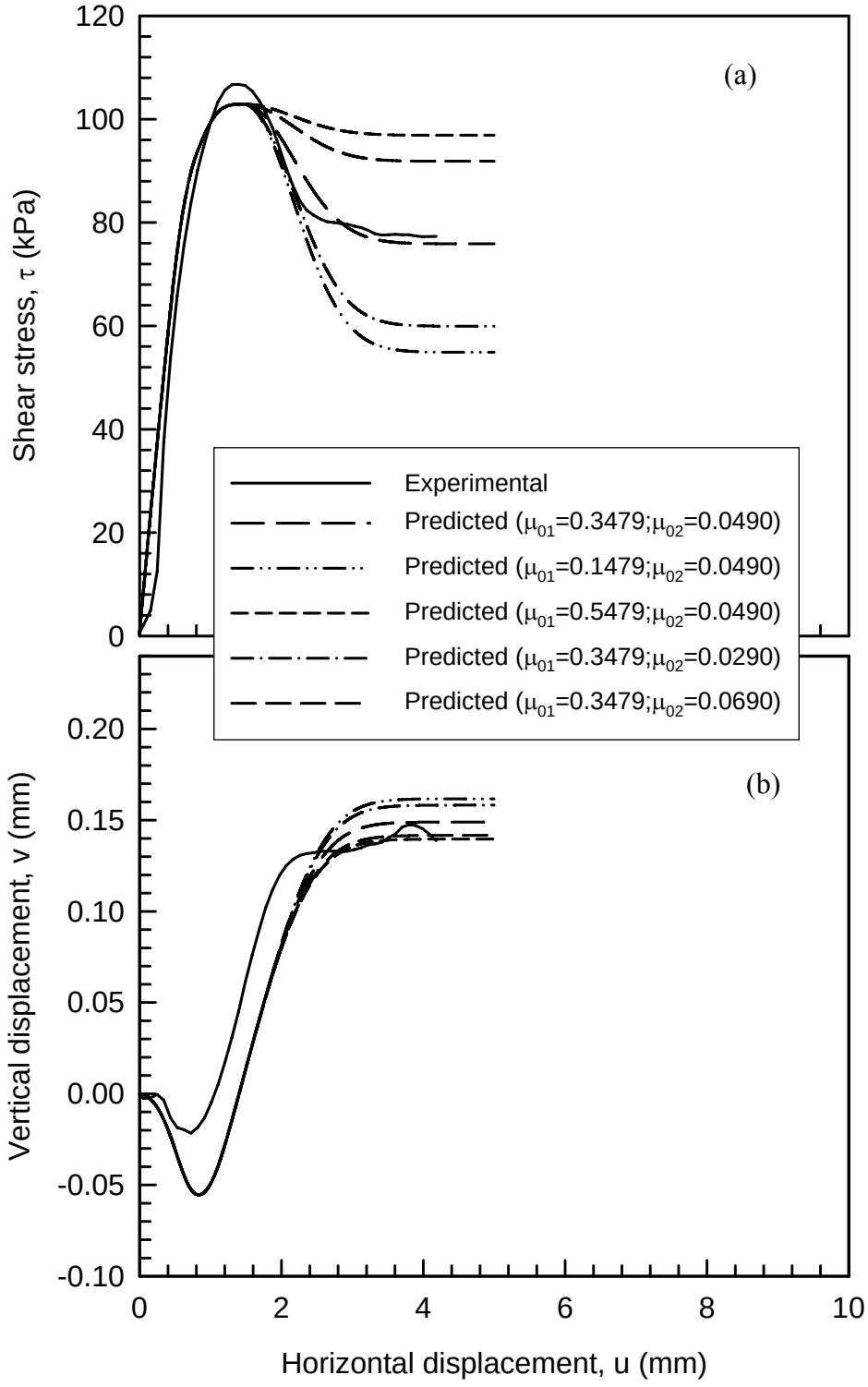

Figure 7.37: Effect of varying μ_{o1} & μ_{02} on the predicted (a) τ vs. u and (b) u vs. v, response of the rough interface at u_a-u_w = 100 kPa and σ_n-u_a = 105 kPa

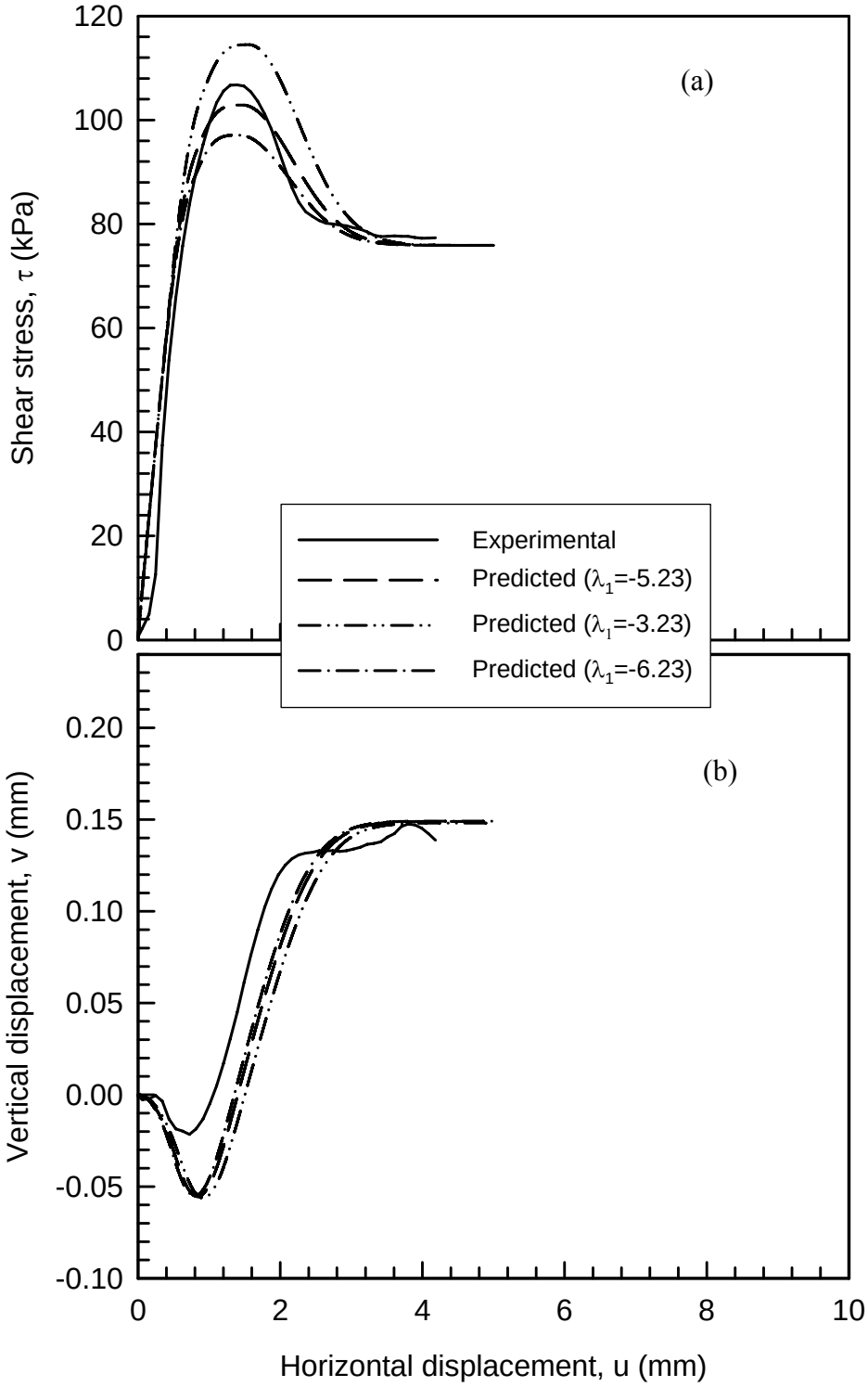

Figure 7.38: Effect of varying λ_1 on the predicted (a) τ vs. u and (b) u vs. v, response of the rough interface at u_a-u_w = 100 kPa and σ_n-u_a = 105 kPa

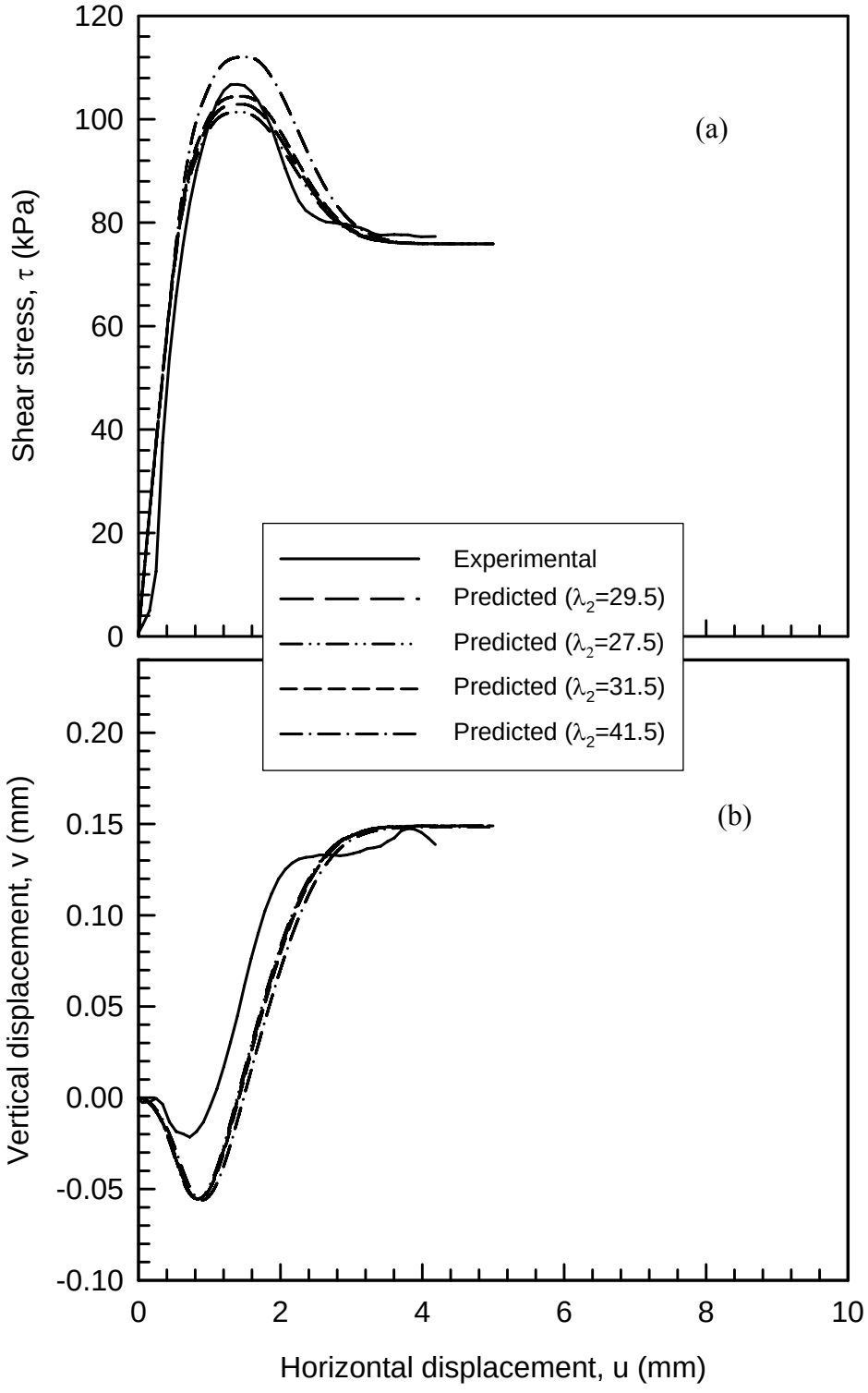

Figure 7.39: Effect of varying λ_2 on the predicted (a) τ vs. u and (b) u vs. v, response of the rough interface at u_a-u_w = 100 kPa and σ_n-u_a = 105 kPa

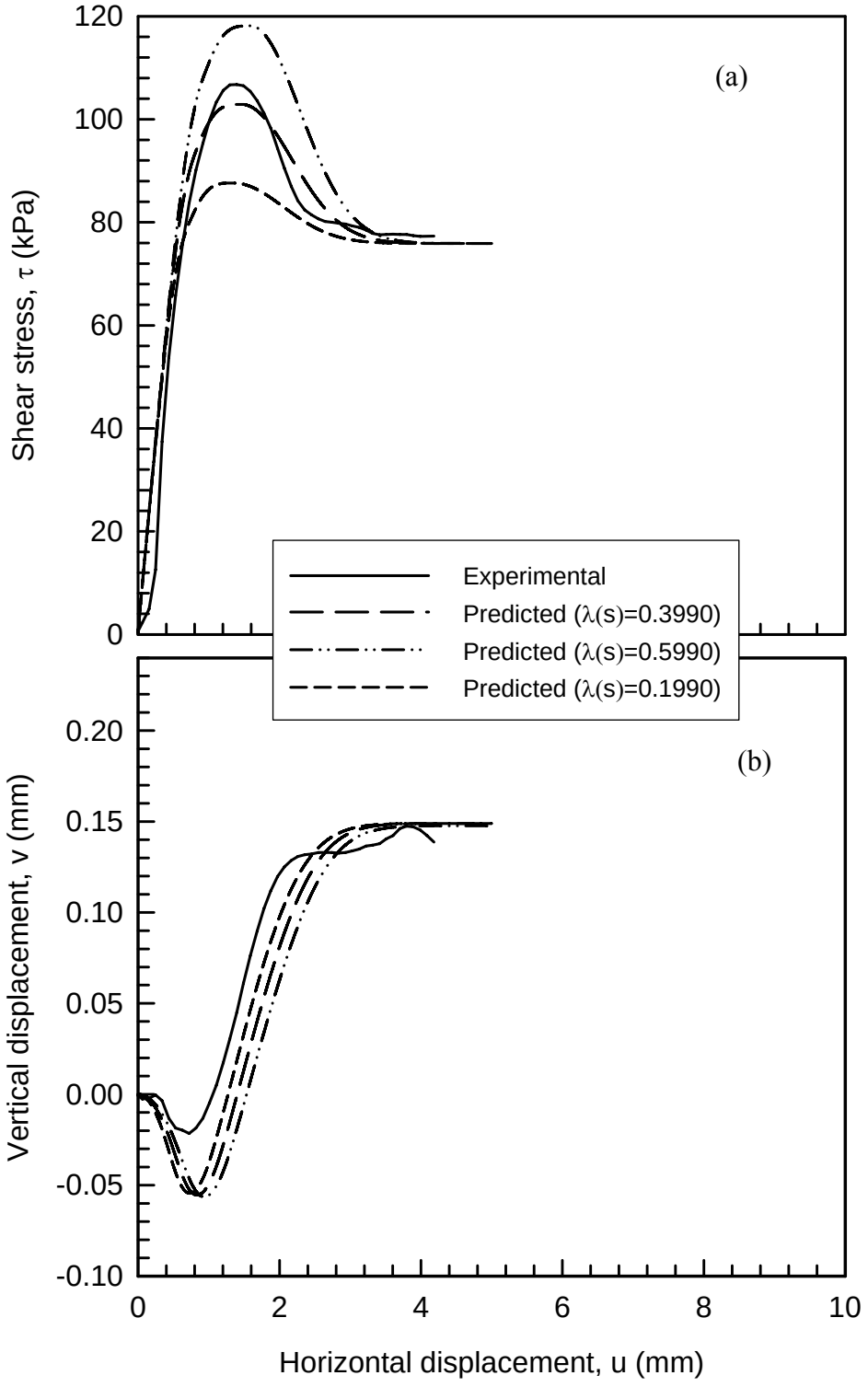

Figure 7.40: Effect of varying λ(s) on the predicted (a) τ vs. u and (b) u vs. v response of the rough interface at u_a-u_w = 100 kPa and σ_n-u_a = 105 kPa

CHAPTER VIII

CONCLUSIONS AND RECOMMENDATIONS

8.1 OVERVIEW

A primary objective of this research was to study the effect of matric suction and net normal stress on the shear strength, residual strength, stress-displacement, and the volume change behavior of unsaturated soil-steel interfaces. Other objectives included the design and construction of an unsaturated interface direct shear device, development of extended Mohr-Coulomb failure criterion for unsaturated interfaces, and development of an elastoplastic constitutive model based on the results of the laboratory testing of unsaturated interfaces. A conventional direct shear test device was modified for performing the experimental program to achieve the objectives of this study. Major modifications included the addition of apparatus for suction-controlled testing using the axis translation method and the construction of shear boxes for testing unsaturated soil and interfaces. The modified device is capable of applying and maintaining matric suction. Performance tests were conducted to verify the device worked correctly.

8.2 CONCLUSIONS

Based on tests and analysis conducted in this study using Minco Silt, the following conclusions are presented.

8.2.1 Development of Unsaturated Interface Direct Shear Apparatus

1. Based on literature review it can be concluded that a device for the measurement of properties of interfaces in unsaturated soil did not exist before this study.

2. In this study a conventional direct shear device was modified and successfully used to determine the strength and volumetric properties of unsaturated soil and unsaturated interfaces.

3. The Unsaturated Interface Direct Shear Apparatus (UIDSA) is capable of applying and controlling suction via the axis translation technique.

4. In this study all tests were performed under constant suction (drained) condition; however, the newly developed device is fully capable of conducting tests under constant water content conditions as well.

5. The newly developed interface direct shear device is versatile in the sense that it can be used for testing of saturated (or dry) and unsaturated soil as well as for testing of interfaces in saturated (or dry) and unsaturated soil.

6. Results of performance tests showed that that the UIDSA was performed well.

7. The observation and analysis of water content data from tests performed in this study showed that the suction was correctly controlled and measured.

8.2.2 Behavior of Unsaturated Soil

1. Shear strength of soil increased with increase in net normal stress for a given suction value.

2. Magnitude of maximum shear stress increased with increase in suction.

3. During shearing, soil initially compressed followed by dilation and steady state behavior.

4. Soil samples tested showed greater strain softening behavior as suction increased.

5. Amount of dilation during shear decreased with increase in net normal stress.

6. Increase in suction caused increase in dilatancy behavior of soil.

7. For a given value of suction the magnitude of vertical compression of soil increased with increase in net normal stress.

8.2.3 Behavior of Unsaturated Interfaces

1. The behavior of unsaturated soil-steel interfaces was a function of matric suction. For example the maximum shear strength value of the rough interface increased from 74 kPa to 107 kPa when matric suction increased from 20 kPa to 100 kPa for a net normal stress of 105 kPa. For the smooth interface under similar conditions the shear strength increased from 41 kPa to 51 kPa.

2. As the magnitude of net normal stress (σ_n-u_a) increased, so did the peak shear strength. For example, in the case of unsaturated soil and smooth steel plate, peak shear strength (τ_{max}) was 51 kPa and 76 kPa for σ_n-u_a =105 kPa and 210 kPa, respectively, at u_a-u_w = 100 kPa. For rough interface under similar conditions τ_{max} increased from 107 kPa to 184 kPa.

3. Residual shear strength of unsaturated soil-steel interfaces increased with increase in net normal stress. For example, in the case of the rough interface the residual shear strength was 71 kPa and 151 kPa for σ_n-u_a=105 kPa and 210 kPa, respectively, at u_a-u_w= 20 kPa. As opposed to the effect of net normal stress, the effect of matric suction on the residual shear strength was not pronounced; residual shear strength either remained unchanged or increased slightly with increase in matric suction. For example, for the

rough interface the residual shear strength was 71 kPa and 77 kPa for 20 kPa and 50 kPa matric suction values, respectively, at a net normal stress of 105 kPa. On the other hand, the corresponding peak shear strength values were 74 kPa and 92 kPa for the matric suction of 20 and 50 kPa. For the smooth interface under similar conditions, residual shear strengths were recorded as 35 kPa and 37 kPa; whereas the corresponding peak shear strength values were 41 kPa to 48 kPa.

4. The smooth interface exhibited stick-slip behavior after reaching the peak shear stress value. After reaching peak shear stress, the shear stress of the smooth interface decreased; however, with increase in horizontal displacement, magnitude of shear stress started increasing and the cycle of increase and decrease in shear stress continued after the maximum shear stress until the end of shearing. The cyclic behavior of increase (stick behavior) and decrease (slip behavior) in shear stress of smooth interface is referred to as stick-slip behavior.

5. During shearing, the rough interface compressed initially and then dilated. The rough interface attained steady state behavior (i.e., no compression or dilation) in the region of residual shear stress. It was also observed that the amount of dilation increased with increase in suction values. However, the amount of dilation decreased with increase in net normal stress.

6. The smooth interface compressed until reaching the peak shear stress. It did not show any compression or dilation after reaching the peak shear stress; it exhibited steady state behavior for the remainder of the shearing phase.

7. For the rough interface, the maximum shear stress occurred at lower values of horizontal displacement with increasing suction, illustrating an increasing brittleness of

the sample with suction. Strain softening behavior also became pronounced with increasing suction. Similar behavior was observed for the smooth interface.

8.2.4 Extended Mohr-Coulomb Failure Criterion for Unsaturated Interfaces

1. The extended Mohr-Coulomb failure envelope for the unsaturated interfaces was developed in a similar manner to unsaturated soil.

2. The extended Mohr-Coulomb failure criterion as used for the unsaturated soil can be used to predict the shear strength of unsaturated soil- steel interfaces.

3. Non-linearity was observed in failure envelopes plotted in shear stress (τ)-net normal stress (σ_n-u_a) plane; however, further testing is required to verify this observation. Considering experimental errors, failure envelopes plotted in τ-(σ_n-u_a) plane were assumed linear and parallel. Based on linear regression analysis an average value of $\phi' = 35^0$ is determined for Minco Silt. Similarly, $\delta' = 35^0$ and $\delta' = 14^0$ were determined for rough and smooth interfaces, respectively.

4. Failure envelopes plotted in τ-(u_a-u_w) plane were assumed linear for the range of u_a-u_w and σ_n-u_a used in this study. Based on this assumption the value of ϕ^b was determined to be 25.7^0. Similarly, $\delta^b = 18.7^0$ and $\delta^b = 7.6^0$ were determined for rough and smooth interfaces, respectively.

5. Values of effective adhesion ($c_a^{'}$) were determine to be 0 kPa and 10 kPa for rough and smooth interfaces, respectively. For soil, the value of effective cohesion (c') was 26 kPa.

8.2.5 Elastoplastic Constitutive Model for Unsaturated Interfaces

1. An elastoplastic model for predicting unsaturated interface behavior was successfully developed. The model is applicable for the constant net normal stress and constant suction conditions.

2. Predictions made with the modified elastoplastic model agreed well with the experimental results.

3. The modified elastoplastic constitutive model is capable of capturing the volumetric behavior of the interface before and after the peak shear stress.

8.3 RECOMMENDATIONS

1. The present study focused on interfaces between compacted soil and steel. However, unsaturated natural soils are also very widespread throughout the world and the behavior of these natural soils may be very different to that of compacted fills (because of the different soil structures). Therefore, experimental research should be carried out to establish whether the proposed constitutive model and conclusions made regarding the behavior of unsaturated interfaces can also be applied to interfaces between unsaturated natural soils and construction materials.

2. The proposed model in its present from requires 17 parameters. Therefore, it will be necessary in the future to simplify the model as much as possible and to devise a suitable and simplified testing program to measure the relevant interface parameters.

3. Further work should be done on the implementation of the proposed constitutive model within finite element programs and analyze the load deformation response and the stability of soil-structure systems.

4. It is clear that the structure of unsaturated soil plays a major role in the mechanical behavior. Therefore an experimental program of research is required to explore the influence of the initial structure (e.g., water content, void ratio) on the behavior of unsaturated soil-steel behavior.

5. In order to measure both sliding displacement between unsaturated soil and steel as well as shear deformation of unsaturated soil, a simple shear device should be modified to test the unsaturated interfaces.

6. Broaden the study to include other soil types and counterface materials.

7. In this research the thickness of the soil above the counterface was similar for all tests. A research program to study the effects of sample thickness on the observed interface behavior is recommended.

8. Use a broader range of u_a-u_w and σ_n-u_a than used in present study.

9. Study the behavior of unsaturated interfaces under constant water content conditions.

10. Study the effect of horizontal displacement rate on the strength and volumetric behavior of unsaturated soil and unsaturated interfaces.

11. Study the behavior of unsaturated interfaces under cyclic loading.

12. Modify the unsaturated interface direct shear device to conduct constant normal stiffness and constant volume tests.

13. Test various types of soil, e.g., lean clay, fat clay, etc.

14. Measure suction at the interface with embedded sensors.

APPENDIX I

Table I.1: Summary of water content data at the end of equalization and testing from controller data and oven dry method

Test ID	σ_n-u_a	u_a-u_w	w	w at the end of equalization From controller data	w at the end of test	
					From controller data	From oven dry method
	(kPa)	(kPa)	%	%	%	%
SOIL						
40904	105	20	20.3	*	16.5	16.4
81804	155	20	20.6	18.1	16.8	16.3
100204	210	20	19.9	17.0	16. 5	15.9
40504	105	50	19.3	*	14.7	14.6
62404	140	50	20.5	*	14.3	14.5
80104	210	50	20.9	16.0	14.2	14.6
90804	105	100	21.2	14.9	13.4	13.7
72504	155	100	20.7	14.0	12.8	12.9
10304	210	100	20.2	14.3	12.7	13.7
ROUGH						
51504	105	20	20.8	17.5	16.5	15.8
101704	140	20	20.5	16.4	16.1	16.1
92904	210	20	20.5	16.4	16.0	15.7
42004	105	50	20.1	15.5	14.8	14.9
61504	140	50	20.4	16.1	15.1	14.9
62004	210	50	20.8	15.6	14.7	14.8
42604	105	50	20.5	16.5	15.2	15.0
82304	105	100	20.3	14.3	13.5	14.0
102504	140	100	20.3	14.9	14.0	14.2
63004	155	100	20.4	14.6	13.7	13.9
101304	210	100	20.6	14.7	13.6	13.9
SMOOTH						
60404	105	20	21.6	17.9	17.1	16.4
111904	140	20	20.5	17.5	16.3	16.1
100104	210	20	20.8	16.7	16.7	16.5
52004	105	50	20.8	15.8	15.2	15.1
81304	140	50	20.7	15.7	15.6	15.4
100604	210	50	20.7	15.6	15.3	15.5
90404	105	100	21.0	14.9	14.4	14.7
112404	140	100	20.2	15.6	14.9	14.9
71504	155	100	20.7	14.3	13.9	13.8
102004	210	100	20.5	15.2	15.0	15.1

Table I.2: Summary of τ_p and τ_r for different values of u_a-u_w for a given value of σ_n-u_a

Test ID	ua-uw (kPa)	Peak Shear Stress (τ_p) (kPa)	Residual Shear Stress (τ_r) (kPa)
SOIL σ_n-u_a=105 kPa			
	20	91	88
	50	115	112
	100	125	89
SOIL σ_n-u_a=140 kPa			
	50	149	123
SOIL σ_n-u_a=155 kPa			
	20	130	130
	100	173	142
SOIL σ_n-u_a=210 kPa			
	20	158	155
	50	191	173
	100	206	189
ROUGH σ_n-u_a=105 kPa			
	20	74	71
	50	92	77
	100	107	77
ROUGH σ_n-u_a=140 kPa			
	20	108	97
	50	117	97
	100	130	101
ROUGH σ_n-u_a=210 kPa			
	20	155	148
	50	166	148
	100	184	149
SMOOTH σ_n-u_a=105 kPa			
	20	41	35
	50	48	37
	100	51	44
SMOOTH σ_n-u_a=140 kPa			
	20	46	42
	50	56	51
	100	61	53
SMOOTH σ_n-u_a=210 kPa			
	20	68	60
	50	72	62
	100	76	69

Table I.3: Summary of τ_p and τ_r for different values of σ_n-u_a for a given value of u_a-u_w

Test ID	σ_n-u_a (kPa)	Peak Shear Stress (τ_p) (kPa)	Residual Shear Stress (τ_r) (kPa)
SOIL u_a-u_w=20 kPa			
	105	91	88
	155	130	130
	210	158	155
SOIL u_a-u_w =50 kPa			
	105	115	112
	140	149	123
	210	191	173
SOIL u_a-u_w =100 kPa			
	105	125	89
	155	173	142
	210	206	189
ROUGH u_a-u_w =20 kPa			
	105	74	71
	140	108	97
	210	156	148
ROUGH u_a-u_w =50 kPa			
	105	92	77
	140	117	97
	210	166	148
ROUGH u_a-u_w =100 kPa			
	105	106	77
	140	130	101
	210	184	149
SMOOTH u_a-u_w =20 kPa			
	105	41	35
	140	46	42
	210	68	60
SMOOTH u_a-u_w =50 kPa			
	105	48	37
	140	56	51
	210	72.37	62
SMOOTH u_a-u_w =100 kPa			
	105	51	44
	140	61	53
	210	76	69

APPENDIX II

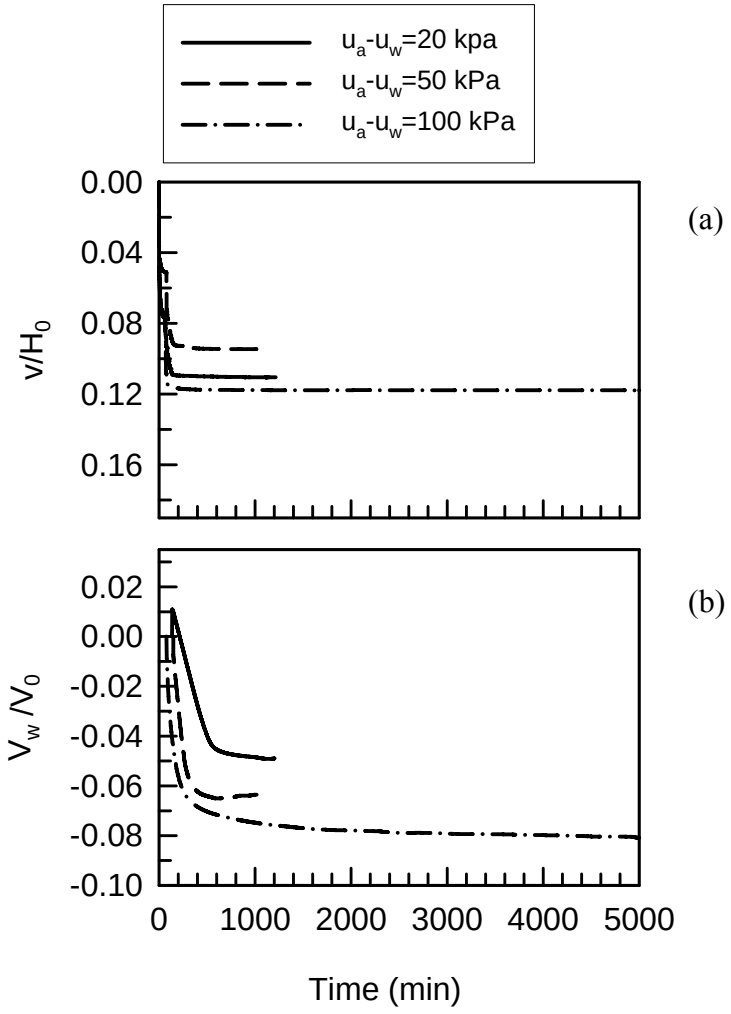

Figure II.1: Effect of u_a-u_w on (a) v/H_0 and (b) V_w/V_0 during equalization for soil (σ_n-u_a = 105 kPa)

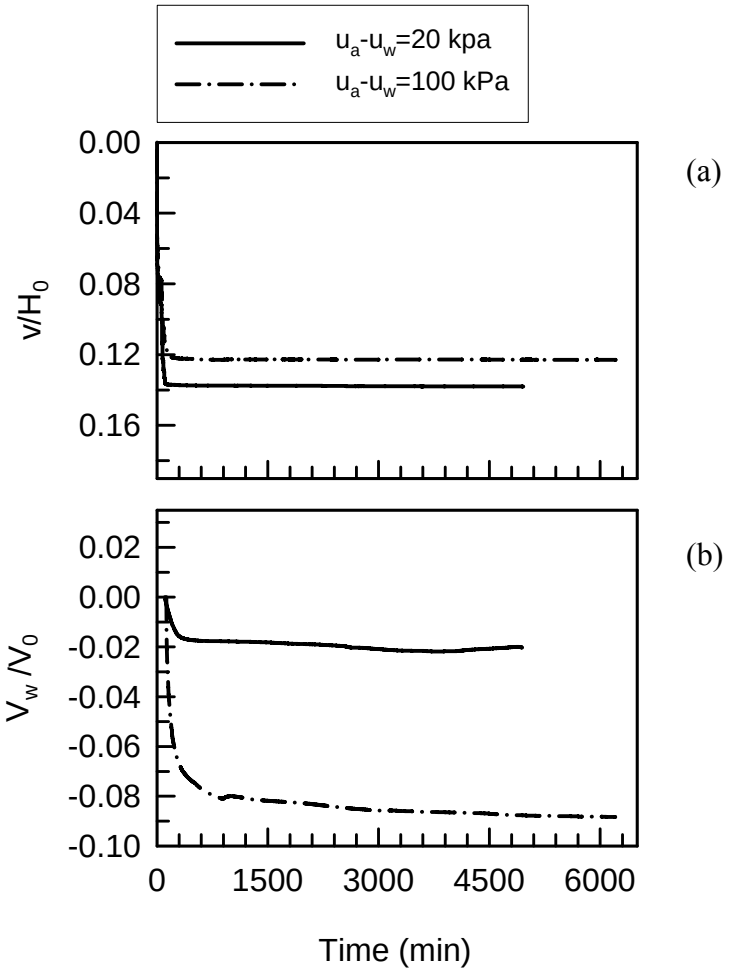

Figure II.2: Effect of u_a-u_w on (a) v/H_0 and (b) V_w/V_0 during equalization for soil (σ_n-u_a = 155 kPa)

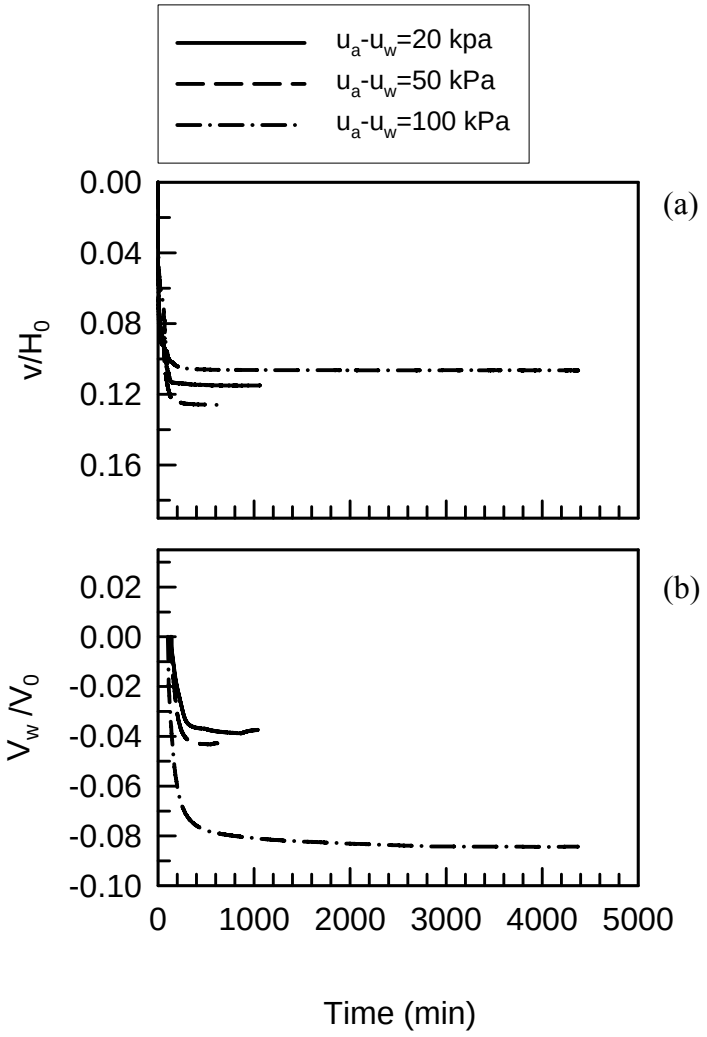

Figure II.3 : Effect of u_a-u_w on (a) v/H_0 and (b) V_w/V_0 during equalization for rough interface. (σ_n-u_a = 105 kPa)

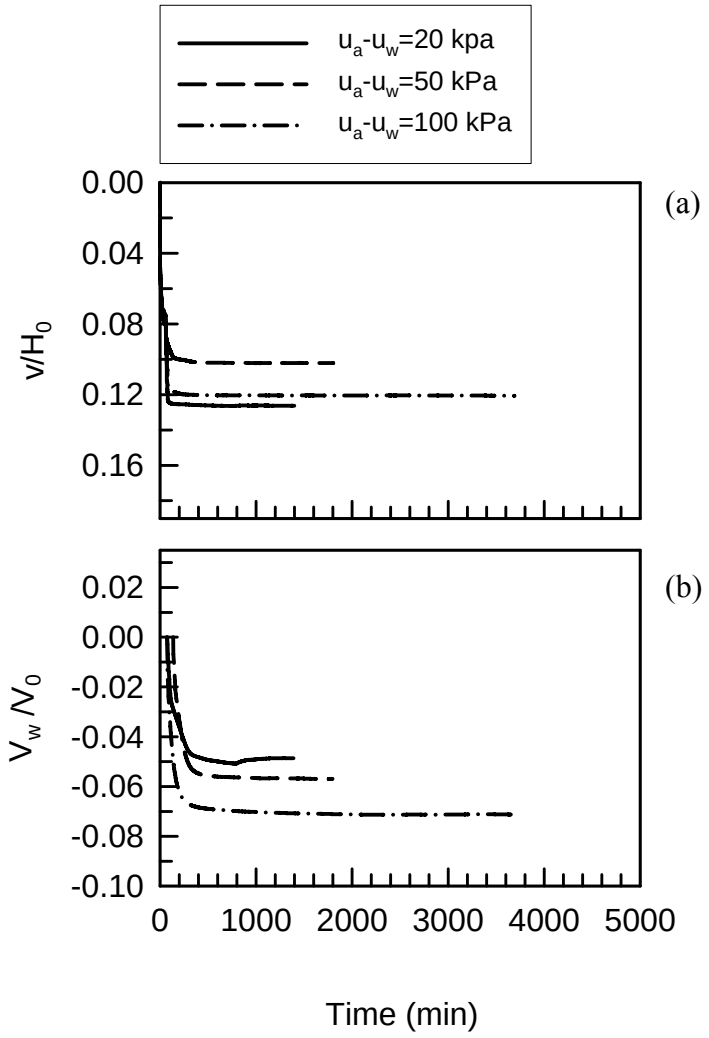

Figure II.4: Effect of u_a-u_w on (a) v/H_0 and (b) V_w/V_0 during equalization for rough interface. (σ_n-u_a = 140 kPa)

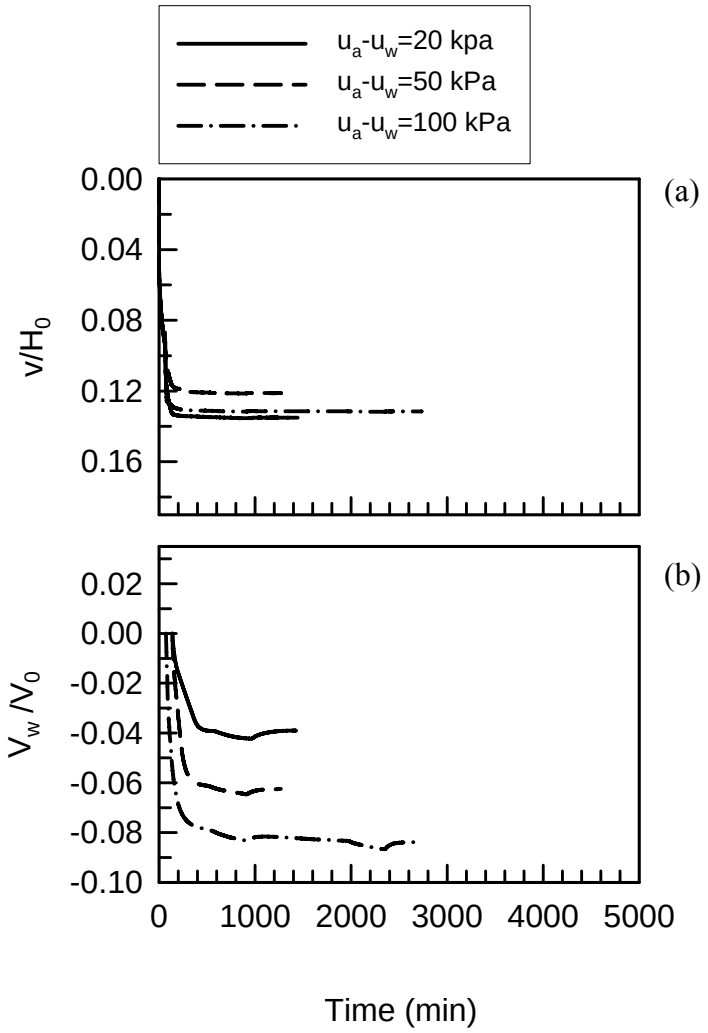

Figure II.5: Effect of u_a-u_w on (a) v/H_0 and (b) V_w/V_0 during equalization for smooth interface. (σ_n-u_a = 105 kPa)

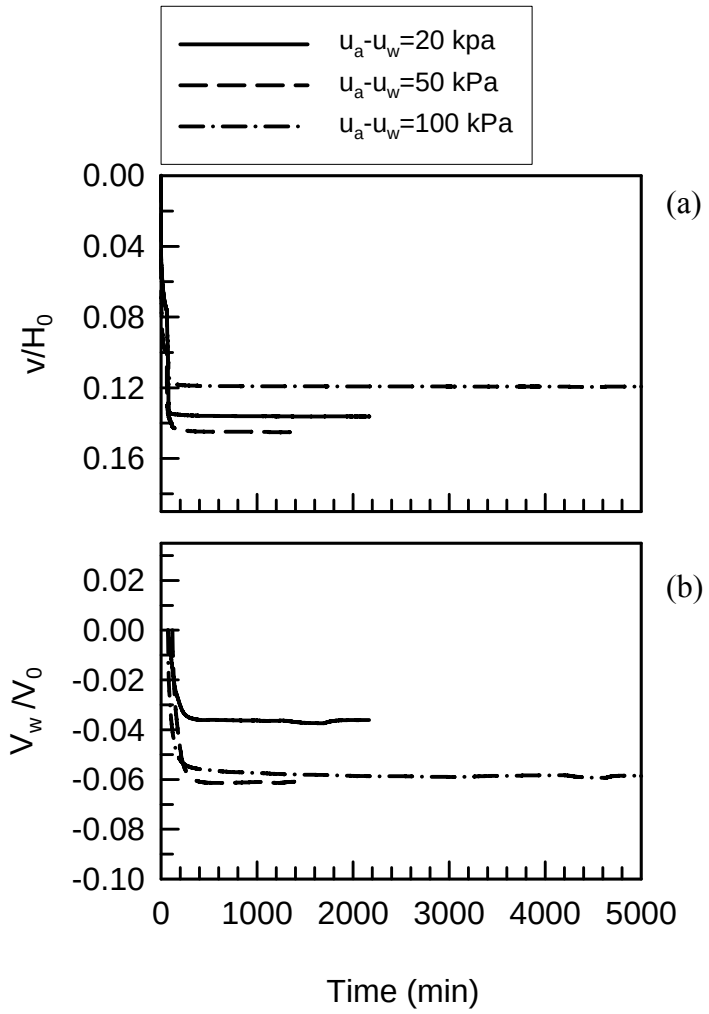

Figure II.6: Effect of u_a-u_w on (a) v/H_0 and (b) V_w/V_0 during equalization for smooth interface. (σ_n-u_a = 140 kPa)

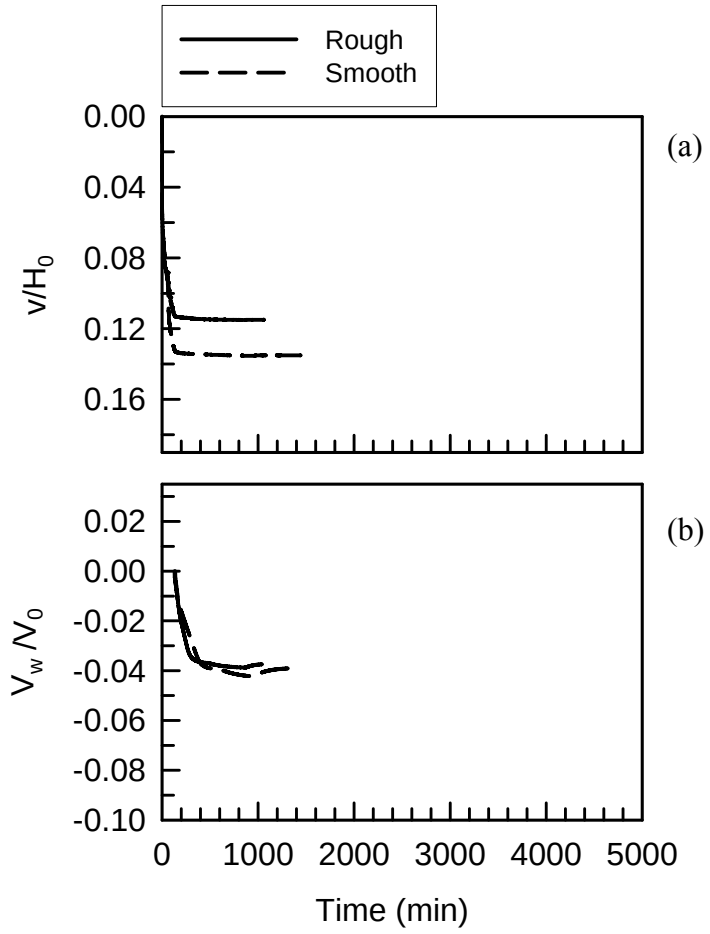

Figure II.7: Effect of surface roughness on (a) v/H_0, (b) V_w/V_0 during equalization (σ_n-u_a = 105 kPa; u_a-u_w = 20 kPa)

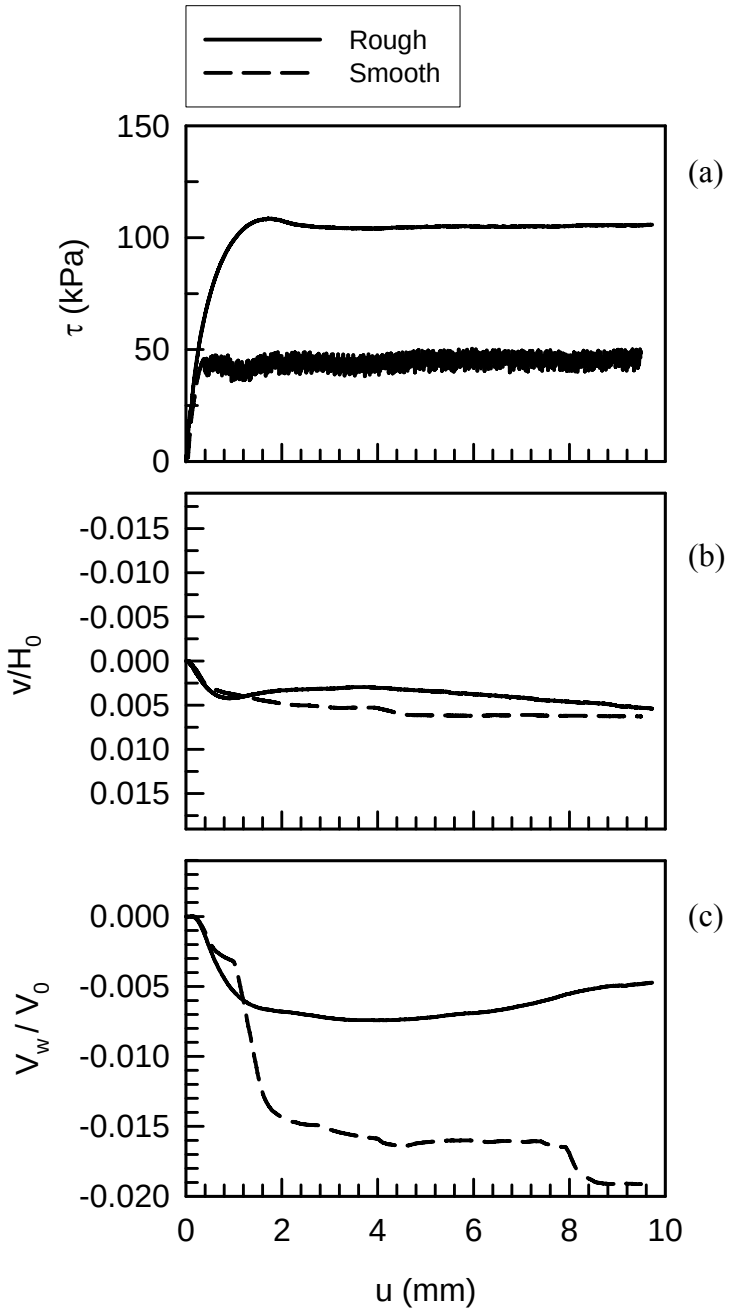

Figure II.8: Effect of surface roughness on (a) τ, (b) v/H_0, (c) V_w/V_0 during shearing (σ_n-u_a = 140 kPa ; u_a-u_w = 20 kPa)

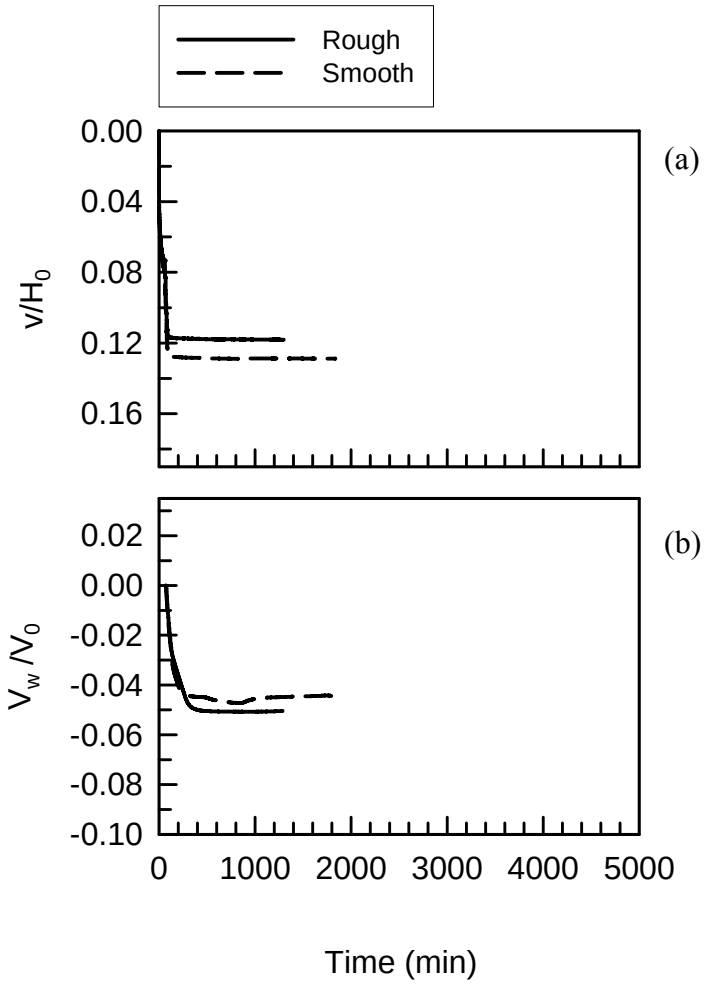

Figure II.9: Effect of surface roughness on (a) v/H_0, (b) V_w/V_0 during equalization (σ_n-u_a = 210 kPa; u_a-u_w = 20 kPa)

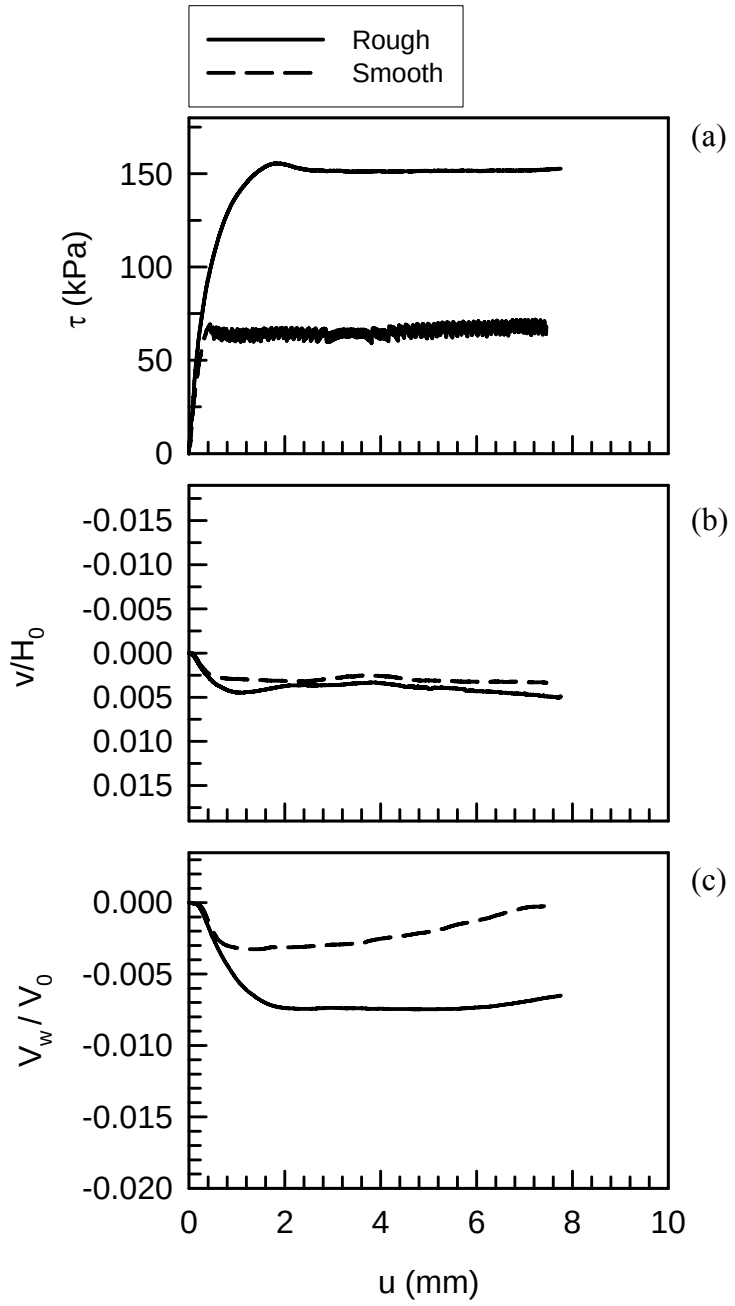

Figure II.10: Effect of surface roughness on (a) τ, (b) v/H_0, (c) V_w/V_0 during shearing (σ_n-u_a = 210 kPa; u_a-u_w = 20 kPa)

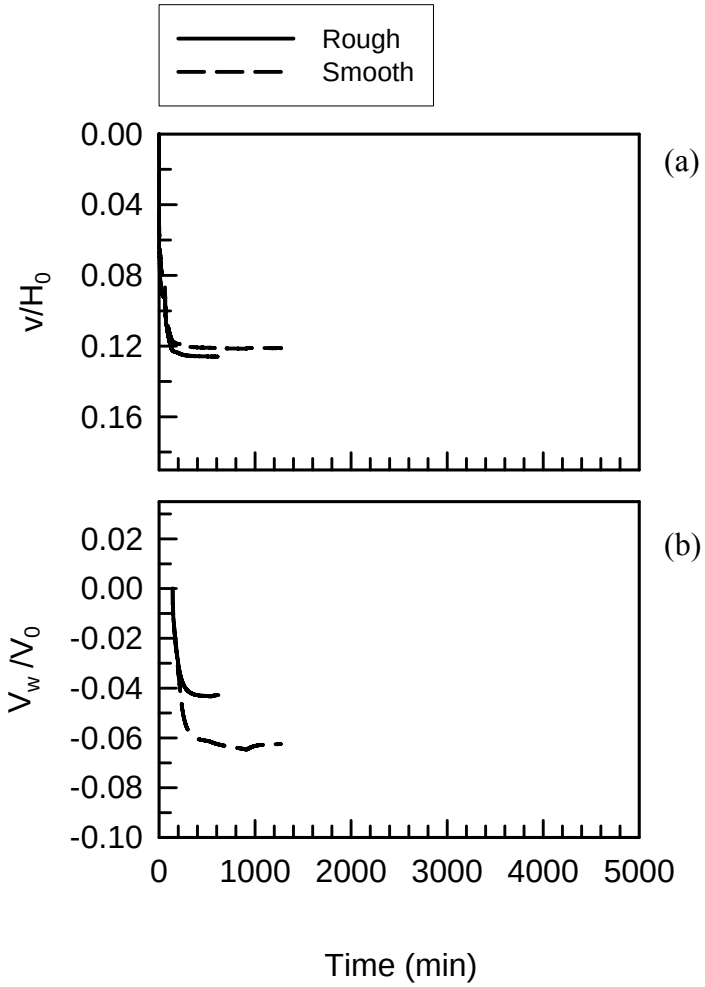

Figure II.11: Effect of surface roughness on (a) v/H_0, (b) V_w/V_0 during equalization (σ_n-u_a = 105 kPa; u_a-u_w = 50 kPa)

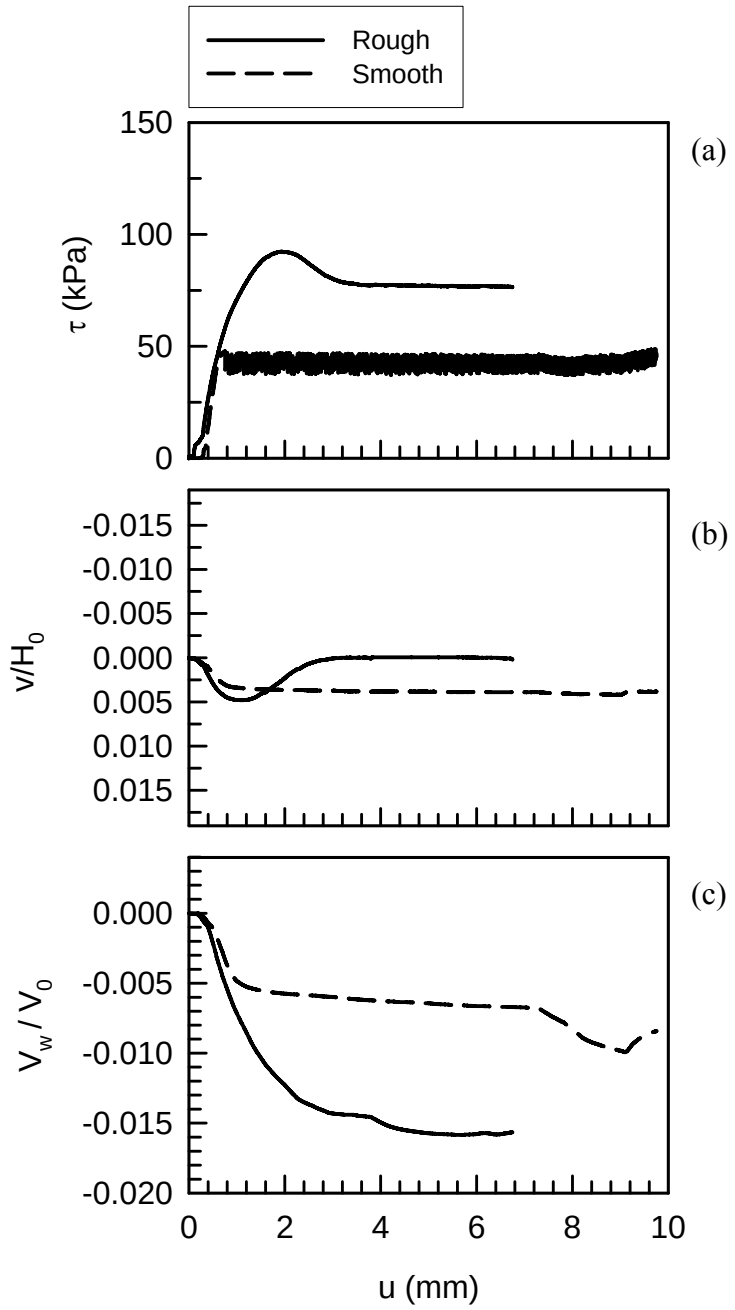

Figure II.12: Effect of surface roughness on (a) τ, (b) v/H_0, (c) V_w/V_0 during shearing (σ_n-u_a = 105 kPa; u_a-u_w = 50 kPa)

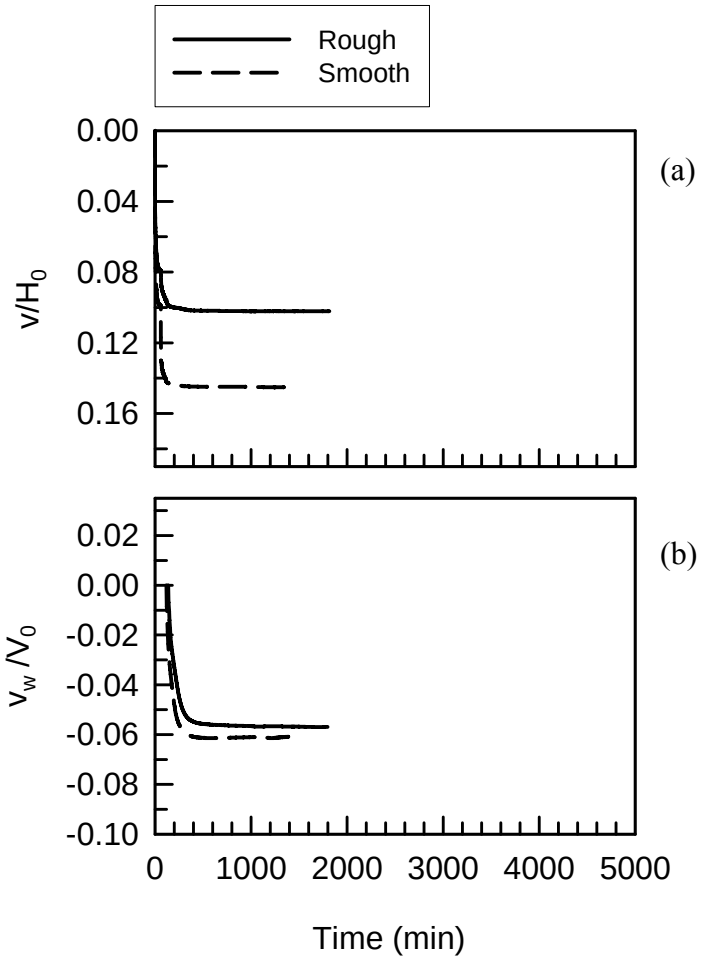

Figure II.13: Effect of surface roughness on (a) v/H_0, (b) V_w/V_0 during equalization (σ_n-u_a = 140 kPa; u_a-u_w = 50 kPa)

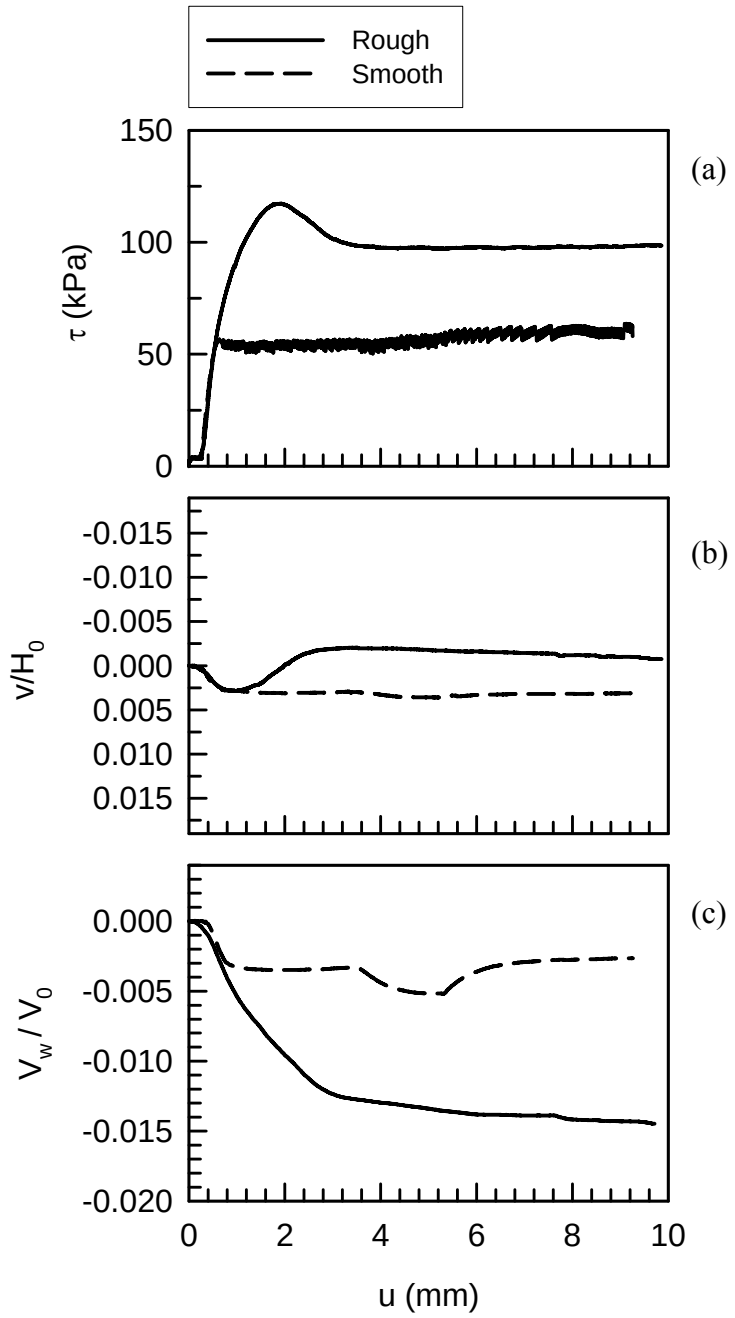

Figure II.14: Effect of surface roughness on (a) τ, (b) v/H_0, (c) V_w/V_0 during shearing (σ_n-u_a = 140 kPa; u_a-u_w = 50 kPa)

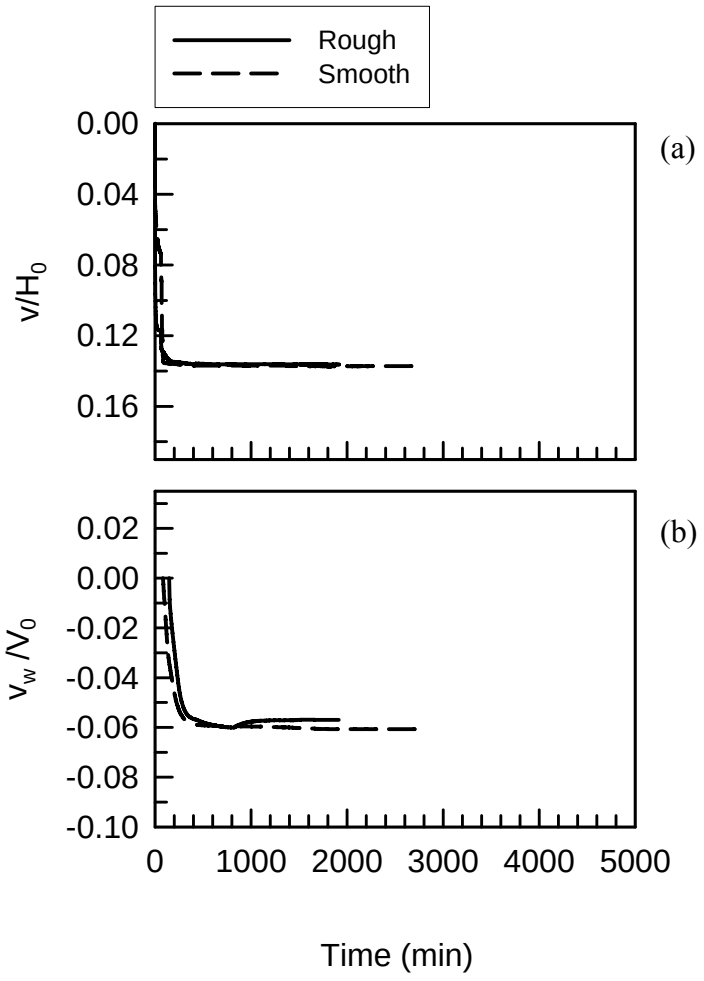

Figure II.15: Effect of surface roughness on (a) v/H_0, (b) V_w/V_0 during equalization (σ_n-u_a = 210 kPa; u_a-u_w = 50 kPa)

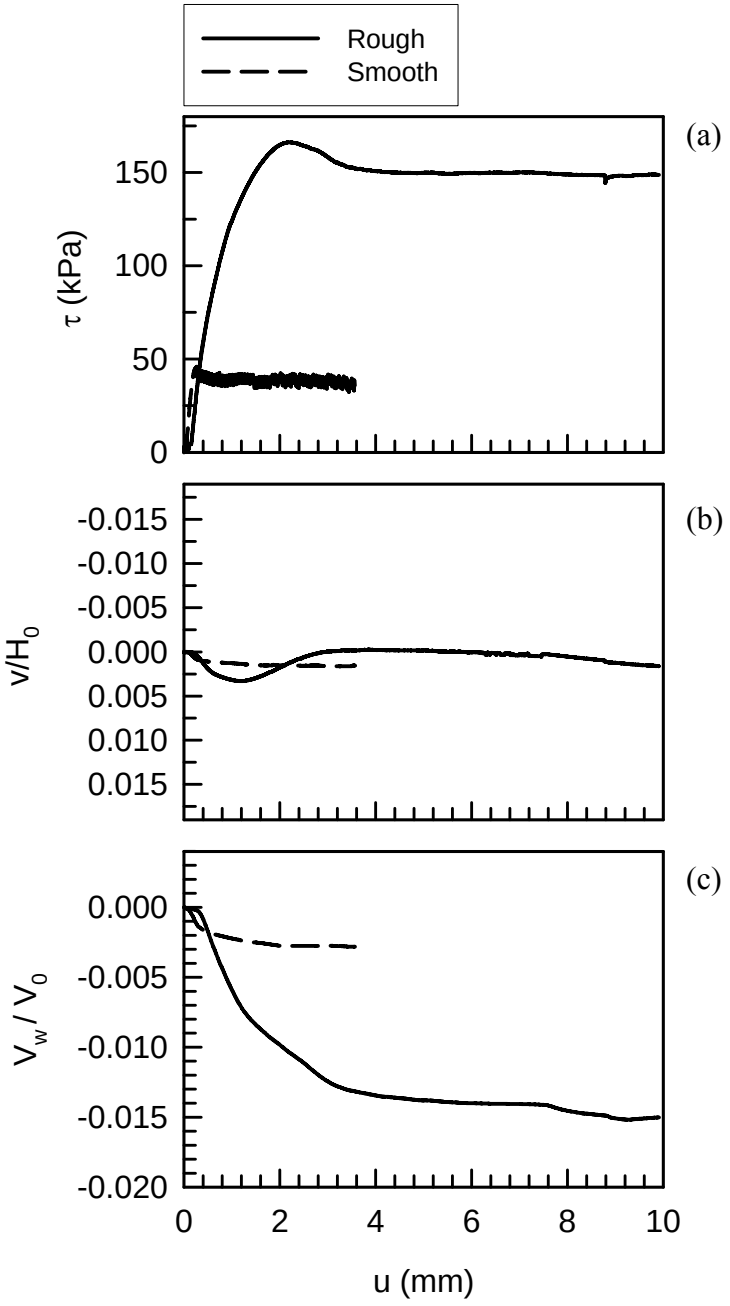

Figure II.16: Effect of surface roughness on (a) τ, (b) v/H_0, (c) V_w/V_0 during shearing (σ_n-u_a = 210 kPa; u_a-u_w = 50 kPa)

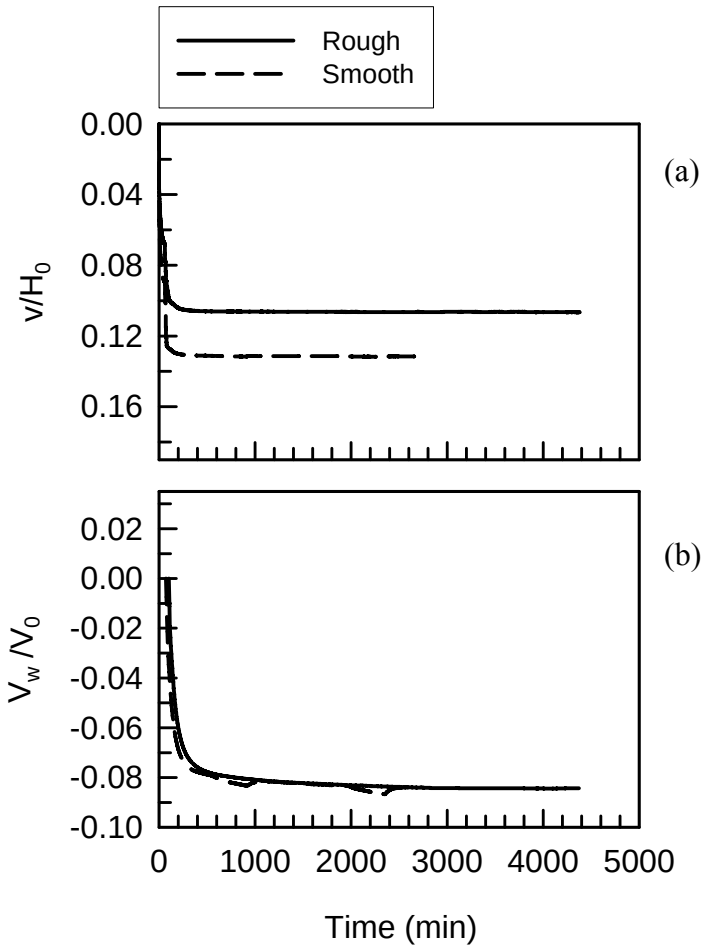

Figure II.17: Effect of surface roughness on (a) v/H_0, (b) V_w/V_0 during equalization (σ_n-u_a = 105 kPa; u_a-u_w = 100 kPa)

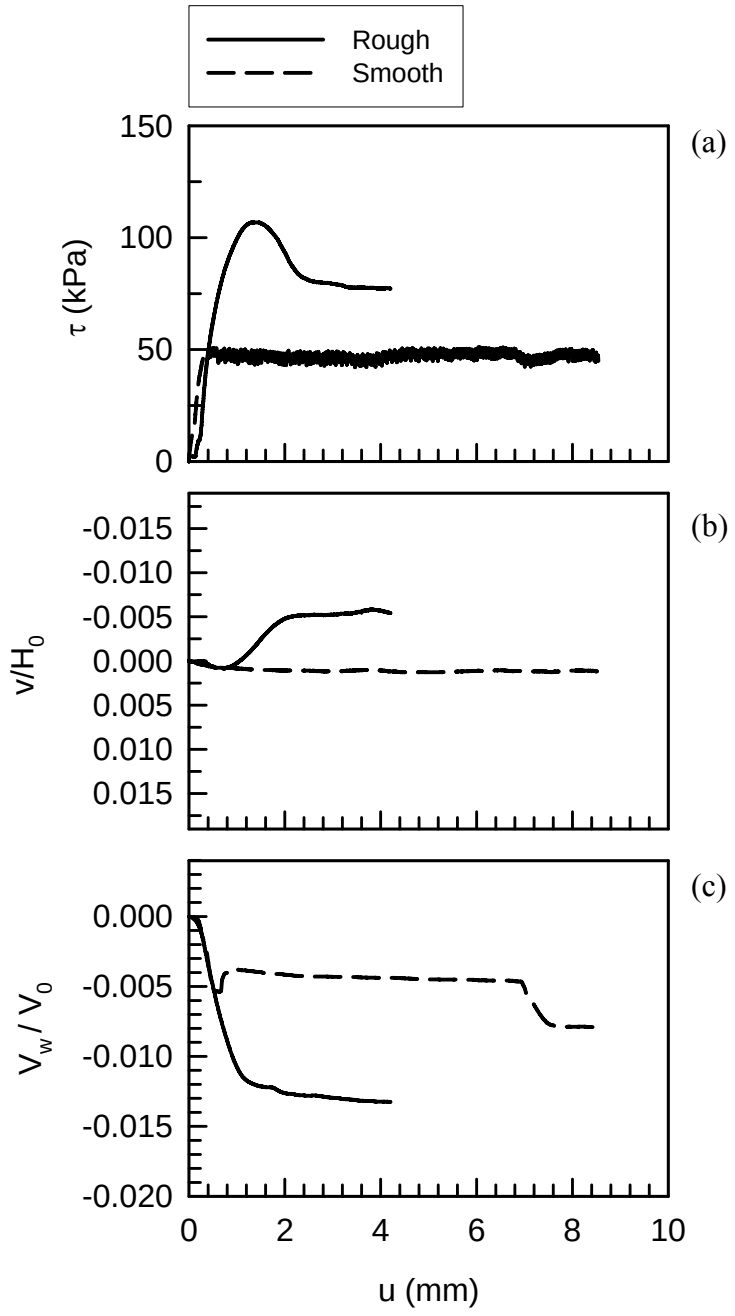

Figure II.18: Effect of surface roughness on (a) τ, (b) v/H_0, (c) V_w/V_0 during shearing (σ_n-u_a = 105 kPa; u_a-u_w = 100 kPa)

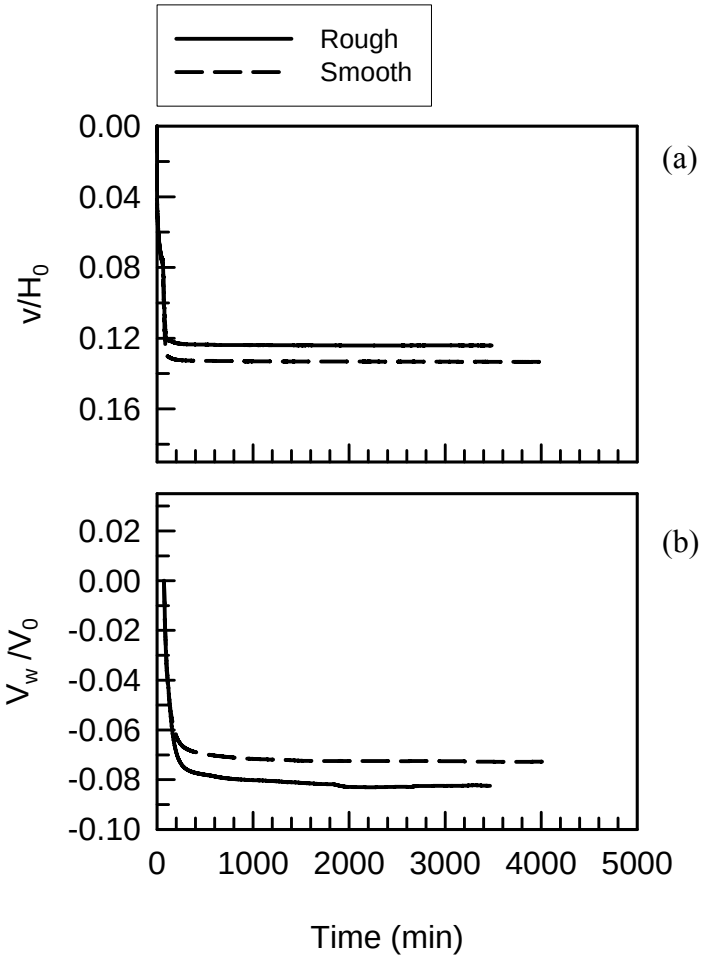

Figure II.19: Effect of surface roughness on (a) v/H_0, (b) V_w/V_0 during equalization (σ_n-u_a = 210 kPa; u_a-u_w = 100 kPa)

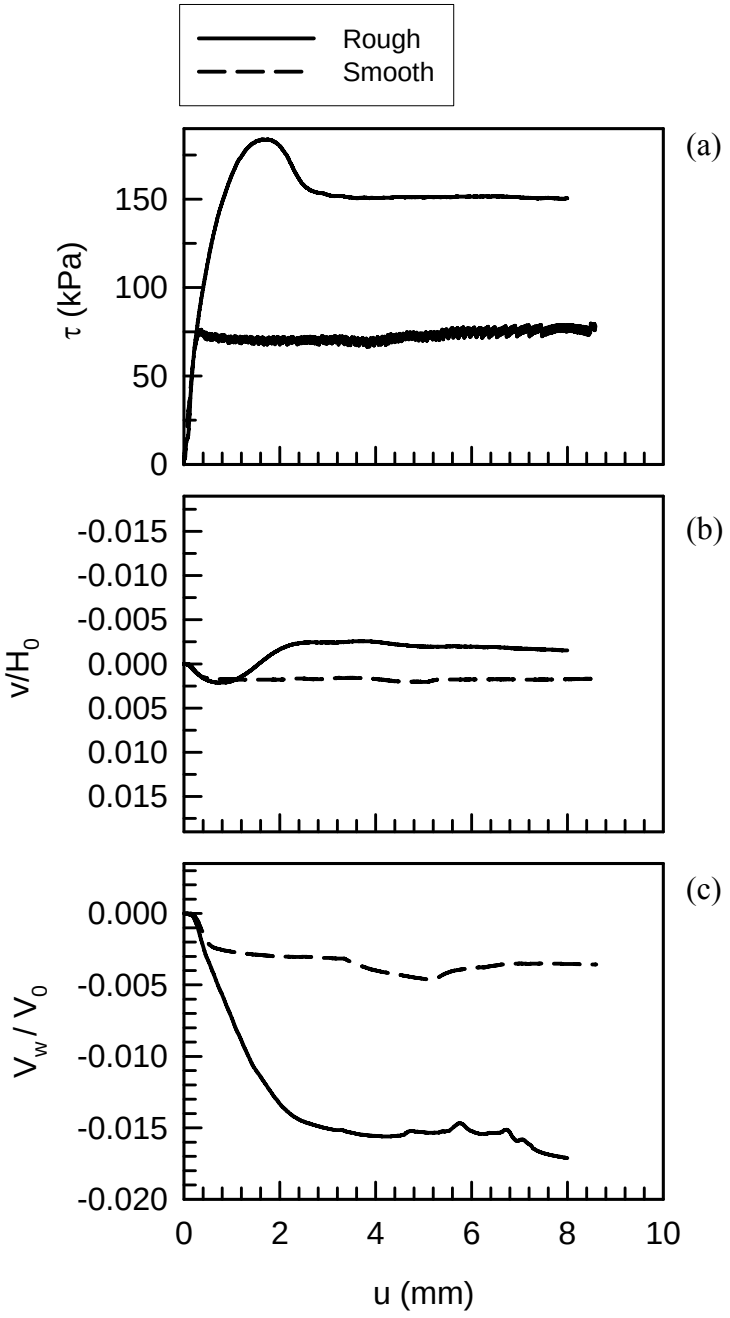

Figure II.20: Effect of surface roughness on (a) τ, (b) v/H_0, (c) V_w/V_0 during shearing (σ_n-u_a = 210 kPa; u_a-u_w = 100 kPa)

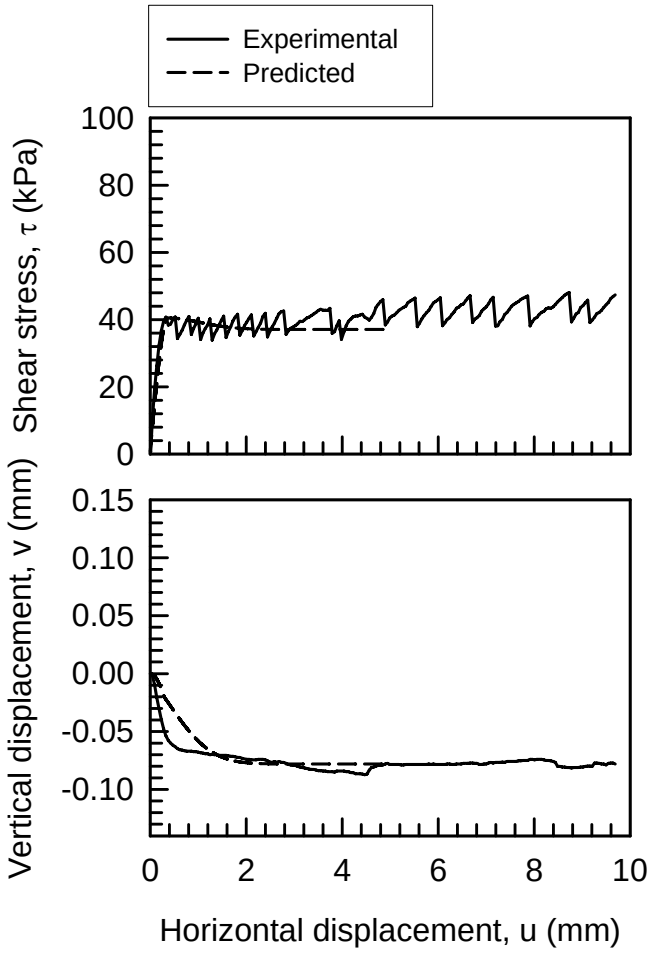

Figure II.21: Comparison between predicted and experimental results for u_a-u_w = 20 kPa and σ_n-u_a = 105 kPa; smooth interface

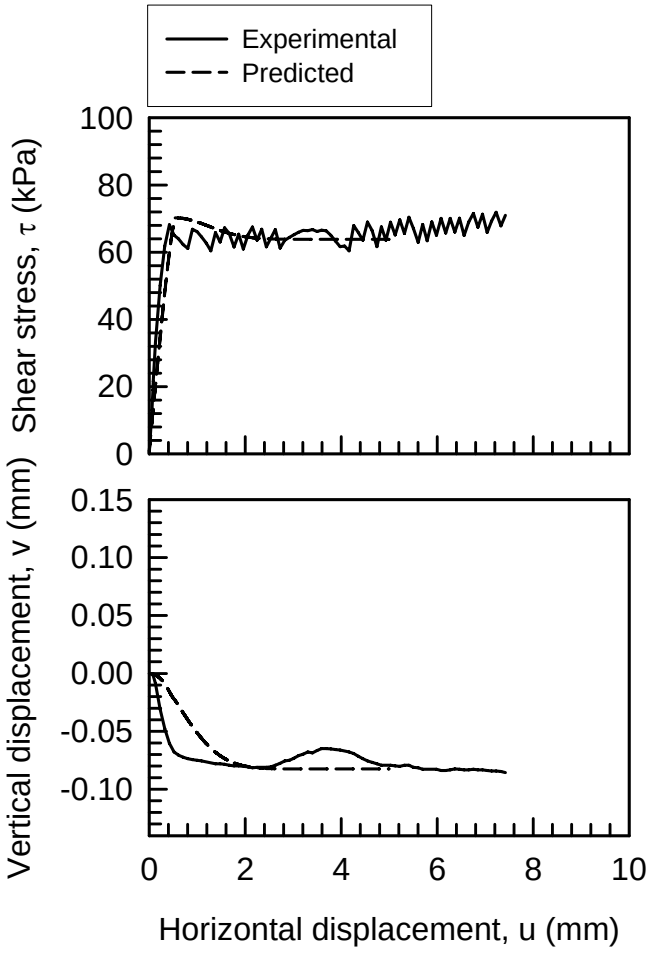

Figure II.22: Comparison between predicted and experimental results for u_a-u_w = 20 kPa and σ_n-u_a = 210 kPa; smooth interface

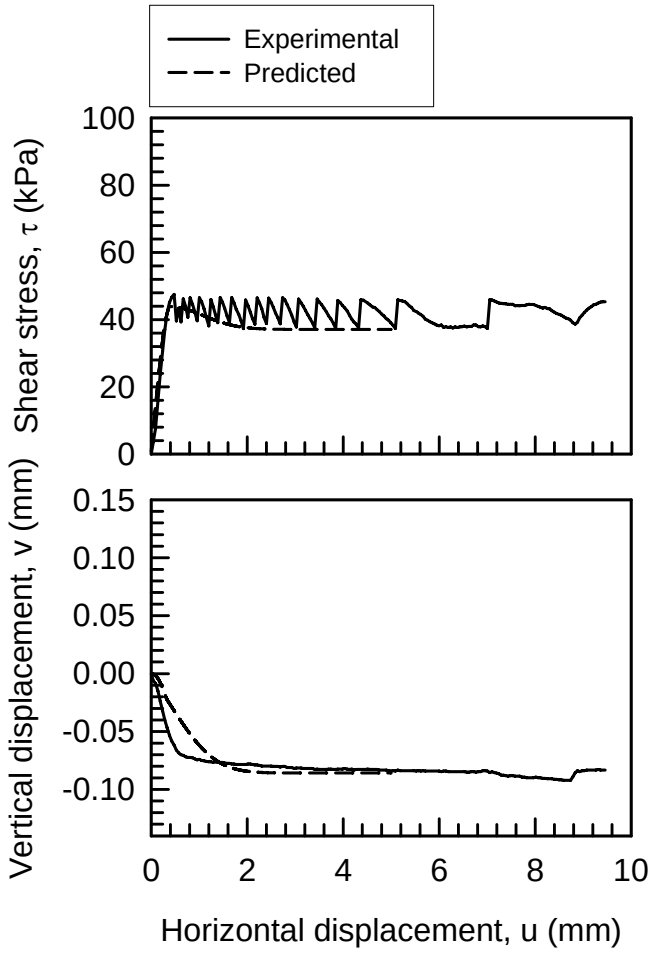

Figure II.23: Comparison between predicted and experimental results for u_a-u_w = 50 kPa and σ_n-u_a = 105 kPa; smooth interface

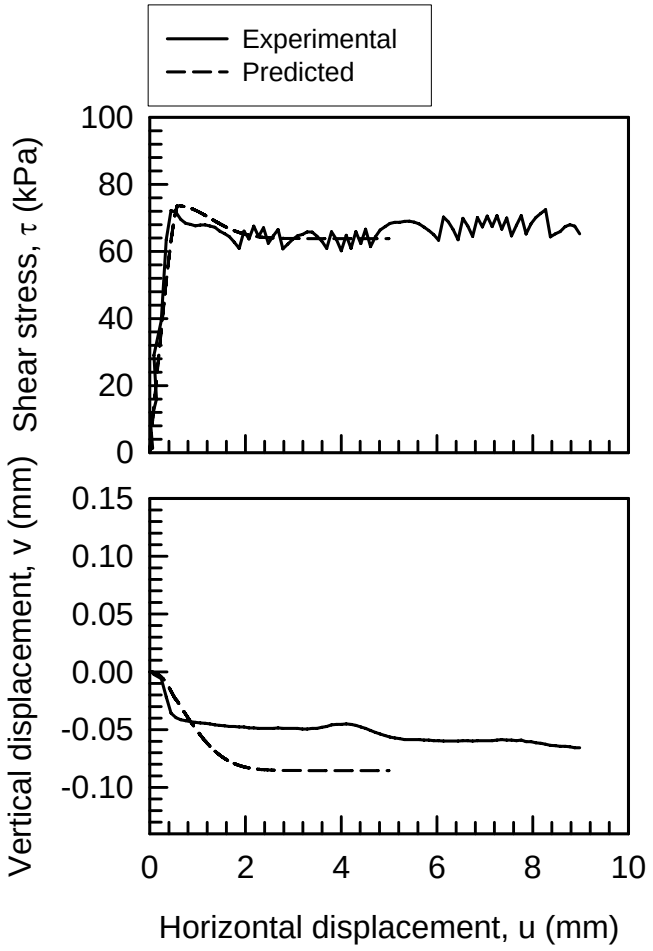

Figure II.24: Comparison between predicted and experimental results for u_a-u_w = 50 kPa and σ_n-u_a = 210 kPa; smooth interface

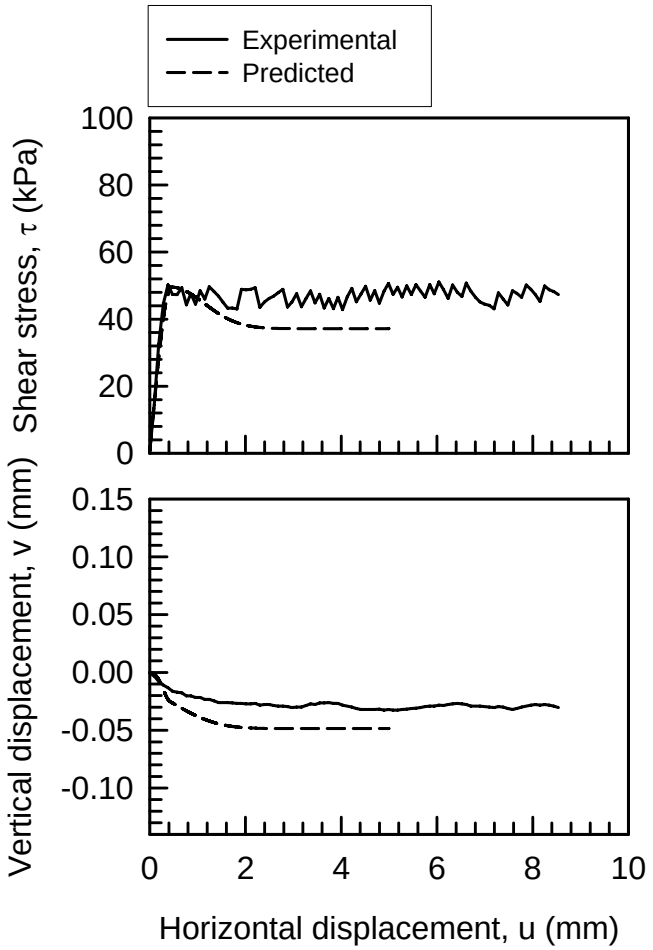

Figure II.25: Comparison between predicted and experimental results for u_a-u_w = 100 kPa and σ_n-u_a = 105 kPa; smooth interface

REFERENCES

Acar, Y.B., Durgunoglu, H.T., Tumay, M. T., 1982, "Interface Properties of Sand," *Journal of Geotechnical Engineering,* ASCE, Vol. 108, No. GT4, pp. 648-654.

Aitchison, G. D., 1961, "Relationship of Moisture and Effective Stress Functions in Unsaturated Soils," *Proceedings of Pore Pressure and suction in Soils*, England, Butterworths, pp. 47-52.

Alonso, E.E, Gens, A., and Josa, A., 1990, "A Constitutive Model for partially Saturated Soils," *Geotechnique*, Vol. 40, No. 3, pp. 405-430.

Alonso, E.E, Gens, A., and Hight, D. W., 1987, "General Report, Special Problems Soils," 9th ICSMFE, Dublin, Vol. 3, pp. 1087-1146.

ASME B46.1-1995, "Surface Texture, Surface Roughness Waviness and Lay," An ASME National Standard.

Aversa, S. and Nicotera, V., 2002, "A Triaxial and Oedometer Apparatus for Testing Unsaturated Soils," *Geotechnical Testing Journal*, Vol.25, No.1, pp.3-15.

Barden, L., Madedor, A. O., and Sides, G. R., 1969, "Volume Change Characteristics of Unsaturated Clay," *Soil Mechanics and Foundation Division*, ASCE, Vol.95, No. SM1, pp.33-51.

Barden, L. and Sides, G. R., 1970, "Engineering Behavior and Structure of Compacted Clay," *Journal of Soil Mechanics and Foundation Engineering*, ASCE, No.96, SM4, pp. 1171-1201.

Bishop, A.W., 1959, "The Principle of Effective Stress," *Teknisk Ukeblad*, Vol. 106, No. 39, pp. 859-863.

Bishop, A.W., and Blight, G.E., 1963, "Some Aspects of Effective Stress in Saturated and Partly Saturated Soils," *Geotechnique*, Vol. 13, No.3, pp. 177-197.

Bishop, A.W, and Donald, I.B., 1961, "The Experimental Study of Partially Saturated Soils in the Triaxial Apparatus," *Proceedings of the 5th ICSMFE*, Paris, Vol.1, pp. 13-21.

Bolzon, G., Schrefler, B.A., and Zienkiewicz, O.C., 1996, "Elastoplastic Soil Constitutive Laws Generalized to Partially Saturated States," *Geotechnique*, Vol. 46, No.2, pp. 279-289.

Boulon, M. and Nova, R., 1990, "Modeling of Soil-Structure Interface Behaviour-A Comparison Between Elastoplastic and Rate Type Laws," *Computers and Geotechnique*, Vol. 9, pp. 21-46.

Boulon, M. and Plytas, C., 1986, "Soil Structure Directionally Dependent Interface Constitutive Equations-Application to the Prediction of Shaft Friction Along Piles," *Proceedings, 2nd International Symposium on numerical Models in Geomechanics*, pp. 43-54.

Brackley, I. J. A., 1971, "Partial Collapse in Unsaturated Expansive Clay," *Proceedings of 5th Regional Conference of Soil Mechanics and Foundation Engineering*, South Africa, pp. 23-30.

Briaud, J. L., Smith, T. D., and Meyer, B., 1982, "Design of Laterally Loaded Piles Using Pressuremeter Test Results," *Symposium on the Pressuremeter and Its Marine Application*, Paris. pp. 377-395.

Brumund, W. F. and Leonards, G. A., 1973, "Experimental Study of Static and Dynamic Friction Between Sand and Typical Construction Materials," *Journal of Testing and Evaluation*, JTEVA, Vol. 1, No. 2, pp. 162-165.

Burland, J.B., 1964 "Effective Stress in Partly Saturated Soils," Correspondence to the Secretary of the Institution of Civil Engineers, *Geotechnique*, Vol. 14, pp. 64-68.

Burland, J. B., and Ridley, A. K., 1996, "The Importance of Suction in Soil Mechanics," *Twelfth Southeast Asian Conference*, 6-10 May 1996, Kuala Lumpur.

Chandler, R. J., 1968, "Shaft Friction of Piles in Cohesive Soils in Terms of Effective Stress," *Civil Engineering*, Vol. 63, No. 738, pp. 48-49+51.

Clough, G. W., and Duncan, J. M.,1971, "Finite element analyses of retaining wall behavior," *Journal of the Soil Mechanics and Foundations Division,* ASCE, Vol. 97, No. SM12, pp.1657-1673.

Cui, Y. J., and Delage, P., 1996, "Yielding and Plastic Behavior of Unsaturated Compacted Silt," *Geotechnique*, Vol. 46, No. 2, pp. 291-311.

Desai, C. S., 1974, "A Consistent Finite Element Technique for Work Softening Behavior," *Proceedings of International Conference on Computational Methods in Non-linear Mechanics*, University of Texas at Austin, TX.

Desai, C. S., 1980, "A General basis for Yield, Failure and Potential Functions in Plasticity," *International Journal of Numerical and Analytical Methods in Geomechanics*, Vol. 4, pp. 361-375.

Desai, C. S., 2001, "Mechanics of Materials and Interfaces: The Disturbed State Concept," CRC Press, Boca Raton, Florida.

Desai, C. S., Drumm, E. C., and Zaman, M. M., 1985, "Cyclic Testing and Modeling of Interfaces," ASCE, *Journal of Geotechnical Engineering*, Vol.111, No.6, pp.793-815.

Desai, C. S. and Faruque, M. O., 1984, "Constitutive Model for (Geological) Materials," *Journal of Engineering Mechanics Division*, ASCE, Vol. 110, No.9, pp. 1391-1408.

Desai, C. S., and Fishman, K. L., 1991, "Plasticity-Based Constitutive model with Associated Testing for Joints," *Int. j. of Rock Mech. Min. Sci. & Geomech. Abstr*. Vol. 28, No.1, pp. 15-26.

Desai, C. S., and Ma, Y., 1992, "Modelling of Joints and Interfaces Using the Disturbed State Concept," *International Journal of Numerical and Analytical Methods in Geomechanics*, Vol. 16, pp. 623-653.

Desai, C. S., Somasundaram, S., Frantziskonis, G., 1986, "A Hierarchical Approach for Constitutive Modelling of Geologic l Materials," *International Journal of Numerical and Analytical Methods in Geomechanics*, Vol. 10, pp. 225-257.

Desai, C. S., Zaman, M. M., Lightner, J. G., and Siriwardane, H. J., 1984, "Thin Layer Element for Interfaces and Joints," *International Journal of Numerical and Analytical Methods in Geomechanics*, Vol. 8, pp. 19-43.

Drumm, E. C., and Desai, C. S., 1986, "Determination of Parameters for a Model for the Cyclic Behaviour of Interfaces," *Earthquake Engineering and Structural Dynamics*. Vol. 14, pp.1-18.

Escario, V., 1980, "Suction Controlled Penetration and Shear Tests," *Proceedings, 4th International Conference on Expansive Soils*, Vol. 2, pp. 781-797.

Escario, V., and Juca, J.F.T., 1989 "Strength and Deformation of Partly Saturated Soils," *Proceedings of the 12th ICSMFE*, Vol.1, pp.43-46.

Escario, I., and Saez, J., 1986, "The Shear Strength of Partly Saturated Soils," *Geotechnique*, Vol. 36, pp. 453-456.

Fakharian, K., 1996, "Three-Dimensional Monotonic and Cyclic Behaviour of Sand-Steel Interfaces: Testing and Modelling," Ph.D. dissertation submitted to Department of Civil Engineering, University of Ottawa.

Fakharian, K. and Evgin, E., 1996, "An Automated Apparatus for Three-Dimensional Monotonic and Cyclic Testing of Interfaces," *Geotechnical Testing Journal*, Vol. 19, No. 1, pp. 22-31.

Fishman, K. L., 1988, "Constitutive Modeling of Idealized Rock Joints Under Quasi-Static and Cyclic Loading," Ph.D. dissertation submitted to Department of Civil Engineering and Engineering Mechanics, The University of Arizona.

Fredlund, D.G., 1975, "A Diffused Air Volume Indicator for Unsaturated Soils," *Canadian Geotechnical Journal*, Vol. 12, pp. 533-539.

Fredlund, D.G. and Rahardjo, H., 1993, "*Soil Mechanics for Unsaturated Soils*", John Wiley and Sons, Inc. New York, N.Y.

Fredlund, D.G., Morgenstern, N.R., 1976Constitutive Relations for Volume Change in Unsaturated Soils," *Canadian Geotechnical Journal*, Vol. 13, No. 3, pp. 261-276.

Fredlund, D.G., Morgenstern, N.R., 1977, "The Shear Strength of Unsaturated Soils," *Proceedings ASCE*, Vol. 103, No.SM5, pp. 447-466.

Fredlund, D.G., Morgenstern, N.R., and Widger, R.A., 1978, "The Shear Strength of Unsaturated Soils," *Canadian Geotechnical Journal*, Vol. 15, No. 3, pp. 313-321.

Fredlund, D.G. and Rahardjo, H., Gan, J. K. M., 1987, "Non-Linearity of Strength Envelope for Unsaturated Soil," *Proceedings 6th International Conference on Expansive Soils*, New Delhi, India. pp. 49-54.

Gachet, P., Klubertanz, G., Vulliet, L., and Laloui, L., 2003, " Interfacial Behavior of Unsaturated Soil with Small- Scale Models and Use of Image Processing Techniques," *Geotechnical Testing Journal*, Vol. 26, No.1.

Gan, J. K. M. and Fredlund, D. G., 1988, "Multistage Direct Shear Testing of Unsaturated Soils," *Geotechnical Testing Journal*, Vol. 11, No.2, pp. 132-138.

Gan, J. K. M., Fredlund, D. G., and Rahardjo, 1988, "Determination of Shear Strength Parameters of an Unsaturated Soil Using Direct Shear Test," *Canadian Geotechnical journal*, Vol.25, No. 8, pp. 500-510.

Geiser, F., 2000, "Applicability of a General Effective Stress Concept to Unsaturated Soil," *Unsaturated Soils for Asia*, Rahardjo, H. et al. (eds.) Balkema:Roterdam, pp.101-105.

Geiser, F., Laloui, L. & Vulliet, L., 2000, "Modelling the Behaviour of Unsaturated Silt," *Experimental Evidence and Theoretical Approaches in Unsaturated Soil*, Rotterdam:Balkema, pp. 155-175.

Gens, A., Alonso, E.E, and Josa, A., 1989, "Elasto-plastic Modelling of Partially Saturated Soils," *proceedings of NUMOG*, Ed. Pietruszczak, S., and Pande, G. N., No. 3, pp. 163-170.

Ghaboussi, J. and Wilson, E. L., 1973, "Finite Elements for Rock Joints and Interfaces," *Journal of the Soil Mechanics and Foundation Division*, ASCE, Vol. 99, No. SM10, pp. 833-848.

Ghionna, V. N. and Mortara, G., 2002, "An Elastoplastic Model for Sand-Structure Interface Behaviour," *Geotechnique*, Vol. 52, No. 1, pp. 41-50.

Ho, D.Y.F., and Fredlund, D. G., 1982, "Multi-stage Triaxial Tests for Unsaturated Soils," *Geotechnical Testing Journal*, Vol. 5, pp. 18-25.

Jewell, R. A., 1989, "Direct Shear Test on Sand," *Geotechnique*, Vol. 39, No. 2, pp. 309-322.

Hilf, J. W., 1948, "Estimating Construction Pore Pressures in Rolled Earth Dams," *Proceedings 2nd ICSMFE*, The Netherlands, Vol. 3, pp. 234-240.

Hu, L. and Pu, J., 2004, "Testing and Modeling of Soil-Structure Interface," *Journal of Geotechnical and Geoenvironmental Engineering*, Vol. 130, No. 8, pp. 851-860.

Idriss, I. M., Dobby, R., and Singh, R. D., 1978, Nonlinear Behavior of Soft Clays During Cyclic Loading," *Journal of Geotechnical Engineering Division,* ASCE, Vol. 104, No. GT12, pp. 1427-1447.

Jennings, J. E. and Burland, J. B., 1962, Limitations to the Use of Effective Stresses in Partly Saturated Soils," *Geotechnique*, Vol. 12, No. 2, pp. 125-144.

Josa, A., Alonso, E.E., Lloret, A., and Gens, A., 1987, " Stress-Strain Behavior of Partially Saturated Soils," *Proceedings of the 9th European Conference on Soil Mechanics and Foundation Engineering*, Dublin, 31 august-3 September.

Karube, D. and Kato, S., 1989, "Yield Function of Unsaturated Soils," *Proceedings of 12th ICSMFE*, Rio de Janeiro, Vol. 1, pp. 615-618.

Khalili, N., 2000, "Application of the Effective Stress principle to Volume Change in Unsaturated Soils," *Unsaturated Soils for Asia*, Rahardjo, H. et al. (eds.) Balkema: Roterdam, pp.119-124.

Kim, M. H., and O'Neill. M. W., 1998, "Side Shear Induced in Drilled Shaft by Suction," *Journal of Geotechnical and Geoenvironmental Engineering*, ASCE, Vol. 124, No. 8, pp. 771-780.

Kishida, H. and Uesugi, M., 1987, "Tests of Interface Between Sand and Steel in the Simple Shear Apparatus," *Geotechnique*, Vol. 37, No. 1, pp. 45-52.

Kohgo, Y., Nakano, M., and Miyazaki, T., 1993, "Theoretical Aspects of Constitutive Modelling for Unsaturated Soils," *Soils and Foundations*, Vol. 33, No.4, pp. 49-63.

Krahn, J., Fredlund, D. G., and Klassen, M. J., 1989, "Effect of Suction on Slope Stability at Notchhill," *Canadian Geotechnical Journal*, Vol. 26, No.2, pp. 269-278.

Leichnitz, W., 1985, "Mechanical Properties of Rock Joints," *International Journal of Rock Mechanics and Mining Sciences & Geomechanics Abstracts*. Vol. 28, No.1, pp. 313-321.

Loret, B., and Alonso, E. E., 1985, "State Surfaces for Partly Saturated Soils," *Proceedings 11th ICSMFE*, San Francisco, Vol. 2, pp. 557-562.

Loret, B. and Khalili, N., 2000, "A Three-Phase Model for Unsaturated Soil," *International Journal for Numerical and Analytical Methods in Geomechanics*, Vol.24, pp. 893-927.

Matyas, E.L. and Radhakrishna, H.S., 1968, "Volume Change Characteristics of Partly Saturated Soils," *Geotechnique*, Vol. 18, pp. 432-448.

Mitchell, J. K., 1976, "Fundamental of Soil Behavior," New York, John Wiley & Sons Inc.

Navayogarajah, N., 1990, "Constitutive Modeling of Static and Cyclic Behavior of Interfaces and Implementation in Boundary Value Problems," Ph.D. Dissertation, Department of Civil and Engineering Mechanics, University of Arizona, Tucson, USA.

Navayogarajah, N., Desai, C. S., and Kiousis, P.D., 1992, "Hierarchical Single Surface Model for Static and Cyclic Behaviour of Interfaces," *Journal of Engineering Mechanics*, ASCE, Vol. 118, No.5, pp. 990-1011.

Oloo, S. Y., and Fredlund, D. G., 1996, "A Method for Determination of ϕ^b for Statically Compacted Soils," *Canadian Geotechnical Journal*, Vol. 33, pp. 272-280.

Paikowsky, S. G., Player, C. M., and Connors, P. J., 1995, " A Dual Apparatus for Testing Unrestricted Friction of Soil Along Solid Surfaces," *Geotechnical Testing Journal*, Vol. 18, No. 2, pp. 168-193.

Potyondy, J. G., 1961, "Skin Friction Between Various Soils and Construction Materials," *Geotechnique*, Vol. 11, No. 4, pp. 831-853.

Rahardjo, H and Fredlund, D.G., 1996, "Consolidation Apparatus for Testing Unsaturated Soils," *Geotechnical Testing Journal*, Vol.19, No.4, pp. 341-353.

Ramberg, W. and Osgood, W. R., 1943, "Description of Stress-Strain Curves by Three Parameters," Technical Note 902, National Advisory Committee for Aeronautics, Washington, D.C.

Richards, B. G., 1966, "The Significance of Moisture Flow and Equilibria in Unsaturated Soils in Relation to the Design of Engineering Structures Built on Shallow Foundations in Australia," Symposium on Permeability and Capillary, ASTM, NJ.

Saeb, S., and Amadei, B., 1992, "Modelling Rock Joints Under Shear and Normal Loading," *International Journal of Rock Mechanics and Mining Sciences & Geomechanics Abstracts*. Vol. 29, No.3, pp. 267-278.

Seeds, H. B., and Chan, C.K., 1959, "Structure and Strength Characteristics of Compacted Clays," *Soil Mechanics and Foundation Division*, ASCE, Vol.85, No. SM5, pp.87-128.

Smith, T. R., and ray, B., 1986, "Shear Mobilization on Laterally Loaded Shafts," *Geotechnical Aspects of Stiff and Hard Clays, Ed. Khera and Lovell,* ASCE, New York, pp. 60-68.

Streeter, V.L., Wylie, E.B., and Richart, F. E., 1974, "Soil Motion Computations by Characteristics Method," *Journal of Geotechnical Engineering Division,* ASCE, Vol. 100, No. GT3, pp. 247-263.

Subba Rao, K. S., Allam, M. M. and Robinson, R. G., 2000, "Drained Shear Strength of Fine-Grained Soil-Solid Surface Interfaces," *Proceedings Institution of Civil Engineers, Geotechnical Engineering*, Vol. 143, pp. 75-81.

Toll, D.G., 1990, "A framework for Unsaturated Soil Behavior," *Geotechnique*, Vol. 40, No. 1, pp. 31-44.

Tsubakihara, Y. and Kishida, 1993, "Frictional Behavior Between Normally Consolidated Clay and Steel by Two Direct Shear Type Apparatus," *Soils and Foundations*, Vol. 33, No. 2, pp. 1-13.

Tsubakihara, Y., Kishida, H., and Nishiyama, T., 1993, "Friction Between Cohesive Soils and Steel," *Soils and Foundations*, Vol. 33, No. 2, pp. 145-156.

Uesugi, M. and Kishida, H., 1986, "Frictional Resistance at Yield Between Dry Sand and Mild Steel," *Soils and Foundations*, Vol. 26, No. 4, pp. 139–149.

Uesugi, M., Kishida, H., and Tsubakihara, Y., 1989, "Friction Between Sand and Steel Under Repeated Loading," *Soils and Foundations*, Vol. 29, No. 3, pp. 127–137.

Uesugi, M., Kishida, H., and Uchikawa, Y., 1990, "Friction Between Dry Sand and Concrete Under Monotonic and Repeated Loading," *Soils and Foundations*, Vol. 30, No. 1, pp. 115–128.

Vanapalli, S.K., Fredlund, D.G., Pufahl, D.E., and Clifton, A.W., 1996, "Model for the Prediction of Shear Strength with Respect to Soil Suction," *Canadian Geotechnical Journal*, Vol. 33, pp. 379-392.

Wheeler, S.J., 1986, "The Stress-Strain Behaviour of Soils Containing Gas Bubbles," D. Phil Thesis, University of Oxford.

Wheeler, S.J., 1988, "The Undrained Shear Strength of Soils Containing Large gas Bubbles," *Geotechnique*, Vol. 38, No.3, pp. 399-413.

Wheeler, S.J., 1991, "An Alternative Framework for Unsaturated Soil Behavior," *Geotechnique*, Vol. 41, No.2, pp. 257-261.

Wheeler, S.J., and Sivakumar, V., 1992, "Development and Application of a Critical State Model for Unsaturated Soil,' *Predictive Soil Mechanics*; *Proceedings of the Wroth Memorial Symposium*, Oxford, 27-29 July. pp. 709-728.

Wheeler, S.J., and Sivakumar, V., 1995, "An Elasto-Plastic Critical Framework for Unsaturated Soil," *Geotechnique*, Vol. 45, No. 1, pp. 35-53.

Wheeler, S.J., Gallipoli, D., and Karstunen, M., 2002, "Comments on Use of the Barcelona Basic Model for Unsaturated Soils," *International Journal for Numerical and Analytical Methods in Geomechanics*, Vol.26, pp. 1561-1571.

Yoshimi, Y. and Kishida, T., 1981, "Friction Between Sand and Metal Surface," *Proceedings, 10th International Conference on Soil Mechanics and Foundation* Engineering, Vol. 1, pp. 831-834.

Zaman, M. M., Desai, C. S., and Drumm, E. C., 1984, "Interface Model for Dynamic Soil-Structure Interaction," *Journal of Geotechnical Engineering*, ASCE, Vol. 110, No. 9, pp. 1257-1273.

Zaman, M. M., 1982, "Influence of Interface Behavior in Dynamic Soil-Structure Interaction Problems," Ph.D. Dissertation, Department of Civil and Engineering Mechanics, University of Arizona, Tucson, USA.

Zeghal, M. and Edil, T. B., 2002, "Soil Structure Interaction Analysis: Modeling the Interface," *Canadian Geotechnical journal*, Vol.39, pp. 620-628.